SCi
ENERGY SYSTEMS DIVISION
SYSTEMS CONTROL, INC. ■ 1801 PAGE MILL ROAD ■ PALO ALTO, CA 94304 ■ TELEX 348-433 ■ (415) 494-1165

DOE/ET/29031--T2

DE83 014063

DEVELOPMENT AND IMPLEMENTATION OF ADVANCED AUTOMATIC GENERATION CONTROL

FINAL REPORT OF TASK 2
DEFINITION OF PERFORMANCE CRITERIA AND DEVELOPMENT OF PROTOTYPE ALGORITHMS

SCI

ENERGY SYSTEMS
DIVISION

DOE/ET/29031--T2

DOE Contract EC-77-01-2118

AC01-77ET29031

SCI Project 5212

DEVELOPMENT AND IMPLEMENTATION OF ADVANCED AUTOMATIC GENERATION CONTROL

FINAL REPORT OF TASK 2

DEFINITION OF PERFORMANCE CRITERIA AND DEVELOPMENT OF PROTOTYPE ALGORITHMS

Prepared for:

Department of Energy
20 Massachusetts Avenue
Washington, D.C. 20545

Attention: Lester H. Fink

Prepared by:

D. Ross
T. Athay
S. Kim
G. Ackerman
R. Podmore
S. Virmani

SYSTEMS CONTROL, INC. ■ 1801 PAGE MILL ROAD □ PALO ALTO, CA 94304 ■ TELEX 348-433 ■ (415) 494-1165

TABLE OF CONTENTS

TABLE OF CONTENTS

TABLE OF CONTENTS

TABLE OF CONTENTS

1. TASK 2 - INTRODUCTION AND OVERVIEW

1.1 OVERVIEW OF TASK 2

Task 2 of the advanced automatic generation control project has been concerned with two principal areas of investigation: (1) the formulation of quantitative criteria which can be used for measuring AGC performance, and (2) the development of prototype AGC algorithms.

The Project Management Plan, drawn up in August, 1977 identified four specific work topics (subtask) within Task 2; they were:

1. Performance Criteria: Quantitative criteria were to be formulated for measuring AGC performance. Recommendations were to be made regarding the application of the performance measures in comparing alternative AGC logics -- in both simulation studies and on-line studies on the Wisconsin Electric Power Company system.

2. Load Prediction Algorithm: A prototype load prediction algorithm was to be developed for the purpose of providing "look ahead" capability for an economic dispatch that is subject to unit rate limits and which may include the dispatch of valve-point loaded units.

3. Dynamic Optimal Dispatch Algorithm: A prototype algorithm was to be developed for the purpose of economically dispatching generation to the predicted load during the upcoming time horizon. The convergence characteristics and computational efficiency of the algorithm were to be investigated. The algorithm was to include the capability for valve point loading.

4. Load Tracking Algorithm: A prototype load frequency algorithm was to be developed and evaluated for: close control of interchange; minimization of unnecessary control action; robustness for model errors, deadband, non-linearities; changes to unit configuration; and poor unit response. The performance of the prototype control algorithm was to be compared with proportional plus integral control of ACE.

As the Task 2 work developed, these four subtasks of the Management Plan expanded into a number of specific activities that are identified (along with their place on the project time-line) in Figure 1.1. These activities are described in detail in Chapters 2 through 6 of this Report. Brief summaries of these Task 2 activities follow:

1. Performance Measures Selected: An analysis was made of several candidate quantitative measures of the comparative performance of alternative AGC schemes. Specific measures were selected for evaluating the quality of control, the control effort, and the production costs of the AGC.

2. Need for Dynamic Dispatch Identified: A preliminary analysis was made of WEPCO load data, unit commitment data and economic dispatch data to see whether there are situations in which static, equal incremental cost, economic dispatch requires unit movement that conflicts with unit rate limits. The equal incremental cost dispatch did require some units to increase output faster than their rate limits in one morning pickup period analyzed. This indicated at least a need to explicitly recognize rate limits in the dispatch, if not to dispatch dynamically instead of statically.

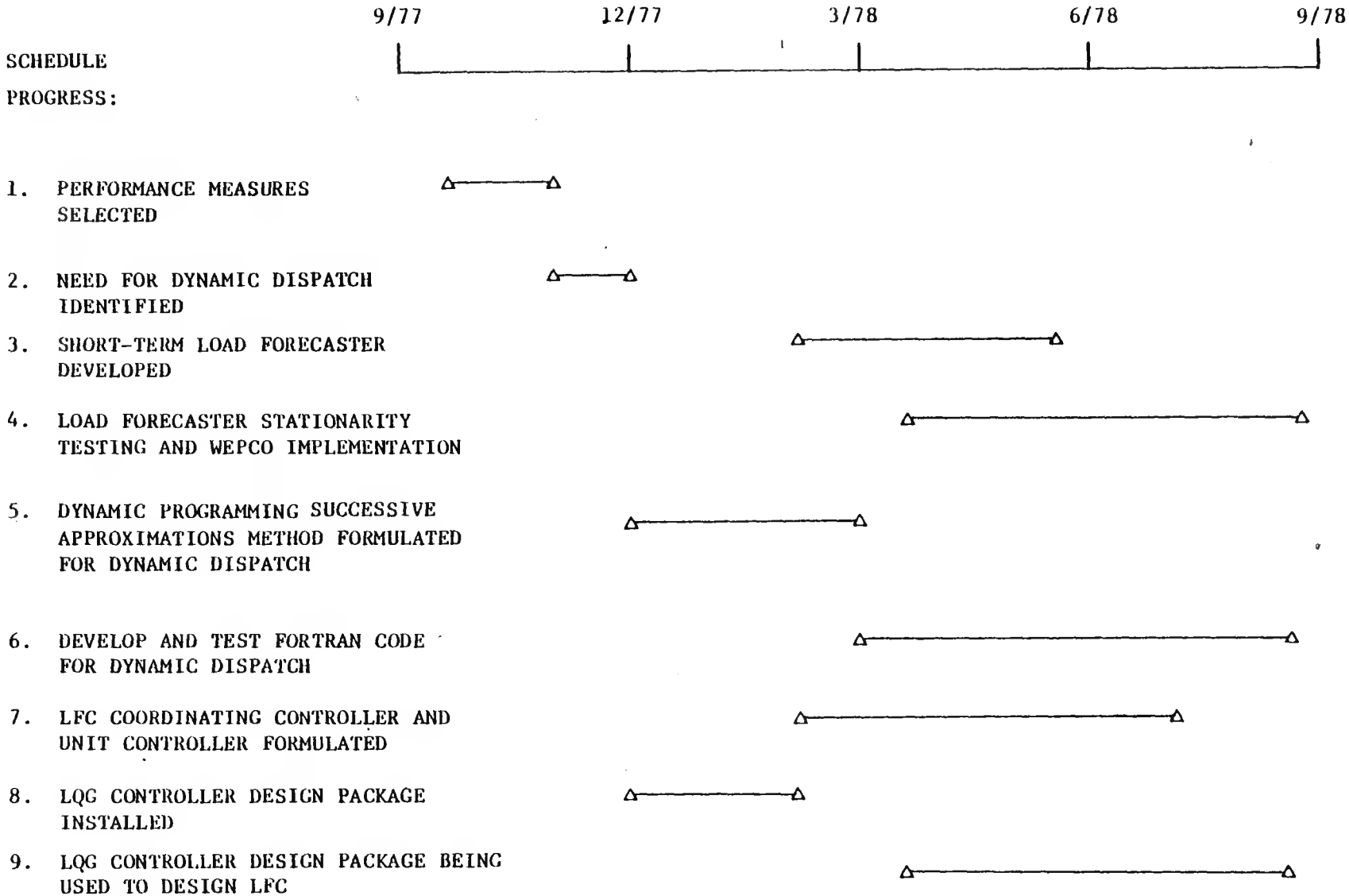

FIGURE 1.1 TASK 2 ACTIVITIES

3. Short-Term Load Forecaster Developed: Hourly and 5-minute load predictor algorithms were derived empirically from samples of WEPCO load data. The algorithms were based on models of load behavior developed using Box-Jenkins time series analysis methods.

4. Load Forecaster Stationarity Testing and WEPCO Implementation: The structure and parameter values of the load predictor models were re-estimated on several new WEPCO load data sets. The purpose of these tests was to determine whether or not the models were stationary. The initially estimated models showed considerable variability -- and eventually new models evolved that were very robust.

   The (initial) hourly and 5-minute predictors were also implemented and tested on-line on the WEPCO Cyber computer.

5. Dynamic Programming Successive Approximations Method Formulated for Dynamic Dispatch: An algorithm was devised for the economic dispatch of generation to load over a prediction horizon, subject to unit rate limits, and allowing for valve-point loading of units. The algorithm was based on successive approximations dynamic programming.

6. Develop and Test FORTRAN Code for Dynamic Dispatch: The successive approximations dynamic programming method for dynamic economic dispatch was coded and tested for its computational efficiency and convergence properties.

7. LFC Coordinating Controller and Unit Controller Formulated: A design approach was taken for the LFC that coordinated the two objectives of (1) having total area generation track area load plus schedule, and (2) having unit generation

track its desired economic trajectory. Suboptimal regulator design techniques have been applied to develop two coordinating controller structures. Both are robust designs that provide reset on area control error. Analyses of gain and phase margins of the controllers demonstrated their robustness.

Linear optimal control design methods have been used to develop a feedback controller design for the units, enabling each unit to track its desired generation.

8. LQG Controller Design Package Installed: A Linear-Quadratic-Gaussian (LQG) controller design software package used in past SCI project work was installed on the Univac 1108 computer for use in designing the coordinating controller and the unit controller.

9. LQG Controller Design Package Used to Design LFC: As mentioned previously, the LQG design package was used to design the coordinating controller and unit controller.

1.2 INTERACTION OF TASK 2 WITH OTHER PROJECT TASKS

Task 2 has been conducted in parallel to Task 1, "Modeling and Analysis of WE System". One interaction of these two tasks has been that Task 1 has resulted in the collection of data on the WEPCO system generating units, load and existing AGC. These data have been necessary to conduct analyses of the prototype AGC algorithms developed in Task 2. The other principal interaction of the two Tasks involves the development, in Task 1, of an AGC simulation package. The performance measures developed in Task 2 have been embodied in the simulation. Also, the coordinating controller and unit controller algorithms have

been embodied in the simulation. The load prediction cannot be implemented in the simulation -- since it would involve modeling the WEPCO daily load and the WEPCO 24-hour load forecasting method -- clearly beyond the scope of our effort. The dynamic economic dispatch algorithm will be run off-line from the simulation program itself on the predicted loads for the various load scenarios treated in the on-line simulation (allows the analyst wants to investigate the effect of the coordinating controller).

Task 2 also interacts with Task 3, "Development of New AGC Software". Task 3 starts in October 1978 (at the same time that Task 2 ends); it involves the specification, coding, and testing (both simulation testing and on-line testing at WEPCO) of the new AGC schemes. Accordingly, the prototype algorithms developed in Task 2 will be converted into operational programs in Task 3.

1.3 AGC ALGORITHMS DEVELOPED AND THEIR INTERRELATIONSHIPS

Chapters 3-6 of this Report discuss the advanced prototype AGC algorithms that have been developed, to date, in this project. The purpose of the present section is to summarize the functioning of the various algorithms and their interactions.

Figure 1.2 identifies the separate AGC algorithms that have been developed and depicts, graphically, their interactions. Brief functional descriptions and analytical/algorithmic bases of the AGC algorithms identified in Figure 1.2 are:

Hourly (Integrated) Load Predictor

Predicts integrated hourly load for at least three hours into the future. It is run once per hour so that the prediction can be updated using the value of the actual hourly integrated load of the most recently completed hour. The predictions provide the basic information that is eventually used in the Dynamic Economic Dispatch algorithm.

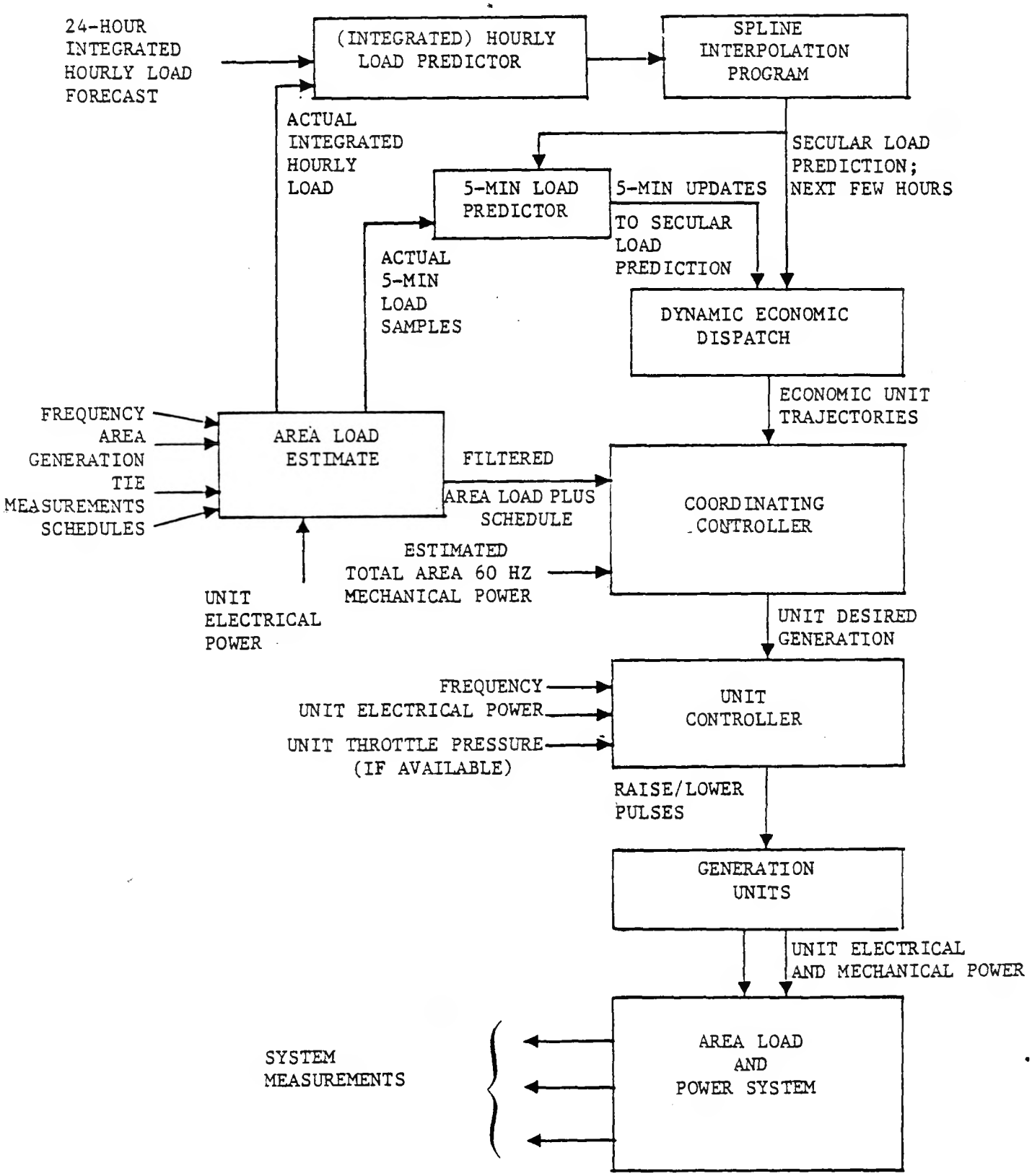

FIGURE 1.2 AGC ALGORITHMS AND THEIR INTERACTIONS

The predictor is based on an auto-regressive time-series model of the errors between actual hourly integrated load and the forecasted 24-hour hourly integrated loads.

Spline Interpolation Program

Interpolates the (discrete) hourly load predictions made by the Hourly Load Predictor. It is run once per hour, immediately after the Hourly Load Predictor has been run. It interpolates the hourly predictions and produces predicted instantaneous load at 5-minute intervals throughout the prediction horizon of the Hourly Load Predictor. It therefore generates, each hour, a revised future nominal load shape extending at least two hours into the future. This can be used to run a new multi-hour dynamic economic dispatch, each hour.

A spline-function interpolation procedure is the basis of this algorithm.

5-Minute Load Predictor

Predicts instantaneous area load at each 5-minute interval in the future, for at least one hour into the future. It therefore provides, as an hour progresses, update/corrections to the load values produced by the Spline Interpolation Program. These load prediction corrections apply to at least one full-hour beyond the current 5-minute point in the current hour. These load corrections can be used by the Dynamic Economic Dispatch, if it is re-run each 5 minutes, to adjust the dispatch of units for the load corrections.

The predictor is based on an auto-regressive time-series model of the errors (at 5-minute intervals) between actual instantaneous load and the load values produced by the Spline Interpolation Program.

Dynamic Economic Dispatch

Once each hour this economic dispatch program is executed to provide economic trajectories for the units on AGC. These trajectories extend out over the interpolation horizon of the Spline Interpolation Program (i.e., at least two hours into the future).

Once each 5-minutes during each hour this program is used (generally on a subset of all units on AGC) to develop an update of the economic unit trajectories.

The purpose of dispatching units over a load prediction horizon that can include many 5-minute dispatch intervals is to provide "look ahead" information to the economic dispatch so that potential problems caused by unit rate limits and/or valve-point loading of certain units can be considered.

The Dynamic Economic Dispatch algorithm is based on the combined use of a minimum marginal cost method and a dynamic programming successive approximations method.

Coordinating Controller

Produces, each AGC cycle, the generation demand (unit desired generation) for each unit on AGC. In doing so it "coordinates" the two tracking objectives: (a) total area generation tracks area load plus schedule, and (b) unit generation tracks a desired economic trajectory. At the same time, it prevents the AGC from interfering with the area primary response (governor/frequency loop).

The coordinating controller design is based upon state - space robust controller design techniques.

Unit Controller

Produces control input to each unit that will cause that unit to match generation output to generation demand (unit desired generation). The controller is of a feedback design (rather than a model-referenced, open-loop design -- which is common in the state-of-the-art) in which throttle pressure and turbine power conditions (internal unit conditions) are estimated and used in the feedback control.

The controller design is based on the application of Kalman filtering and LQG Controller Design methods.

Three technical papers that discuss the coordinating and unit controllers, load predictor, and the dynamic economic dispatch respectively are included as Appendices A, B and C.

2. PERFORMANCE MEASURES

2.1 INTRODUCTION

Early in the project, four fundamental aspects of AGC performance measurement were identified: (1) AGC "economics" or production costs of the generation; (2) the "quality of control" provided by AGC, which indicates how well a control area is meeting its responsibilities as part of an interconnection; (3) the "control effort" of the AGC, which indicates how much control variation is being applied to the generation units; and, (4) "operator interactions" measures, which indicate the ease of use and the amount of operator attention to or intervention with the AGC.

It was decided, in the course of the project work, that the first three aspects of AGC performance measurement were amenable to quantitative assessment, but that the operator interactions was more qualitative in nature -- being dependent upon operator attitudes and possibly varying considerably among the system operators. Accordingly, work has concentrated on defining quantitative performance measures for the first three aspects of AGC; no formal performance evaluation approach is planned in regard to operator interactions. However, when actual tests of the advanced AGC software are conducted, significant operator actions and comments will be reported.

The performance measures will be used to provide quantitative indications of the differences between the advanced AGC being developed in this project and existing, state-of-the-art, AGC logics. The performance measures will be used in both simulation tests and on-line tests on the WEPCO system.

Section 2.2 - 2.4 below discuss the performance measures that have been selected, as well as the analyses made in support of the selected measures.

2.2 QUALITY OF CONTROL

2.2.1 Meaning of Quality of Control

The objective in defining quality of control performance measure(s) is to provide a systematic procedure for assessing how well a control area is meeting its responsibilities as part of an interconnection. These responsibilities have been defined as performing three functions which are described below.

A. An area should absorb its own local load changes (referred to 60 Hz). This is an obligation function.

B. An area should share in control of frequency. This is also an obligation function.

C. An area's AGC should coordinate with governing response to remote load changes. This is a contribution function.

It is implicit that if the first two functions are performed satisfactorily then the area will minimize the amount of assistance which it receives from the interconnection.

2.2.2 Candidate Measures of Quality of Control

At the outset of the project, several possible quality of control measures were postulated. First, area control error (ACE), as conventionally defined:

$$ACE = M - S + 10B\Delta f \qquad (2.1)$$

where M = Metered interchange

S = Scheduled interchange

B = Bias factor

Δf = Frequency deviation

was identified as a possible measure. Several different operations could be performed on ACE to define the quality of control measure. For example, rms ACE, the time-integral of ACE, and the spectral power of ACE were all proposed.

Another candidate measure that was initially proposed was inadvertent accumulation:

$$\text{inadvertent} = \int (M - S)\, dt \qquad (2.2)$$

Associated with inadvertent was the notion of developing a performance measure that was based on the interchange error, M - S.

Another concept that was considered [2-1] was that the interchange error, M - S, was a measure of a control area's mismatch between its own generation and load-plus-schedule (unreferenced to frequency) -- and that the bias term, $10B\Delta f$, in Equation (2.1) was associated with the control area's assistance to the interconnection for frequency control. Accordingly, a system's operation corresponds to motion in the two-dimensions, M - S and $10\ B\Delta f$. Based on an argument that area load changes should be predominately uncorrelated with system frequency deviations, it was argued that if the interchange error were separated into two components -- one uncorrelated with Δf (say, IE_o) and one correlated with Δf (say, $IE_{\Delta f}$) -- then:

- IE_o should be a measure of the quality of the control in regard to matching area generation to area load
- $IE_{\Delta f} + 10B\Delta f$ should be a measure of the quality of the control in regard to providing assistance to the interconnection for frequency regulation.

(Note that $IE_o + IE_{\Delta f} + 10B\Delta f = ACE$)

Of these various initial ideas for measuring quality of control, it was finally decided to use ACE in defining a quality of control performance measure. This use of ACE is described in the next subsection.

Inadvertent (Equation 2.2) was judged inappropriate as a performance measure because it could be zero at any system frequency and therefore it did not reflect the control areas' responsibility to share in the control of frequency or to coordinate its AGC with governing responses to remote load changes.

The notion of measuring the quality of control via the quantities IE_o and $IE_{\Delta f} + 10B\Delta f$ was also discarded. This was discarded because one of the tacit assumptions that had been made was the $IE_{\Delta f}$, the component of interchange error that is correlated with system frequency deviation, was due to the load/generation mismatches for the external area. In fact, it was later shown [2-2] that $IE_{\Delta f}$ was NOT generally dominated by load/generation imbalances for the external area. Actually, the control area's load/generation imbalance itself could have nearly the same contribution to the $IE_{\Delta f}$ as the external area load/generation imbalance. This meant that $IE_{\Delta f}$ was NOT generally a good measure of how well the area was assisting the interconnection. Conversely, IE_o was NOT a good measure of the area's load/generation imbalance.

2.2.3 Selection of rms ACE as Quality of Control Performance Measure

Qualitative Appeal of ACE^2 as a Performance Measure

To gain an understanding of the significance of ACE in measuring control performance, consider Figure 2.1. Figure 2.1 is a pictorial representation of ACE as a function of metered interchange and frequency deviation. The horizontal axis represents the deviation between metered and scheduled interchange with export, or over-generation being positive. The vertical axis represents the bias factor times frequency deviation with deviations above scheduled value being positive. The line B-B´ represents

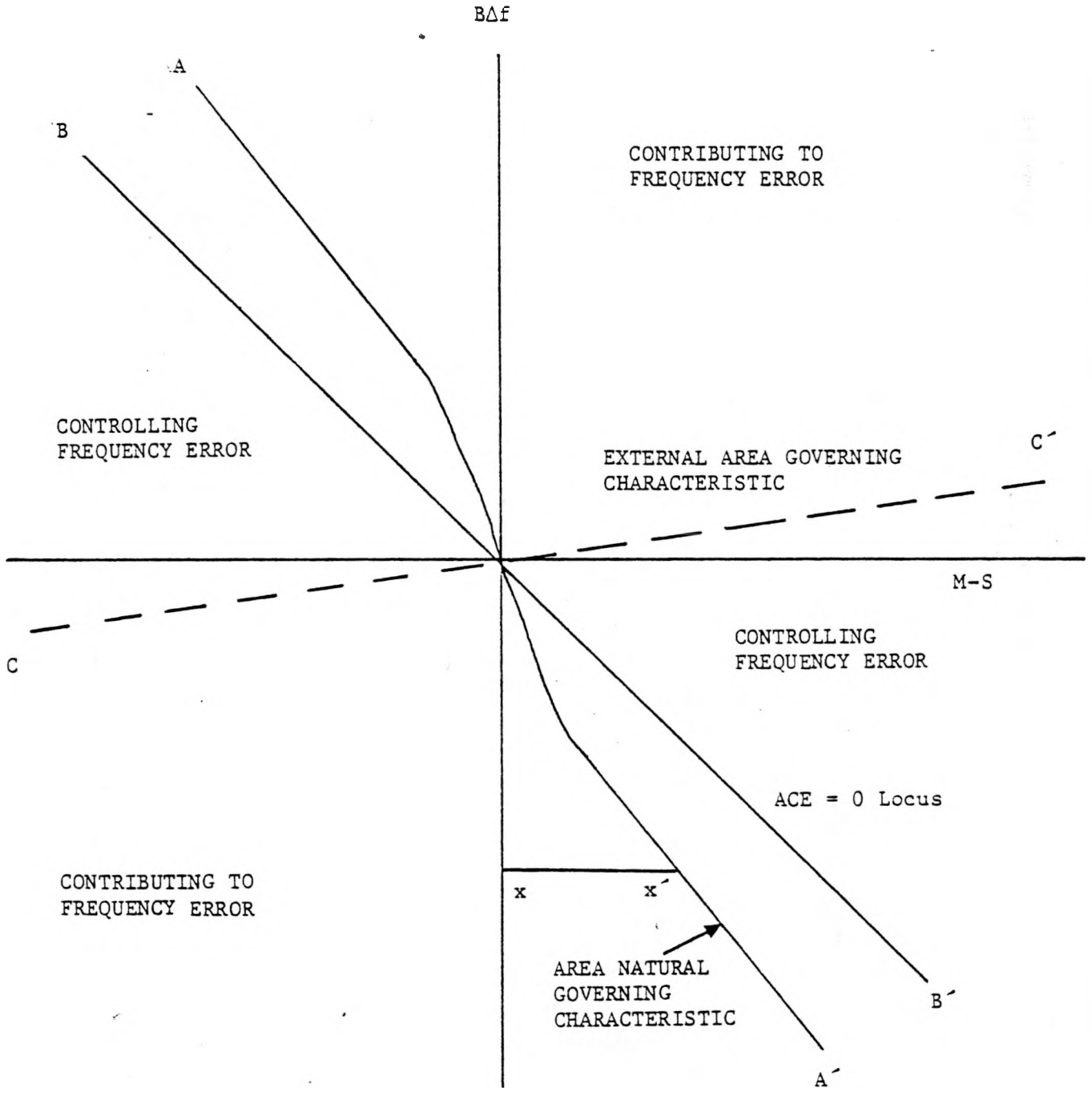

FIGURE 2.1 PICTORIAL REPRESENTATION OF ACE

the locus along which ACE is zero. The locus A-A´ represents the natural governing characteristic of the area in concern. The locus C-C´ represents the governing characteristics for the rest of the interconnection. The performance of the system can be portrayed by a time varying trajectory in this plane. If the frequency deviation is initially zero and the area's metered interchange matches schedule then the trajectory lies at the origin. If a load change occurs internal to the area and no supplementary control action is taken, then the trajectory will move along the locus C-C´. On the other hand, if an external load change occurs and no supplementary control action is taken then the trajectory will move along the locus A-A´.

The four quadrants of the diagram can be divided into two categories. In the first and third quadrants the area is contributing to the frequency error of the interconnection and may be viewed as receiving assistance from the interconnection. In the second and fourth quadrants, the area is contributing to the control of the frequency error and may be viewed as providing assistance to the interconnection. The actual amount of assistance which it is providing is determined by the horizontal distance from the Y axis as shown by the line X-X´. The ACE for any point in the plane is given by the horizontal distance between the point and the locus B-B´. From simple geometry, it follows that the minimum distance of any point in the plane from the B-B´ line is equal to $1/\sqrt{2}$ x ACE. Minimization of ACE^2 can therefore be thought of as minimizing a quadradic penalty function which is 0 centered about the line B-B´. The weighting of this penalty function could be less when the frequency deviations are larger; the reasoning for this is that larger frequency deviations are most likely due to large load changes or loss-of-generation in the rest of the interconnection and should be largely unrelated to how well load changes are being met. However, under normal operating conditions the variations in $B\Delta f$ tend to be smaller than the variations in metered minus schedule and so such frequency dependent scaling would have little effect anyway. Consideration could be given to measuring the amount of assistance received from the interconnection as the percentage of time which was spent in the

first and third quadrants with some small allowable deadband region about the origin. However a quadradic penalty on ACE will automatically penalize receiving assistance from the interconnection and therefore the percentage of time spent in the first and third quadrants is considered to be of interest but not critical for performance evaluation.

To summarize, the pictorial representation of ACE provides insight into how this measure simultaneously assesses an area's performance in four respects:

A. Matching its own changes by tracking deviations in metered interchange.

B. Contributing to control of frequency by lying in the second or fourth quadrant.

C. Providing assistance to the interconnection through primary governing response by staying close to the ACE = 0 line.

D. By performing the above three functions then the area automatically minimizes its assistance from the interconnection.

Accordingly, a performance measure defined in terms of ACE^2 has considerable appeal.

Applicability of ACE to Dynamic Performance Measurement

Analyses were conducted [2-3] that showed that the M - S term in ACE provides an accurate enough representation of the mismatch between an area's mechanical power generated and load. The equation for the metered interchange of Area 1 is as follows:

$$M_1 = \frac{H_2}{H_T}(P_{M1} - P_{L1}) - \frac{H_1}{H_T}(P_{M2} - P_{L2}) \qquad (2.3)$$

The above equation is based upon a coherent system wide model and is a good representation for frequencies below .1 Hz since synchronizing oscillations tend to be in the .3 to 2 Hz range. For oscillations in the range of .1 Hz to 1 cpm the changes in the mechanical power term become more significant and the accelerating power term becomes less significant as the frequency of oscillation decreases. For oscillations below 1 cpm the changes in mechanical power can be based upon the steady state response of governors and the accelerating power term is insignificant. Appendix A of Reference [2-3] provides an analysis which shows that the governors can follow a 1 cpm load change with very little error between total mechanical power and total load power. The analysis in Appendix B of Reference [2-3] shows that the accelerating power term for a 3000 MW system can be expected to be less than 1/2 MW for frequencies less than 1 cpm.

The impact of the foregoing observations is that the definition of ACE on the basis of a steady state relationship between metered interchange and various generation/load changes as well as a steady state relationship between turbine output and frequency changes is not as severe as one might initially expect. In fact, it is believed that these relationships are reasonably valid for all dynamic conditions which can be represented by frequencies below 1 cpm. Further, since there is little possibility of using the supplementary control loop to control load changes which are faster than 1 cpm, the foregoing assumptions do not appear to be restrictive at all. An additional note is that even if the turbine response significantly lags a frequency change, then the temporary effect on ACE is such that additional assistance to the interconnection is provided through supplementary control.

Measurement of Quality of Control Using ACE

The previous discussions (based on the analyses of Reference [2-3]) have shown that:

- ACE^2, simultaneously measures an area's performance in regard to (a) matching its own load changes, (b) contributing to control of frequency by lying in the second or fourth quadrants of Figure 2-1, (c) providing assistance to the

to the interconnection through primary governor response, and (d) minimizing its assistance from the interconnection.

- ACE is a reasonably valid measure of control area load/generation mismatch for all dynamic conditions which can be represented by frequencies below 1 cpm. Here, ACE is assumed to be defined according to the NAPSIC guidelines [2-4].

On the basis of these conclusions, it has been decided to use the rms value of the component of the ACE signal which has spectral frequencies below 1 cpm as the quality of control performance measure.

Three alternative procedures have been formulated for evaluating quality of control performance using rms ACE. The procedures consist of:

- A time domain procedure
- A frequency domain procedure
- A graphical procedure

When used for the purpose of comparing algorithms, the evaluation procedure should be applied to a recording of ACE which is obtained under normal conditions when the system frequency deviates from scheduled value by less than .05 Hz. The time domain procedure consists of the following steps:

- Record n samples of area control error at intervals T. Let the k^{th} sample be A(k)
- Filter samples using Butterworth digital filter with cut-off frequency at 1 cpm. Call the filtered signal $A'(k)$
- Calculate the rms value using

$$R = \frac{1}{n} \Sigma_k A'(k)^2 \qquad (2.4)$$

Time periods in the range of 30 minutes to 1 hour will be used. A gross measure of overall performance will be obtained by evaluating the mean value of R over all the observation periods with the new and old control algorithms respectively.

The frequency domain procedure utilizes Parceval's Theorem which can be used to show that the rms value of A may be alternatively expressed in the form:

$$C \sum |\bar{A}(s)|^2 \qquad (2.5)$$

where $\bar{A}(s)$ is the discrete Fourier transform of A(k). It follows that A'(k) can be obtained by integrating the power spectral density function of A(k) only over those frequencies which exceed the cut off value.

The frequency domain procedure can be performed as follows:

A. Take 1024 samples of ACE at 4 second intervals for a period of 68.26 minutes.

B. Process the signal with a single or double Hanning function to remove the leakage effects due to time domain translation. The single Hanning function is

$$\chi(t) = \frac{1}{2} - \frac{1}{2} \cos \frac{2\pi t}{Tc} \quad 0 \leq t < T.$$

C. Take the Fast Fourier transform of the signal produced in Step 2.

D. Calculate the power spectral density of the signal in Step 3.

E. Calculate the area under the power spectral density function of Step 4 up to the cut off frequency.

At various times when field tests are being performed or when the operation of the system is being casually observed it will be handy

to have a simple procedure for obtaining a rough measure of the system performance which can be obtained graphically as follows:

- Take the ACE chart
- Sketch through the average value of ACE to smooth out the "hash"
- Graphically integrate the rms value of ACE by counting squares under the ACE curve for each 10 MW band, assigning weights to the squares in each band and totaling the weighted values as follows (the weights are approximately for computing the rms value);

MW band	Weight	No. Squares	Weight x No. Squares
0 - 10	1		
10 - 20	3		
20 - 30	5		
30 - 40	7		
40 - 50	9		
60 - 70	11		
			Total

This procedure may appear to be so simple minded as to be unworthy of consideration by sophisticates. However, it should give results which agree quite closely with the other procedures and will be useful for initial appraisals.

2.3 CONTROL EFFORT

2.3.1 Meaning of Control Effort

"Control effort" is taken to be some quantitative measure of amount of regulation or control variation being applied to a generation unit. There are two primary reasons for introducing control effort measures into the AGC analysis. First, while the dollar costs of plant control variations are (at this time) uncertain, it is often implied that control variations do have associated fuel and maintenance costs. Secondly, establishing a measure of control effort provides a means of assessing

how well a particular control logic is keeping plant operation within "soft" constraints. One example of such a "soft" constraint is the desirable aim of keeping boiler stored energy fluctuations small so as to not stress the thermal system greatly. Kwatny, et.al. [2-5] have shown that the power spectrum of boiler output peaks in a certain frequency range. Reflecting, "control effort" in the control design may, for example, be a way of reflecting the desire to keep boiler stored energy fluctuations small.

2.3.2 Candidate Measures of Control Effort

The amount of control variation applied to a generation unit could be measured in a number of ways. The control variation can evidence itself in any of three principal generation unit quantities: pulses applied to the unit speedchanger motor; the output of the speed-changer, or the unit desired generation; the electrical power output of the unit.

Early in the project, candidate control effort measures based upon each of the three principal unit quantities were proposed. These were:

- Amount of unit pulsing (which could be measured in a number of ways -- e.g., sum of absolute values, sum of pulse-squared values, -- etc. over a period of time)
- Power spectrum of unit desired generation (with, say, some scheme for weighting the various frequency components in the spectrum)
- Power spectrum of unit output

We quickly rejected the variation in unit output; it is not a useful measure of control effort because it includes the governor response which is outside the AGC control loop.

The choice of unit pulsing or unit desired generation as a basis for a control effort measured is not distinct because the two quantities are directly related; one is the input to the speedchanger motor and the other is its output. The analysis below yields a control effort measure that is computed in the time domain from unit pulses. This measure is motivated by some physical considerations involving frequency-domain analysis of unit desired generation.

2.3.3 Analysis Leading to Choice of Control Effort Measure

As mentioned previously, Kwatny, et.al. [2-5] have shown that the power spectrum of boiler output peaks in a certain frequency range and for that reason it is desirable (in order to reduce boiler stress) to confine the control variation to a low frequency band below the "peaking" range of boiler output fluctuations. This partially motivates a control effort measure defined in the frequency domain. Let $S_{uu}(\omega)$ be the power spectral density observed for the unit desired generation, UDG, over a given time period. Then, a plausible control effort measure is:

$$J_u = \int_0^{\omega^*} \omega^2 S_{uu}(\omega)\, d\omega \qquad (2.6)$$

where ω^* = half the Nyquist frequency associated with the AGC control cycle (= πT where T = AGC control cycle in seconds).

In Equation (2.6), the weighting of the spectrum $S_{uu}(\omega)$ by the square of the frequency, ω^2, arises from weighting the frequency components of UDG(t) linearly with frequency. This linear weighting of the frequency components of UDG is, in turn, motivated by the increase, with frequency, of the amplitude of boiler stored energy fluctuations. As frequency increases, these fluctuations increase and can cause boiler stress. This

weighting is therefore consistent with the objectives of (1) providing a measure of control-variation, and (2) providing a measure of how well the control keeps the plant operation within "soft" constraints.

The control effort measure given by Equation (2.6) can also be expressed as:

$$J_u = \int_0^{\omega^*} \omega^2 \, |H(j\omega)|^2 S_{XX}(\omega) \, d\omega \qquad (2.7)$$

where $S_{XX}(\omega)$ is the power spectral density of the input to the speedchanger motor

$H(j\omega)$ is the transfer function for the speedchanger motor

since $H(j\omega) = K/j\omega$, it is seen that

$$J_u = K^2 \int_0^{\omega^*} S_{XX}(\omega) d\omega \qquad (2.8)$$

That is, the control effort measure is also proportional to the power in the input (within the frequency range $[0,\omega^*]$). Through Parceval's theorem, it follows that the control effort measure is also related to the rms value of the speedchanger input. To carry this time-domain interpretation farther, consider a string of raise/lower pulses that form the input to the speedchanger. Let the pulse areas be α_0, α_1, α_2, ...; the pulses occur at intervals of T seconds, where T is the WEPCO control cycle (presently 4 sec.). The Fourier transform of this pulse sequence is:

$$|F(j\omega)|^2 = \int_{-\infty}^{\infty} f(t) e^{-j\omega t} dt = (\alpha_0 + \alpha_1 e^{-j\omega t} + \alpha_2 e^{-j\omega t} + \ldots) \frac{\sin(\omega\tau/2)}{(\omega\tau/2)} \qquad (2.9)$$

In the frequency range $[o,\omega^*]$ (which is approximately the range [0,0.79] rad/sec) $\sin(\omega\tau/2)/(\omega\tau/2) \cong 1$. If the sequence of complex exponentials in Equation (2.9) is truncated at some value N, then it can be shown that:

$$\frac{1}{N}\left|F(j\omega)\right|^2 = S_{XX}(\omega) \cong \frac{1}{N}\sum_{k=0}^{N}\alpha_k^2 + 2\cos\omega T\sum_{k=0}^{N-1}\alpha_k\alpha_{k+1} \qquad (2.10)$$

$$+ 2\cos 2\omega T\sum_{k=0}^{N-2}\alpha_k\alpha_{k+2} + \text{----}$$

$$+ 2\cos N\omega T\,(\alpha_0\alpha_N)$$

Thus Equation (2.9) has the form:

$$\left|F(j\omega)\right|^2 = A_0 + 2A_1\cos\omega T + 2A_2\cos 2\omega T \qquad (2.11)$$

$$+ \text{---} + 2A_k\cos k\omega T + \text{--} + 2A_N\cos N\omega T$$

Therefore:

$$\frac{1}{N}\int_0^{\omega^*}\left|F(j\omega)\right|^2 d\omega = \frac{1}{N}\int_o^{\pi/T}\left|F(j\omega)\right|^2 d\omega = \frac{1}{N}\frac{\pi}{T}A_0 \qquad (2.12)$$

From Equations (2.8) and (2.12) it is seen that the control effort measure is proportional to A_0/N. And, since A_0 is the sum of the squares of the raise/lower pulse areas, it follows that:

$$J \propto \frac{1}{N}\sum_{k=0}^{N}\alpha_k^2 \qquad (2.13)$$

Accordingly, we have selected the control effort measure defined in relation (2.13) for use in evaluating different control logics. It is the mean squared-amplitude (area) of the unit raise/lower pulses. The averaging period, NT, should be long enough to capture the frequency

components of the control variation; an averaging period of at least 30 minutes, and possibly as long as 1 hour is planned.

2.3.4 A Note On A Generalization of the Control Effort Measure

The basic unit variable or quantity used to define a measure of control effort is the output of the governor speedchanger motor, which will be referred to as the unit desired generation (UDG). A conceptually useful and practical vehicle for defining a measure of control effort is the power spectral density of unit desired generation, $S_{uu}(\omega)$. If control effort "costs" can be determined as a function of frequency, either theoretically or experimentally, then a weighting function $W(\omega)$ can be constructed and an associated measure of control effort is the integral

$$J_u = \int_0^{\omega_2} W(\omega)\ S_{uu}(\omega)\ d\omega \qquad (2.14)$$

where ω_2 is one half the Nyquist frequency associated with the AGC control cycle.

We remark that, given $W(\omega)$, (2.14) can be very efficiently evaluated (in real-time if desired) using fast Fourier Transform techniques. The problem of course is determining what the costs of control are, i.e., determining the weighting function $W(\omega)$. Presumably if a unit is regulated about a base point with a period in the order of a few minutes (so that thermal equilibrium is not maintained) then some losses are incurred, for example. Although this is an active research area [2-6], we are not aware of any significant, currently available data or analytical results which indicate what those costs are.

2.3.5 Summary

In summary, the control effort measure that has been selected is the average of the squared areas of the unit raise/lower pulses as given by relation (2.13). The AGC system operation would be observed over time periods of about 30-60 minutes in duration, and the control effort measure would be computed from this observation record. Total system AGC control effort is simply the sum of the unit control efforts.

2.4 ECONOMICS OR PRODUCTION COST

2.4.1 Approaches to Measuring Production Costs

Direct Analysis of Production Costs -- Difficulties

The obvious measure of economic performance is the total production cost of the electric energy generated. This production cost consists of two primary components: the total fuel costs and the total maintenance costs.

The simple-minded means of measuring the production cost associated with the operation of a particular AGC system is to rely upon actual fuel-usage and maintenance records. This, however, would not be a satisfactory approach due to the many departures of the various elements of each generating unit from "average" conditions. There are, for example, a variety of factors affecting fuel consumption of each unit: deposits in the heat exchangers, slag deposits in boilers, evaporator condition, wet coal (or BTU content of fuel), pulverizer condition, and water inlet temperature. In short, direct performance measurement of economics is apt to be clouded by variations of different factors from average conditions.

Thus, to develop an economic comparison of one AGC system with another, it is more appropriate to use average conditions as a reference. In particular, average performance characteristics -- such as embodied in heat rate curves -- can be used for developing comparative production costs. This is discussed in succeeding sections.

Estimating Fuel Costs From Average Unit Heat Rate Data

Unit heat rate data together with average fuel cost can be used to estimate fuel costs. The relationship is:

$$\begin{matrix}\text{Fuel Cost Rate} \\ (\$/\text{HR})\end{matrix} = F_i C_i H_i(P_i) \qquad (2.15)$$

where:

F_i = (Seasonal) performance factor for the i^{th} unit; used to adjust the incremental heat curve.

C_i = Fuel cost for the i^{th} unit ($/MBTU)

$H_i(\ )$ = Thermal energy input rate (MBTU/HR)

P_i = Net generation (MW)

Equation (2.15) is a valid approximation to the fuel cost under the condition of thermal equilibrium for the unit boiler system. That is, the average heat rate data are developed from tests on the unit in which the unit is placed at one load point at a time and held there for about 1-1/2 hours to insure stable readings [2-7]. This means that the heat rate data are not valid for evaluating the costs of dynamical variations in unit output that do not approximate thermal equilibrium. Accordingly, it would be inappropriate to insert the actual unit output, $P_i(t)$, into Equation (2.15) to estimate production costs. Only the costs associated with the low frequency components of $P_i(t)$ are validly approximated by Equation (2.15). Apparently thermal equilibrium conditions, for which the average heat rate data are valid, pertain to low frequency components of $P_i(t)$ that have periods that are many minutes in duration -- perhaps 20 minutes or longer.

Including Maintenance Costs and Transmission Losses

Besides the fuel costs, the other major cost categories to be included in the production cost evaluations are maintenance costs and transmission losses. Some utilities (including WEPCO) perform economic dispatch using unit incremental cost curves that incorporate both heat rate data and maintenance data. Letting $M_i(P_i)$ be the maintenance cost rate ($/HR) associated with generation level P_i, Equation (2.15) can be augmented to include the maintenance costs:

$$\text{Total Production Cost Rate (\$/HR)} = F_i C_i H_i(P_i) + M_i(P_i) \qquad (2.16)$$

Additionally, a transmission loss penalty factor can be applied to the generation. Letting this penalty factor be designated $T_i(P_i)$, we have:

$$\text{Total Production Cost Rate, Including Losses (\$/HR)} = T_i(P_i)\ [F_i C_i H_i(P_i) + M_i(P_i)] \qquad (2.17)$$

Valve Point Representation and Plant Test Data Needed

The heat rate curves, $H_i(P_i)$ discussed above will -- in the evaluation of production costs (as well as in the new dynamic economic dispatch) -- differ from the conventional smooth-curve representation. Instead, valve-point unit inefficiences will be represented. Two types of data collection efforts are expected to supply sufficient information to represent the valve-point inefficiencies. These two data collection efforts are: (1) detailed heat runs on one or more units; and (2) unit efficiency monitoring on all units during normal on-line operation.

The heat runs on one or two units would serve to identify, via controlled experiment how the valve operation is related to plant variables (pressures, temperatures, etc.) that can be measured. The heat runs and the measurements recorded during the runs would be analyzed to determine an approximate representation of unit heat rates as a function of the measurable plant variables. For instance, one relation that has already been suggested [2-8] is that the unit heat rate is mainly a function of the MW output of the unit and throttle pressure.

It would be too costly, in time and effort, to conduct such heat runs on all WEPCO units within the scope of this project. Accordingly, the knowledge gained on unit valve-point operation on one or two WEPCO units needs to be extrapolated to other units. Unit efficiency monitoring on all units, during normal on-line operation can aid in this extrapolation of the limited heat run experience. Unit efficiency data at different MW outputs can be used to infer valve point regions of all units, and the "shape" of the heat rate curve in the vicinity of valve points.

The net result of the heat runs and the efficiency calculations will be the representation of unit heat rate "curves", $H_i(P_i)$ -- including valve-point effects. It is expected that these new heat rate curves will have sharp rates of increase in heat rate at valve-openings. This contrasts with the smooth heat rate curves currently used in WEPCO economic dispatch, as shown below in Figure 2.2 (note that Figure 2.2 depicts heat rates, rather than incremental heat rates).

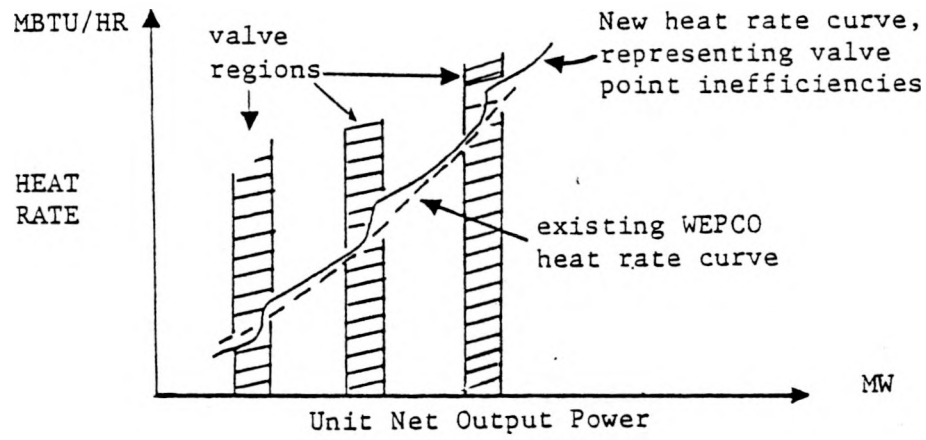

FIGURE 2.2 SIMPLIFIED DEPICTION OF UNIT HEAT RATE CURVES

Low-Pass Filtering of Unit Outputs

As briefly discussed above, the heat rate curves, $H_i(P_i)$, are valid for unit outputs $P_i(t)$ that are slowly varying. Since Equations (2.15) - (2.17) are valid only for low frequency components of $P_i(t)$, it is proposed that production costs be evaluated by filtering recorded values of unit output, $P_i(t)$, and then using Equation (2.17) to estimate production costs using only the low frequency "trend" components of $P_i(t)$.

2.4.2 Economic Performance Measurement, Using Simulations As An Aid

A procedure, aided by computer simulation, is outlined in this Section that enables a comparison of production costs arising from (1) the operation of the existing WEPCO AGC system, and (2) the operation of the new AGC logic. A fundamental problem, that simulation helps resolve, is that since the old and new AGC logic will be operating on different days -- no direct comparison of the two logics operating on identical loads is possible. However, simulated operation of the two logics for identical loads is possible, and this fact is used in structuring an evaluation procedure that combines both actual and simulated production cost data.

Difficulties in Measuring Production Cost Differences from Actual Unit Outputs

Total production costs for a day (or a sub-period of a day) can be determined via (integrating) Equation (2.17) over the time period of interest (assuming that filtered $P_i(t)$ values are used). Thus if, say, tests are scheduled in which two weeks of the existing WEPCO AGC operation are observed, followed by two weeks' operation under the new AGC software -- then a systematic means exists (Equation (2.17) to calculate the production costs ($/MWH) during the operation of each AGC system. Unfortunately, the calculations of the production costs of the two different AGC systems are based upon different loads and possible differences in unit committment (or at least slight differences in the times at which given units are on-line or are being regulated). Of course, the experiment design for the

production cost comparisons should have roughly comparable loads and unit committments in the data sets for the two AGC system observations; nevertheless, replication of the load and unit committment conditions will not be possible in actual operation.

One can view the production cost comparisons as the test of the effects of two AGC systems upon specific load/unit committment situations or scenarios drawn from a population of all scenarios. The various random factors affecting load and unit committment cause the scenarios in the population to have a probabilistic distribution. This probability distribution, in turn induces probability distributions for the production costs incurred by each of the two AGC schemes.

The distributions of production costs incurred in the operations of the two AGC schemes might appear as depicted in Figure 2.3.

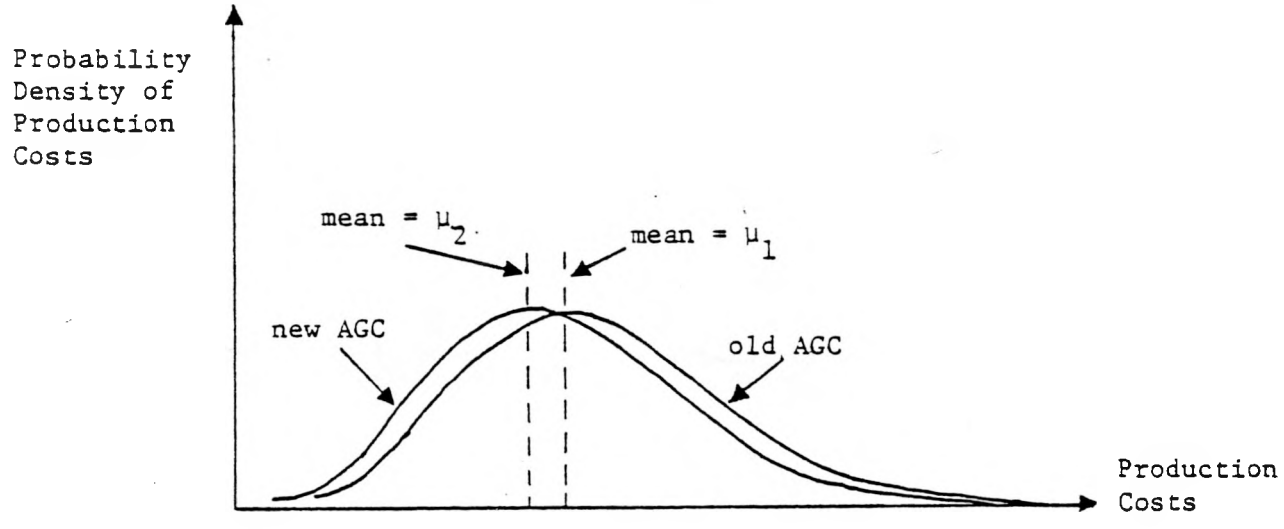

FIGURE 2.3 HYPOTHETICAL DISTRIBUTION OF PRODUCTION COSTS

Without having the ability to fix the load to the same value for both AGC schemes, the observer of test results has no way of pairing test results to "remove" the effect of the extraneous factor -- the load. Accordingly, the best that one can do is to consider each of the two sets of production costs to be distributed in some manner, and then to perform statistical tests on how the two distributions differ. One such test would be on the differences between the means of the two production costs differences (i.e., the difference between the μ_2 and μ_1 values depicted in Figure 2).

To get an idea of what one would be able to conclude about the differences in the mean production costs of the two AGC schemes from two weeks' operation on the WEPCO system with each scheme, a simple analysis was conducted. The incremental cost curves of the WEPCO units were reviewed to get a rough idea of how production costs would vary when load varied. The mean production cost would seem to be about $20/MWH and its standard deviation about $5/MWH. Assume that the production costs for the two AGC schemes are normally distributed ($\sigma_1 = \sigma_2 = \$5/MWH$) but have different means (i.e., $\mu_2 \neq \mu_1$). Assume that ten days of tests ($N_1 = N_2 = 10$) are performed on each AGC scheme. In this case, the statistic (see Ref [2-9], page 271):

$$d = \frac{\mu_1 - \mu_2}{\sigma \sqrt{\frac{1}{N_1} + \frac{1}{N_2}}} = \frac{\mu_1 - \mu_2}{\sigma \sqrt{2/N}} \qquad (2.18)$$

can be used to test the hypothesis that the mean production costs differ by a specified amount. From Table A-12b of [2-9], in order for a sample size N=10 to be sufficient to detect, with 90% probability, a significant difference in means at the 95% confidence level -- there would have to be an observed difference of at least about 9% in the means. That is:

$$\mu_1 - \mu_2 \geq (P/100)\left(\frac{\mu_1 + \mu_2}{2}\right) \qquad (2.19)$$

with $P \tilde{=} 9$. Since the true difference in mean production costs is likely to be very small -- on the order of 1% or less, much less than 9% -- the conclusion is that a sample size of N=10 would be inadequate. In fact, (again using (2.18) and Table 12-b of [2-9]) in order to be able to detect, with 90% probability, a 1% difference in mean production costs at the 95% confidence level -- one would need over 700 samples of production costs with each AGC scheme!

Thus, it is seen that under plausible assumptions ($\sigma_1 = \sigma_2 = \sigma$ = \$5/MWH, and $(\mu_1 + \mu_2)/2$ = \$20/MWH) -- an inordinately large sample size would be needed of production costs for each AGC scheme!

Augmenting Actual Operating Data With Simulation Results

As the discussion above has revealed, an evaluation of the production cost differences of the two AGC schemes based solely on actual system operation will require very large samples. The key reason for this is that since both AGC schemes cannot be tested on identical load data, the load variability remains a significant extraneous factor that masks differences in the AGC schemes.

Simulation has an advantage over tests of actual operation. Namely, it is possible to fix the load to be the same for a pair of simulations -- one in which the old AGC scheme is in effect, and one in which the new AGC scheme is in effect. Under these conditions, the load is no longer an extraneous factor. One can then pair the production costs -- so that if N load scenarios are simulated and X_1^n and X_2^n are the simulated production costs for the n^{th} scenario (n = 1, 2, ..., N) -- one obtains the N pairs of observations:

$$(X_1^1, X_2^1), (X_1^2, X_2^2), (X_1^3, X_2^3) \ldots (X_1^N, X_2^N)$$

By pairing observations and removing the extraneous factor of load, one gains information for comparison of the differences:

$$X_1^n - X_2^n$$

The AGC simulation model developed in Task 1 can be used to test the old and new AGC schemes.

With the simulation, actual production cost data can be augmented with simulated production costs. For each day of actual tests of the AGC schemes, one obtains either the data triple X_1, X_2, Y_1 or X_1, X_2, Y_2. Here the indices have the meaning: 1 = old AGC logic, 2 = new AGC logic. The X's are simulated production costs, and the Y's are actual production costs (i.e., calculated from actual unit outputs). The X_1, Y_1 values obtained on days in which the old AGC logic is in operation on the WEPCO system can be regressed to obtain Y_1 as a function of X_1. That is, the actual production costs, Y_1, can be functionally related to the simulated production costs, X_1, obtained under the same load conditions. Similarly, X_2 and Y_2 can be functionally related through a regression relation. These regressions allow estimates of actual production costs, $\hat{Y}_1$ and $\hat{Y}_2$, to be made, where:

$\hat{Y}_1$ = Estimated (from regression of Y_1 on X_1 and the computed X_1 value) actual production cost for a day in which actual Y_2 data was obtained.

$\hat{Y}_2$ = Estimated (from regression of Y_2 on X_2 and the computed X_2 value) for a day in which actual Y_1 data was obtained.

The differences in actual production costs can then be estimated from the sample values of the sets of regression differences, $\hat{Y}_1 - \hat{Y}_2$, obtained for the same load conditions.

2.4.3 Recommended Procedure for Evaluating Production Cost Performance

An analysis has been conducted (see Table 3 in [2-10]) that indicates that a sample size (No. of load period over which actual WEPCO system operation is to be observed) somewhere in the range of N=40 to N=80 may be needed in order to detect 1% differences in the production costs (with competing AGC logics) at a 90% confidence level. The N load period can be accommodated within say, a two week (10 observation days) by subdividing each day into a number of load periods, each of several hours duration.

Once an initial testing program (selected days and N load periods from these days) has been devised, the flow chart that is presented below gives the recommended steps in the evaluation of production costs.

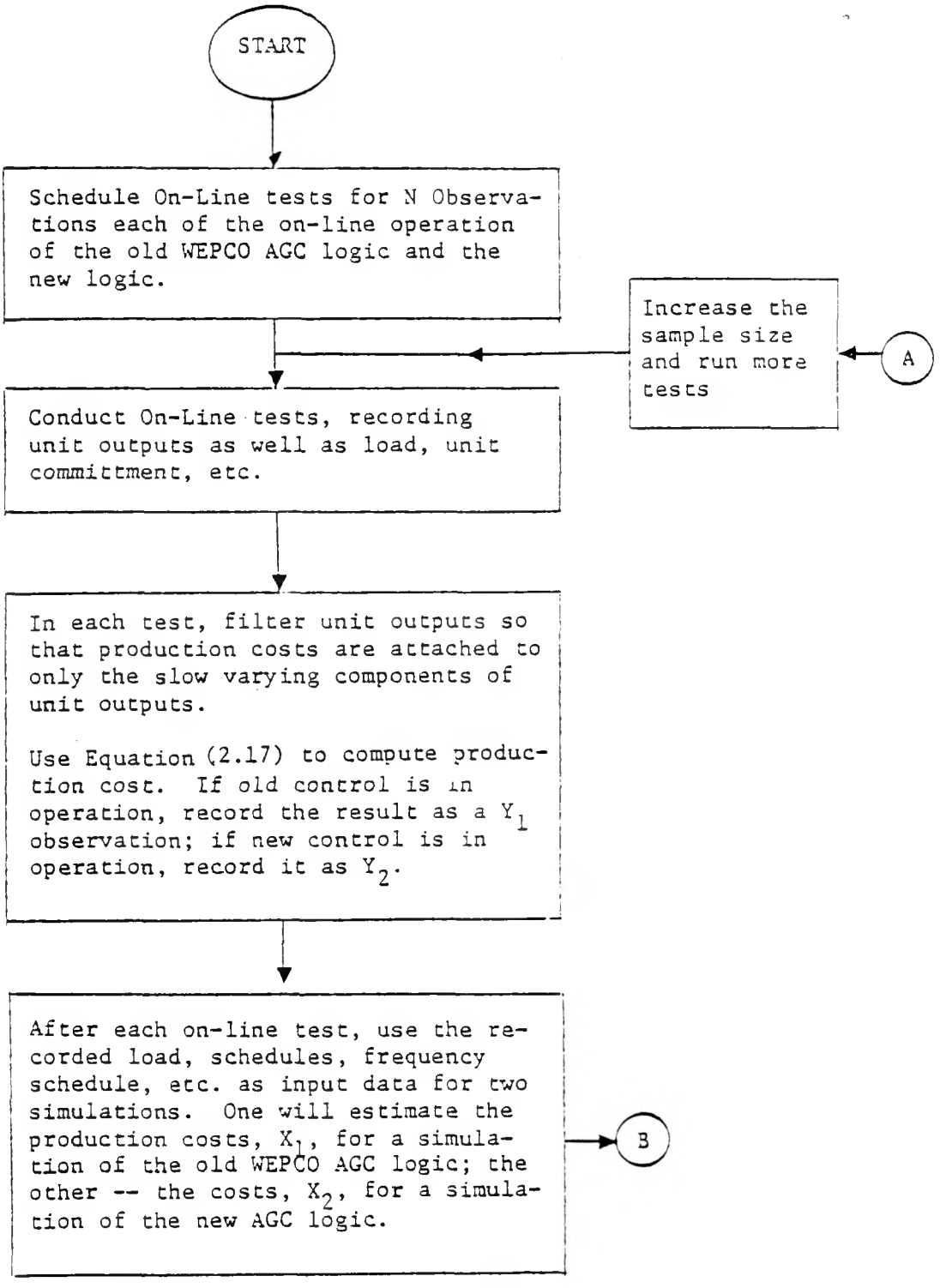
START
Schedule On-Line tests for N Observations each of the on-line operation of the old WEPCO AGC logic and the new logic.
Increase the sample size and run more tests
A
Conduct On-Line tests, recording unit outputs as well as load, unit committment, etc.
In each test, filter unit outputs so that production costs are attached to only the slow varying components of unit outputs.
Use Equation (2.17) to compute production cost. If old control is in operation, record the result as a Y_1 observation; if new control is in operation, record it as Y_2.
After each on-line test, use the recorded load, schedules, frequency schedule, etc. as input data for two simulations. One will estimate the production costs, X_1, for a simulation of the old WEPCO AGC logic; the other -- the costs, X_2, for a simulation of the new AGC logic.
B

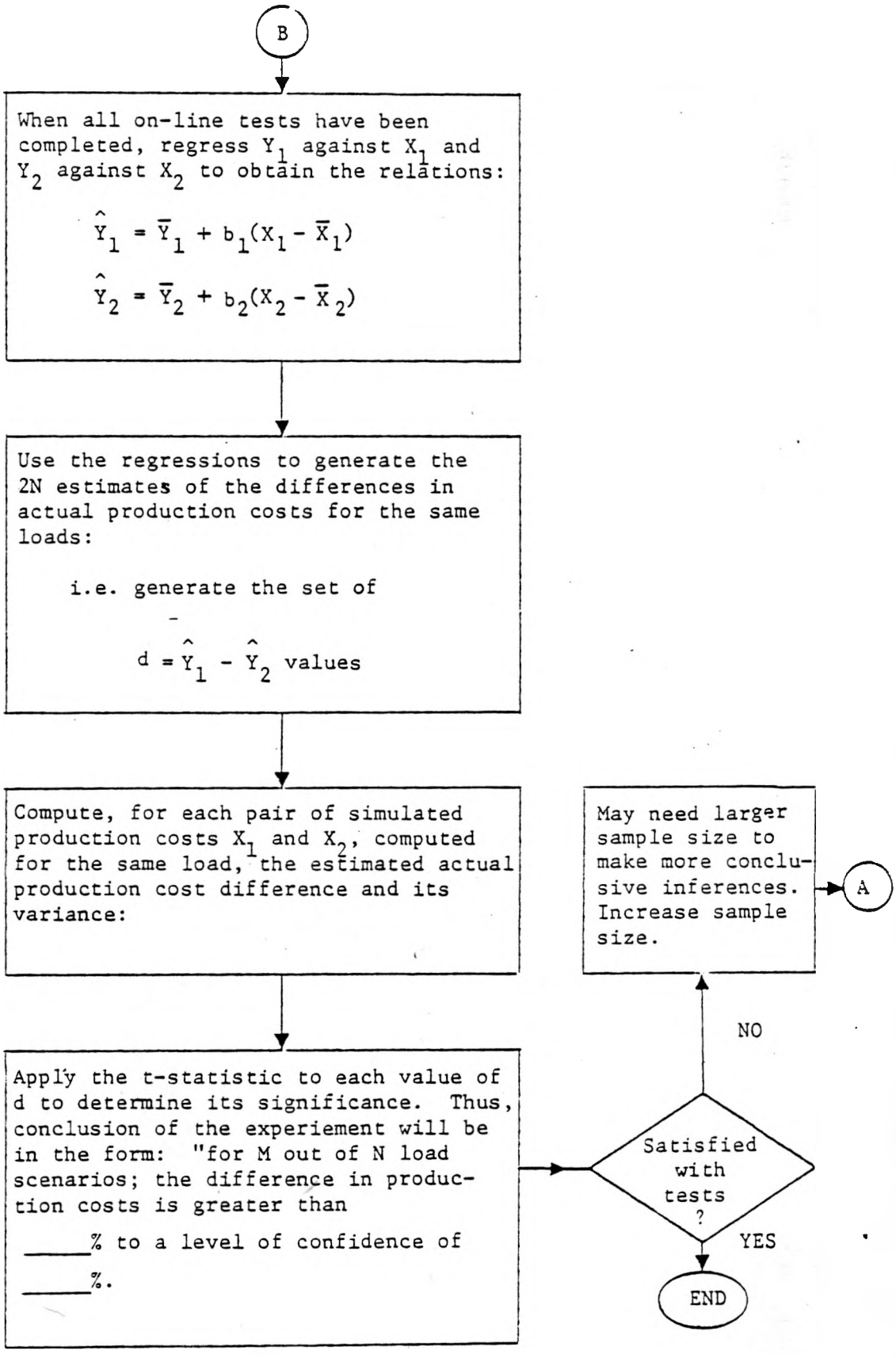
B
When all on-line tests have been completed, regress Y_1 against X_1 and Y_2 against X_2 to obtain the relations:
$\hat{Y}_1 = \bar{Y}_1 + b_1(X_1 - \bar{X}_1)$
$\hat{Y}_2 = \bar{Y}_2 + b_2(X_2 - \bar{X}_2)$
Use the regressions to generate the 2N estimates of the differences in actual production costs for the same loads:
i.e. generate the set of
$d = \hat{Y}_1 - \hat{Y}_2$ values
Compute, for each pair of simulated production costs X_1 and X_2, computed for the same load, the estimated actual production cost difference and its variance:
Apply the t-statistic to each value of d to determine its significance. Thus, conclusion of the experiement will be in the form: "for M out of N load scenarios; the difference in production costs is greater than
_____% to a level of confidence of
_____%.
Satisfied with tests ?
NO
YES
May need larger sample size to make more conclusive inferences. Increase sample size.
A
END

References - Section 2

2-1 D. Ross, "Quality of Control Performance Measures", SCI Project 5212 Memorandum, Oct. 3, 1978.

2-2 D. Ross, "Analytical Proof That Correlating Tie Error With Frequency Deviation is Not Purposeful", Project 5212 Memorandum, Oct. 20, 1978.

2-3 R. Podmore, "Quality of Control Performance Measures", Project 5212 Memorandum, Oct. 29, 1977.

2-4 North American Power Systems Interconnection Committee (NAPSIC), Operating Guide No. 2, "Frequency Bias Setting", approved July 21, 1964.

2-5 H. Kwatny, et.al., "An Optimal Tracking Approach to Load-Frequency Control", IEEE Transactions on Power Apparatus and Systems, Vol PAS-94, No. 5, Sept/Oct., 1975.

2-6 Project RP 1048-2, "Determination of Three Sample Dynamic Models", research project being conducted by Power Technologies Inc. under contract to the Electric Power Research Institute (1978-80).

2-7 Roy W. Thomas, "Determination of the Incremental Heat Rate Characteristic by Performance Testing", paper presented at AIEE Fall General Meeting, Chicago, October, 1957.

2-8 R. Podmore, "Telephone Conversation with R. Bischke of WEPCO", SCI Project 5212 Memo, October 20, 1977.

2-9 W.J. Dixon, F.J. Massey, Jr., Introduction to Statistical Analysis, McGraw Hill, New York, 1969.

2-10 D. Ross, "Economic Performance Measures", SCI Project 5212 Memo, October 28, 1977, (Revised, November 3, 1977).

3. LOAD PREDICTION ALGORITHM

3.1 INTRODUCTION

Accurate information about future system disturbances or demands can, and should, be used to improve the quality of control. With such information the deleterious effects of system delays or large time constants effectively can be reduced. Moreover, any tracking functions that a system must fulfill will be greatly enhanced by a controller provided with advanced knowledge. Thus it is advantageous to exploit any information available which is useful in describing the future environment.

Automatic Generation Control (AGC) is a prime example of a control problem where future information is vital to successful control. Obviously, a power generating system must fulfill a tracking function; and the inertia associated with the various generating machinery leads to large time constants. Anticipatory control is essential, and forecasts of future loads must be computed. Construction of these forecasts, in general, is a challenging problem since electrical load is affected by many factors including weather -- an exogenous disturbance which man still has only marginal success in predicting. There is, however, a wealth of statistical information available in the form of system load time series. Whether compiled on a minute-by-minute or hourly basis, sufficiently long sequences of data are available which permit a thorough time series analysis treatment. Thus, even with the uncertainty present in weather induced load changes, it is possible to extract enough information to provide an accurate load forecast which greatly enhances the performance of an AGC system.

The remainder of this chapter describes the specification, estimation, and implementation of two short-term load predictors: one using an hourly time scale, and another using a 5-minute period. Both will provide inputs to the dynamic economic dispatch, which will be discussed later in Chapter 4. A diagram of the relationship between forecasting models can be found in Figure 3.1. Further, the evolution of an appropriate hourly predictor model is delineated herein in order to give the reader some appreciation for the mixture of science and art necessary to identify a time series model. The methodology employed in the statistical analyses is a derivation of that popularized by Box and Jenkins [3-1]. The estimation algorithm employed to obtain an optimal set of predictor coefficients is maximum likelihood.

3.2 MODEL SPECIFICATIONS AND EMPIRICAL DETERMINATION

3.2.1 General Model for Time Behavior of Load

AGC requires an accurate predictor of future electrical load, both on an hourly basis and on a 5-minute sampled basis. The predictor follows from the structure of the model used to represent the actual load evolution over time, and, in general, is given by a nonlinear function.

$$y_t = f(\, y^t,\, \chi^t,\, t, \varepsilon_t) \tag{3.1}$$

where

- y_t = actual system load in megawatts (expressed as integrated hourly load in the case of the hourly predictor; and as instantaneous 5-minute load in the case of the 5-minute predictor).
- y^t = $\{\chi_\tau; -\infty < \tau \leq t-1\}$, i.e., all past observed exogenous variables
- t = time index
- ε_t = additive random disturbances representing all unobserved effects on the system load

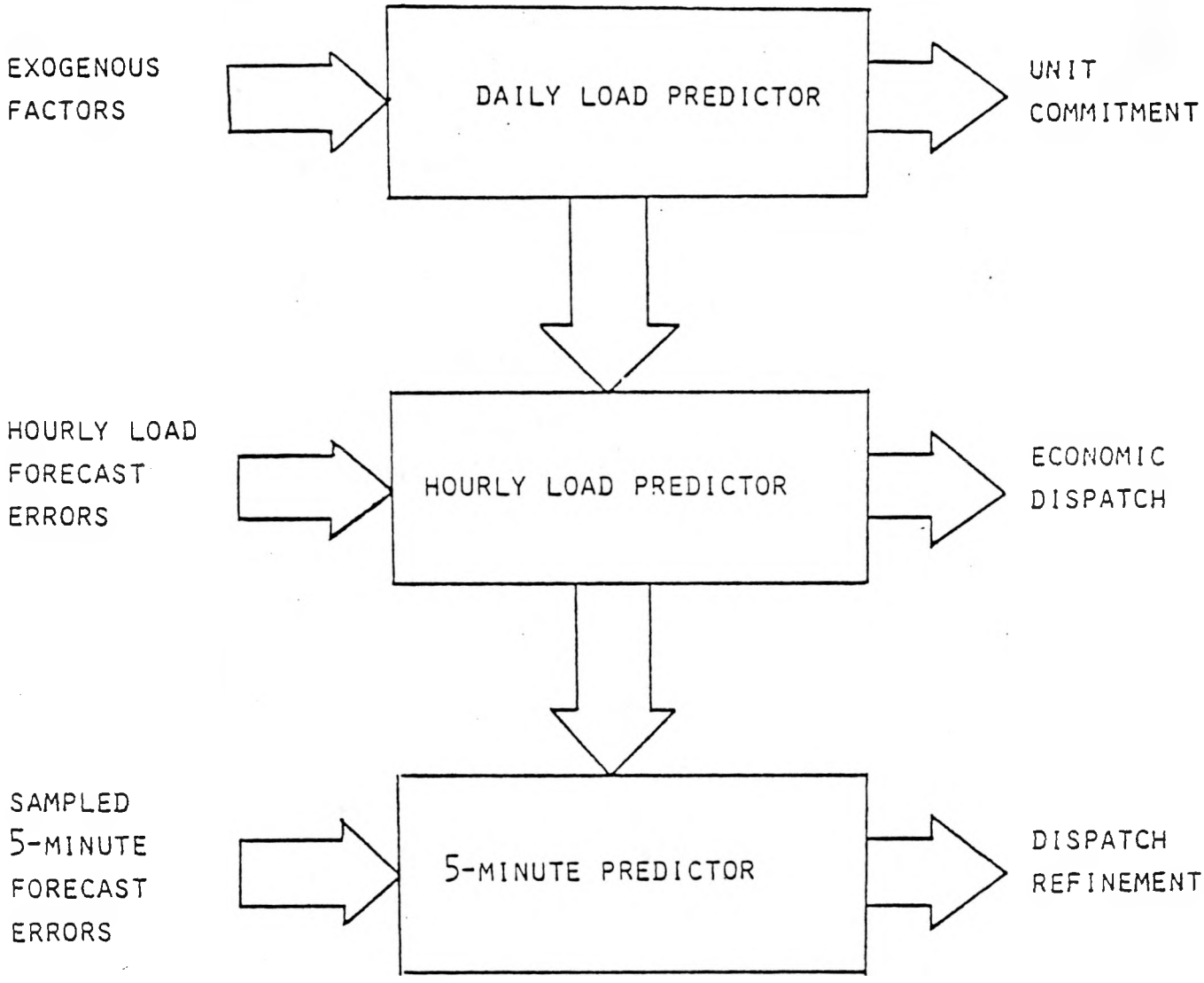

FIGURE 3.1 HIERARCHICAL STRUCTURE

Attempting to develop a precise representation for $f(\cdot)$ can be very costly. and although a very accurate predictor would result, it is an open question whether the improvement in accuracy over a more simple representation would justify the extra modeling effort. It may be possible to obtain sufficient accuracy with a quite simple representation. Therefore, it is advisable to begin with a simplified form for $f(\cdot)$ and elaborate upon it only as required in order to meet performance requirements. Such an approach leads one to the trivial representation:

$$y_t = \chi_t + e_t \tag{3.2}$$

where χ_t is now a scalar variable representing the value of the load at t as predicted by a regression of the load on all observed exogenous factors. The new additive random (unobserved) error, e_t, now represents both the truly random disturbances and the modeling errors inherent in replacing $f(\cdot)$ with χ_t. For the purposes of AGC and the chosen test site (WEPCO) of this project, χ_t is taken as the WEPCO hourly integrated load forecast and is computed as an aggregate of all causal effects, including weather.

The optimal predictor for y_t can be obtained by formally taking conditional expectations across Equation (3.2).

$$y_{t+k|t-1} = \chi_{t+k} + e_{t+k|t-1} \tag{3.3}$$

where $y_{t+k|t-1}$ denotes $\{y_{t+k}|I^{t-1}\}$ and I^{t-1} symbolizes all the information available at time t-1. Likewise for $e_{t+k|t-1}$. The conditional expectation on χ_{t+k} reduces to χ_{t+k} itself since it is assumed that this value is always known into the future. From (2) it is seen that the structure imposed by (1) reduces the development of the optimal predictor to the development of an optimal predictor for e_t.

Similar arguments may be applied to the 5-minute predictor. The only difference being in the time scale and forecast horizon; i.e., replace t by τ to indicate time in units of 5-minutes instead of hours, and k=1 since we are only interested in one-step-ahead forecasts. The resulting predictor is then given by:

$$y'_{\tau+1|\tau} = \chi'_{\tau+1} + e'_{\tau+1|\tau} \qquad (3.4)$$

where

y'_τ = actual instantaneous system load at time τ

χ'_τ = some forecast of actual instantaneous load at time τ (derived from χ_t)

The primes are employed merely to differentiate the 5-minute sampled instantaneous load variables from the hourly integrated load variables.

All the known structure, representing all a priori information concerning observed cause-and-effect relationships is captured in the χ_t and χ'_τ variables. All the unknown structure, representing all the additional information which may be extracted from empirical data, is contained in the e_t and e'_τ variables. If systematic (serial correlation, for example) variation exists in these error terms then it can be employed to devise additional structure which will yield a more accurate forecast. The examination of e_t is a problem in statistical time series analysis and is discussed below in Section 3.2. A discussion of modeling e'_τ can be found in Section 3.3.

3.2.2 Empirical Structure Determination

The analysis of the error term in equation (3.2) and the estimation of a model for prediction of the error terms consitutes a problem in statistical time series analysis. The details of the methodology employed here are given in [3-1] and will not be presented. Only a summary of the relevant steps comprising the methodology is given to facilitate and understanding of the rationale behind the predictors selected for implementation in the AGC system.

In short, the Box-Jenkins methodology is an iterative procedure by which a model is constructed. The process proceeds from the most simple structure, with the least number of parameters, to as complex a structure as is required to obtain an "adequate" model -- "adequate" in the sense of yielding white residuals. This process of building increasingly complex models embodies their own philosophy of parsimony: "include only as many parameters as you really need." A schematic of the procedure is given in Figure 3.2. The first step is an identification of structure and employs sample autocorrelation patterns. After a structure has been chosen the next step involves an estimation of the coefficients inherent in the structure description. Next the optimal parameter estimates are inserted into the model to generate its estimated residuals. These are then subjected to diagnostic procedures to determine if they are indeed "white". If not, their sample correlogram is used to hypothesize a new structure and the cycle is begun anew. If the model satisfies all diagnostic tests it may then be implemented for on line testing. The benefits of such a methodology are many, but primarily one will always be assured of a model which has the fewest possible parameters while still explaining all the systematic variation in the random errors.

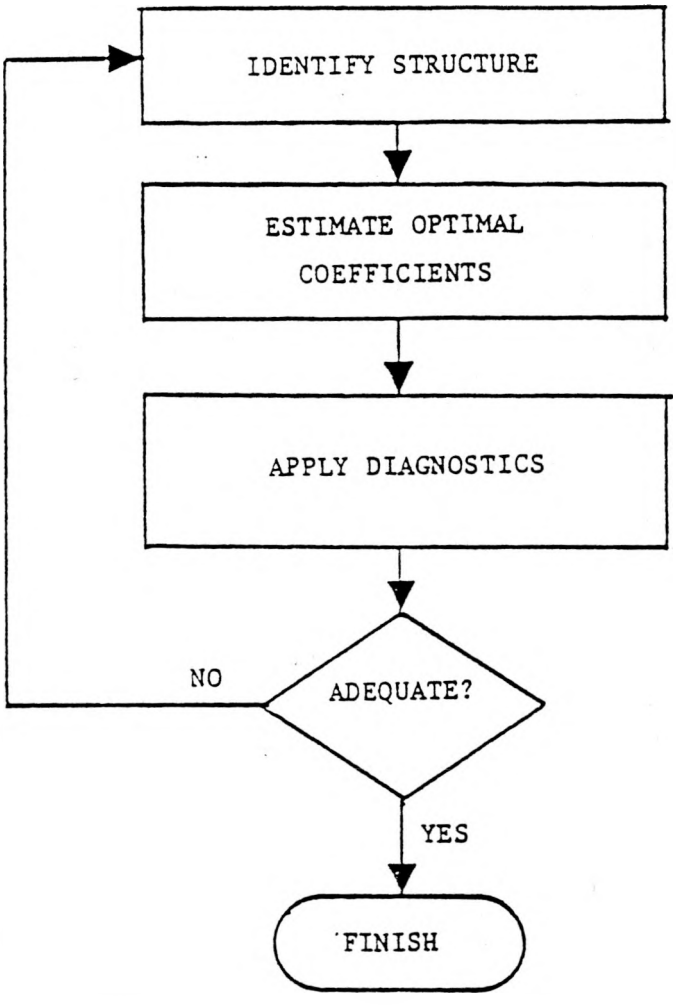

FIGURE 3.2 THE BOX-JENKINS METHODOLOGY

The particular form for e_t and e_t' assumed by the Box-Jenkins methodology is the rational form:

$$e_t = \frac{c(L)}{d(L)} \eta_t \tag{3.5}$$

where

$$c(L) = 1 + c_1 L + .. + d_q L^q \tag{3.6}$$

$$d(L) = 1 + d_1 L + .. + d_p L^p \tag{3.7}$$

where L is a shift (or lag) operator, i.e., $L^k \chi_t = \chi_{t-k}$, and η_t is a white noise process with the same normal distribution for every value of t. Thus by structure identification we mean specification of the integers p and q. In the econometric terminology (3.5) represents an autoregressive/moving-average ARMA(p,q) model. By examining the auto-correlation function for e_t it is possible to gain information regarding the values of p and q. This is the first step in the procedure.

Estimation of a set of coefficients $\{c_i, d_i\}$ is effected with the aid of maximum likelihood estimation algorithm described in [3-2].

3.3 THE HOURLY LOAD PREDICTOR: EVOLUTION OF THE TIME SERIES MODEL

3.3.1 Specification I of the Hourly Predictor

In April of 1978, generation of the e_t series was carried out by simply differencing actual observed system hourly integrated load and the adjusted (by dispatcher) WEPCO predicted hourly integrated load. Two series were examined at that time, five consecutive days in January 1978 (1/10-1/14) and three consecutive days in March (3/7-3/9).*

---

* These data sets were supplied to SCI by Robert Bischke of WEPCO, from WEPCO data files of past system operation.

The estimated autocorrelation functions for the January series is presented in Figure 3.3. It seems clear that a periodic error existed with a 24 hour component, and that there was at least a first order serial correlation. Two options were open: First, the e_t series could be differenced according to

$$\tilde{e}_t = e_t - e_{t-24}$$

and a new structure search initiated on $\tilde{e}_t$. Second, we could fit a first order ARMA(1,B) model to e_t and apply the diagnostic tests. Both approaches were used and both indicated that the 24-hour period must be removed by 24^{th} order differencing. The autocorrelation for $\tilde{e}_t$ is presented in Figure 3.4. Fitting a first order autoregressive model to $e_t - e_{t-24}$ appeared highly advisable. Such a fit was carried out, producing a model with the residual autocorrelation function of Figure 3.5. This model yielded a residual series with non-zero autocorrelations that were well within the bounds of acceptable sample error. Thus, the model was deemed adequate.

Almost identical results were obtained for the hourly errors compiled with the March 1978 data. Both estimates were performed with "mean" subtraction represented by the letter m, and are presented here for comparison:

$$e_t - m = \underset{(\pm.059)}{\frac{1}{1 - 0.762L}} \eta_t \qquad (3.8)$$

with $\eta_t \sim N(0,702.6)$ and m = -6.74 for January 10-14, 1978; and

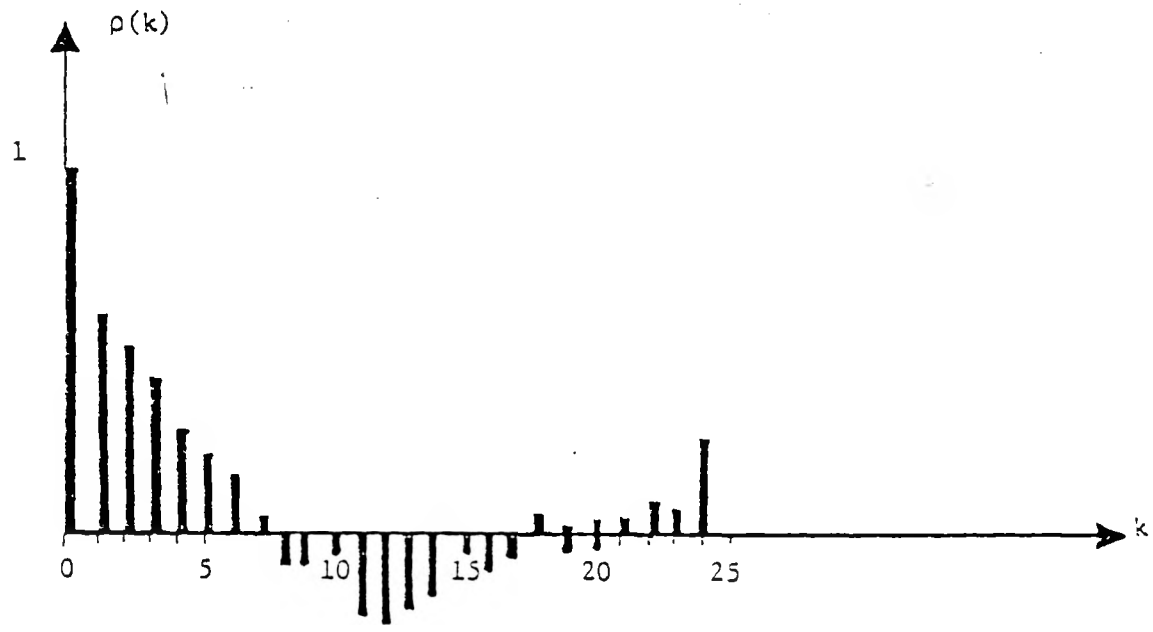

FIGURE 3.3 SAMPLE AUTOCORRELATION FUNCTION FOR JANUARY 1978 DATA

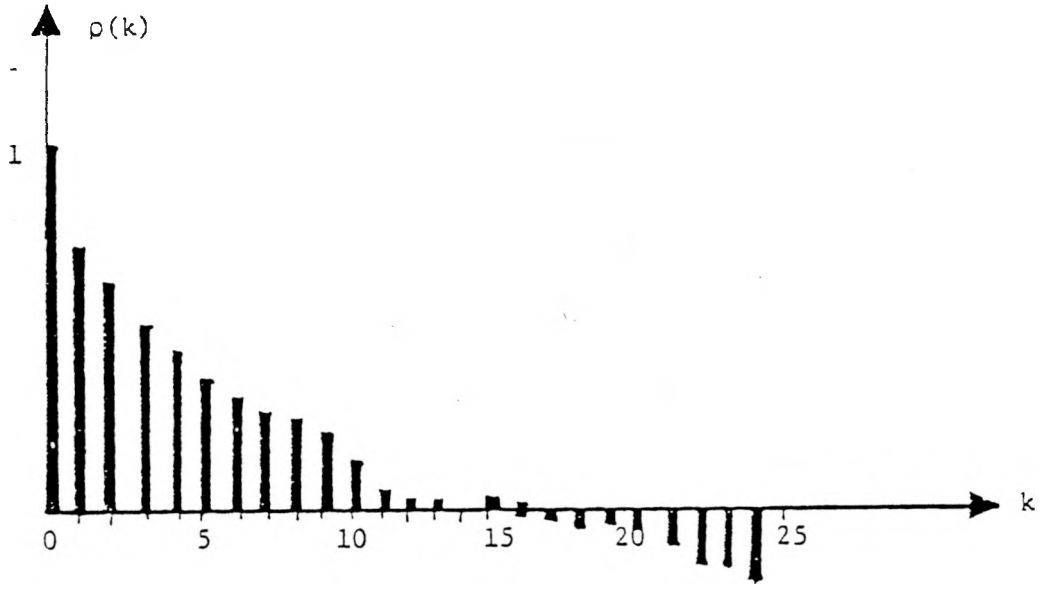

FIGURE 3.4 SAMPLE AUTOCORRELATION FUNCTION FOR $e_t - e_{t-24}$

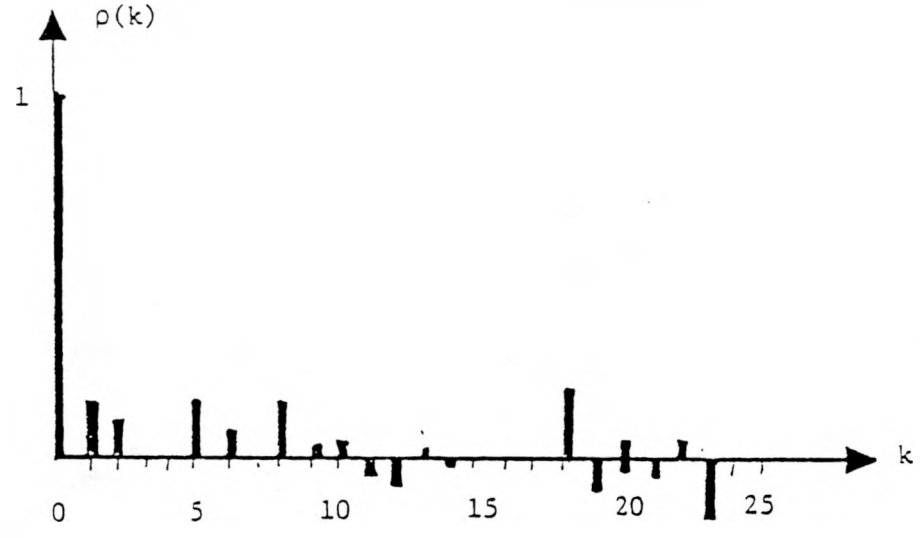

FIGURE 3.5 SAMPLE AUTOCORRELATION OF FINAL MODEL

$$\tilde{e}_t - m = \frac{1}{1 - 0.663L}\ \eta_t \qquad (3.9)$$

with $\eta_t \sim N(0, 946.3)$ and $m = -2.667$ for March 7-9, 1978. Both coefficients and both estimated σ^2 and η_t are well within the 95% confidence intervals of each other. This was the first of several subsequent specifications in the analysis of WEPCO hourly loads. Hence, we shall refer to it as Specification I throughout the remainder of this section.

3.3.2 Specification II of the Hourly Predictor

What appeared to be an attractive specification for January and March data, failed to satisfy two requirements. First, application of the 24^{th} order differencing to later data sets from June and August 1978 weekdays* exhibited non-stationary properties in the sample autocorrelation functions. This indicated either that 24^{th} order differencing might be appropriate for some but not all data sets, or that an alternative specification was required. Second, estimation of the AR(1) model on the 24^{th} order differences exhibited parameter estimates for the autoregressive coefficient which were significantly different from the estimates made on January and March data (see left-most portion of Table 3.2 later in this subsection). In August of 1978, more detailed experimentation was performed on the WEPCO data sets for January (four consecutive weekdays), March (three consecutive weekdays), June (two sets of five consecutive weekdays) and August (two sets of five consecutive weekdays).

As an alternative to 24^{th} order differencing, first order differencing of consecutive observations of e_t was performed on each of the six data sets. The motivation to examine an alternative order of differencing was purely experimental. That is to say, it was not clear

---

* As before, these data sets were supplied to SCI by Robert Bischke of WEPCO, from WEPCO data files of past system operation.

upon examination of the raw data that first order differencing would yield stationary sample autocorrelation functions. However, it was found that in each data set first order differencing exhibit autocorrelations which "spiked" (i.e., has a value significantly different from zero) at lags one and twenty-four, and all the intermediate correlations were small and followed a random pattern. An example of this using the January data set can be found on Figure 3.6. Further, a comparison of the residual standard error for the one-step-ahead forecasts between 24^{th} order differences and first order differences can be found on Table 3.1. Although a comparison of residual standard errors between different dependent variables (i.e., e_t vs $e_t - e_{t-24}$ vs $e_t - e_{t-1}$) is not statistically correct, the numbers on Table 3.1 tend to support the notion that first order differencing has less residual variation than 24^{th} order differencing. The increase in residual variation in the differenced data, both first order and 24^{th} order, relative to the raw data in both June data sets should not be interpreted as favoring a time series model of the raw data. The point of comparing residual variation is to help indicate between competing specifications which form of the dependent variable is more likely to exhibit stationary characteristics.

Based on the sample autocorrelation of the first order differences for each data set, an alternative specification (Specification II) was suggested. Specification II is a 24^{th} order autoregressive (without any autoregressive terms for lags 1 through 23), first order moving average (MA) model of the first order consecutive differences of e_t. Expressed in the notation established above, we have

$$e_t - e_{t-1} = d_1 L^{24} (e_t - e_{t-1}) + (1 + C_1 L^1)\, \eta_t \qquad (3.10)$$

Where L^n is a lag operator of order n such that $L^n e_t = e_{t-n}$, and η_t is a random disturbance term. The two specifications imitate each other to a degree. Specification I assumes a 24^{th} order autoregressive (AR)

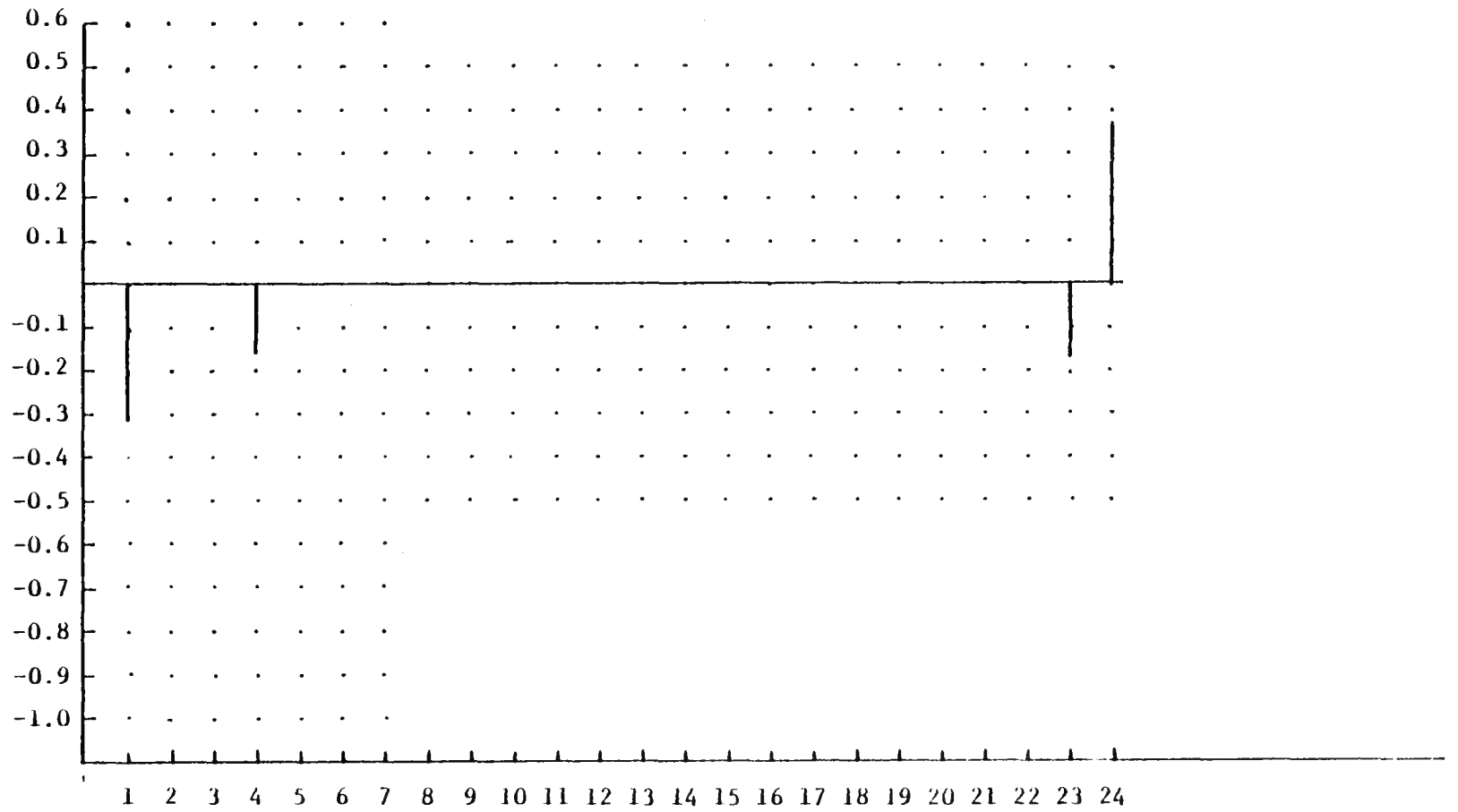

FIGURE 3.6 SAMPLE AUTOCORRELATION FOR $e_t - e_{t-1}$

TABLE 3.1

COMPARISON OF RESIDUAL STANDARD ERRORS (MW)

DATA SET	RAW DATA (e_t)	FIRST ORDER DIFFERENCING ($e_t - e_{t-1}$)	24TH ORDER DIFFERENCING ($e_t - e_{t-24}$)
January	38.0	29.1	36.9
March	36.5	33.8	40.8
June 5-9	62.1	66.6	76.2
June 12-16	63.2	67.3	81.7
August 7-10	83.8	48.8	107.8
August 14-17	100.8	58.2	81.7

term which for a stationary time series model must be in the range -1.0 to 1.0. The results on Table 3.2 show that the estimates for the six data sets considered ranged from .04 to .66.[1] Alternatively, Specification II assumes an AR(1) parameter value of -1.0 due to first order differencing. Specification I calls for estimates of the AR(1) parameter which based on the results seen in Table 3.2 are significantly less, in absolute value, then unity. A maximum likelihood estimator is used to derive the results seen on Table 3.2. Both specifications exhibited widely varying parameter values for their respective autoregressive term. Specification II showed a range of values for C_1 ranging from -.79 to .07. This implied that for some data the model might be ARMA(24,1) (e.g., January), AR(24) (e.g., August 14-17), or MA(1) (e.g., June 12-16).

3.3.3 Specification III of the Hourly Predictor

At this point in the analysis, it was decided that due to the dismal results of Specifications I and II a closer look at the raw data might reveal some of the inherent problems and suggest possible solutions. Casual inspection of the data often reveals sources of inconsistency or non-stationarity. It was noted upon re-examination that in the WEPCO data, the system load dispatcher infrequently adjusts the 24 hour predicted hourly load. For example, in the January data set, the first 24 hourly predictions were adjusted by the dispatcher, but every subsequent hour remained unadjusted. For other data sets, the adjustments, if made at all, were at various times of the day. It was believed that infrequent insertion of extraneous information changed the nature of the time series.

---

1 If the AR term were placed on the left hand side of Specification II, the parameters would take on negative values. Hence, Specification II could be rewritten as follows:

$$e_t - d_1 e_{t-24} = e_{t-1} - d_1 e_{t-25} + (1+C_1 L^1)\ \eta_t \qquad (3.11)$$

TABLE 3.2

FULL INFORMATION MAXIMUM LIKELIHOOD ESTIMATION OF
TWO TIME SERIES SPECIFICATIONS ON WEPCO HOURLY LOADS

	Specification I					Specification II					
	$e_t - e_{t-24} = \frac{1}{1 + d_1 L} \eta_t$					$e_t - e_{t-1} = d_1 L^{24} (e_t - e_{t-1}) + (1+c_1 L^1) \eta_t$					
Data Set	No. of Obs.	d_1	$\hat{\sigma}_{d_1}$	$\hat{\sigma}_\eta$	R^2	d_1	$\hat{\sigma}_{d_1}$	c_1	$\hat{\sigma}_{c_1}$	$\hat{\sigma}_\eta$	R^2
January	96	-.76	.06	26.51	48.34	.54	.10	-.28	.13	24.01	31.92
March	72	-.66	.09	30.76	43.16	.39	.12	-.35	.16	31.16	15.07
June 5-9	120	-.32	.09	72.52	21.21	.16	.10	-.79	.07	59.12	21.20
June 12-16	120	-.40	.09	75.47	14.67	.04	.10	-.73	.09	58.45	24.57
August 7-10	96	-.87	.05	53.80	75.09	.23	.12	-.29	.10	49.02	0.0
August 14-17	95	-.85	.05	42.73	72.65	.66	.10	.07	.10	48.70	29.98

NOTES: d_1 is an autoreggressive parameter

c_1 is a moving average parameter

$\hat{\sigma}$ is the estimated standard error

L^n is a polynomial lag operator of order n such that $L^n e_t = e_{t-n}$.

R^2 is the percent of variation in the dependent variable explained by the model.

Several solutions to the problem were proposed. One idea was to note when the 24 hour predictor was adjusted by the Load Dispatcher using an indicator variable that would assume either a value of zero if there was no adjustment, or unity otherwise. This idea was rejected because an indicator variable could only absorb the effect of a different mean value of e_t with and without load dispatcher adjustment to the 24 hour forecast.

Next, it was proposed that the adjustments made by the Load Dispatcher should be ignored and the time series e_t should represent the error in the WEPCO 24 hour load predictor. The raw data, then, was altered to ignore the effect of load dispatcher adjustments on January, June and August data sets. The sample autocorrelation function of these data showed a consistent pattern such as the one shown on Figure 3.7 for the August 7-10 data set. The pattern of the sample autocorrelations suggested that a simple AR(1) model might be a satisfactory candidate.

The results of maximum likelihood estimation on the third specification (Specification III) can be found on Table 3.3. Casual observation of the results indicate that Specification III is more robust across different data sets then the other two specifications. It should be noted that the sample autocorrelations of the noise process, n_t, indicated that greater complexity could be added to the AR(1) model. However, experimentation with more complex models never reduced the residual standard error by more than 5%, thus, the AR(1) model was selected to represent the hourly load predictor error process. In order to confirm the conclusion presented above, one additional data set for August 17-22 was subject to all three specifications. This data set was slightly different in that the third and fourth days were a Saturday and Sunday; respectively. All other data sets only considered weekdays.

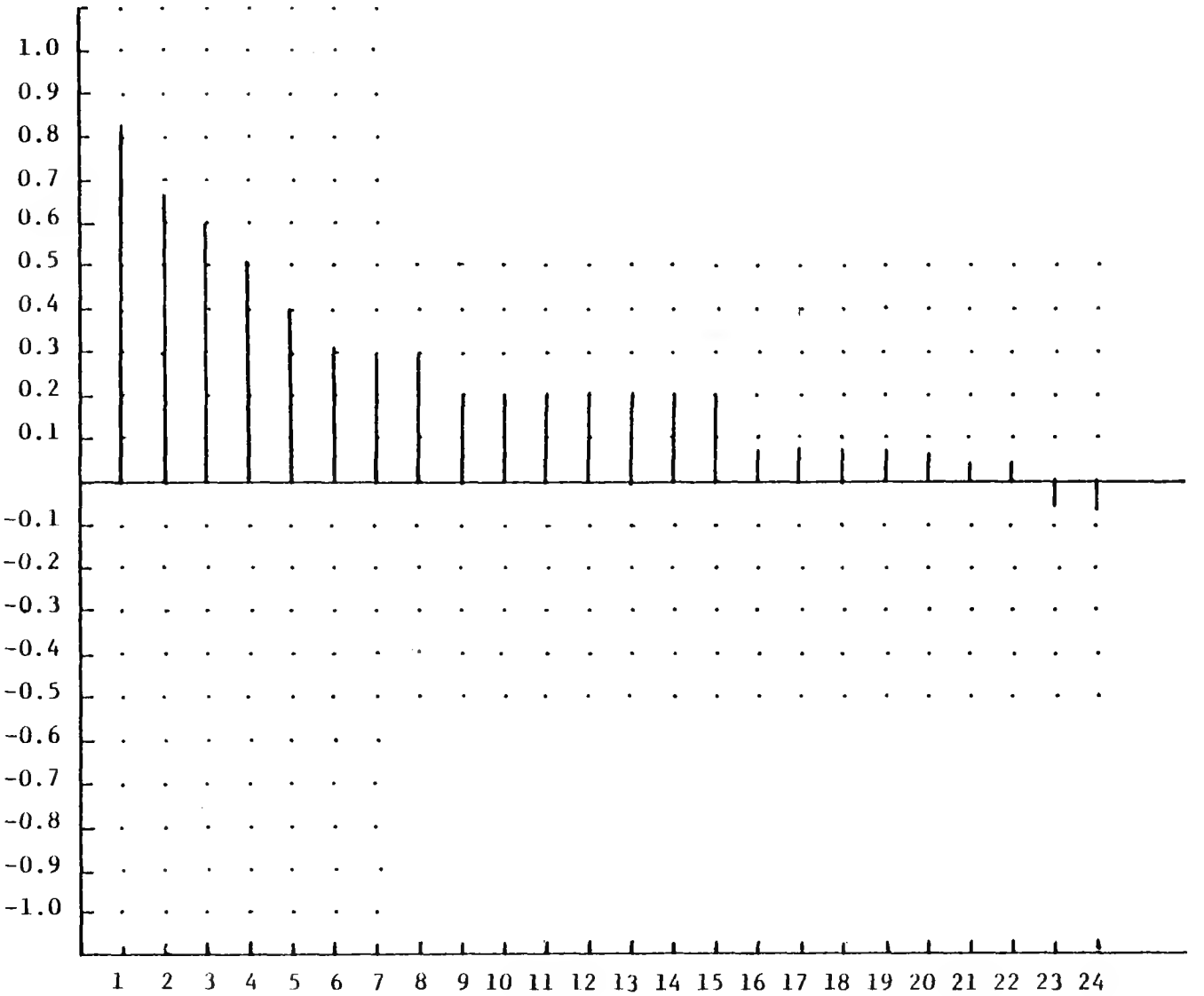

FIGURE 3.7 SAMPLE AUTOCORRELATION FOR "NEW" RAW DATA

TABLE 3.3

FULL INFORMATION MAXIMUM LIKELIHOOD ESTIMATION
OF AR(1) MODEL ON WEPCO HOURLY LOADS

DATA SET	$e_t = \cdot \frac{1}{1 + d_1 L} \eta_t$			
	d_1	$\hat{\sigma}_{d_1}$	$\hat{\sigma}_{\eta}$	R^2
January	-.78	.05	12.49	89.91
June 5-9	-.78	.06	40.20	60.75
June 12-16	-.82	.05	41.79	66.42
August 7-10	-.86	.05	41.33	73.47
August 14-17	-.76	.07	63.37	55.89

TABLE 3.4

ESTIMATION OF THREE COMPETING SPECIFICATIONS ON WEPCO
UNADJUSTED HOURLY LOAD ERROR: AUGUST 17-22

	d_1	$\hat{\sigma}_{d_1}$	c_1	$\hat{\sigma}_{c_1}$	$\hat{\sigma}_\eta$
SPECIFICATION I: $e'_t - e'_{t-24} = \frac{1}{1+d_1 L'} \eta_t$	-.92	.03	--	--	42.99
SPECIFICATION II: $e'_t - e'_{t-1} = d_1 L^{24}(e'_t - e'_{t-1}) + (1+c_1 L')\eta_t$	.49	.08	.19	.09	40.38
SPECIFICATION III: $e'_t = \frac{1}{1 + d_1 L'} \eta_t$	-.87	.04	--	--	44.51

Note: e'_t represents the error in the unadjusted 24 hour load predictor

The results which can be found on Table 3.4 already indicate that the AR(1) model's parameter estimates are similar to the processes estimated for the other five data sets. Specification I had an estimated AR parameter value of -.92, significantly larger than any previous estimate. Specification II estimation shows a significant (at roughly a 95% confidence interval) AR(24) parameter value of .49, but the MA parameter is barely significant with 95% confidence for the August 17-22 data set. As discussed earlier, estimation of Specification II on different WEPCO data sets supported different structural forms; AR(24), MA(1) or ARMA(24,1).

It is our contention that an AR(1) model of the unadjusted hourly load error data is a simple and fruitful model to help predict hourly loads on the WEPCO system. The strength of the AR(1) model is the consistency of its parameter estimates for different types of days (e.g., weekdays vs. weekend) over different times of the year, and the model's ease in implementation.

3.3.4 Summary of Prediction Error Statistics

From Table 3.4 it is seen that the predicted standard error, $\hat{\sigma}_\eta$, of the Specification III load prediction for one-step-ahead (one hour) is:

$$\hat{\sigma}_\eta = 44.51 \text{ MW}$$

Since the predictor model is a 1st-order autoregressive error model, the prediction error variance asymptotically approaches (as the number of time-steps ahead increases) a limit -- whose standard error is $\hat{\sigma}_\eta(1/(1-d_1))$, or:

$$\hat{\sigma}_{t\to\infty} = 342.4 \text{ MW}$$

The size of the "error-envelope" of the predictor, as a function of the number of hours ahead is given in Table 3.5.

TABLE 3.5

ESTIMATED STANDARD ERRORS OF HOURLY LOAD PREDICTOR

NO. OF HOURS AHEAD	STANDARD ERROR OF PREDICTED LOAD (MW)
1	44.5
2	83.2
3	116.9
4	146.2
5	171.7
.	.
.	.
.	.
∞	342.4

Thus the predictor accuracy deteriorates with increasing prediction time; the prediction error envelope is centered about the 24-hour load forecast adjusted upward or downward by the mean error of the predictor.

3.3.5 WEPCO Implementation of the Hourly Predictor

As discussed in Section 3.2.1 - 3.2.3, the Hourly Load Predictor has evolved, through a series of model estimation studies on several sets of WEPCO load data, into the design of Specification III.

The elements of an implementation at WEPCO of the (Specification III) Hourly Predictor are:

1. Actual integrated hourly load must be computed and stored for the most recently completed hour. At the end of one

hour and the start of another, let this actual integrated hourly load be designated as y_{t-1}. Let the corresponding WEPCO system load forecast (from the WEPCO unadjusted SLF data file) for that same hour be χ_{t-1}.

2. Compute the residual, e_{t-1}, as:

$$e_{t-1} = y_{t-1} - \chi_{t-1} \tag{3.12}$$

3. Update a running-average of the mean of past values of e_t. A simple exponential averaging method is proposed:

$$m = \alpha e_{t-1} + (1-\alpha)m \tag{3.13}$$

where α is a smoothing constant in the range $0 < \alpha < 1$.

4. Subtract the mean m from e_{t-1} to obtain the zero-mean variable to which the Specification III autoregressive model applies:

$$\tilde{e}_{t-1} = e_{t-1} - m \tag{3.14}$$

5. Use the AR(1), Specification III autoregressive model to predict values of $\tilde{e}_{t+k}$ for future hours (i.e., for k = 0,1,2,--K) via (see Table 3.3):

$$\tilde{e}_{t+k|t-1} = d_1^{k+1}\, \tilde{e}_{t-1} \tag{3.15}$$

(From Table 3.3, it is seen that the mean value of d_1 found from our model estimations was $d_1 = 0.81$).

6. Add the mean m back to the predicted values of $\tilde{e}_{t+k|t-1}$ to obtain the predicted differences, $\tilde{e}_{t+k|t-1}$ between actual integrated hourly load and the WEPCO 24-hour load forecast:

$$\hat{e}_{t+k|t-1} = \tilde{e}_{t+k|t-1} + m \qquad (3.16)$$

for k = 0,1,2,---,k.

7. Use the general model of Equation (3.3) to predict the system integrated hourly load:

$$y_{t+k|t-1} = \chi_{t+k} + \hat{e}_{t+k|t-1} \qquad (3.17)$$

for k = 0,1,2,---,k. Where:

$y_{t+k|t-1}$ = predicted hourly integrated load for hour t+k, in megawatts.

χ_{t+k} = the WEPCO (unadjusted) hourly integrated load forecast for hour t+k, in megawatts

$\hat{e}_{t+k|t-1}$ = predicted error between actual and forecasted hourly integrated load -- given observations of actual load through hour t-1.

Equations (3.12) - (3.17) are the essential elements of the implementation of the Hourly Predictor. To date, only Specification I (see Section 3.2.1) has been implemented and tested on the WEPCO Cyber computer system. However, as has already been discussed in Sections 3.2.1 through 3.2.3, Specifications I and II happened to be disappointing in regard to stationarity of predictor model structure and parameters. The

disappointing predictor model estimation results were somewhat bourne out by the online results obtained at WEPCO with the implementation of Specification I.

In the early stages of Task 3, we will revise the WEPCO implementation of the Hourly Predictor so that it conforms to Specification III, and online tests will again be conducted. We can then experiment with the predictor implementation to obtain the best prediction performance with the model structure of the Specification III model. This experimentation could include trials made that examine the manner by which the residual mean, m, is updated (Equation 3.13 is one possible implementation). Also, even though the model estimation work already done on the Specification III Hourly Predictor has shown fairly strong stationarity of the AR(1) parameter, the time-invariance assumption could be tested further. If deemed necessary, the Specification III predictor could be appended with an estimator of its (possibly time-varying) parameters; an approach based on Kalman Filtering was outlined during our Task 2 work [3-3].

3.3.6 Use of the Hourly Load Predictor

The purpose of the Hourly Load Predictor (as well as of the 5-Minute Predictor, which will be discussed in Section 3.3 below) is to provide a short-term forecast of the load -- so that the dynamic economic dispatch of the generation units can (1) reconcile anticipated upcoming load changes with the rate limits on dispatched units, and (2) plan the movement, from valve-point to valve-point, of any valve-point loaded units.

The process by which the Hourly Load Predictor is used is construct a short-term load prediction is described by the following three steps:

1. First-Order Autoregressive Error Model

   Recall that a first-order autoregressive time series model has been constructed of the error, e_t, between the actual integrated hourly load and WEPCO's forecasted integrated hourly load. This is the Specification III model discussed earlier.

   This time series model for e_t is then used to predict the integrated hourly load via:

$$y_{t+k|t-1} = \chi_{t+k} + \hat{e}_{t+k|t-1} \tag{3.18}$$

   where $y_{t+k|t-1}$ is the prediction of integrated hourly load for time t+k, given the observations on actual integrated hourly loads through time t-1; χ_{t+k} is the WEPCO hourly load forecast (which, incidentally considers temperature, season, cloud cover, ---); and $\hat{e}_{t+k|t-1}$ is the error predicted from the error time series model.

2. Ascribe Value of Integrated Hourly Load to Mid-Point of Each Hour and Interpolate Among These Points

   The dynamic dispatch requires a load forecast that is defined for each dispatch interval (every 3-5 minutes) of the several-hour future time-horizon. This is achieved by (1) ascribing the predicted integrated hourly load to the mid-point (half-hour) of each hour, and then (2) interpolating among these points. The process is sketched in Figure 3.8, below:

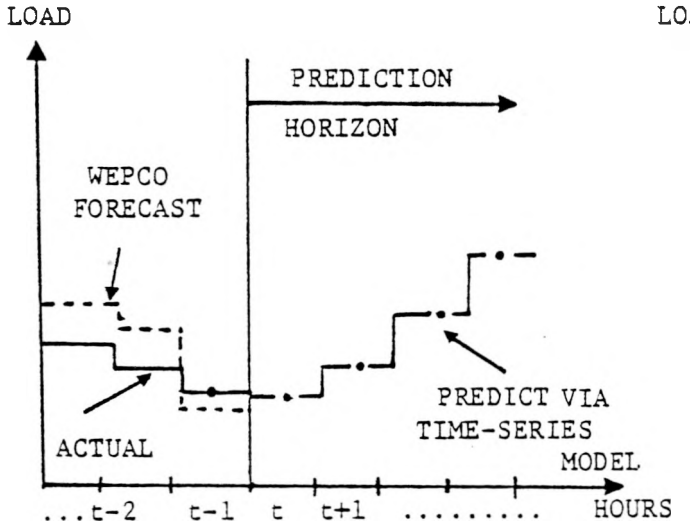

(a) Prediction of Integrated Hourly Load

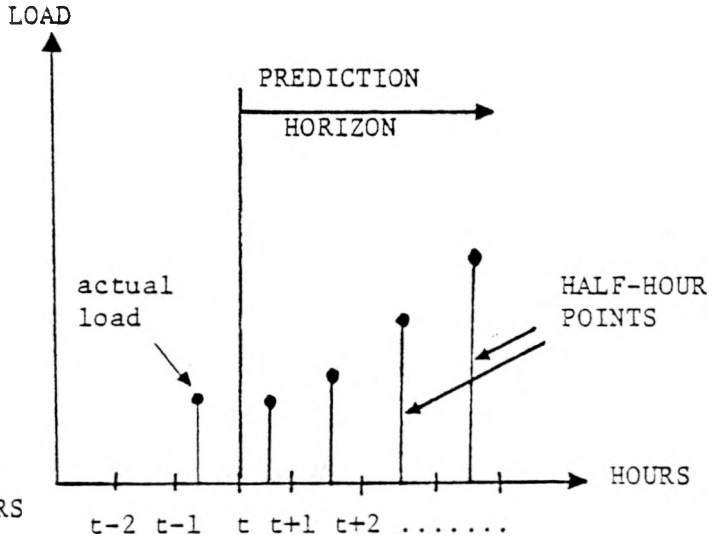

(b) Ascribe Value to Mid-Point of Each Hour

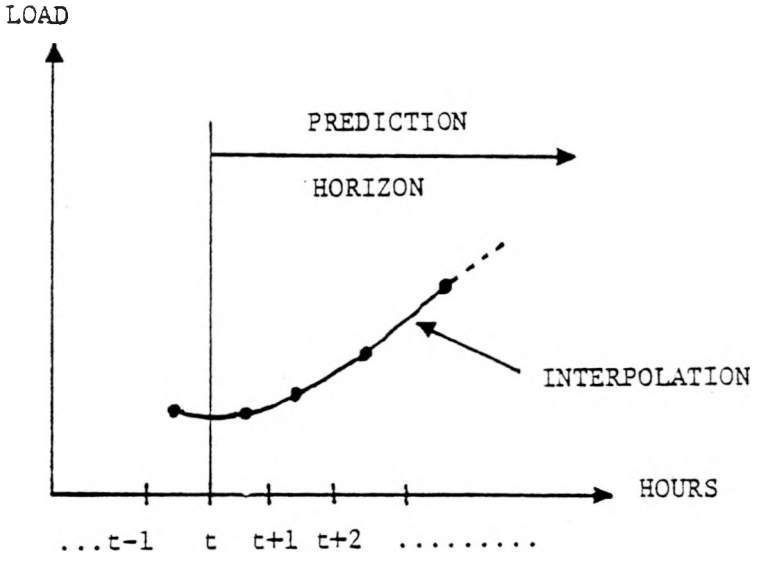

(c) Interpolate Among Ascribed Load Points

FIGURE 3.8 HOURLY LOAD PREDICTION PROCEDURE FOR DYNAMIC DISPATCH

The interpolation among the predicted load points is done via spline interpolation techniques. A standard spline interpolation method has been adapted to this application [3-4]. The load values, obtained by evaluating the spline interpolation at 5-minute intervals, would be the predicted load inputs to the dynamic dispatch algorithm.

3. Update The Prediction Each Hour -- "Moving Window" Prediction

Since a new observation of actual integrated hourly load becomes available once each hour, the prediction procedure outlined in steps 1 and 2 above is repeated each hour and an update to the dynamic dispatch is then made.

Thus the prediction (obtained via the first-order auto-regressive model and the spline interpolation) would be updated each hour, as depicted in Figure 3.9.

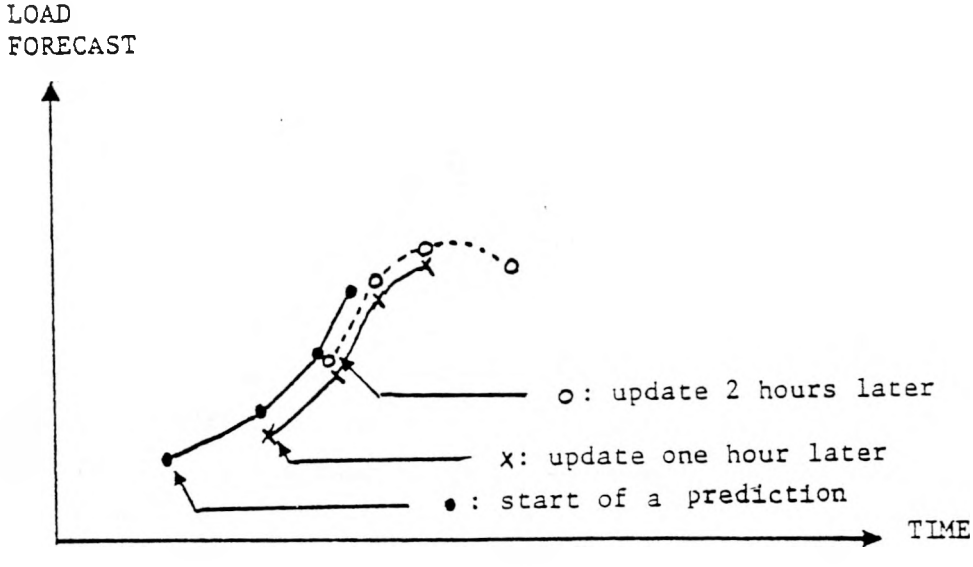

FIGURE 3.9 MOVING-WINDOW LOAD PREDICTION FOR DYNAMIC DISPATCH

3.4 THE 5-MINUTE PREDICTOR: ITS EVOLUTION

3.4.1 Specification of the 5-Minute Predictor

The formulation of a general model for a 5-Minute Predictor follows basically the same arguments as those for the Hourly Predictor (see Section 3.1.1). The only difference being in the time scale and forecast horizon; i.e., replace t by τ to indicate time in units of 5-minutes instead of hours. The resulting predictor is then given by:

$$y'_{\tau+k|\tau} = \chi'_{\tau+k} + e'_{\tau+k|\tau} \tag{3.19}$$

where

y'_τ = actual instantaneous system load at time τ

χ'_τ = some forecast of actual instantaneous load at time τ (derived from χ_τ); in particular, the spline interpolation derived from the Hourly Predictor Execution.

e'_τ = error between actual load and forecasted load

All the known structure, representing all a priori information concerning observed cause-and-effect relationships is captured in the χ'_τ variable. All the unknown structure, representing all the additional information which may be extracted from empirical data, is contained in the e'_τ variable. If systematic (serial correlation, for example) variation exists in these error terms then it can be employed to devise additional structure which will yield a more accurate forecast. The examination of e'_τ is a problem in statistical time series analysis and is discussed below.

Generation of the e'_τ series was carried out in a manner consistent with the way in which the predictor would actually be implemented. First χ'_τ was computed by sampling a cubic spline interpolation on the predictions of hourly integrated load when they were fixed at the half-hour of each hour. (see Figure 3.8 and accompanying discussion). Next the actual instantaneous minute-by-minute load was passed through a simple filter to compensate for any aliasing which might arise due to the 5-minute sampling process [3-5]. Finally these two sampled series were differenced to obtain e'_τ.

The sample autocorrelation for e'_τ using data for December 7, 1977 appears in Figure 3.10. There is significant serial correlation and at least first-order autoregression appears likely. In fact, higher orders are called for, but an ARMA(1,0) was initially fit to illustrate the use of the autocorrelation diagnostic. Upon estimation the ARMA(1,0) model produced the autocorrelation diagnostic. Upon estimation the ARMA(1,0) model produced the autocorrelation function of Figure 3.11. There still appeared to be significant autocorrelation in the residuals, so an ARMA(2,0) model was estimated. Its residuals produced the sample autocorrelation function of Figure 3.12. The second order model is all that is necessary to adequately describe <u>all</u> of the systematic variation in e'_τ.

Similar results were obtained for data taken over March 7, 1978 and March 8, 1978. The three models are presented below:

$$e'_\tau - m = \frac{1}{\underset{}{1} \underset{(\pm.057)}{- 1.537L} + \underset{(\pm.057)}{0.579L^2}} \eta_t \qquad (3.20)$$

with $m = -8.45$ and $\eta_t \sim N(0.22.2)$ for the December 7, 1977 data.

$$e'_\tau - m = \frac{1}{\underset{}{1} \underset{(\pm.058)}{- 1.537L} + \underset{(\pm.057)}{0.564L^2}} \eta_t \qquad (3.21)$$

with $m = 0.510$ and $\eta_t \sim N(0,14.92)$ for the March 7, 1978 data.

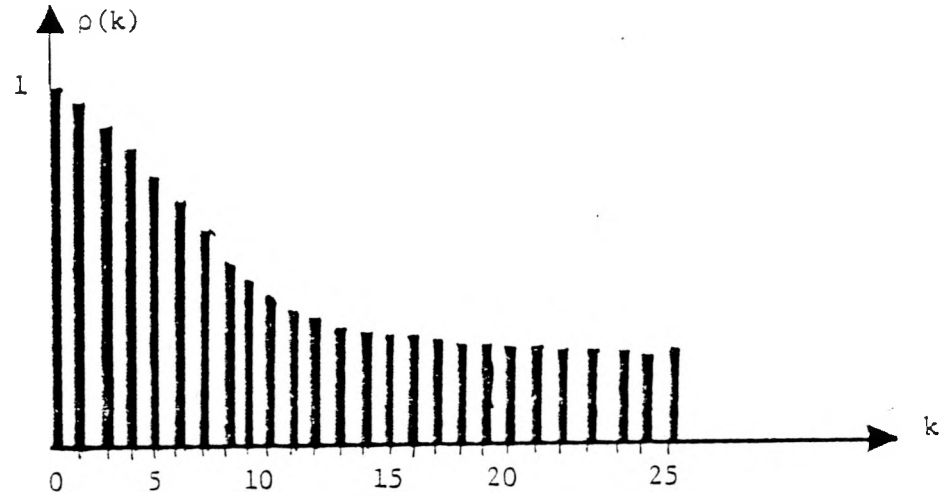

FIGURE 3.10 SAMPLE AUTOCORRELATION FOR 5-MINUTE DATA

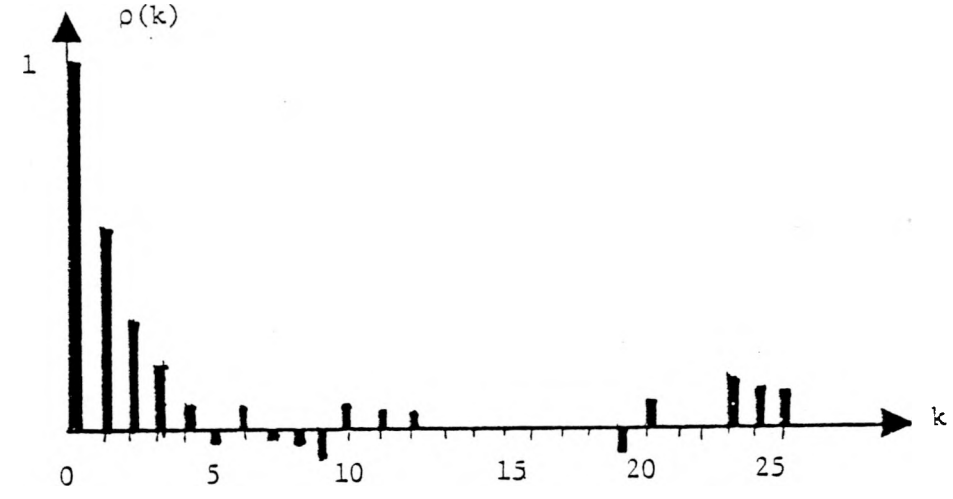

FIGURE 3.11 SAMPLE AUTOCORRELATION FOR ARMA(1,0) MODEL of e'_t

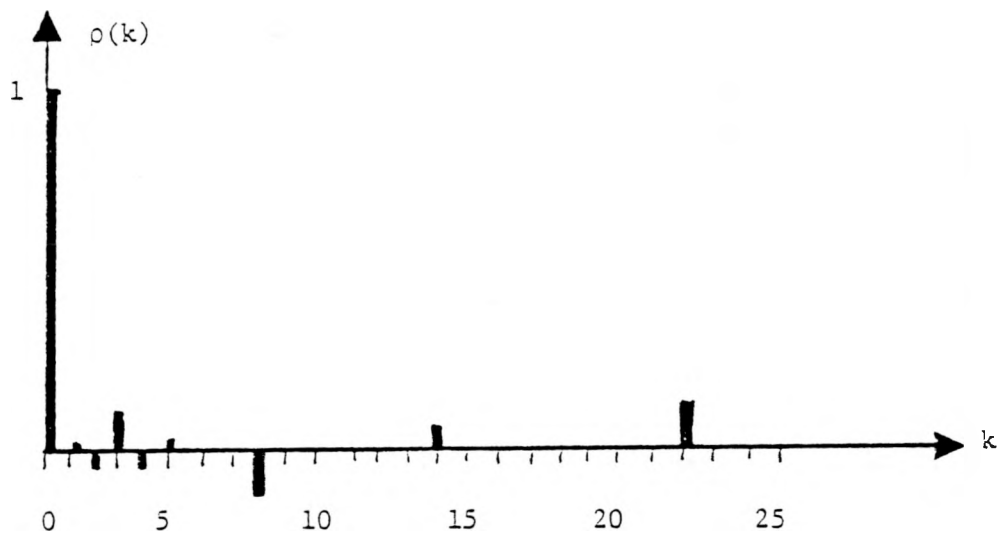

FIGURE 3.12 SAMPLE AUTOCORRELATION FUNCTION FOR ARMA(2,0) MODEL OF e'_t

$$e'_t - m = \frac{1}{1 - 1.474L + 0.551L^2}\ \eta_t \qquad (3.22)$$

with $m = 2.34$ and $\eta_t \sim N(0,16.86)$ for the March 1978 data.

3.4.2 Revisions That May be Needed In The Predictor Specifications

As mentioned in subsection 3.3.1, the estimation procedure for the 5-Minute Predictor started with the generation of the e'_t series. This series was generated by passing 1-minute raw samples of load through a low pass filter (cutoff frequency at one cycle each 10 minutes or lower [3-5]) and then subtracting the corresponding spline interpolation values (of the hourly load predictions) at each 5-minute interval -- thus obtaining the e'_t series (values each 5-minutes).

One can see that, by definition of the construction of the e'_t series, the resulting predictor is only capable of predicting the filtered load at 5-minute intervals. But the filtered load will have large time lag (on the order of 10 minutes) relative to actual load. We became aware of this problem during the later stages of the model estimation work on the Hourly Predictor and have not addressed the problem yet because we only recently completed the Hourly Predictor specification.

The problem can be resolved, so that actual (not lagged) load is predicted, as follows:

1. First, the smoothed actual load should be generated by low-pass filtering the raw 1-minute samples of load first forward in time, and then filtering the forward-pass filter outputs backwards in time.

The net effect of the two filtering operations will be to smooth the load, yet without introducing any time lag.

2. Next, the difference between the smoothed time series of actual load (time-lag now eliminated) and the spline interpolation (from Hourly Predictor) is computed, each 5-minutes, to generate the e'_τ time series.

3. The 5-minute predictor is re-estimated using the new e'_τ time series.

4. When the 5-minute predictor is implemented, it will be necessary to filter actual load <u>but</u> then to compensate the filter output for the filter time lag. A simple linear or polynomial extrapolation of past filter outputs should suffice to place enough prediction on the filter output to compensate for the lag of the filter.

The above revisions to the 5-Minute Predictor estimation procedure and its implementation are assumed for the WEPCO implementation which is discussed later in Section 3.3.4.

3.4.3 Prediction Error Statistics

As seen from the discussion of the estimation results (Equations (3.20) - (3.22)), the estimated prediction error, defined as $\pm$ one standard error for one 5-minute interval is worst-case value found in the model estimations):

$$\sigma = 4.71 \text{ MW}$$

The estimated forecast error for intervals beyond one step ahead requires solution of a second order difference equation [3-5]. The prediction error as a function of number of 5-minute steps into the future is given in Table 3.6

TABLE 3.6

ESTIMATED STANDARD ERRORS OF 5-MINUTE LOAD PREDICTOR

NO. OF 5-MINUTE INTERVALS AHEAD	STANDARD ERROR OF PREDICTED LOAD (MW)
1	4.71
2	11.9
3	20.4
4	29.1
5	37.6
(30 min) 6	45.7
7	53.1
8	60.0
9	66.1
10	71.5
11	76.4
(1 hour) 12	80.7

Table 3.6 shows the degree to which the predictor accuracy deteriorates with increasing prediction time; the prediction error envelope is centered about the spline interpolation curve which has been fit to the hourly load predictions -- adjusted upward or downward by the mean error of the 5-minute predictor.

3.4.4 WEPCO Implementation of the 5-Minute Predictor

As discussed in Section 3.3.2, there may be some revisions needed to the 5-Minute Load Predictor. As currently estimated, the elements of the WEPCO implementation* of the 5-Minute Predictor are:

1. Each minute, a new sample load (at WEPCO this is called "1-minute snapshot load") is obtained and input to a digital Butterworth filter. The filter prevents aliasing when the load data is used to develop the 5-minute load predictions. SCI has developed a program for Butterworth filter designs that is useful here [3-6].

2. Each minute, after the 1-minute load has been filtered, the filter output is passed through a simple predictor that compensates for the filter lag (see previous discussion in Section 3.3.2).

3. Every 5th minute (or at whatever interval the dynamic economic dispatch is to be updated -- but the model estimated by SCI is for 5-minute intervals), the residual, e'_τ, is computed as:

$$e'_\tau = y_\tau - \chi_\tau \tag{3.23}$$

where

y_τ = current output of the filtered and lag-compensated actual load

χ_τ = the (pre-computed) value of load, at the present time, as estimated by the spline interpolation to the hourly load predictions.

---

* Robert Bischke implemented this predictor on the WEPCO Cyber computer system in July-August, 1978.

4. Update a running-average of the mean of the past values of e'_τ. A simple exponential averaging method can be used:

$$m = \alpha e'_\tau + (1-\alpha)\, m \tag{3.24}$$

where α is a smoothing constant in the range $0 < \alpha < 1$.

5. Subtract the mean, m, from e'_τ to obtain the zero-mean variable to which the autoregressive predictor model applies:

$$\tilde{e}_\tau = e'_\tau - m \tag{3.25}$$

6. Obtain the zero-mean residual of 5-minutes (one time step) ago, $\tilde{e}_{\tau-1}$, and recursively predict values of $\tilde{e}_{\tau+k}$ for an hour of future 5-minute intervals (i.e., for k = 1,2,3,---12), using:

$$\tilde{e}_{\tau+k} = d_1 \tilde{e}_{\tau+k-1} + d_2 \tilde{e}_{\tau+k-2} \tag{3.26}$$

(From Equations (3.20) - (3.22) it is seen that $d_1 = 1.52$ and $d_2 = 0.565$ are the average parameter values found from the model estimation work).

7. Add the mean, m, back to the predicted values of $\hat{e}_{\tau+k|\tau}$ between actual WEPCO load and the spline interpolation values at each of the twelve 5-minute intervals of the next hour:

$$\hat{e}_{\tau+k|\tau} = \tilde{e}_{\tau+k} + m \tag{3.27}$$

for k = 1,2,3,---12

8. Use the general model of Equation (3.19) to predict the system load at the 5-minute intervals:

$$y_{\tau+k|\tau} = \chi_{\tau+k} + \hat{e}_{\tau+k|\tau} \qquad (3.28)$$

for k = 1,2,3,---12

where:

$y_{\tau+k|\tau}$ = predicted secular load at time $\tau+k$, in megawatts

$\chi_{\tau+k}$ = the spline interpolation (at time $\tau+k$) of the hourly load predictions

$\hat{e}_{\tau+k|\tau}$ = predicted error between actual load and the spline interpolation of the hourly load predictions

Equations (3.23) - (3.28) are the essential elements of the implementation of the 5-Minute Predictor. This predictor model had already been implemented at WEPCO before we realized that it was essential to compensate for the lag introduced by the filtering of the 1-minute load "snapshots". Some further work may be necessary to revise the estimated model and its implementation, as has been outlined in Section 3.3.2. Once these revisions have been made online tests will be conducted at WEPCO. We can then experiment with the predictor implementation to obtain the best performance within the estimated model structure. This experimentation could include trials made that examine the manner by which the residual mean, m is updated. Also, even though the initial model estimation work has shown fairly strong stationerity in the AR(2) parameters (see Equations (3.20) - (3.22)) the time-invariance assumption could be tested further. If necessary the 5-Minute Predictor could be appended with an estimator of its (possibility time-varying) parameters; the approach in [3-3] could be used.

3.4.5 Use of the 5-Minute Predictor

The principal use, within the advanced AGC logic, of the 5-Minute Predictor is to provide frequent updates of the short-term load predictions throughout each hour. These 5-minute updates to the short-term load prediction can, in turn, be used to produce updates to the dynamic economic dispatch of the generation units. The Hourly Load Predictor is updated only once per hour -- so that within any given hour information on departures of actual load from the (spline interpolation of) hourly load prediction cannot affect the control of the units unless updates of the load prediction are made throughout the hour.

The use of the 5-Minute Predictor is best understood by considering the way in which it is planned to implement the dynamic economic dispatch. Consider Figure 3.13, which depicts the use of the load predictions. The spline interpolation of the hourly load predictions provides a nominal load prediction through the current hour, the next hour, and possibly for hours beyond the first two. (The spline interpolation to the hourly load predictions must, for reasons explained later, be defined throughout the current hour and the next). At each 5-minute time-point within the hour, the 5-Minute Predictor program is to be run to produce a refined prediction of the load beyond that 5-minute time-point. For instance, Figure 3.13 shows a refinement in the load prediction being made at 5-minute time-point A, followed 5 minutes later by another refinement at point B. As the figure shows, both load prediction refinements will converge to within m MWs of the spline interpolation, where m is the mean error between actual load and the spline interpolation.

The load prediction refinements that are made at 5-minute intervals will be carried forward only 1 hour -- as depicted in Figure 3.13. One reason for not carrying them forward for more than one hour is that at the start of the next hour, the Hourly Predictor will be re-run so that the spline interpolation or nominal load prediction curve will then be changed for the next hour and for hours beyond that. Since the spline interpolation is an exogenous input to the 5-Minute Predictor, the 5-Minute Predictor results for the next hour and beyond will be affected. The predictions, made each 5 minutes for a one hour horizon, will "slide" along, as the current hour progresses, until the prediction made at the 55th minute of the current hour spans the entire next hour. The 1-hour "sliding" horizon for the 5-Minute Predictor is therefore consistent with the minimum two-hour horizon proposed for the spline interpolation of the hourly predictions.

It is planned that the load predictions made, each 5-minutes, for a 1-hour horizon will be used in an execution (also each 5-minutes) of the dynamic economic diaptach program (see Chapter 4). These executions, each 5-minutes, of the dynamic economic dispatch will be partial in that they will involve a subset of all dispatchable units (possibly operator-selected), and will serve to partially update the economic dispatch. At the start of each new hour, a full dynamic economic dispatch will be performed -- among all dispatchable units, and for a time horizon that goes at least two hours into the future (corresponding to the nominal two-hour spline interpolation of hourly load predictions).

The continuous curves depicted in Figure 3.13 are not actually so; they are discrete load values predicted for each 5-minute time-point. Accordingly once these discrete load predictions are available from the 5-Minute Predictor, and the dynamic economic dispatch has been run to produce the 5-minute dispatch targets for each input, -- an interpolation scheme has to be applied to provide each unit's economic target, in real-time. This interpolation process is depicted in Figure 3.14.

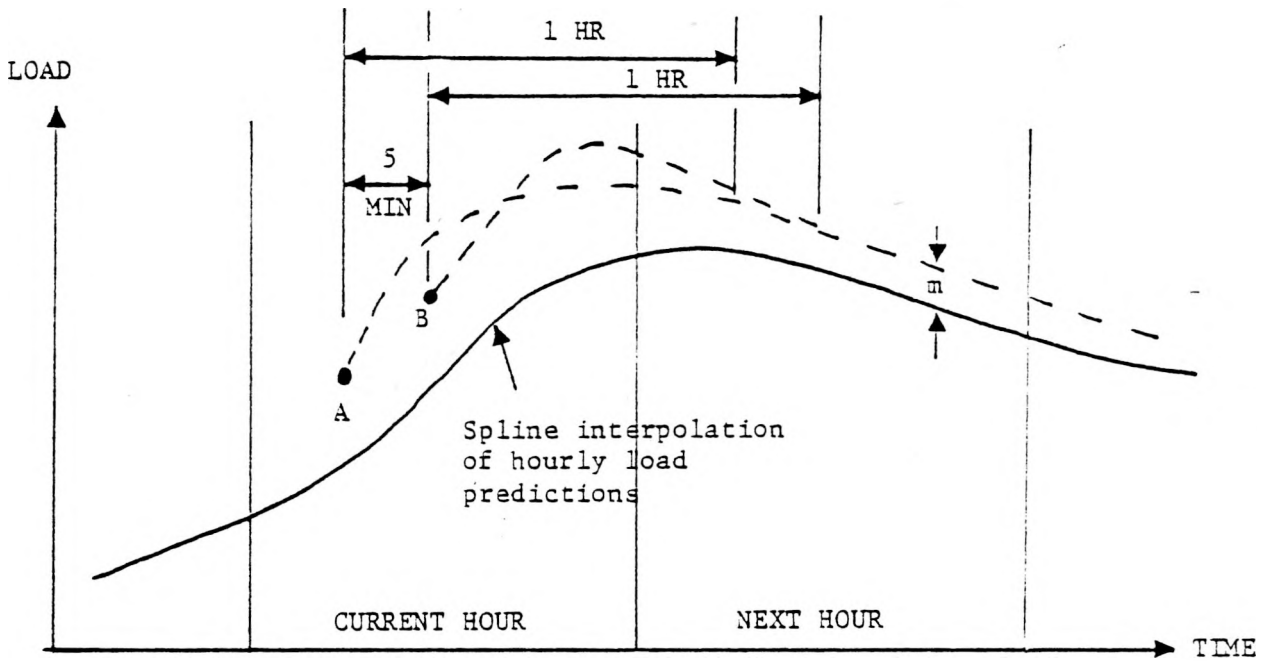

FIGURE 3.13 RELATION BETWEEN HOURLY LOAD PREDICTION AND 5-MINUTE LOAD PREDICTIONS

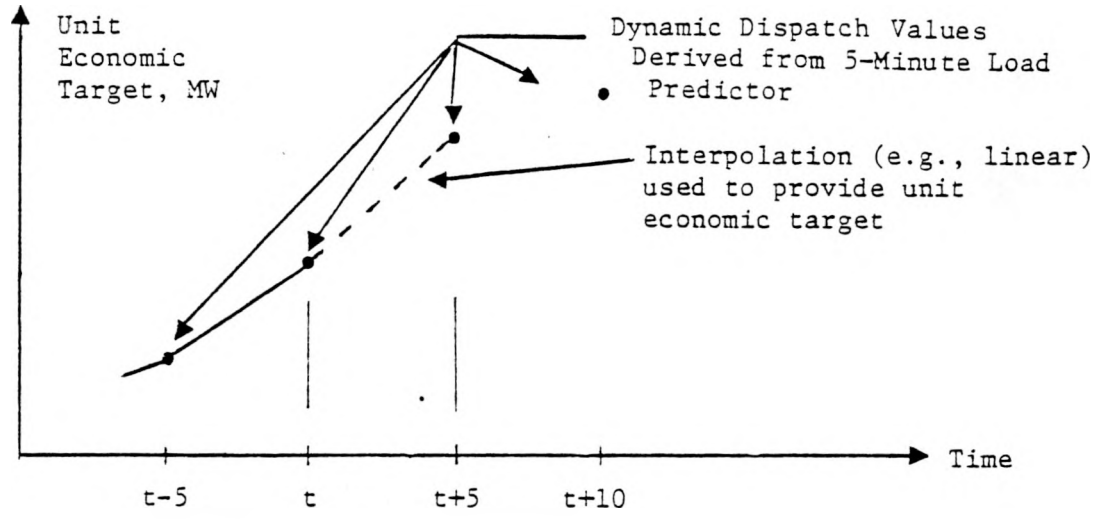

FIGURE 3.14 INTERPOLATION BETWEEN DISPATCH VALUES DERIVED FROM 5-MINUTE LOAD PREDICTIONS

One final point that has been only briefly touched upon above, is that special logic must be invoked at the start of each new hour. This is due to the fact that the Hourly Predictor is re-run at the start of each new hour -- thereby creating a new spline interpolation curve that fits future hourly load predictions. As depicted in Figure 3.15, this can cause the spline interpolation to be discontinuous at the hour boundary. This continuity requires that the 5-Minute Predictor be reinitialized at the start of each hour. That is, the initial error states, $\tilde{e}_{t-1}$ and $\tilde{e}_{t-2}$ of the AR(2) 5-Minute Predictor would both be reset to zero. If the mean error between actual load and the spline interpolation curve had the value $\bar{m}$ prior to the reinitialization, and if the discontinuity in the spline interpolation was ΔL megawatts (see Figure 3.15), then the mean error, m, should be reset to:

$$m = \bar{m} - \Delta L \tag{3.29}$$

Chapter 4 will discuss the interface between the load predictors and the dynamic economic dispatch further.

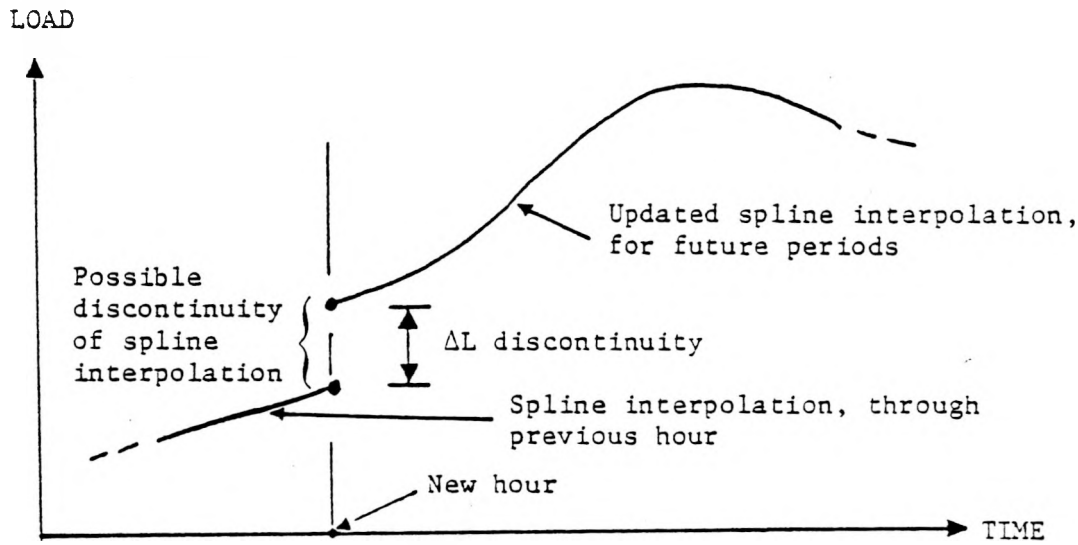

FIGURE 3.15 SPLINE UPDATE AT EACH NEW HOUR

References for Chapter 3

3-1 Box, G.E.P. and Jenkins, G., Time Series Analysis: Forecasting and Control, San Francisco, Holden-Day, 1970.

3-2 Wall, K.D., "Estimation of Rational Distributed Lag Structural Form Models", Annals Econ. Social Meas., Vol. 5, No. 2, pp 53-63, 1976.

3-3 Wall, K.D., "Recursive Updating Algorithm for the Parameters of the Short-Term Load Predictor", SCI Project 5212 memo, May 25, 1978.

3-4 D. Ross, "Spline Interpolation Routines for use in the Short-Term WEPCO Load Predictors", SCI Project 5212 memo, May 31, 1978.

3-5 D. Ross, "Short-Term Load Forecasting Techniques", SCI Project 5212 memo, March 10, 1978.

3-6 D. Ross, "Low-Pass Digital Filter Design Using Butterworth Filter Design Methods", SCI Project 5212 memo, June 15, 1978.

4. DYNAMIC ECONOMIC DISPATCH

4.1 INTRODUCTION

The basic purpose of the economic dispatch function is to schedule the outputs of the on-line power generators serving a particular area so as to meet the net area load at least cost. The state-of-the-art in methods for economic dispatch is that "static" optimization techniques, such as the equal-incremental-cost method, are used to solve the economic load allocation problem. These techniques are "static" in that they do not use, as input load data, anything more than the estimated current load. They do not "look ahead" over the future time horizon, using predicted load trends (say, of 1-2 hours ahead) to determine the economic allocation of generation to the load. Such predictive or "look ahead" capability on the economic dispatch would be beneficial for several reasons:

- The use of predicted load in the economic dispatch would compensate some of the lag that occurs in the generation response with state-of-the-art economic dispatch. Much of this lag is due to the fact that a static dispatch, having no "look ahead" capability, cannot foresee that the present loading of units can affect the total generation rate-of-response capability at a future time. In order to fully utilize the sustained response capability of units, manual prescheduling of units is necessary. A "dynamic" economic dispatch, which determines the economic allocation of generation with knowledge of both the present and future load could lessen these problems.
- The potential benefits of valve-point loading cannot be obtained without having load prediction capability, and using it to dynamically dispatch generation (some units being dispatched to valve-points). As discussed in [4-1], one basic requirement for successful implementation of valve-point loading is that the amount of regulating capacity necessary to take up the difference between block-loaded generation and actual load is a function, among other things, of the amount of time required to pick up or drop

one or more blocks of generation. Furthermore, some minimum amount of time, say 10 minutes, must be provided during which a unit remains at a given valve position without a reversal of load, otherwise the economic benefit of the valve-point loading will not be achieved. These considerations mean that successful valve point loading requires foreknowledge of the load trend.

The first area of potential benefit (elimination of lag) discussed above was analyzed earlier in the project for some WEPCO load situations [4-2], [4-3]. In [4-2] it was concluded that in periods of rapid load change and large load magnitude, the static WEPCO automatic dispatch logic tends to load most units to maximum output -- leaving insufficient rate-of-response among the remaining units to follow load in a statically-optimum economic sense. Additionally, it was postulated that, in actual WEPCO operation, better (than by static dispatch) load following results would probably be obtained via manual dispatch actions. It was postulated that the dispatcher probably manually ramp units so that they reach future target values and follow the load ramping. Reference [4-2] never did analyze actual dispatcher actions. Accordingly, that study was updated by [4-3] to show how the dispatcher actually handled an a.m. pickup scenario. These analyses, although they were limited in scope, gave credence to the usefulness of a dynamic economic dispatch. The succeeding sections of this chapter discuss a dynamic economic dispatch algorithm that has been developed and tested in the project.

4.2 DYNAMIC ECONOMIC DISPATCH ALGORITHM

4.2.1 Previous Work On Optimal Dynamic Dispatch

The subject of optimal dynamic dispatch of thermal units has not previously received a significant amount of attention. More attention has been devoted to the related problem of combined scheduling of hydro and

thermal units. Some of the techniques which have been applied to this latter problem are also applicable to optimal dynamic dispatch of thermal units. The optimal dynamic dispatch of thermal units was originally described in Reference [4-4] which is one of the few available on this subject. In this reference, economic load allocation and supplementary control action were combined into a single dynamic optimal control problem. An optimal feedback controller was designed using Pontryagin's Maximum Principle. The procedure was limited to a two-generator system due to computational problems in storing complex switching surfaces for greater numbers.

A multi-pass dynamic programming approach to the dynamic economic dispatch problem was taken in Reference [4-5]. Optimal trajectories were generated for up to five dispatched units. Valve-point loading was considered. Basically, the approach employed "coarse-grid, fine-grid" methods to reduce the dimensionality problems usually associated with dynamic programming.

4.2.2 Mathematical Statement of the Problem

The optimal dynamic dispatch problem is that of allocating generation from n "dispatchable" units so that operating constraints are satisfied and the production costs are minimized. It is assumed that a load prediction is available over the entire dispatch horizon (of two or more hours). Furthermore it is assumed that the predicted load is specified at uniform discrete time intervals (say, of 5 minutes) indexed as $t = 0,1,2,...T$. Since (a) not all units will be on AGC and, (b) the area generation requirement must be adjusted for the net scheduled interchange — it is assumed that the load prediction, the manually operated generation's output, and planned tie schedules have been combined to obtain the net generation requirement for all units on AGC over the time horizon $t = 0,1,2,...,T$. With these preliminaries, a statement of the optimal dynamic dispatch problem is contained in the discussion below.

The net generation requirement is to be met at each time instant by the sum of the outputs of the generators being scheduled. Formally,

$$\sum_{i=1}^{n} x_i(t) = NETG(t) \qquad (4.1)$$

$$t = 0,1,\ldots,T$$

where

$x_i(t)$ = output of ith generator at time t
n = number of generating units scheduled
T = number of time intervals in scheduling intervals

The output of each generator can be changed directly. Formally,

$$x_i(t+1) = x_i(t) + u_i(t) \qquad (4.2)$$

where

$u_i(t)$ = change in output of ith generator over time interval t.

These changes are bounded through the equations

$$RL_i \leq u_i(t) \leq RU_i \qquad (4.3)$$

where

RU_i = maximum increase in output of generator i over one time interval

RL_i = maximum decrease in output of generator i over one time interval

Finally, the cost of operating each generator over the scheduling interval can be expressed as

$$J_i = \sum_{t=1}^{T} f_i(x_i(t)) \tag{4.4}$$

where

J_i = total cost of operating generator i over the scheduling interval

$f_i(x_i(t))$ = cost of operating generator i at output $x_i(t)$ over time interval t

The problem can then be written as follows: given a set of generators with initial outputs $x_i(0)$, find a set of changes to output $u_i(t)$. $t = 0,1,\ldots,T-1$ such that total cost J, where

$$J = \sum_{i=1}^{n} J_i = \sum_{i=1}^{n} \sum_{t=1}^{T} f_i(x_i(t)) \tag{4.5}$$

is minimized, subject to the system dynamic equation

$$x_i(t+1) = x_i(t) + u_i(t),$$

and the constraint on change in generator outputs (4.3) and the constraint that the net system load must be met at each time instant

$$\sum_{i=1}^{n} x_i(t) = \text{NETG}(t)$$

As previously discussed in Section 3.3.5 of this report, it is planned to perform a dynamic dispatch each 5 minutes. The first dynamic dispatch of each hour will involve all dispatchable units and the time horizon for this dispatch will be at least two hours into the future. At intermediate 5-minute points between the starts of successive hours, the dynamic economic dispatch will be "partial" in that it will involve a subset of all dispatchable units -- and over a 1-hour horizon. The partial dispatch serves to partially update the dynamic economic dispatch throughout an hour.

Besides being executed, in full (i.e., all dispatchable units), at the start of each hour, the dynamic economic dispatch will also be executed, in full, with any change in the availability of or operating limits of a dispatchable unit. Such changes include loss of a unit, change in the (sustained) rate limit(s) of a unit, or (unplanned) change in status of a unit (say from automatic to manual mode of operation).

4.2.3 Successive Approximations Dynamic Programming Algorithm

An algorithm for dispatching generation to (predicted) load over a given time-horizon has been developed that uses the dynamic programming successive approximation technique [4-6]. Normally, this technique involves solving a sequence of dynamic programming problems, each having one state variable. For the reasons given below, the usual approach has been modified to entail solving a sequence of dynamic programming problems, each having two state variables.

If load must be met exactly at each time in the dispatch horizon then it is not possible to allow independent variation of the output of a single generator. One means of overcoming this difficulty would be to vary one unit's output while all the remaining units are constrained to move at equal incremental cost within an allowable band constructed about their current trajectories. Yet another, and simpler approach, is to allow one unit's output to be varied while a second unit's output is simultaneously adjusted so that the load constraint is satisfied. In the state space, this constrains the successive approximation searches to lie along the lines depicted in Figure 4.1.

In this pairing approach, various pairing schemes can be applied among the set of dispatchable units. These are discussed in later sections.

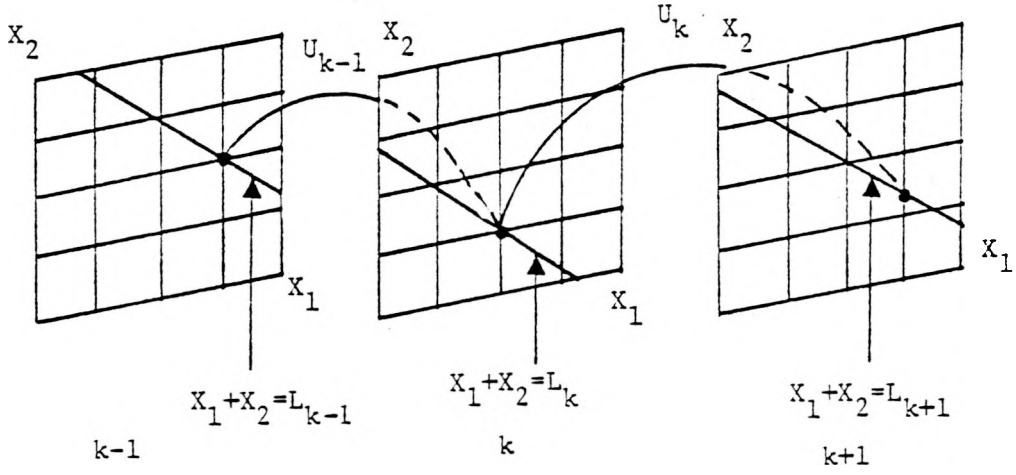

X_1 = Output of 1st unit

X_2 = Output of 2nd unit

L_k = Net generation requirement, k^{th} stage

FIGURE 4.1 PAIRING OF UNITS IN SUCCESSIVE APPROXIMATIONS DYNAMIC PROGRAMMING

The basic idea of the successive approximations technique is to break the large problem of Equations (4.1) - (4.5) containing many control variables (the change in generation variables, $u_i(t)$) into a number of subproblems that each contain only one control variable. By considering the generation units in pairs, each subproblem has only one control variable and only one state variable. Since the computational requirements of dynamic programming increase exponentially with the number of state variables, there is a large reduction in the computational difficulty. Accordingly, although dynamic programming would be infeasible, if applied straightforwardly to the dynamic economic dispatch problem -- it becomes quite feasible if applied iteratively to one pair of units at a time.

The dynamic programming successive approximations (DPSA) algorithm that has been developed for problem (4.1) - (4.5) is characterized in three ways: (1) the iterations or successive approximations are based upon pairings of units (an "artificial unit" is included among the units, as discussed later), (2) each resulting one-dimensional dynamic program is solved by forward dynamic programming, and (3) the special structure of the cost function, Equation (4.5), and the dynamics, Equation (4.2), yield a simple solution procedure for applying Bellman's Principal of Optimality [4-7] at each time-stage of the dynamic program. Each of these characteristics is summarized next.

Pairings of Units

General successive approximations dynamic programming requires independent variation of each control variable. This cannot be done directly in the problem of Equations (4.1) - (4.5) for the reason that the net generation requirement is a given input to the problem which constrains the units; thus if the trajectories of N-1 trajectories are fixed, the trajectory of the other unit is also fixed.

However, if each successive approximations iteration considers the adjustment of two units' trajectories, with the N-2 other units' trajectories being held fixed for the iteration, then Equation (4.1) can be used to reduce the problem at each iteration to one with a single state variable.

Having experimented with a number of pairing schemes, we find that no particular scheme results in the best (with respect to convergence time) overall computational results. One scheme, that we call a "circular" pairing scheme, is described to illustrate how unit pairing is done. With this scheme, the units are indexed by i = 1,2,...,N with i = 1 corresponding to the "cheapest" unit and i = N corresponding to the "most expensive" unit. The "cheapest" unit is the one whose incremental cost curve lies below all other units' incremental cost curves (within the MW range of this "cheapest" unit). The next cheapest unit is taken to be the one with the next lowest cost curve -- and so on. The cirular pairing scheme then considers the units in the pairs: 1-2, 2-3, 3-4,..., (N-1), N-1 — as depicted in Figure 4.2.

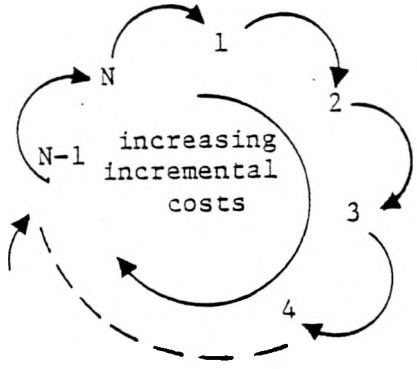

FIGURE 4.2 CIRCULAR PAIRING SCHEME

Prior to the application of successive approximations dynamic programming to the problem solution, it is necessary to initialize the output trajectories of the units over the entire dispatch horizon. A static dispatch technique (namely, a minimum marginal cost algorithm which is discussed in Section 4.3) is used to initialize the unit outputs over the dispatch horizon. In order to guarantee that the static dispatch can initialize the units so that their initial trajectories are feasible (meet all constraints), an artifice is used. Namely, an additional ficticious unit, called the "artificial" unit is used in the dispatch. This artificial unit has much higher production costs than the other (actual) units and has very high rate limits. It is loaded by the static dispatch algorithm at time-stages for which the other units cannot satisfy the net generation requirement. The articial unit therefore expands the total number of units from N to N*(=N+1).

The minimum marginal cost algorithm for initializing unit trajectories considers all units together; that is, there is no need for it to use successive approximations. Once, however, the initial unit trajectories are passed to the DPSA algorithm, the final dynamic dispatch is achieved by the successive approximations method with pairing of two units at each iteration. In effect, DPSA iteratively attempts to both: (a) unload the (expensive) artificial unit -- shifting its generation to the (cheaper) actual units while obeying rate limits on the units, and (b) shift generation, for two units at a time, among the actual units to further reduce the total production costs.

The artificial unit is introduced into the pairing scheme (used in the DPSA computations) as follows. First, the artificial unit is paired with each actual unit in succession. Secondly, a set of "circular" pairings among all units is conducted. These two types of pairing schemes ogether comprise what we call a "single DPSA iteration". This iteration is depicted in Figure 4.3.

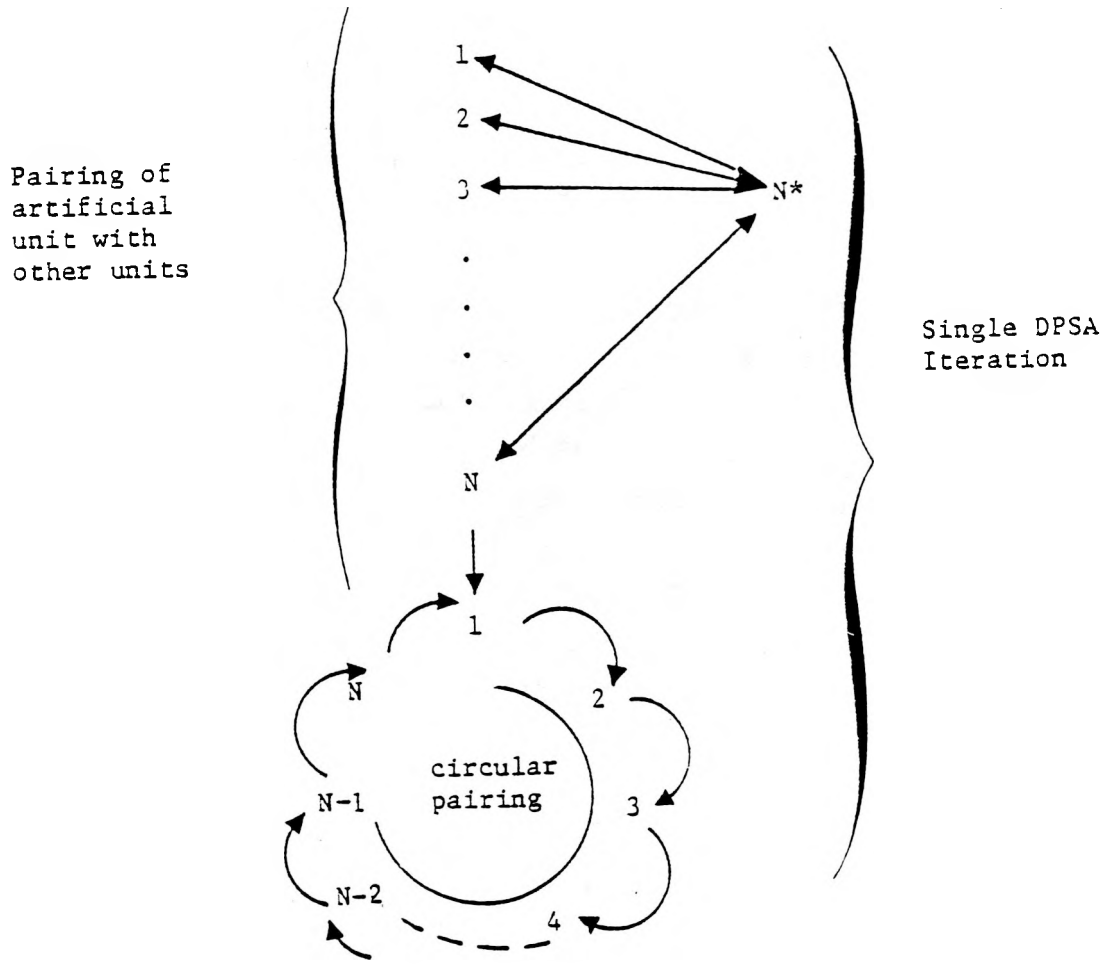

FIGURE 4.3 PAIRING SCHEME FOR A SINGLE DPSA ITERATION

As the circular pairing portion (bottom of Figure 4.3) of each DPSA iteration is being conducted, an attempt is made to unload (at least some) of the artificial unit onto each pair of actual units. The trajectories (obtained by dynamic programming) of each pair of actual units and the trajectory of the artificial unit are examined, one time-stage at a time, and possible shifts of generation from the artificial unit to the two other units are identified. Such shifts must violate neither the rate limits nor the dispatch limits of the two units. Figure 4.4 depicts a possible shift of 2 MW between the artificial unit and a pair of actual units.

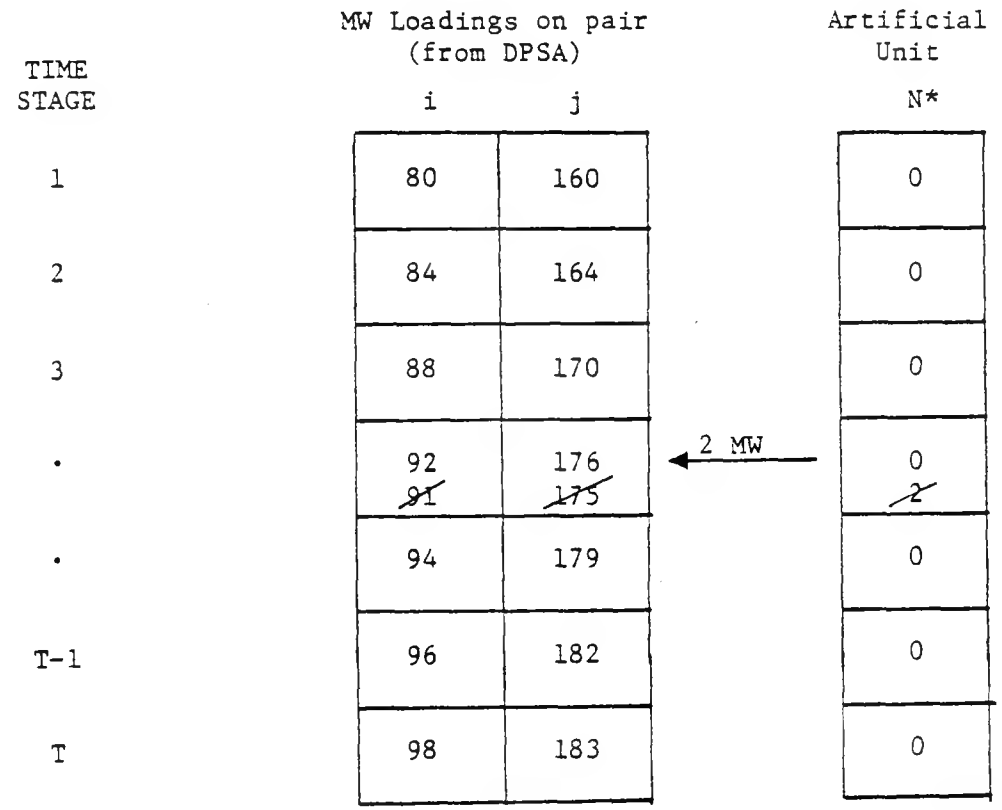

Rate Limits	Dispatch Limits
$R_i = 4$	$30 \leq x_i \leq 110$
$R_j = 6$	$40 \leq x_j \leq 270$

FIGURE 4.4 EXAMPLE SHIFT OF GENERATION FROM ARTIFICIAL UNIT TO PAIR OF OTHER UNITS

The logic to unload the artificial unit, as depicted in Figure 4.4, was added to the simple pairing scheme depicted in Figure 4.3 because that scheme often left some residual loading on the artificial unit of a few MW, and was blind to opportunities to maneuver the outputs of two units in such a way that residual generation on the artificial unit could be absorbed.

A few final comments concerning the use of the artificial unit are:

- It guarantees a feasible solution from DPSA, even when actual load rate exceeds area generation response capability (e.g., during a schedule change). In such cases, the amount of residual generation on the artificial unit corresponds to the drawing of power over the tie lines.
- It admits the possibility of adjusting the production costs on the artificial unit to obtain either rigid matching of generation to load or an approximate matching of generation to load that perhaps taxes the rate-of-response limits of the units less.

Forward Dynamic Programming

As each pair of units is encountered in the pairing scheme depicted in Figure 4.3, a single state-variable/single control variable dynamic program is solved to determine the optimum dynamic dispatch for the pair, with the loadings on the other units held fixed. At the time that the dynamic economic dispatch is computed, the current outputs of the units are known. Accordingly, the dynamic programming proceeds forward in time, starting from the current unit loadings. Thus the algorithm iterates forward in time-stages, using Bellman's Principle of Optimality:

$$I(x,k) = \min_{u(k-1)} \left\{ \sum_i f_i(x_i(k)) + I(x-u_{k-1},k-1) \right\} \qquad (4.6)$$

where $I(x,k)$ is the minimum cost to state x at stage k.

Equation (4.6) is particularly simple to solve because the unit production costs, $f_i(\ )$, are not functions of the control -- but are only functions of the unit outputs (more will be said about this below).

Special Structure of Cost Function -- And Bellman's Principle of Optimality

At each time-stage, k, of the one state-variable forward dynamic program, Bellman's Principle of Optimality (4.6) must be applied to determine the optimum control (generation change) that will bring the unit to an output level, x. Equation (4.6) is solved for the minimizing control by fixing the output, x, of the unit at time-stage k. Then all controls u(k) that will yield output x at time k, starting from some feasible state x_{k-1} at the previous time-stage are found. The minimizing control is the one that solves Equation (4.6) for feasible x_{k-1}.

Due to the fact that the production cost functions, $f_i(x_i(k))$, in Equation (4.6) do not depend explicitly on u(k-1) or x(k-1), and also because $x_k - u_{k-1} = x_{k-1}$, Equation (4.6) reduces to:

$$I(x,k) = \sum_i f_i(x_i(k)) + \min_{\substack{\text{possible} \\ \text{prior} \\ x_{k-1}}} I(x_{k-1},k-1) \qquad (4.7)$$

Therefore (4.6) and (4.7) is minimized by simply searching among the possible prior state levels for the one that has the minimum cost! This optimum previous state is saved and the new optimum cost through stage k is computed from (4.7).

Furthermore, the prior stage's feasible states, x_{k-1} that correspond to the given value of x_k are found directly from the unit rate limits, as depicted in Figure 4.5

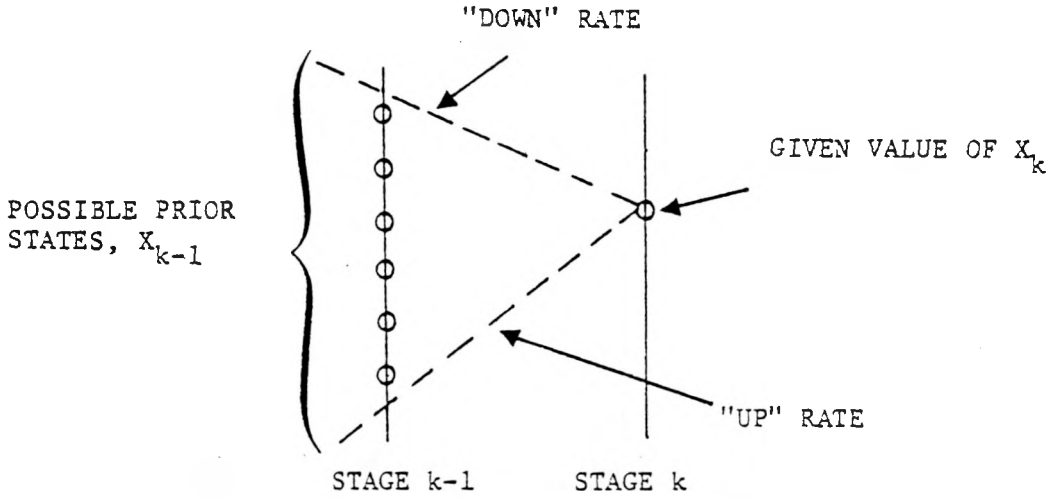

FIGURE 4.5 PRIOR STAGE FEASIBLE STATES FOUND BY APPLYING KNOWLEDGE OF RATE LIMITS

In summary then, the special structure of the dynamic economic dispatch problem has been used to advantage in simplifying the dynamic program.

4.3 MINIMUM MARGINAL COST ALGORITHM

As discussed above in Section 4.2.2, the DPSA algorithm requires an initial set of low-cost feasible trajectories before the dynamic programming successive approximations iterations can proceed. The method that has been developed to produce the initial dynamic dispatch of unit output trajectories is a minimum marginal cost algorithm. This algorithm is a static economic dispatch method. That is, it allocates generation to

the net generation requirement one time-stage at a time -- with no "look ahead" to the requirement at future time-stages. Such a static dispatch would, in general, generate infeasible trajectories because lack of look ahead capability would cause the units' rate-of-response to be misallocated in favor of incremental economics. However, with the addition of an expensive, fast, artificial unit to the set of dispatchable units -- this potential problem is resolved. The use of the artificial unit guarantees that feasible trajectories will be generated.

Figure 4.6 illustrates how the minimum marginal cost algorithm functions. The principal steps in the algorithm (executed once for each time-stage in the dynamic dispatch horizon) are:

1. The rate limits (in both up and down directions) on each unit determine the number of generation increments by which the unit output can be raised/lowered from its last output value. These become the candidate increments available on each unit. The candidate increments for the artificial unit are its entire output range.

2. Before determining which of the available generation increments will be used on each unit, the algorithm assumes that each unit starts from the lowest output level within its current range of increments.

3. The candidate increments among all units are placed in a list called the "candidate list".

4. The increments on the candidate list are ranked by their cost into a ranking array.

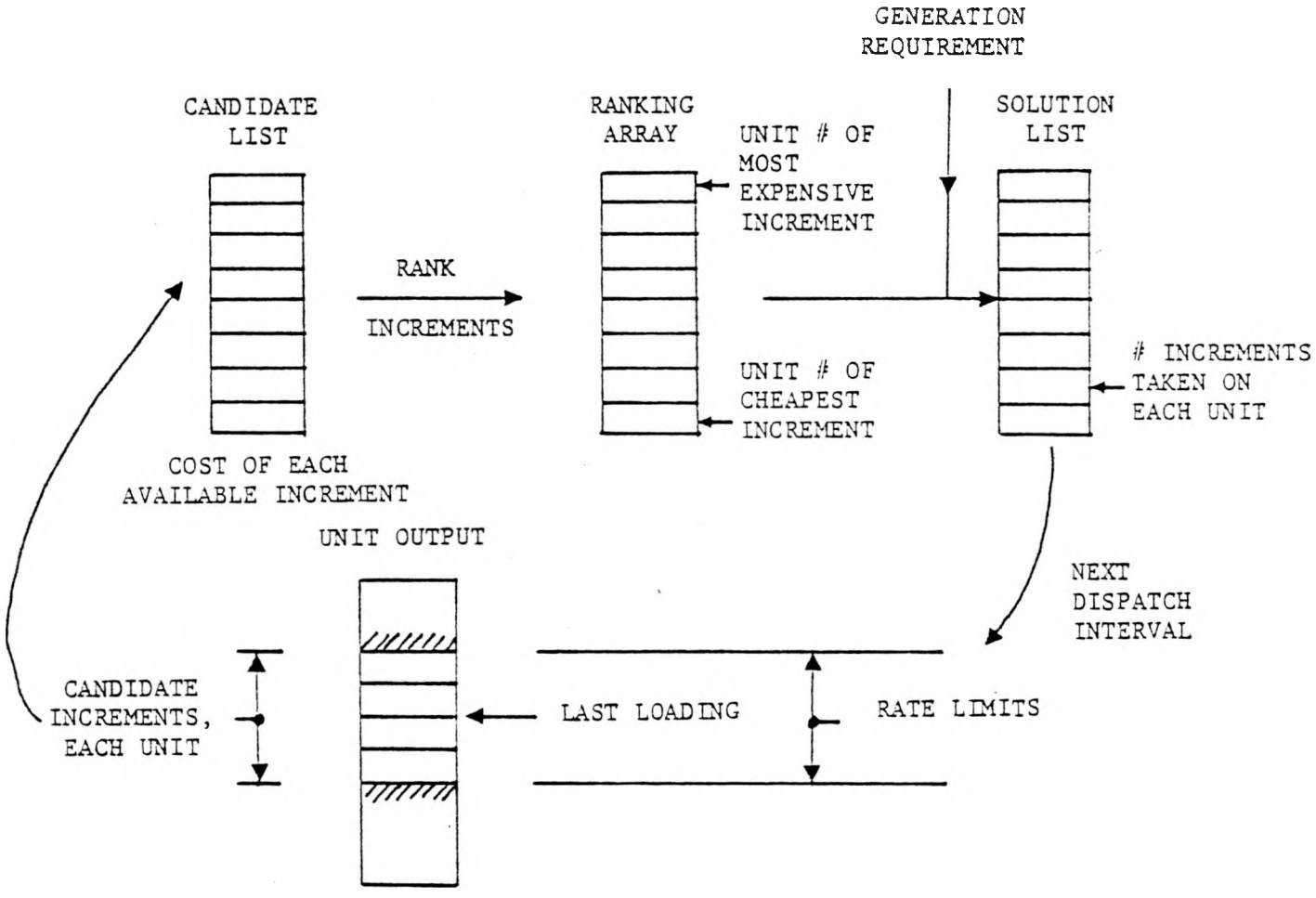

FIGURE 4.6 MINIMUM MARGINAL COST ALGORITHM -

5. The increments are chosen one-by-one until the total generation requirement for the time-stage is met. Increments are chosen in the order of increasing cost under the further condition that a new increment may not be allocated to a unit unless all other increments between the low end of the available increments and the new increment have already been allocated. As increments are thus chosen from the ranking array, they are placed on a "solution list".

6. The solution list gives the new economic dispatch results for the units. The new unit loadings become the last output values considered again (in Step 1) at the next time-stage.

7. Steps 1 - 6 are repeated successively for the later time-stages in the dispatch horizon.

4.4 VALVE POINT LOADING

Both the successive approximations dynamic programming algorithm (DPSA) and the minimum marginal cost algorithm (MINMAR) have been adapted to also handle valve point loading of units. The algorithms themselves needed no modification for this function; valve-point loading is accomplished via the representation of the valve points in both the unit incremental production cost functions (used by MINMAR) and the unit production cost functions (used by DPSA).

Recall that MINMAR serves to initialize the unit output trajectories for the DPSA executions. Accordingly, we felt that an approximate representation of the unit incremental cost functions that reflected the desirability of operating units at their valve points was justified even though the approximations could be quite crude. Figure 4.7 depicts the approximation made. This figure shows that a step

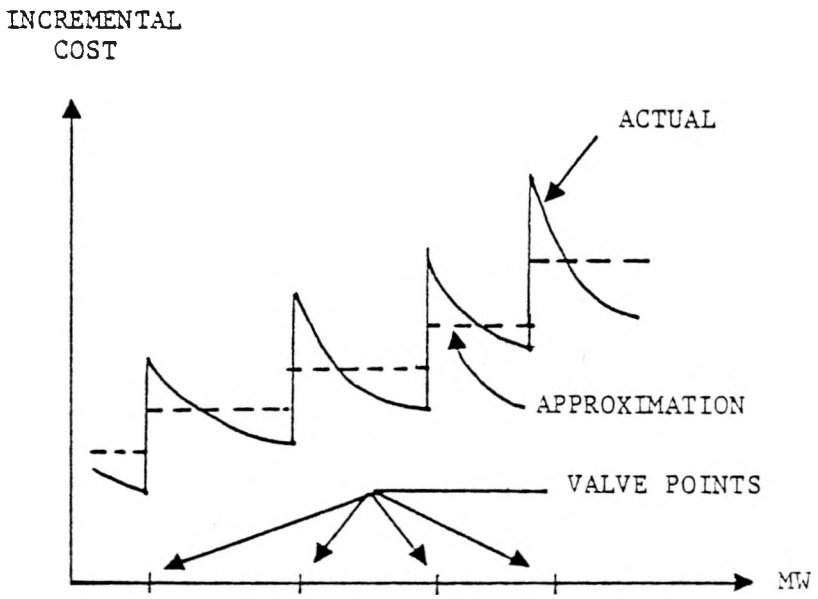

FIGURE 4.7 APPROXIMATION OF INCREMENTAL COST FUNCTION FOR MINMAR VALVE-POINT LOADING

approximation is made to the actual incremental cost. The step approximation is equal to the (estimated) average incremental cost between each pair of valve points. The approximation tends to hold a unit at a valve point until the incremental cost of generation on other units (as they pick up additional load) becomes equal to the incremental cost of the valve-point-loaded unit at its next valve point. At that point, the valve-point-loaded unit will move toward its next valve-point (in a load-rise period). Obviously this is only a crude approximation -- and the fact that the incremental cost representation does not have the sharp increases of the actual incremental cost curves may yield MINMAR solutions that have the unit away from valve-points for long periods. However, further DPSA iterations provide the mechanism for improving the solution.

When DPSA dispatches valve-point loaded units, it considers the unit cost function to have incremental cost discontinuities, as depicted in Figure 4.8, at the valve points. This representation is consistent with that of the actual incremental cost (Figure 4.7).

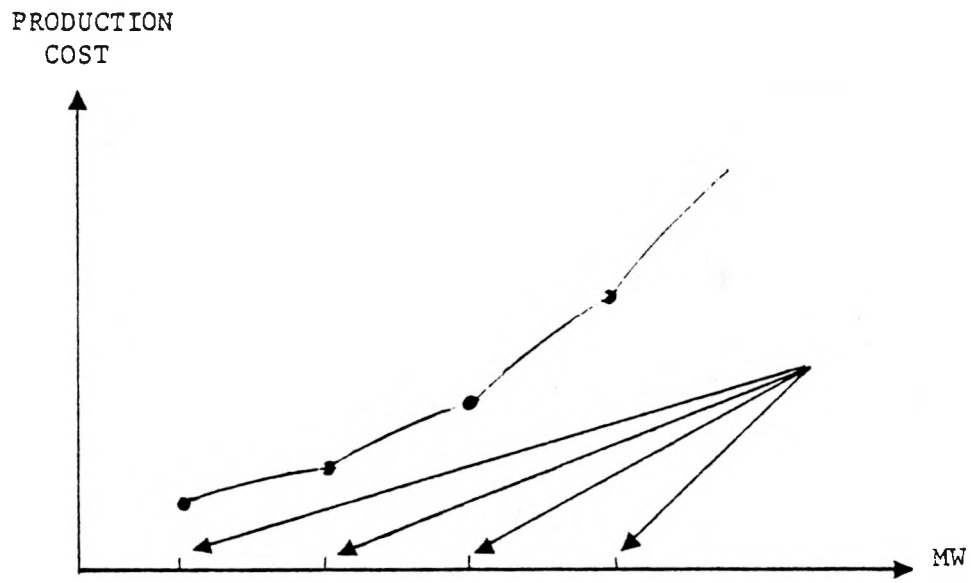

FIGURE 4.8 APPROXIMATION OF PRODUCTION COST FUNCTION FOR DPSA VALVE-POINT LOADING

Preliminary computational results for valve-point loading with DPSA and MINMAR are presented in Section 4.5.3.

4.5 KEY RESULTS

Presented in this section are results of studies done with the batch mode program, DPSA, applied on WEPCO units assuming all WEPCO units are to be dispatched except the base generation units, such as Point Beach units, Lakeside units and hydro units. The first page of the batch mode program lists all these unit data. (See Figure 4.9.) The contents of the figure are:

1st column	Unit number
2nd column	Rate limit in MW/MIN
3rd column	A*
4th column	B*
5th column	C*
6th column	Upper economic limit "in MW"
7th column	Lower economic limit "in MW"
8th column	Initial generation "in MW"

* A, B, C are coefficients of the cost function, when it is represented as a quadratic equation of unit generation, i.e.,

$$COST = A*(MW)^2 + B*(MW) + C$$

There are 15 generating units and one artificial unit to be dispatched. All 16 units are ordered in the order of their incremental costs. They are:

Unit 1	0.C.6
Unit 2	0.C.5
Unit 3	0.C.8
Unit 4	0.C.7
Unit 5	0.C.3
Unit 6	0.C.2
Unit 7	0.C.4
Unit 8	0.C.1

	RATE MW/MIN	COST FUNCTION COEFFICIENTS A,B,C			HIGH LIMIT MW	LOW LIMIT MW	INITIAL GENERATION MW
1	3.000	.005	5.627	261.180	225.000	70.000	190.000
2	3.000	.006	5.500	264.630	240.000	70.000	173.000
3	5.000	.004	6.383	190.502	285.000	110.000	162.000
4	5.000	.005	6.295	230.154	282.000	110.000	140.000
5	1.500	.007	6.654	112.922	114.000	30.000	64.000
6	1.500	.012	6.362	143.092	91.000	30.000	51.000
7	1.500	.012	6.515	135.334	105.000	40.000	45.000
8	1.500	.016	6.265	154.298	104.000	30.000	44.000
9	1.800	.022	7.750	95.100	70.000	35.000	35.000
10	1.800	.024	8.062	89.200	63.000	35.000	35.000
11	1.800	.030	7.667	99.960	77.000	35.000	35.000
12	1.800	.029	7.716	105.640	66.000	35.000	35.000
13	1.800	.030	8.317	91.140	77.000	35.000	35.000
14	3.000	.010	11.752	100.059	118.000	20.000	20.000
15	3.000	.009	11.993	101.790	116.000	20.000	20.000
16	100.000	.000	100.000	.000	50.000	-50.000	.000

FIGURE 4.9 PRINTOUT OF ALL UNIT DATA

Unit 9	P.W.5
Unit 10	P.W.3
Unit 11	P.W.4
Unit 12	P.W.1
Unit 13	P.W.2
Unit 14	V.2
Unit 15	V.1
Unit 16	Artificial Unit

Before any results are presented, it is necessary to explain the output format of the program, because some results will be presented merely in the form of computer outputs in later sections. The output format for both MINMAR and DPSA are identical and shown in Figure 4.10. The contents of the figure are:

FIRST LINE

First Column	Stage Number
Second Column	Net Generation Requirement (MW)
Third through Twelfth Columns	Dispatched Generations for each unit. When there are more than ten units, more than one line may be used (MW)

SECOND LINE

First Column	Total Optimum Cost up to the corresponding stage (dollars)
Second Column	Net Generation (MW)
Third through Twelfth Column	Incremental cost of each unit at its dispatched output. When there are more than ten units, more than one line may be used. ($/MWH)

The first and second lines explained above will be repeated as many times as the number of stages.

STAGE REQUIRED MW
COST ACTUAL MW

UNIT GENERATIONS
UNIT INCREMENTAL COSTS

1	1110	190	170	170	131	67	52	46	45	35	35
		35	35	35	20	20	0				
861	1110	7.651	7.652	7.646	7.647	7.651	7.641	7.648	7.666	9.300	9.750
		9.750	9.750	10.400	12.150	12.350	100.000				
2	1125	190	180	173	144	69	54	47	45	35	35
		35	35	35	20	20	0				
1732	1125	7.671	7.676	7.668	7.676	7.680	7.690	7.672	7.666	9.300	9.750
		9.750	9.750	10.400	12.150	12.350	100.000				
3	1138	200	182	177	140	70	54	48	46	35	35
		35	35	35	20	20	0				
2611	1138	7.692	7.701	7.698	7.695	7.695	7.690	7.697	7.697	9.300	9.750
		9.750	9.750	10.400	12.150	12.350	100.000				
4	1163	200	185	182	150	73	56	50	48	35	35
		35	35	35	20	20	0				
3506	1163	7.733	7.737	7.735	7.734	7.740	7.739	7.746	7.759	9.300	9.750
		9.750	9.750	10.400	12.150	12.350	100.000				
5	1175	200	187	185	152	74	57	51	48	35	35
		35	35	35	20	20	0				
4409	1175	7.754	7.761	7.757	7.753	7.755	7.764	7.771	7.759	9.300	9.750
		9.750	9.750	10.400	12.150	12.350	100.000				
6	1213	212	192	193	159	79	60	53	50	35	35
		35	35	35	20	20	0				
5339	1213	7.816	7.821	7.817	7.820	7.829	7.838	7.820	7.822	9.300	9.750
		9.750	9.750	10.400	12.150	12.350	100.000				
7	1275	222	201	207	170	85	64	57	54	35	35
		35	35	35	20	20	0				
6305	1275	7.919	7.930	7.921	7.926	7.918	7.936	7.918	7.906	9.300	9.750
		9.750	9.750	10.400	12.150	12.350	100.000				
8	1300	225	204	213	175	88	66	59	55	35	35
		35	35	35	20	20	0				
7289	1300	7.950	7.960	7.965	7.974	7.983	7.985	7.968	7.977	9.300	9.750
		9.750	9.750	10.400	12.150	12.350	100.000				
9	1338	225	211	223	182	94	69	62	57	35	35
		35	35	35	20	20	0				
8299	1338	7.950	8.050	8.039	8.041	8.052	8.059	8.042	8.039	9.300	9.750
		9.750	9.750	10.400	12.150	12.350	100.000				
10	1388	225	219	237	192	100	73	66	61	35	35
		35	35	35	20	20	0				
9343	1388	7.950	8.147	8.143	8.137	8.142	8.157	8.140	8.164	9.300	9.750
		9.750	9.750	10.400	12.150	12.350	100.000				
11	1438	225	227	250	203	107	77	70	64	35	35
		35	35	35	20	20	0				
10421	1438	7.950	8.243	8.240	8.242	8.246	8.256	8.238	8.257	9.300	9.750

		9.750	9.750	10.400	12.150	12.350	100.000				
12	1475	225	233	260	211	112	80	73	66	35	35
		35	35	35	20	20	0				
11525	1475	7.950	8.310	8.314	8.319	8.320	8.330	8.312	8.319	9.300	9.750
		9.750	9.750	10.400	12.150	12.350	100.000				
13	1525	225	240	276	223	114	84	78	70	35	35
		35	35	35	20	20	0				
12063	1525	7.950	8.400	8.433	8.434	8.350	8.428	8.435	8.443	9.300	9.750
		9.750	9.750	10.400	12.150	12.350	100.000				
14	1563	225	240	285	237	114	90	83	74	35	35
		35	35	35	20	20	0				
13828	1563	7.950	8.400	8.500	8.568	8.350	8.575	8.558	8.568	9.300	9.750
		9.750	9.750	10.400	12.150	12.350	100.000				
15	1600	225	240	285	259	114	91	90	81	35	35
		35	35	35	20	20	0				
15020	1600	7.950	8.400	8.500	8.774	8.350	8.640	8.731	8.785	9.300	9.750
		9.750	9.750	10.400	12.150	12.350	100.000				
16	1630	225	240	285	276	114	91	97	87	35	35
		35	35	35	20	20	0				
16235	1630	7.950	8.400	8.500	8.942	8.350	8.600	8.903	8.972	9.300	9.750
		9.750	9.750	10.400	12.150	12.350	100.000				

FIGURE 4.10 SAMPLE OUTPUT OF MINMAR OR DPSA ECONOMIC DISPATCH OF GENERATING UNITS

4.5.1 Demonstration of Look Ahead Ability of DPSA As Opposed to Stage-Wise MINMAR Dispatch

In general, the most rapid change in load can be seen during the early morning pickup of a typical peak summer day. Also, because of the high peak load in the early afternoon period, a quite large schedule import often occurs. Throughout such a load scenario, the base generations, such as outputs from Point Beach units, Lakeside units and hydro units, remain unchanged. Case 1 of Figure 4.11 indicates the portion of load to be dispatched for such an early summer morning pickup which is obtained by subtracting the base generations from the load during the period. The summer morning load data used here was obtained by interpolating the actual hourly integrated WEPCO load for the peak 1977 summer day. Also seen on the same figure is a case with a schedule change. A large schedule import was suggested by WEPCO to make the load scenario correspond to large changes in generation requirement that sometime occur at WEPCO. Here, a 325 MW schedule is to be imported during the 10 minute interval between 5 minutes before and 5 minutes after 7:00 a.m.

Figure 4.12 and 4.13 show optimal economic dispatching of generating units for Case 1 using MINMAR and DPSA respectively. Since there was no rate limit violation that occurred in the stage-wise MINMAR economic dispatching of actual units only, the two figures theoretically should look identical. The two figures exhibit slight differences in the overall trajectories of some units, however, the total costs of both methods are the same. For instance, in stage 4, i.e., four 5-minute intervals into the dispatch horizon, the MINMAR and DPSA results for units 2 and 4 differ by 1 MW. There are numerous such 1 MW differences throughout the dispatch horizon. Yet these differences lead to no cost differences between the MINMAR and DPSA solutions, neither at individual stages nor for the entire dispatch horizon.

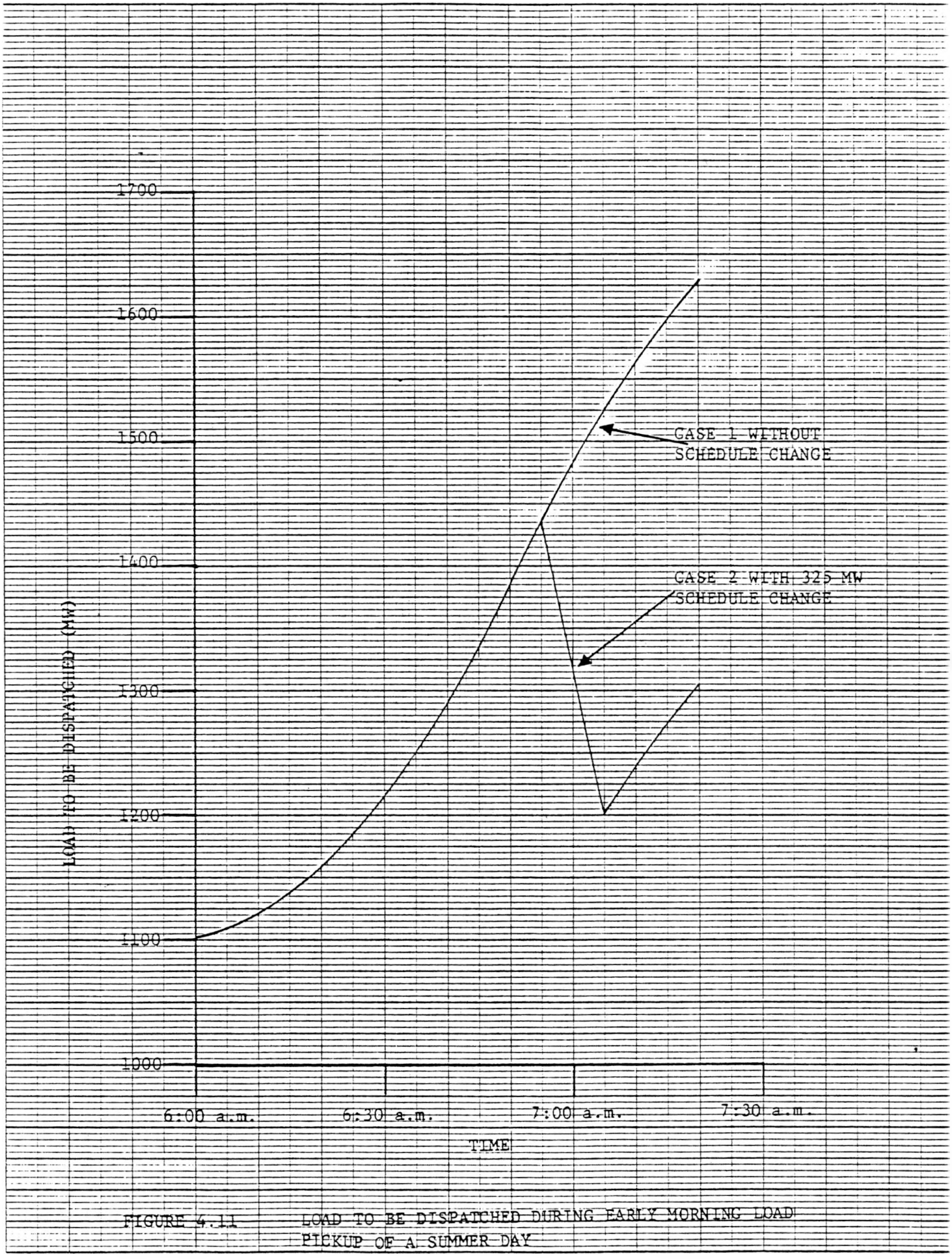

FIGURE 4.11 LOAD TO BE DISPATCHED DURING EARLY MORNING LOAD PICKUP OF A SUMMER DAY

STAGE REQUIRED MW COST ACTUAL MW		UNIT GENERATIONS UNIT INCREMENTAL COSTS									
1	1110	190 35	170 35	170 35	141 20	67 20	52 0	48	45	35	35
981	1110	7.651 9.750	7.652 9.750	7.648 10.400	7.647 12.150	7.651 12.350	7.641 100.000	7.648	7.600	9.300	9.
2	1125	190 35	180 35	173 35	144 20	69 20	54 0	47	45	35	35
1732	1125	7.671 9.750	7.676 9.750	7.668 10.400	7.676 12.150	7.680 12.350	7.690 100.000	7.672	7.666	9.300	9.750
3	1138	200 35	182 35	177 35	146 20	70 20	54 0	48	46	35	35
2611	1138	7.692 9.750	7.701 9.750	7.698 10.400	7.695 12.150	7.695 12.350	7.690 100.000	7.697	7.697	9.300	9.750
4	1163	200 35	185 35	182 35	150 20	73 20	56 0	50	48	35	35
3506	1163	7.733 9.750	7.737 9.750	7.735 10.400	7.734 12.150	7.740 12.350	7.739 100.000	7.746	7.759	9.300	9.750
5	1175	200 35	187 35	185 35	152 20	74 20	57 0	51	48	35	35
4409	1175	7.754 9.750	7.761 9.750	7.757 10.400	7.753 12.150	7.755 12.350	7.764 100.000	7.771	7.759	9.300	9.750
6	1213	212 35	192 35	193 35	159 20	79 20	60 0	53	50	35	35
5136	1213	7.816 9.750	7.821 9.750	7.817 10.400	7.820 12.150	7.829 12.350	7.818 100.000	7.820	7.822	9.300	9.750
7	1275	222 35	201 35	207 35	170 20	85 20	64 0	57	54	35	35
6305	1275	7.919 9.750	7.930 9.750	7.921 10.400	7.926 12.150	7.918 12.350	7.936 100.000	7.919	7.946	9.300	9.750
8	1300	225 35	204 35	213 35	175 20	88 20	66 0	59	55	35	35
7289	1300	7.950 9.750	7.966 9.750	7.965 10.400	7.974 12.150	7.983 12.350	7.985 100.000	7.968	7.977	9.300	9.750
9	1338	225 35	211 35	223 35	192 20	94 20	69 0	62	57	35	35
8299	1338	7.950 9.750	8.050 9.750	8.039 10.400	8.041 12.150	8.052 12.350	8.059 100.000	8.042	8.039	9.300	9.750
10	1368	225 35	219 35	237 35	192 20	100 20	73 0	66	61	35	35
9343	1368	7.950 9.750	8.147 9.750	8.143 10.400	8.137 12.150	8.142 12.350	8.157 100.000	8.140	8.164	9.300	9.750
11	1438	225 35	227 35	250 35	203 20	107 20	77 0	70	64	35	35
10421	1438	7.950	8.243	8.240	8.242	8.246	8.256	8.238	8.257	9.300	9.750

		9.750	9.750	10.400	12.150	12.350	100.000				
12	1475	225 35	233 35	260 35	211 20	112 20	80 0	73	66	35	35
11525	1475	7.950 9.750	8.316 9.750	8.314 10.400	8.319 12.150	8.320 12.350	8.330 100.000	8.312	8.319	9.300	9.750
13	1525	225 35	240 35	276 35	223 20	114 20	84 0	78	70	35	35
12003	1525	7.950 9.750	8.400 9.750	8.433 10.400	8.434 12.150	8.350 12.350	8.428 100.000	8.435	8.443	9.300	9.750
14	1563	225 35	240 35	285 35	237 20	114 20	90 0	83	74	35	35
13828	1563	7.950 9.750	8.400 9.750	8.500 10.400	8.568 12.150	8.350 12.350	8.575 100.000	8.558	8.568	9.300	9.750
15	1600	225 35	240 35	285 35	259 20	114 20	91 0	90	81	35	35
15020	1600	7.950 9.750	8.400 9.750	8.506 10.400	8.774 12.150	8.350 12.350	8.600 100.000	8.731	8.795	9.300	9.750
16	1630	225 35	240 35	285 35	278 20	114 20	91 0	97	87	35	35
16235	1630	7.950 9.750	8.400 9.750	8.500 10.400	8.942 12.150	8.350 12.350	8.600 100.000	8.903	8.972	9.300	9.

FIGURE 4.12 MINMAR ECONOMIC DISPATCH OF GENERATING UNITS FOR CASE 1

/ AGE REQUIRED MW
COST ACTUAL MW

UNIT GENERATIONS
UNIT INCREMENTAL COSTS

1	1110	190	175	169	142	67	52	46	45	35	35
		35	35	35	20	20	0				
861	1110	7.651	7.652	7.638	7.657	7.651	7.641	7.648	7.666	9.300	9.750
		9.750	9.750	10.400	12.150	12.350	100.000				
2	1125	198	180	173	144	69	54	47	45	35	35
		35	35	35	20	20	0				
1732	1125	7.671	7.676	7.668	7.676	7.660	7.690	7.672	7.666	9.300	9.750
		9.750	9.750	10.400	12.150	12.350	100.000				
3	1138	200	182	177	146	70	54	48	46	35	35
		35	35	35	20	20	0				
2611	1138	7.692	7.701	7.698	7.695	7.695	7.690	7.697	7.697	9.300	9.750
		9.750	9.750	10.400	12.150	12.350	100.000				
4	1163	204	184	182	151	73	56	50	48	35	35
		35	35	35	20	20	0				
3506	1153	7.733	7.725	7.735	7.743	7.740	7.739	7.746	7.759	9.300	9.750
		9.750	9.750	10.400	12.150	12.350	100.000				
5	1175	206	187	185	152	74	57	51	48	35	35
		35	35	35	20	20	0				
4409	1175	7.758	7.761	7.757	7.753	7.755	7.764	7.771	7.759	9.300	9.750
		9.750	9.750	10.400	12.150	12.350	100.000				
6	1213	212	192	193	159	79	60	53	50	35	35
		35	35	35	20	20	0				
5339	1213	7.810	7.821	7.817	7.820	7.829	7.838	7.820	7.822	9.300	9.750
		9.750	9.750	10.400	12.150	12.350	100.000				
7	1275	222	201	207	170	85	64	57	54	35	35
		35	35	35	20	20	0				
6305	1275	7.919	7.930	7.921	7.926	7.918	7.936	7.918	7.946	9.300	9.750
		9.750	9.750	10.400	12.150	12.350	100.000				
8	1300	225	204	213	174	89	66	59	55	35	35
		35	35	35	20	20	0				
7289	1300	7.950	7.965	7.965	7.964	7.978	7.985	7.968	7.977	9.300	9.750
		9.750	9.750	10.400	12.150	12.350	100.000				
9	1338	225	210	224	182	94	68	62	58	35	35
		35	35	35	20	20	0				
8299	1338	7.952	8.038	8.047	8.041	8.052	8.034	8.042	8.070	9.300	9.750
		9.750	9.750	10.400	12.150	12.350	100.000				
10	1388	225	219	230	195	100	73	66	61	35	35
		35	35	35	20	20	0				
9303	1388	7.950	8.147	8.136	8.140	8.142	8.157	8.140	8.164	9.300	9.750
		9.750	9.750	10.400	12.150	12.350	100.000				
11	1438	225	220	250	204	107	76	71	64	35	35
		35	35	35	20	20	0				
10421	1438	7.950	8.231	8.240	8.252	8.246	8.231	8.263	8.257	9.300	9.750

		9.750	9.750	10.400	12.150	12.350	100.000				
12	1475	225	233	260	211	112	79	74	66	35	35
		35	35	35	20	20	0				
11525	1475	7.950	8.316	8.314	8.319	8.320	8.305	8.337	8.319	9.300	9.750
		9.750	9.750	10.400	12.150	12.350	100.000				
13	1525	225	240	276	223	114	84	78	70	35	35
		35	35	35	20	20	0				
12003	1525	7.950	8.400	8.433	8.434	8.350	8.428	8.435	8.443	9.300	9.750
		9.750	9.750	10.400	12.150	12.350	100.000				
14	1563	225	240	285	237	114	89	84	74	35	35
		35	35	35	20	20	0				
13428	1563	7.950	8.400	8.500	8.566	8.550	8.551	8.583	8.568	9.300	9.750
		9.750	9.750	10.400	12.150	12.350	100.000				
15	1600	225	240	285	259	114	91	91	80	35	35
		35	35	35	20	20	0				
15020	1600	7.950	8.400	8.500	8.779	8.550	8.600	8.755	8.754	9.300	9.750
		9.750	9.750	10.400	12.150	12.350	100.000				
16	1638	225	240	285	270	114	91	98	86	35	35
		35	35	35	20	20	0				
16235	1638	7.950	8.400	8.500	8.942	8.550	8.600	8.928	8.941	9.300	9.750
		9.750	9.750	10.400	12.150	12.350	100.000				

FIGURE 4.13 DPSA ECONOMIC DISPATCH OF GENERATING UNITS FOR CASE 1

This fact indicates that depending on the discretization of both MW outputs and cost curves in the program, there may exist multiple optimum trajectories within the tolerance.

Figure 4.14 and 4.15 are optimal economic dispatching of generating units for Case 2 using MINMAR and DPSA respectively. Here, we notice that on Figure 4.14, the artificial unit is dispatched at 12th and 13th stage. The negative output dispatch of the artificial unit indicates that the load was decreasing at the higher rate than the stage-wise dispatch can handle. Even though the aggregate rate limit of actual units can follow the sudden schedule change, the stage-wise dispatching approach of MINMAR could not yield a dispatch without using the artificial unit. The reason for this is that Units 9 through 15 had been operated at their lower economic limits during the previous stages and therefore could not contribute to meeting the sudden decrease in the load without the look ahead capability. However, using the trajectories given in Figure 4.14 as the initial trajectories, DPSA is able to remove the output of the artificial unit and reallocate it to the actual units (see Figure 4.15). Also to be noted on the same figure is that Units 9 and 10 generate more output at the 10th and 11th stages than in the stage-wise dispatch of MINMAR which is compensated for by slight drops in the outputs of Units 2, 3, 5-8. Even though the total units' output at these stages exactly meets the net generation requirement, the rate of response capability for later time stages has been increased by moving Units 9 and 10 up from their minimum outputs. This extra generation of Units 9 and 10 at Stages 10 and 11 is later used as "reserved" rate of response when there is a sudden decrease in the load. This is the look ahead capability of the DPSA method of economic dispatch which any stage-wise dispatching scheme does not have.

STAGE REQUIRED MW / COST ACTUAL MW		UNIT GENERATIONS / UNIT INCREMENTAL COSTS									
1	1110	196	176	170	141	67	52	46	45	35	35
		35	35	35	20	20	0				
861	1110	7.651	7.652	7.646	7.647	7.651	7.641	7.648	7.666	9.300	9.750
		9.750	9.750	10.400	12.150	12.350	100.000				
2	1125	198	180	173	144	69	54	47	45	35	35
		35	35	35	20	20	0				
1732	1125	7.671	7.676	7.668	7.676	7.680	7.690	7.672	7.666	9.300	9.750
		9.750	9.750	10.400	12.150	12.350	100.000				
3	1138	200	182	177	146	70	54	48	46	35	35
		35	35	35	20	20	0				
2611	1138	7.692	7.701	7.698	7.695	7.695	7.690	7.697	7.697	9.300	9.750
		9.750	9.750	10.400	12.150	12.350	100.000				
4	1161	204	185	182	150	73	56	50	48	35	35
		35	35	35	20	20	0				
3506	1161	7.733	7.737	7.735	7.734	7.740	7.739	7.746	7.759	9.300	9.750
		9.750	9.750	10.400	12.150	12.350	100.000				
5	1175	206	187	185	152	74	57	51	48	35	35
		35	35	35	20	20	0				
4404	1175	7.754	7.761	7.757	7.753	7.755	7.764	7.771	7.759	9.300	9.750
		9.750	9.750	10.400	12.150	12.350	100.000				
6	1213	212	192	193	159	79	60	53	50	35	35
		35	35	35	20	20	0				
5330	1213	7.816	7.821	7.817	7.820	7.829	7.838	7.820	7.822	9.300	9.750
		9.750	9.750	10.400	12.150	12.350	100.000				
7	1275	222	201	207	170	85	64	57	54	35	35
		35	35	35	20	20	0				
6305	1275	7.919	7.930	7.921	7.926	7.918	7.936	7.918	7.906	9.300	9.750
		9.750	9.750	10.400	12.150	12.350	100.000				
8	1300	225	204	213	175	88	66	59	55	35	35
		35	35	35	20	20	0				
7289	1300	7.950	7.946	7.965	7.974	7.963	7.985	7.966	7.977	9.300	9.750
		9.750	9.750	10.400	12.150	12.350	100.000				
9	1336	225	211	223	182	94	69	62	57	35	35
		35	35	35	20	20	0				
8299	1336	7.950	8.050	8.039	8.041	8.052	8.059	8.042	8.039	9.300	9.750
		9.750	9.750	10.400	12.150	12.350	100.000				
10	1360	225	219	232	192	100	73	66	61	35	35
		35	35	35	20	20	0				
9343	1360	7.950	8.147	8.143	8.137	8.142	8.157	8.140	8.164	9.300	9.750
		9.750	9.750	10.400	12.150	12.350	100.000				
11	1436	225	227	250	203	107	77	70	64	35	35
		35	35	35	20	20	0				
10421	1436	7.950	8.243	8.240	8.242	8.246	8.256	8.238	8.257	9.300	9.750

10/02/78 10:21:38 SKIM 0373AAv.15 000373 3 99 DATE 100278 PAGE 29

		9.750	9.750	10.400	12.150	12.350	100.000				
12	1313	211	212	225	178	100	70	63	57	35	35
		35	35	35	20	20	18				
11577	1313	7.905	8.082	8.054	8.062	8.102	8.084	8.066	8.039	9.300	9.750
		9.750	9.750	10.400	12.150	12.350	100.000				
13	1200	197	197	200	153	93	63	56	50	35	35
		35	35	35	20	20	24				
12712	1200	7.881	7.881	7.869	7.862	8.038	7.911	7.894	7.822	9.300	9.750
		9.750	9.750	10.400	12.150	12.350	100.000				
14	1239	212	195	199	163	86	61	55	52	35	35
		35	35	35	20	20	0				
13056	1238	7.816	7.857	7.861	7.850	7.933	7.862	7.869	7.884	9.300	9.750
		9.750	9.750	10.400	12.150	12.350	100.000				
15	1275	222	201	207	170	85	64	57	54	35	35
		35	35	35	20	20	0				
14024	1275	7.919	7.930	7.921	7.926	7.918	7.936	7.918	7.906	9.300	9.750
		9.750	9.750	10.400	12.150	12.350	100.000				
16	1305	225	205	215	175	89	66	60	55	35	35
		35	35	35	20	20	0				
15012	1305	7.950	7.978	7.980	7.974	7.978	7.985	7.992	7.977	9.300	9.750
		9.750	9.750	10.400	12.150	12.350	100.000				

FIGURE 4.14 MINMAR ECONOMIC DISPATCH OF GENERATING UNITS FOR CASE 2

STAGE REQUIRED MW
COST ACTUAL MW

UNIT GENERATIONS
UNIT INCREMENTAL COSTS

1	1110	196	177	170	142	87	52	46	45	35	35
		35	35	35	20	20	0				
881	1110	7.651	7.640	7.646	7.657	7.651	7.641	7.648	7.646	9.300	9.
		9.750	9.750	10.400	12.150	12.350	100.000				
2	1125	198	180	173	144	89	54	47	45	35	35
		35	35	35	20	20	0				
1732	1125	7.671	7.676	7.666	7.676	7.680	7.690	7.672	7.666	9.300	9.750
		9.750	9.750	10.400	12.150	12.350	100.000				
3	1138	200	182	177	146	70	54	48	46	35	35
		35	35	35	20	20	0				
2611	1138	7.692	7.701	7.698	7.695	7.695	7.690	7.697	7.697	9.300	9.750
		9.750	9.750	10.400	12.150	12.350	100.000				
4	1163	204	184	182	151	73	56	50	48	35	35
		35	35	35	20	20	0				
3506	1163	7.733	7.725	7.735	7.743	7.740	7.739	7.746	7.759	9.300	9.750
		9.750	9.750	10.400	12.150	12.350	100.000				
5	1175	206	187	185	154	74	57	51	48	35	35
		35	35	35	20	20	0				
4409	1175	7.754	7.761	7.757	7.753	7.755	7.764	7.771	7.759	9.300	9.750
		9.750	9.750	10.400	12.150	12.350	100.000				
6	1213	212	192	193	159	79	60	53	50	35	35
		35	35	35	20	20	0				
5330	1213	7.818	7.821	7.817	7.820	7.829	7.838	7.820	7.822	9.300	9.750
		9.750	9.750	10.400	12.150	12.350	100.000				
7	1275	222	201	207	170	85	64	57	54	35	35
		35	35	35	20	20	0				
6305	1275	7.919	7.930	7.921	7.926	7.918	7.936	7.918	7.946	9.300	9.750
		9.750	9.750	10.400	12.150	12.350	100.000				
8	1300	225	204	212	175	89	66	59	55	35	35
		35	35	35	20	20	0				
7259	1300	7.950	7.946	7.958	7.974	7.976	7.985	7.968	7.977	9.300	9.750
		9.750	9.750	10.400	12.150	12.350	100.000				
9	1338	225	210	224	182	94	68	62	58	35	35
		35	35	35	20	20	0				
8299	1338	7.950	8.036	8.047	8.041	8.052	8.034	8.042	8.070	9.300	9.750
		9.750	9.750	10.400	12.150	12.350	100.000				
10	1388	225	218	237	193	100	73	62	58	42	35
		35	35	35	20	20	0				
9344	1388	7.950	8.135	8.143	8.146	8.142	8.157	8.042	8.070	9.610	9.750
		9.750	9.750	10.400	12.150	12.350	100.000				
11	1438	225	221	244	200	101	75	66	61	50	39
		37	38	35	20	20	0				
10425	1438	7.950	8.171	8.195	8.271	8.157	8.207	8.140	8.164	9.984	9.983

		9.869	9.929	10.400	12.150	12.350	100.000				
12	1313	210	200	219	181	94	68	59	54	42	35
		35	35	35	20	20	0				
11419	1313	7.795	7.990	8.010	8.031	8.052	8.034	7.968	7.946	9.610	9.750
		9.750	9.750	10.400	12.150	12.350	100.000				
13	1200	197	191	194	158	87	61	52	47	35	35
		35	35	35	20	20	0				
12339	1200	7.661	7.809	7.824	7.791	7.948	7.882	7.795	7.728	9.300	9.750
		9.750	9.750	10.400	12.150	12.350	100.000				
14	1238	212	195	200	165	82	61	55	53	35	35
		35	35	35	20	20	0				
13283	1238	7.816	7.857	7.864	7.878	7.874	7.882	7.869	7.915	9.300	9.750
		9.750	9.750	10.400	12.150	12.350	100.000				
15	1275	222	201	207	170	85	64	57	54	35	35
		35	35	35	20	20	0				
14251	1275	7.919	7.930	7.921	7.926	7.918	7.936	7.918	7.946	9.300	9.750
		9.750	9.750	10.400	12.150	12.350	100.000				
16	1305	225	205	215	175	89	66	60	55	35	35
		35	35	35	20	20	0				
15239	1305	7.950	7.978	7.980	7.974	7.978	7.985	7.992	7.977	9.300	9.
		9.750	9.750	10.400	12.150	12.350	100.000				

FIGURE 4.15 DPSA ECONOMIC DISPATCH OF GENERATING UNITS FOR CASE 2

4.5.2 Effect of Pairing Choices on the Convergence Behavior

As explained in previous section, in addition to the initial trajectories of units, DPSA also needs a specification of the pairings between units. Obviously, one way of pairing units for DPSA is to pair units in all possible combinations. Even though this pairing scheme will yield a true optimal dispatch of all generating units, it will require a large number of pairs, that is, n x (n-1)/2 pairs when n units are to be dispatched, and thus requires very long computational time per iteration. Other than the all-possible-pairing scheme, we studied three simpler pairing schemes. For all schemes described below the units are numbered in the order of their incremental costs, i.e., the first unit being the cheapest and the n-th unit being the most expensive unit. For all three schemes, the artificial unit will be introduced into the pairing scheme as follows. First, the artificial unit is paired with each actual unit in succession. This is done as the first attempt to unload the output of the artificial unit into actual units. Secondly, the actual units will be paired according to the pairing scheme chosen. These two steps together comprises what we call a "single DPSA iteration".

Scheme 1: Circular Pairing

In this scheme, a unit is paired with the next cheapest unit. In other words, Unit 1 is paired with Unit 2, then Unit 2 with Unit 3, and when nth unit is paired with Unit 1, it will complete a circle. Using 15 units, an example of this pairing is shown in Figure 4.16.

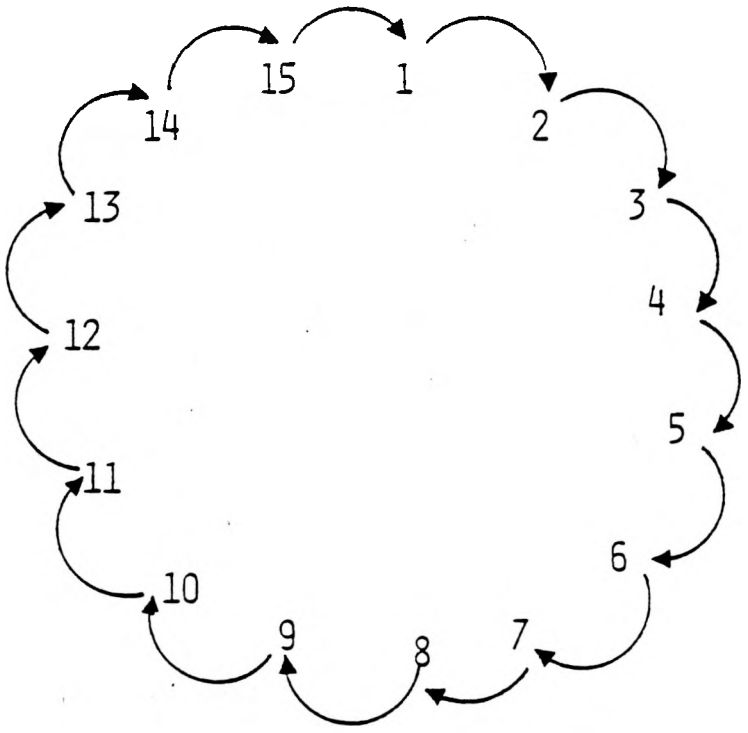

Pair 1	1 and 2	Pair 9	9 and 10
Pair 2	2 and 3	Pair 10	10 and 11
Pair 3	3 and 4	Pair 11	11 and 12
Pair 4	4 and 5	Pair 12	12 and 13
Pair 5	5 and 6	Pair 13	13 and 14
Pair 6	6 and 7	Pair 14	14 and 15
Pair 7	7 and 8	Pair 15	15 and 1
Pair 8	8 and 9		

FIGURE 4.16 CIRCULAR PAIRING OF 15 UNITS

Scheme 2: Spiral Pairing

In this scheme, the cheapest unit will be paired with the most expensive unit, at first. Then the most expensive unit will be paired with the second cheapest unit, then, the second cheapest unit with the second most expensive unit, and so forth. Using 15 units, an example is shown in Figure 4.17.

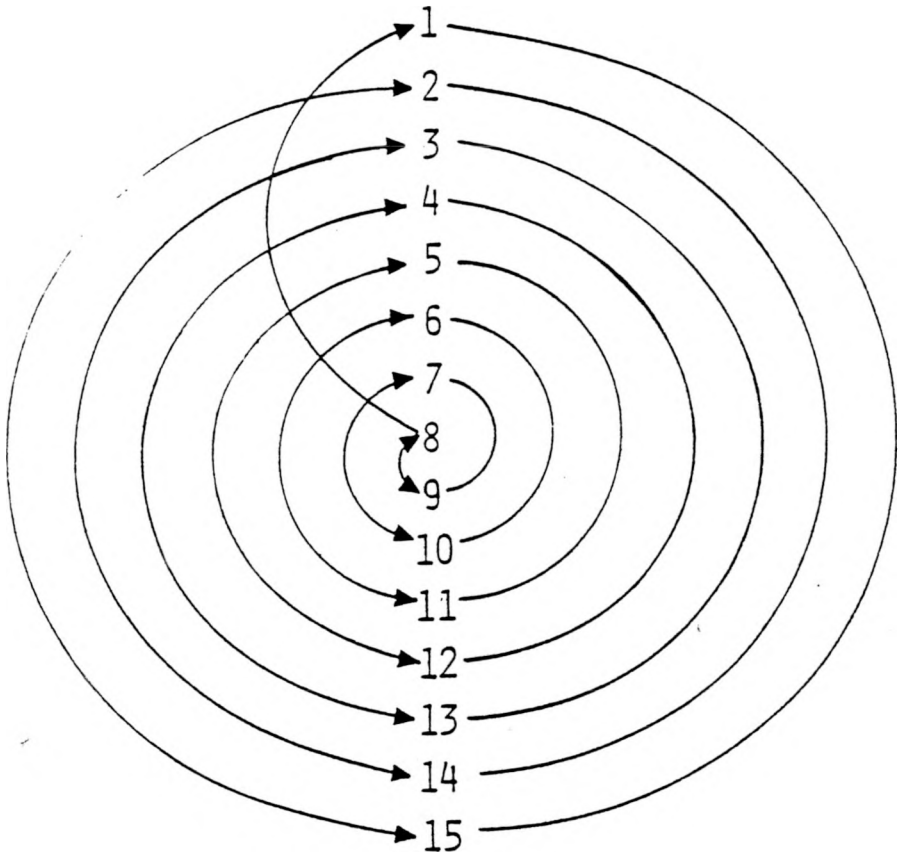

Pair 1	1 and 15	Pair 9	5 and 11
Pair 2	15 and 2	Pair 10	11 and 6
Pair 3	2 and 14	Pair 11	6 and 10
Pair 4	14 and 3	Pair 12	10 and 7
Pair 5	3 and 13	Pair 13	7 and 9
Pair 6	13 and 4	Pair 14	9 and 8
Pair 7	4 and 12	Pair 15	8 and 1
Pair 8	12 and 5		

FIGURE 4.17 SPIRAL PAIRING OF 15 UNITS

Scheme 3:

This scheme is about midway between the two schemes previously explained. Each pair contains two units which are very similar nor which are drastically different in cost. All pairs in this scheme contain approximately the same difference in cost between the paired units. See Figure 4.18

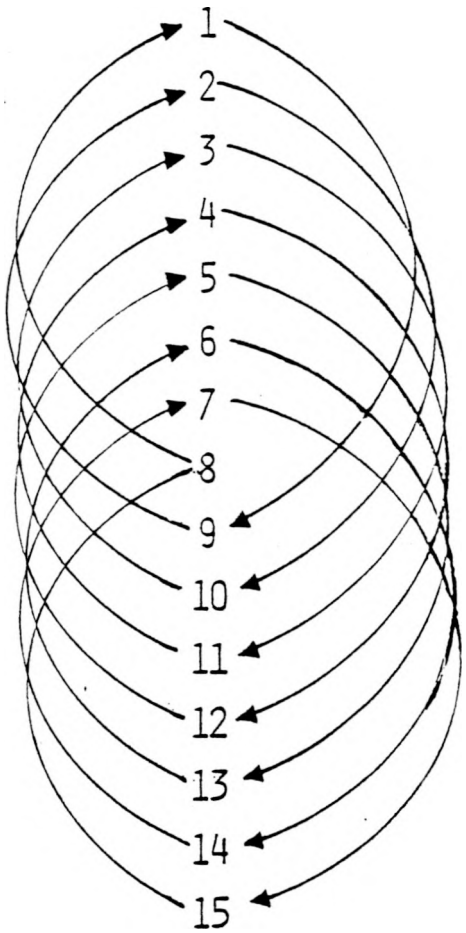

Pair 1	1 and 9
Pair 2	9 and 2
Pair 3	2 and 10
Pair 4	10 and 3
Pair 5	3 and 11
Pair 6	11 and 4
Pair 7	4 and 12
Pair 8	12 and 5
Pair 9	5 and 13
Pair 10	13 and 6
Pair 11	6 and 14
Pair 12	14 and 7
Pair 13	7 and 15
Pair 14	15 and 8
Pair 15	8 and 1

FIGURE 4.18 ILLUSTRATION OF PAIRING SCHEME 3

- To study the convergence behavior of each pairing scheme, the initial trajectories of units should be consistent for all schemes. This is done by dispatching units initially through the MINMAR method. Case 2 is used for the load to be dispatched in our study. Then, the all-possible-pairing scheme is first used to find the true optimal trajectories of units and the true optimal total cost. The true optimal cost becomes a reference against which the three pairing schemes are compared.

Each of the three different pairing schemes are used, one at a time, in conjunction with DPSA dispatch method. Figure 4.19 through 4.23 are results from these runs. To see the convergence behavior more clearly, total cost versus CPU time for all pairing schemes are plotted together on Figure 4.24. The Pairing Scheme 1 yielded the closest optimum cost of $15,239 versus $15,238 of all pairing schemes, and Scheme 3 yielded the fastest convergence. However, as shown in Figure 4.24, the differences between different pairing schemes are quite minimal. Having experimented with the above three pairing schemes, we concluded that no particular scheme results in the best overall computational results.

STAGE REQUIRED MW
COST ACTUAL MW

UNIT GENERATION
UNIT INCREMENTAL COSTS

1	1110	190	175	170	141	87	52	46	45	35	35
		35	35	35	20	20	0				
881	1110	7.651	7.652	7.646	7.647	7.651	7.641	7.648	7.666	9.300	9.7
		9.750	9.750	10.400	12.150	12.350	100.000				
2	1125	196	180	173	144	89	54	47	45	35	35
		35	35	35	20	20	0				
1732	1125	7.671	7.676	7.668	7.676	7.660	7.690	7.672	7.666	9.300	9.750
		9.750	9.750	10.400	12.150	12.350	100.000				
3	1138	200	182	177	146	90	54	48	46	35	35
		35	35	35	20	20	0				
2811	1138	7.692	7.701	7.698	7.695	7.695	7.690	7.697	7.697	9.300	9.750
		9.750	9.750	10.400	12.150	12.350	100.000				
4	1163	204	185	182	150	93	56	50	48	35	35
		35	35	35	20	20	0				
3508	1163	7.733	7.737	7.735	7.734	7.740	7.739	7.746	7.759	9.300	9.750
		9.750	9.750	10.400	12.150	12.350	100.000				
5	1175	208	187	185	152	94	57	51	48	35	35
		35	35	35	20	20	0				
4409	1175	7.754	7.761	7.757	7.753	7.755	7.764	7.771	7.759	9.300	9.750
		9.750	9.750	10.400	12.150	12.350	100.000				
6	1213	212	192	193	159	99	60	53	50	35	35
		35	35	35	20	20	0				
5330	1213	7.816	7.821	7.817	7.820	7.829	7.838	7.820	7.822	9.300	9.750
		9.750	9.750	10.400	12.150	12.350	100.000				
7	1275	222	201	207	170	85	64	57	54	35	35
		35	35	35	20	20	0				
6305	1275	7.919	7.930	7.921	7.926	7.916	7.936	7.918	7.906	9.300	9.750
		9.750	9.750	10.400	12.150	12.350	100.000				
8	1300	225	204	213	175	88	66	59	55	35	35
		35	35	35	20	20	0				
7269	1300	7.950	7.948	7.965	7.974	7.943	7.985	7.966	7.977	9.300	9.750
		9.750	9.750	10.400	12.150	12.350	100.000				
9	1338	225	211	223	182	94	69	62	57	35	35
		35	35	35	20	20	0				
8299	1338	7.950	8.051	8.038	8.041	8.052	8.059	8.042	8.039	9.300	9.750
		9.750	9.750	10.400	12.150	12.350	100.000				
10	1388	225	219	237	192	100	73	66	61	35	35
		35	35	35	20	20	0				
9343	1388	7.950	8.147	8.143	8.137	8.142	8.157	8.140	8.164	9.300	9.750
		9.750	9.750	10.400	12.150	12.350	100.000				
11	1438	225	227	250	203	107	77	70	64	35	35
		35	35	35	20	20	0				
10421	1438	7.950	8.243	8.248	8.242	8.248	8.256	8.238	8.257	9.300	9.750

		9.750	9.750	10.400	12.150	12.350	100.000				
12	1513	211	212	225	178	100	70	63	57	35	35
		35	35	35	20	20	-18				
11577	1313	7.805	8.062	8.058	8.002	8.142	8.084	8.066	8.039	9.300	9.750
		9.750	9.750	10.400	12.150	12.350	100.000				
13	1200	197	197	200	153	93	63	56	50	35	35
		35	35	35	20	20	-24				
12712	1200	7.681	7.681	7.869	7.762	8.038	7.911	7.894	7.822	9.300	9.750
		9.750	9.750	10.400	12.150	12.350	100.000				
14	1238	212	195	199	163	96	61	55	52	35	35
		35	35	35	20	20	0				
13658	1238	7.818	7.857	7.861	7.858	7.933	7.842	7.869	7.888	9.300	9.750
		9.750	9.750	10.400	12.150	12.350	100.000				
15	1275	222	201	207	170	85	64	57	54	35	35
		35	35	35	20	20	0				
14629	1275	7.919	7.930	7.921	7.926	7.916	7.936	7.918	7.906	9.300	9.750
		9.750	9.750	10.400	12.150	12.350	100.000				
16	1305	225	205	215	175	89	66	60	55	35	35
		35	35	35	20	20	0				
15612	1305	7.950	7.978	7.980	7.974	7.978	7.985	7.992	7.977	9.300	9
		9.750	9.750	10.400	12.150	12.350	100.000				

FIGURE 4.19 INITIAL TRAJECTORY USED FOR THE CONVERGENCE BEHAVIOR STUDY (MINMAR ECONOMIC DISPATCH FOR CASE 2)

STAGE REQUIRED MW
COST ACTUAL MW

UNIT GENERATIONS
UNIT INCREMENTAL COSTS

1	1110	140	178	170	142	67	52	46	44	35	35
		35	35	35	20	20	0				
661	1110	7.651	7.652	7.646	7.657	7.651	7.641	7.648	7.635	9.300	9.750
		9.750	9.750	10.400	12.150	12.350	100.000				
2	1125	198	180	173	144	69	54	47	45	35	35
		35	35	35	20	20	0				
1732	1125	7.671	7.678	7.668	7.670	7.680	7.690	7.672	7.666	9.300	9.750
		9.750	9.750	10.400	12.150	12.350	100.000				
3	1138	200	182	177	146	70	54	48	46	35	35
		35	35	35	20	20	0				
2811	1138	7.692	7.701	7.698	7.695	7.695	7.690	7.697	7.697	9.300	9.750
		9.750	9.750	10.400	12.150	12.350	100.000				
4	1163	204	188	183	151	73	56	50	47	35	35
		35	35	35	20	20	0				
3506	1163	7.733	7.725	7.742	7.743	7.740	7.739	7.746	7.728	9.300	9.750
		9.750	9.750	10.400	12.150	12.350	100.000				
5	1175	207	187	185	152	74	57	50	48	35	35
		35	35	35	20	20	0				
4409	1175	7.764	7.761	7.757	7.753	7.755	7.764	7.746	7.759	9.300	9.750
		9.750	9.750	10.400	12.150	12.350	100.000				
6	1213	212	192	195	169	79	59	53	50	35	35
		35	35	35	20	20	0				
5330	1213	7.816	7.821	7.817	7.830	7.829	7.813	7.820	7.822	9.300	9.750
		9.750	9.750	10.400	12.150	12.350	100.000				
7	1275	222	201	207	170	85	64	58	53	35	35
		35	35	35	20	20	0				
6305	1275	7.919	7.930	7.921	7.926	7.918	7.936	7.943	7.915	9.300	9.750
		9.750	9.750	10.400	12.150	12.350	100.000				
8	1300	225	204	213	175	89	65	59	55	35	35
		35	35	35	20	20	0				
7269	1300	7.950	7.960	7.965	7.974	7.978	7.961	7.968	7.977	9.300	9.750
		9.750	9.750	10.400	12.150	12.350	100.000				
9	1338	225	211	224	182	93	68	63	57	35	35
		35	35	35	20	20	0				
8299	1338	7.950	8.050	8.047	8.041	8.038	8.034	8.060	8.039	9.300	9.750
		9.750	9.750	10.400	12.150	12.350	100.000				
10	1388	225	214	237	192	100	72	67	60	36	35
		35	35	35	20	20	0				
9343	1348	7.950	8.137	8.143	8.137	8.142	8.133	8.165	8.132	9.344	9.750
		9.750	9.750	10.400	12.150	12.350	100.000				
11	1438	225	223	245	204	99	74	68	63	45	40
		35	39	35	20	20	0				
10424	1438	7.950	8.195	8.203	8.252	8.127	8.182	8.189	8.226	9.743	9.991

		9.929	9.982	10.400	12.150	12.350	100.000				
12	1313	210	208	220	179	92	67	61	56	40	35
		35	35	35	20	20	0				
11419	1313	7.795	8.014	8.017	8.012	8.023	8.010	8.017	8.004	9.521	9.750
		9.750	9.750	10.400	12.150	12.350	100.000				
13	1200	195	193	195	154	85	60	54	49	35	35
		35	35	35	20	20	0				
12337	1200	7.640	7.633	7.631	7.772	7.918	7.836	7.845	7.791	9.300	9.750
		9.750	9.750	10.400	12.150	12.350	100.000				
14	1238	210	196	201	165	82	61	56	52	35	35
		35	35	35	20	20	0				
13281	1238	7.795	7.869	7.876	7.876	7.874	7.862	7.894	7.884	9.300	9.750
		9.750	9.750	10.400	12.150	12.350	100.000				
15	1275	222	201	207	170	85	64	58	53	35	35
		35	35	35	20	20	0				
14250	1275	7.919	7.930	7.921	7.926	7.918	7.936	7.943	7.915	9.300	9.750
		9.750	9.750	10.400	12.150	12.350	100.000				
16	1305	225	205	215	175	89	66	60	55	35	35
		35	35	35	20	20	0				
15256	1305	7.950	7.978	7.980	7.974	7.978	7.985	7.992	7.977	9.300	9.750
		9.750	9.750	10.400	12.150	12.350	100.000				

FIGURE 4.20 DPSA-ECONOMIC DISPATCH FOR CASE 2 USING ALL POSSIBLE PAIRS

STAGE REQUIRED MW
COST ACTUAL MW

UNIT GENERATIONS
UNIT INCREMENTAL COSTS

1	1110	140	177	170	142	67	52	46	45	35	35
		35	35	35	20	20	0				
881	1110	7.691	7.640	7.646	7.657	7.651	7.641	7.648	7.666	9.300	9.
		9.750	9.750	10.400	12.150	12.350	100.000				
2	1125	198	180	173	144	69	54	47	45	35	35
		35	35	35	20	20	0				
1732	1125	7.671	7.676	7.666	7.676	7.680	7.690	7.672	7.666	9.300	9.750
		9.750	9.750	10.400	12.150	12.350	100.000				
3	1138	200	182	177	148	70	54	48	46	35	35
		35	35	35	20	20	0				
2811	1138	7.692	7.701	7.698	7.695	7.695	7.690	7.697	7.697	9.300	9.750
		9.750	9.750	10.400	12.150	12.350	100.000				
4	1161	204	184	182	151	73	56	50	48	35	35
		35	35	35	20	20	0				
3508	1163	7.733	7.725	7.735	7.743	7.740	7.739	7.746	7.759	9.300	9.750
		9.750	9.750	10.400	12.150	12.350	100.000				
5	1175	206	187	185	152	74	57	51	48	35	35
		35	35	35	20	20	0				
4404	1175	7.754	7.761	7.757	7.753	7.755	7.764	7.771	7.759	9.300	9.750
		9.750	9.750	10.400	12.150	12.350	100.000				
6	1213	212	192	193	159	79	60	53	50	35	35
		35	35	35	20	20	0				
5436	1213	7.816	7.821	7.817	7.820	7.829	7.836	7.820	7.822	9.300	9.750
		9.750	9.750	10.400	12.150	12.350	100.000				
7	1275	222	201	207	170	85	64	57	54	35	35
		35	35	35	20	20	0				
6305	1275	7.919	7.930	7.921	7.926	7.918	7.936	7.918	7.946	9.300	9.750
		9.750	9.750	10.400	12.150	12.350	100.000				
8	1300	225	204	212	175	89	66	59	55	35	35
		35	35	35	20	20	0				
7289	1300	7.950	7.960	7.958	7.974	7.978	7.985	7.962	7.977	9.300	9.750
		9.750	9.750	10.400	12.150	12.350	100.000				
9	1338	225	210	224	182	94	68	62	58	35	35
		35	35	35	20	20	0				
8299	1338	7.950	8.036	8.047	8.041	8.052	8.034	8.042	8.070	9.300	9.750
		9.750	9.750	10.400	12.150	12.350	100.000				
10	1389	225	218	232	195	100	73	62	58	42	35
		35	35	35	20	20	0				
9344	1389	7.950	8.135	8.143	8.146	8.142	8.157	8.042	8.070	9.810	9.750
		9.750	9.750	10.400	12.150	12.350	100.000				
11	1438	225	221	244	208	101	75	66	61	50	35
		37	38	35	20	20	0				
10425	1438	7.950	8.171	8.195	8.271	8.157	8.207	8.140	8.164	9.964	9.943

		9.869	9.924	10.400	12.150	12.350	100.000				
12	1313	210	200	219	181	94	68	59	54	42	35
		35	35	35	20	20	0				
11419	1313	7.795	7.990	8.010	8.031	8.052	8.034	7.968	7.946	9.810	9.75
		9.750	9.750	10.400	12.150	12.350	100.000				
13	1200	197	191	194	156	87	61	52	47	35	35
		35	35	35	20	20	0				
12539	1200	7.881	7.809	7.826	7.791	7.948	7.862	7.795	7.728	9.300	9.75
		9.750	9.750	10.400	12.150	12.350	100.000				
14	1238	212	195	200	165	82	61	55	53	35	35
		35	35	35	20	20	0				
13283	1238	7.816	7.857	7.869	7.878	7.874	7.862	7.809	7.915	9.300	9.75
		9.750	9.750	10.400	12.150	12.350	100.000				
15	1275	222	201	207	170	85	64	57	54	35	35
		35	35	35	20	20	0				
14251	1275	7.919	7.930	7.921	7.926	7.918	7.936	7.918	7.946	9.300	9.750
		9.750	9.750	10.400	12.150	12.350	100.000				
16	1305	225	205	215	175	89	66	60	55	35	3
		35	35	35	20	20	0				
15239	1305	7.950	7.978	7.980	7.974	7.978	7.985	7.992	7.977	9.300	
		9.750	9.750	10.400	12.150	12.350	100.000				

FIGURE 4.21 DPSA ECONOMIC DISPATCH FOR CASE 2 USING PAIRING SCHEME 1

STAGE REQUIRED MW
COST ACTUAL MW

UNIT GENERATIONS
UNIT INCREMENTAL COSTS

1	1112	197	179	170	141	67	52	46	44	35	35
		35	35	35	20	20	0				
881	1110	7.681	7.652	7.646	7.647	7.651	7.641	7.648	7.635	9.300	9.750
		9.750	9.750	10.400	12.150	12.350	100.000				
2	1125	198	180	173	144	69	54	47	45	35	35
		35	35	35	20	20	0				
1732	1125	7.671	7.679	7.668	7.676	7.690	7.690	7.672	7.666	9.300	9.750
		9.750	9.750	10.400	12.150	12.350	100.000				
3	1139	200	182	177	146	70	54	48	46	35	35
		35	35	35	20	20	0				
2611	1138	7.692	7.701	7.698	7.695	7.695	7.690	7.697	7.697	9.300	9.750
		9.750	9.750	10.400	12.150	12.350	100.000				
4	1163	205	185	182	150	73	56	50	47	35	35
		35	35	35	20	20	0				
3506	1163	7.746	7.737	7.735	7.734	7.740	7.739	7.746	7.728	9.300	9.750
		9.750	9.750	10.400	12.150	12.350	100.000				
5	1175	206	187	185	152	74	57	51	48	35	35
		35	35	35	20	20	0				
4409	1175	7.764	7.761	7.757	7.753	7.755	7.764	7.771	7.759	9.300	9.750
		9.750	9.750	10.400	12.150	12.350	100.000				
6	1213	212	192	193	159	79	60	53	50	35	35
		35	35	35	20	20	0				
5336	1213	7.816	7.821	7.817	7.820	7.829	7.838	7.820	7.822	9.300	9.750
		9.750	9.750	10.400	12.150	12.350	100.000				
7	1275	223	201	207	170	85	64	57	53	35	35
		35	35	35	20	20	0				
6305	1275	7.929	7.930	7.921	7.920	7.918	7.936	7.918	7.915	9.300	9.750
		9.750	9.750	10.400	12.150	12.350	100.000				
8	1300	225	204	213	175	86	66	59	55	35	35
		35	35	35	20	20	0				
7269	1300	7.950	7.960	7.965	7.974	7.963	7.985	7.968	7.977	9.300	9.750
		9.750	9.750	10.400	12.150	12.350	100.000				
9	1338	225	211	223	182	94	69	62	57	35	35
		35	35	35	20	20	0				
8299	1338	7.950	8.050	8.039	8.041	8.052	8.059	8.042	8.039	9.300	9.750
		9.750	9.750	10.400	12.150	12.350	100.000				
10	1369	226	222	237	192	100	73	66	58	35	35
		35	35	35	20	20	0				
9343	1386	7.950	8.183	8.143	8.137	8.142	8.157	8.140	8.070	9.300	9.750
		9.750	9.750	10.400	12.150	12.350	100.000				
11	1438	217	223	250	203	107	77	70	54	44	43
		35	35	35	20	25	0				
10425	1438	7.997	8.195	8.240	8.242	8.248	8.256	8.238	7.946	9.699	10.136

		9.750	9.750	10.400	12.150	12.439	100.000				
12	1313	202	208	225	178	100	70	63	47	35	35
		35	35	35	20	25	0				
11421	1313	7.713	8.014	8.054	8.002	8.142	8.089	8.060	7.728	9.300	9.750
		9.750	9.750	10.400	12.150	12.439	100.000				
13	1200	187	193	200	153	93	63	56	40	35	35
		35	35	35	20	20	0				
12341	1200	7.556	7.833	7.809	7.762	8.038	7.911	7.894	7.511	9.300	9.750
		9.750	9.750	10.400	12.150	12.350	100.000				
14	1238	202	208	199	163	86	61	55	46	35	35
		35	35	35	20	23	0				
13266	1238	7.713	8.014	7.881	7.858	7.933	7.862	7.809	7.697	9.300	9.750
		9.750	9.750	10.400	12.150	12.404	100.000				
15	1275	212	210	207	170	85	64	57	49	35	35
		35	35	35	20	20	0				
14254	1275	7.816	8.111	7.921	7.920	7.918	7.936	7.918	7.791	9.300	9.750
		9.750	9.750	10.400	12.150	12.350	100.000				
16	1305	223	208	215	175	89	66	60	54	35	35
		35	35	35	20	20	0				
15243	1305	7.929	8.014	7.960	7.974	7.976	7.985	7.992	7.946	9.300	9.750
		9.750	9.750	10.400	12.150	12.350	100.000				

FIGURE-4.22 DPSA ECONOMIC DISPATCH FOR CASE 2 USING PAIRING SCHEME 2

STAGE REQUIRED MW
COST ACTUAL MW

UNIT GENERATIONS
UNIT INCREMENTAL COSTS

1	1110	197	170	170	141	67	52	46	44	35	35
		35	35	35	20	20	0				
801	1110	7.801	7.852	7.846	7.847	7.851	7.841	7.848	7.835	9.300	9.
		9.750	9.750	10.400	12.150	12.350	100.000				
2	1125	198	190	173	144	69	54	47	45	35	35
		35	35	35	20	20	0				
1732	1125	7.871	7.870	7.866	7.870	7.860	7.890	7.872	7.866	9.300	9.750
		9.750	9.750	10.400	12.150	12.350	100.000				
3	1138	200	182	177	140	70	54	48	46	35	35
		35	35	35	20	20	0				
2011	1138	7.892	7.901	7.898	7.895	7.895	7.890	7.897	7.897	9.300	9.750
		9.750	9.750	10.400	12.150	12.350	100.000				
4	1163	205	185	182	150	73	56	50	47	35	35
		35	35	35	20	20	0				
3500	1163	7.744	7.737	7.735	7.734	7.740	7.739	7.746	7.728	9.300	9.750
		9.750	9.750	10.400	12.150	12.350	100.000				
5	1175	206	187	185	152	74	57	51	48	35	35
		35	35	35	20	20	0				
4409	1175	7.754	7.761	7.757	7.753	7.755	7.764	7.771	7.759	9.300	9.750
		9.750	9.750	10.400	12.150	12.350	100.000				
6	1213	212	192	193	159	79	60	53	50	35	35
		35	35	35	20	20	0				
5330	1213	7.810	7.821	7.817	7.820	7.829	7.838	7.820	7.822	9.300	9.750
		9.750	9.750	10.400	12.150	12.350	100.000				
7	1275	221	201	207	170	85	64	57	53	35	35
		35	35	35	20	20	0				
6305	1275	7.929	7.930	7.921	7.929	7.916	7.930	7.918	7.915	9.300	9.750
		9.750	9.750	10.400	12.150	12.350	100.000				
8	1300	225	204	213	175	88	66	59	55	35	35
		35	35	35	20	20	0				
7269	1300	7.950	7.960	7.965	7.974	7.963	7.985	7.960	7.977	9.300	9.750
		9.750	9.750	10.400	12.150	12.350	100.000				
9	1338	225	211	223	182	94	69	62	57	35	35
		35	35	35	20	20	0				
8229	1338	7.950	8.050	8.034	8.041	8.052	8.059	8.042	8.039	9.300	9.750
		9.750	9.750	10.400	12.150	12.350	100.000				
10	1350	225	211	217	192	100	73	66	61	43	35
		35	35	35	20	20	0				
9344	1388	7.950	8.050	8.143	8.137	8.142	8.157	8.140	8.164	9.654	9.750
		9.750	9.750	10.400	12.150	12.350	100.000				
11	1434	220	217	250	205	107	77	70	54	52	4
		35	35	35	20	20	0				
10420	1438	7.844	8.123	8.240	8.242	8.246	8.250	9.230	7.946	10.053	10.136

		9.750	9.750	10.400	12.150	12.350	100.000				
12	1313	205	202	225	178	100	70	63	47	43	35
		35	35	35	20	20	0				
11420	1313	7.914	7.982	8.059	8.002	8.142	8.188	8.066	7.728	9.654	9.75
		9.750	9.750	10.400	12.150	12.350	100.000				
13	1200	190	187	200	153	93	63	56	43	35	35
		35	35	35	20	20	0				
12340	1200	7.589	7.741	7.804	7.762	8.038	7.911	7.804	7.804	9.300	9.750
		9.750	9.750	10.400	12.150	12.350	100.000				
14	1238	205	202	194	163	86	61	55	47	40	3
		35	35	35	20	20	0				
13285	1230	7.744	7.942	7.861	7.858	7.933	7.862	7.869	7.728	9.521	9.750
		9.750	9.750	10.400	12.150	12.350	100.000				
15	1275	216	210	207	170	85	64	57	51	35	3
		35	35	35	20	20	0				
14253	1275	7.857	8.039	7.921	7.929	7.918	7.936	7.918	7.853	9.300	9.750
		9.750	9.750	10.400	12.150	12.350	100.000				
16	1305	225	205	215	175	89	66	60	55	35	3
		35	35	35	20	20	0				
15241	1305	7.950	7.978	7.960	7.974	7.978	7.985	7.992	7.977	9.300	9
		9.750	9.750	10.400	12.150	12.350	100.000				

FIGURE 4.23 DPSA ECONOMIC DISPATCH FOR CASE 2 USING PAIRING SCHEME 3

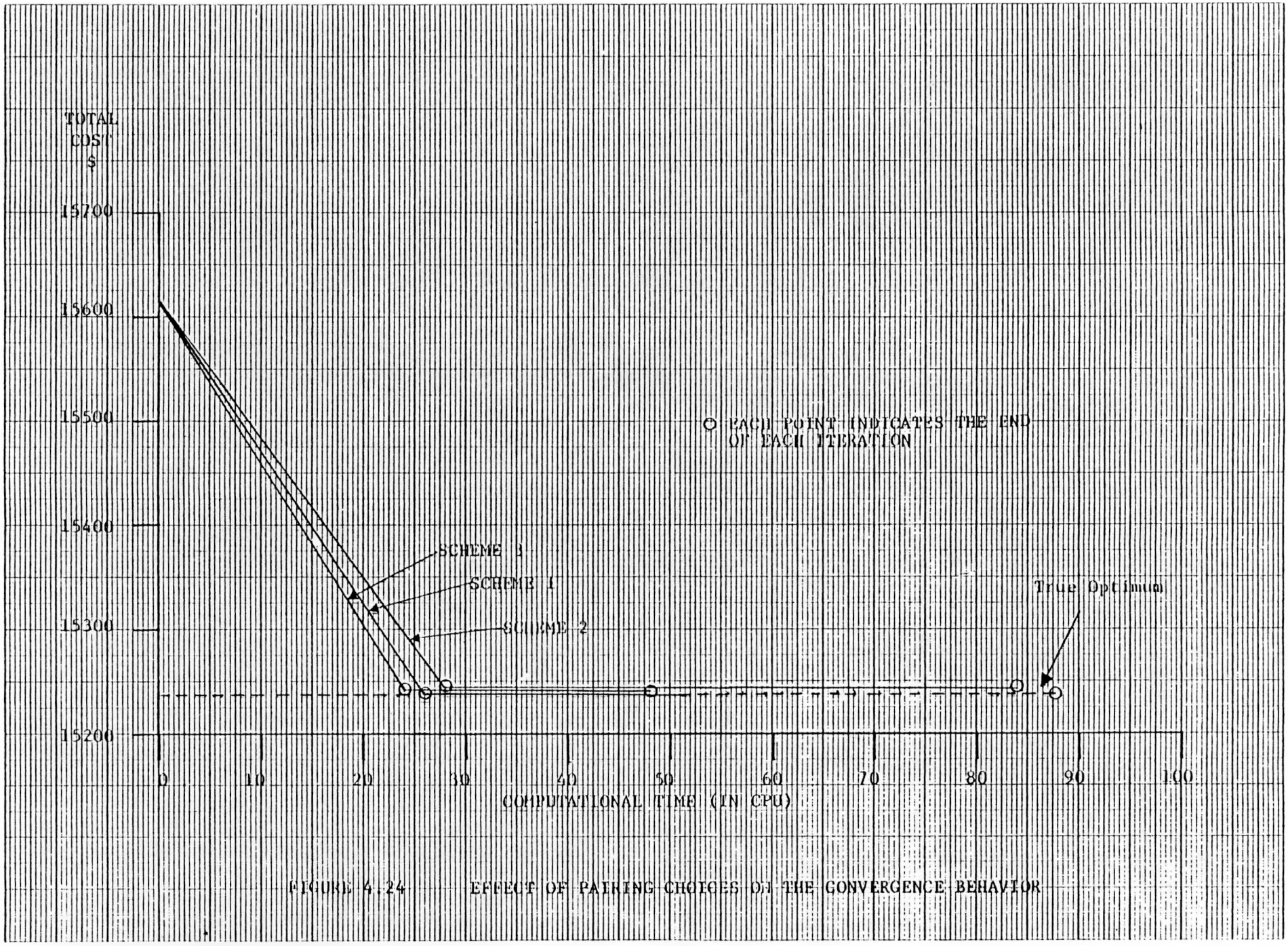

FIGURE 4.24 EFFECT OF PAIRING CHOICES ON THE CONVERGENCE BEHAVIOR

4.5.3 Valve Point Loading

Figure 4.25 is a typical saw tooth incremental cost curve of a valve point loaded unit. Rather than a slight curvature, a straight line is assumed as an approximation for incremental costs between two valve points. Then as shown in the same figure, the step approximation is made to the incremental cost curve to be used in conjunction with the MINMAR algorithm. This approximation tends to hold the units' output at a valve point until the incremental cost of other units become greater than the incremental cost of the valve-point-loaded unit at its next valve point. At that point, the output of the valve point unit will move towards its next valve point. However, the DPSA scheme does not require any approximation. Figure 4.26 represents the cost curve which is obtained by integrating the saw tooth incremental cost curve of Figure 4.25

Unit No. 5, Oak Creek Unit 3, was assumed to be valve point loaded, with the valve points being at 30, 60, 90 and 114 MW. With these assumptions, both Case 1 and Case 2 were dispatched using both MINMAR and DPSA methods. Figure 4.27 through 4.30 are the results obtained. In all figures, one thing in common can be noticed easily. That is, the output of Unit 5 generally remains at a valve point as long as possible, however, when it moves to the next valve point, it moves at its full rate limit. To show this effect, Figure 4.31 and Figure 4.32 is prepared using the DPSA result of both Case 1 and Case 2. These figures compare the dispatched output of the valve point loaded unit and the dispatched output of the same unit when it is not valve point loaded. The cost curve of the same unit for when it is not valve-point-loaded is shown in Figure 4.26. Another thing to be noticed here is the difference and the similarity between Figure 4.27 and 4.28, which are the dispatch output of generating units for Case 1 from MINMAR and DPSA dispatch schemes respectively. These figures show quite different trajectories of Unit 5, and of other units correspondingly. However, the total costs from both schemes differ only by two dollars.

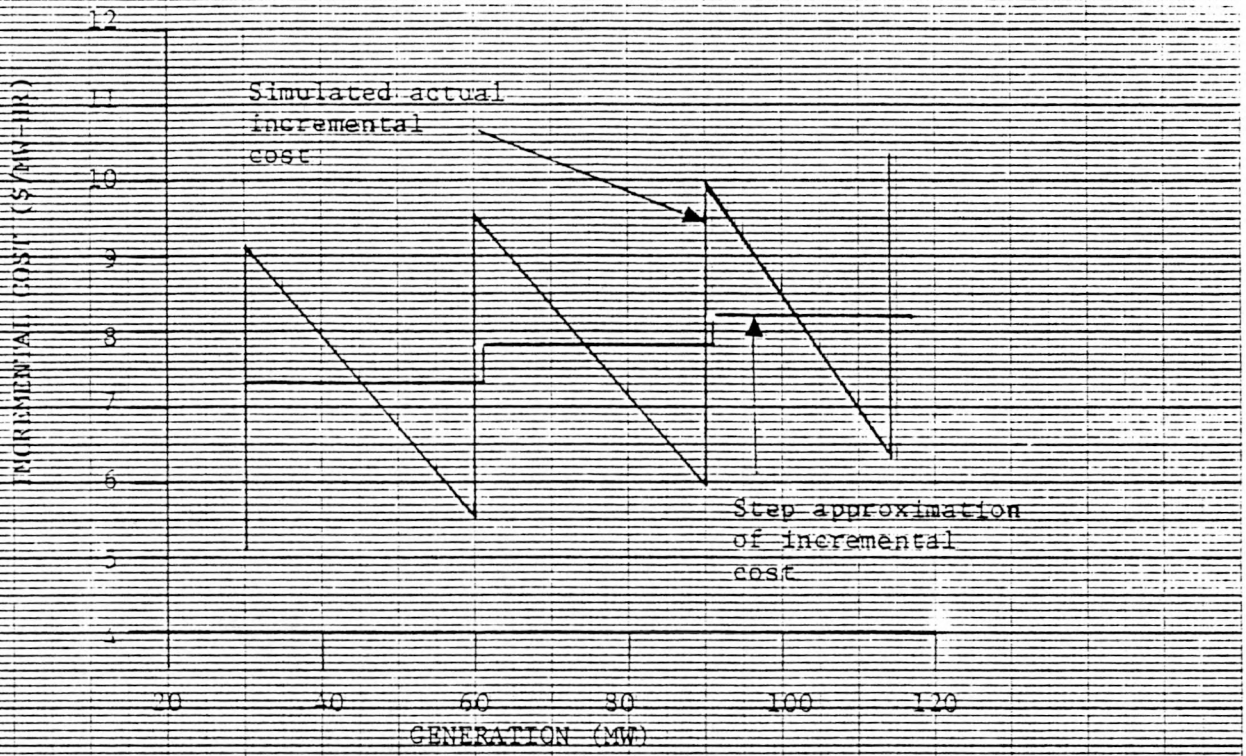

FIGURE 4.25 INCREMENTAL COST CURVE USED FOR O.C.3 UNIT

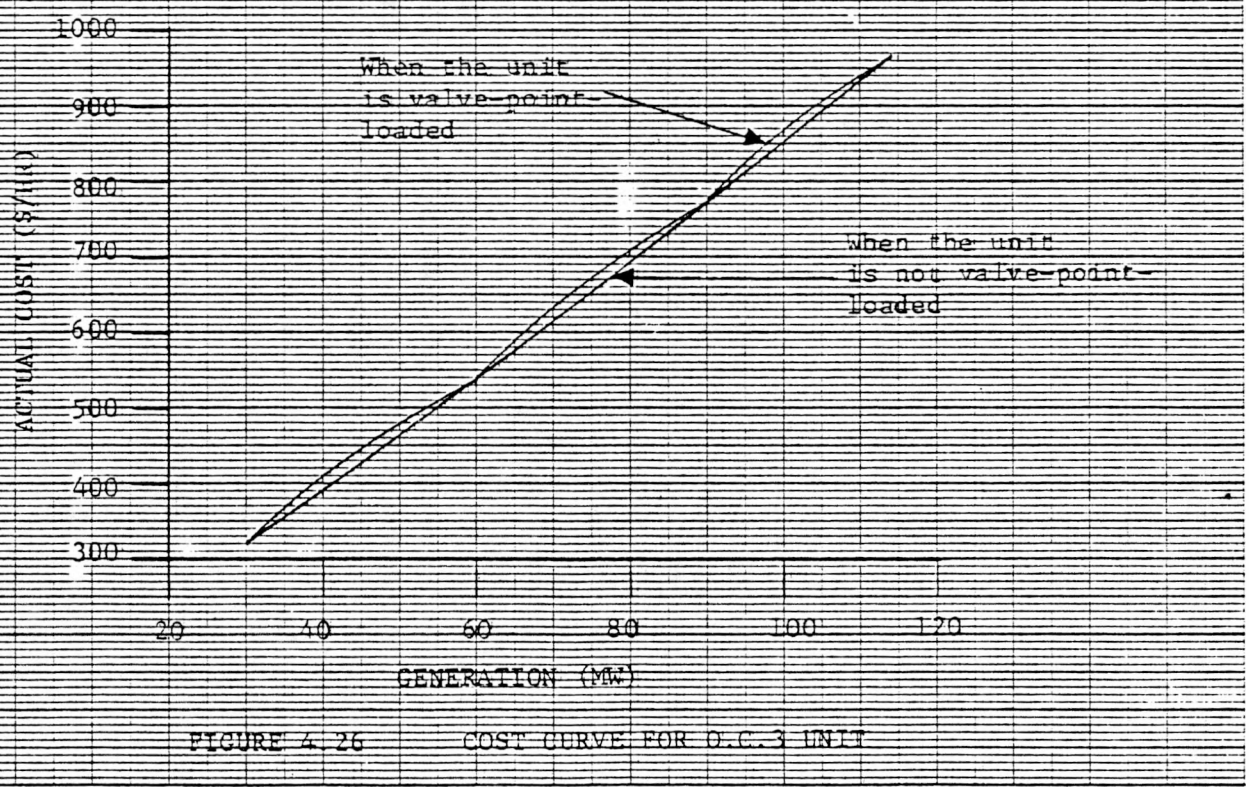

FIGURE 4.26 COST CURVE FOR O.C.3 UNIT

STAGE REQUIRED MW
COST ACTUAL MW

UNIT GENERATIONS
UNIT INCREMENTAL COSTS

1	1110	197	179	172	142	60	53	47	45	35	35
		35	35	35	20	20	0				
801	1110	7.681	7.694	7.691	7.697	7.769	7.696	7.672	7.686	9.300	9.
		9.750	9.750	10.400	12.150	12.350	100.000				
2	1125	200	181	176	145	60	54	48	46	35	
		35	35	35	20	20	0				
1732	1125	7.692	7.694	7.693	7.696	7.769	7.698	7.697	7.697	9.300	9.750
		9.750	9.750	10.400	12.150	12.350	100.000				
3	1138	202	183	179	148	60	55	49	47	35	35
		35	35	35	20	20	0				
2611	1138	7.713	7.713	7.713	7.715	7.769	7.715	7.722	7.728	9.300	9.750
		9.750	9.750	10.400	12.150	12.350	100.000				
4	1163	207	187	185	153	60	57	51	48	35	35
		35	35	35	20	20	0				
3507	1163	7.761	7.761	7.757	7.762	7.769	7.764	7.771	7.759	9.300	9.750
		9.750	9.750	10.400	12.150	12.350	100.000				
5	1175	208	188	187	154	65	58	51	49	35	35
		35	35	35	20	20	0				
4410	1175	7.775	7.773	7.772	7.772	7.769	7.789	7.771	7.791	9.300	9.750
		9.750	9.750	10.400	12.150	12.350	100.000				
6	1213	213	193	195	160	72	60	54	51	35	35
		35	35	35	20	20	0				
5339	1213	7.826	7.833	7.831	7.830	7.769	7.838	7.845	7.853	9.300	9.750
		9.750	9.750	10.400	12.150	12.350	100.000				
7	1275	224	201	209	171	79	64	58	54	35	35
		35	35	35	20	20	0				
6309	1275	7.940	7.930	7.935	7.935	7.769	7.936	7.943	7.946	9.300	9.750
		9.750	9.750	10.400	12.150	12.350	100.000				
8	1300	225	205	214	175	86	68	59	55	35	35
		35	35	35	20	20	0				
7295	1300	7.950	7.970	7.971	7.974	7.769	7.985	7.968	7.977	9.300	9.750
		9.750	9.750	10.400	12.150	12.350	100.000				
9	1338	225	211	220	183	90	69	61	58	35	35
		35	35	35	20	20	0				
8304	1338	7.950	8.050	8.047	8.050	8.171	8.059	8.066	8.070	9.300	9.750
		9.750	9.750	10.400	12.150	12.350	100.000				
10	1388	225	221	240	195	90	74	67	61	35	35
		35	35	35	20	20	0				
9348	1388	7.950	8.171	8.166	8.165	8.171	8.182	8.165	8.164	9.300	9.750
		9.750	9.750	10.400	12.150	12.350	100.000				
11	1438	225	229	253	205	97	78	71	65	35	35
		35	35	35	20	20	0				
10426	1438	7.950	8.261	8.262	8.261	8.171	8.280	8.263	8.268	9.300	9.750

		9.750	9.750	10.400	12.150	12.350	100.000				
12	1475	225	235	262	213	104	80	74	67	35	35
		35	35	35	20	20	0				
11530	1475	7.950	8.340	8.329	8.336	8.171	8.330	8.337	8.350	9.300	9.750
		9.750	9.750	10.400	12.150	12.350	100.000				
13	1525	225	240	277	224	111	85	78	70	35	35
		35	35	35	20	20	0				
12969	1525	7.950	8.400	8.441	8.444	8.171	8.452	8.435	8.443	9.300	9.750
		9.750	9.750	10.400	12.150	12.350	100.000				
14	1563	225	240	285	237	114	90	83	74	35	35
		35	35	35	20	20	0				
13838	1563	7.950	8.400	8.500	8.568	8.175	8.575	8.558	8.568	9.300	9.750
		9.750	9.750	10.400	12.150	12.350	100.000				
15	1600	225	240	285	259	114	91	90	81	35	35
		35	35	35	20	20	0				
15025	1600	7.950	8.400	8.500	8.779	8.175	8.600	8.731	8.785	9.300	9.750
		9.750	9.750	10.400	12.150	12.350	100.000				
16	1630	225	240	285	270	114	91	97	87	35	35
		35	35	35	20	20	0				
16234	1630	7.950	8.400	8.500	8.982	8.175	8.600	8.903	8.972	9.300	9.750
		9.750	9.750	10.400	12.150	12.350	100.000				

FIGURE 4.27 MINMAR ECONOMIC DISPATCH FOR CASE 1
(UNIT 5 IS VALVE POINT LOADED)

STAGE REQUIRED MW / COST ACTUAL MW		UNIT GENERATIONS / UNIT INCREMENTAL COSTS									
1	1110	196	179	173	131	71	53	47	45	35	35
		35	35	35	20	20	0				
862	1110	7.651	7.664	7.664	7.551	7.769	7.000	7.672	7.668	9.300	9.750
		9.750	9.750	10.400	12.150	12.350	100.000				
2	1125	200	180	176	130	78	53	47	46	35	35
		35	35	35	20	20	0				
1734	1125	7.692	7.676	7.690	7.542	7.769	7.000	7.672	7.697	9.300	9.750
		9.750	9.750	10.400	12.150	12.350	100.000				
3	1138	202	183	175	129	85	54	48	47	35	35
		35	35	35	20	20	0				
2614	1138	7.713	7.713	7.663	7.532	7.769	7.690	7.697	7.728	9.300	9.750
		9.750	9.750	10.400	12.150	12.350	100.000				
4	1163	207	187	177	133	90	56	50	48	35	35
		35	35	35	20	20	0				
3510	1163	7.764	7.761	7.698	7.571	8.171	7.739	7.746	7.759	9.300	9.750
		9.750	9.750	10.400	12.150	12.350	100.000				
5	1175	208	186	177	141	90	57	51	48	35	35
		35	35	35	20	20	0				
4412	1175	7.775	7.773	7.698	7.647	8.171	7.764	7.771	7.759	9.300	9.750
		9.750	9.750	10.400	12.150	12.350	100.000				
6	1213	214	192	185	154	90	59	53	51	35	35
		35	35	35	20	20	0				
5340	1213	7.836	7.821	7.757	7.772	8.171	7.813	7.820	7.853	9.300	9.750
		9.750	9.750	10.400	12.150	12.350	100.000				
7	1275	222	201	204	167	90	64	58	54	35	35
		35	35	35	20	20	0				
6308	1275	7.919	7.930	7.898	7.897	8.171	7.936	7.943	7.946	9.300	9.750
		9.750	9.750	10.400	12.150	12.350	100.000				
8	1300	225	204	212	170	97	64	58	55	35	35
		35	35	35	20	20	0				
7253	1300	7.950	7.950	7.958	7.920	8.171	7.936	7.943	7.927	9.300	9.750
		9.750	9.750	10.400	12.150	12.350	100.000				
9	1338	225	211	219	177	104	68	62	57	35	35
		35	35	35	20	20	0				
8304	1338	7.950	8.050	8.010	7.993	8.171	8.030	8.042	8.039	9.300	9.750
		9.750	9.750	10.400	12.150	12.350	100.000				
10	1388	225	221	232	185	111	72	66	61	35	35
		35	35	35	20	20	0				
9348	1388	7.950	8.171	8.106	8.069	8.171	8.133	8.140	8.164	9.300	9.750
		9.750	9.750	10.400	12.150	12.350	100.000				
11	1438	225	229	245	194	114	76	71	64	35	35
		35	35	35	20	20	0				
10420	1438	7.950	8.287	8.203	8.204	8.175	8.231	8.263	8.252	9.300	9.750

		9.750	9.750	10.400	12.150	12.350	100.000				
12	1475	225	235	257	206	114	80	74	67	35	35
		35	35	35	20	20	0				
11529	1475	7.950	8.340	8.292	8.290	8.175	8.330	8.337	8.350	9.300	9.750
		9.750	9.750	10.400	12.150	12.350	100.000				
13	1525	225	240	275	223	114	85	78	70	35	35
		35	35	35	20	20	0				
12667	1525	7.950	8.400	8.426	8.434	8.175	8.452	8.435	8.443	9.300	9.750
		9.750	9.750	10.400	12.150	12.350	100.000				
14	1563	225	240	285	237	114	89	84	74	35	35
		35	35	35	20	20	0				
13832	1563	7.950	8.400	8.500	8.560	8.175	8.551	8.583	8.568	9.300	9.750
		9.750	9.750	10.400	12.150	12.350	100.000				
15	1600	225	240	285	259	114	91	91	80	35	35
		35	35	35	20	20	0				
15023	1600	7.950	8.400	8.500	8.779	8.175	8.600	8.755	8.754	9.300	9.750
		9.750	9.750	10.400	12.150	12.350	100.000				
16	1630	225	240	285	270	114	91	98	86	35	35
		35	35	35	20	20	0				
16237	1630	7.950	8.400	8.500	8.982	8.175	8.600	8.928	8.941	9.300	9.750
		9.750	9.750	10.400	12.150	12.350	100.000				

FIGURE 4.28 DPSA ECONOMIC DISPATCH FOR CASE 1
(UNIT 5 IS VALVE POINT LOADED)

STAGE REQUIRED MW
COST ACTUAL MW

UNIT GENERATIONS
UNIT ENCREMENTAL COSTS

1	1110	197	179	172	142	66	53	47	45	35	35
		35	35	35	20	20	0				
861	1110	7.661	7.644	7.661	7.657	7.749	7.666	7.672	7.666	9.300	9.
		9.750	9.750	10.400	12.150	12.350	100.000				
2	1125	200	181	176	145	60	54	48	46	35	35
		35	35	35	20	20	0				
1732	1125	7.692	7.649	7.690	7.686	7.769	7.690	7.697	7.697	9.300	9.750
		9.750	9.750	10.400	12.150	12.350	100.000				
3	1138	202	183	179	148	60	55	49	47	35	35
		35	35	35	20	20	0				
2911	1138	7.713	7.713	7.713	7.715	7.769	7.715	7.722	7.728	9.300	9.750
		9.750	9.750	10.400	12.150	12.350	100.000				
4	1163	207	187	185	153	60	57	51	48	35	35
		35	35	35	20	20	0				
3507	1163	7.764	7.761	7.757	7.762	7.769	7.764	7.771	7.759	9.300	9.750
		9.750	9.750	10.400	12.150	12.350	100.000				
5	1175	208	188	187	154	65	58	51	49	35	35
		35	35	35	20	20	0				
4410	1175	7.775	7.773	7.772	7.772	7.769	7.789	7.771	7.791	9.300	9.750
		9.750	9.750	10.400	12.150	12.350	100.000				
6	1213	213	193	195	160	72	60	54	51	35	35
		35	35	35	20	20	0				
5339	1213	7.826	7.833	7.831	7.830	7.769	7.838	7.845	7.853	9.300	9.750
		9.750	9.750	10.400	12.150	12.350	100.000				
7	1275	220	201	209	171	79	64	58	54	35	35
		35	35	35	20	20	0				
6309	1275	7.900	7.930	7.935	7.935	7.769	7.936	7.943	7.946	9.300	9.750
		9.750	9.750	10.400	12.150	12.350	100.000				
8	1300	225	205	214	175	86	66	59	55	35	35
		35	35	35	20	20	0				
7294	1300	7.950	7.975	7.973	7.974	7.769	7.985	7.968	7.977	9.300	9.750
		9.750	9.750	10.400	12.150	12.350	100.000				
9	1338	225	211	224	183	90	69	63	58	35	35
		35	35	35	20	20	0				
8304	1338	7.950	8.050	8.047	8.050	8.171	8.059	8.066	8.070	9.300	9.750
		9.750	9.750	10.400	12.150	12.350	100.000				
10	1388	225	221	240	195	90	74	67	61	35	35
		35	35	35	20	20	0				
9348	1388	7.950	8.171	8.166	8.165	8.171	8.182	8.165	8.164	9.300	9.750
		9.750	9.750	10.400	12.150	12.350	100.000				
11	1438	225	229	253	205	97	78	71	65	35	35
		35	35	35	20	20	0				
10428	1438	7.950	8.267	8.262	8.261	8.171	8.280	8.263	8.268	9.300	9.750

		9.750	9.750	10.400	12.150	12.350	100.000				
12	1313	211	214	228	189	90	71	64	58	35	35
		35	35	35	20	20	18				
11562	1313	7.905	8.088	8.077	8.022	8.171	8.108	8.091	8.070	9.300	9.75
		9.750	9.750	10.400	12.150	12.350	100.000				
13	1200	197	199	203	155	83	64	57	51	35	35
		35	35	35	20	20	24				
12717	1200	7.881	7.900	7.891	7.782	7.769	7.936	7.918	7.853	9.300	9.75
		9.750	9.750	10.400	12.150	12.350	100.000				
14	1238	212	195	197	162	90	81	55	51	35	35
		35	35	35	20	20	0				
13001	1238	7.816	7.857	7.846	7.849	8.171	7.862	7.869	7.853	9.300	9.750
		9.750	9.750	10.400	12.150	12.350	100.000				
15	1275	222	200	206	169	90	83	57	53	35	3
		35	35	35	20	20	0				
14029	1275	7.919	7.918	7.913	7.916	8.171	7.911	7.918	7.915	9.300	9.750
		9.750	9.750	10.400	12.150	12.350	100.000				
16	1305	225	205	214	175	90	66	60	55	35	3
		35	35	35	20	20	0				
15617	1305	7.950	7.975	7.973	7.974	8.171	7.985	7.992	7.977	9.300	
		9.750	9.750	10.400	12.150	12.350	100.000				

FIGURE 4.29 MINMAR ECONOMIC DISPATCH FOR CASE 2
(UNIT 5 IS VALVE POINT LOADED)

STAGE REQUIRED MW
COST ACTUAL MW

UNIT GENERATIONS
UNIT INCREMENTAL COSTS

1	1110	195	179	173	131	71	53	47	46	35	35
		35	35	35	20	20	0				
892	1110	7.651	7.664	7.668	7.551	7.769	7.666	7.672	7.666	9.300	9.750
		9.750	9.750	10.400	12.150	12.350	100.000				
2	1125	200	180	176	130	78	53	47	46	35	35
		35	35	35	20	20	0				
1734	1125	7.692	7.679	7.690	7.542	7.769	7.666	7.672	7.697	9.300	9.750
		9.750	9.750	10.400	12.150	12.350	100.000				
3	1138	202	185	175	129	85	54	48	47	35	35
		35	35	35	20	20	0				
2610	1138	7.713	7.713	7.683	7.532	7.769	7.690	7.697	7.728	9.300	9.750
		9.750	9.750	10.400	12.150	12.350	100.000				
4	1161	207	187	177	133	90	56	50	48	35	35
		35	35	35	20	20	0				
3510	1163	7.764	7.761	7.698	7.571	8.171	7.739	7.746	7.759	9.300	9.750
		9.750	9.750	10.400	12.150	12.350	100.000				
5	1175	208	188	177	141	90	57	51	48	35	35
		35	35	35	20	20	0				
4412	1175	7.775	7.773	7.698	7.647	8.171	7.764	7.771	7.759	9.300	9.750
		9.750	9.750	10.400	12.150	12.350	100.000				
6	1213	214	192	185	154	90	59	53	51	35	35
		35	35	35	20	20	0				
5340	1213	7.836	7.821	7.757	7.772	8.171	7.813	7.820	7.853	9.300	9.750
		9.750	9.750	10.400	12.150	12.350	100.000				
7	1275	222	201	208	167	90	64	58	54	35	35
		35	35	35	20	20	0				
6308	1275	7.919	7.930	7.894	7.697	8.171	7.936	7.943	7.906	9.300	9.750
		9.750	9.750	10.400	12.150	12.350	100.000				
8	1300	225	204	212	174	90	66	59	55	35	35
		35	35	35	20	20	0				
7293	1300	7.950	7.960	7.956	7.964	8.171	7.985	7.968	7.977	9.300	9.750
		9.750	9.750	10.400	12.150	12.350	100.000				
9	1338	225	211	224	183	90	69	63	58	35	35
		35	35	35	20	20	0				
8303	1338	7.950	8.050	8.047	8.050	8.171	8.059	8.066	8.070	9.300	9.750
		9.750	9.750	10.400	12.150	12.350	100.000				
10	1386	225	221	240	195	90	74	68	59	40	35
		35	35	35	20	20	0				
9347	1388	7.950	8.171	8.166	8.165	8.171	8.182	8.091	8.101	9.521	9.750
		9.750	9.750	10.400	12.150	12.350	100.000				
11	1438	225	222	244	204	97	78	68	63	49	38
		37	38	35	20	20	0				
10426	1438	7.950	8.193	8.195	8.252	8.171	8.280	8.189	8.226	9.920	9.895

		9.869	9.924	10.400	12.150	12.350	100.000				
12	1313	210	207	219	179	90	71	61	56	40	35
		35	35	35	20	20	0				
11922	1313	7.795	8.002	8.010	8.012	8.171	8.108	8.017	8.008	9.521	9.750
		9.750	9.750	10.400	12.150	12.350	100.000				
13	1200	195	192	198	154	83	64	54	49	35	35
		35	35	35	20	20	0				
12342	1200	7.690	7.821	7.824	7.772	7.769	7.936	7.845	7.791	9.300	9.750
		9.750	9.750	10.400	12.150	12.350	100.000				
14	1238	210	195	198	163	90	61	54	52	35	35
		35	35	35	20	20	0				
13660	1238	7.795	7.857	7.854	7.858	8.171	7.862	7.845	7.884	9.300	9.750
		9.750	9.750	10.400	12.150	12.350	100.000				
15	1275	222	199	206	170	90	63	57	53	35	35
		35	35	35	20	20	0				
14254	1275	7.919	7.906	7.913	7.920	8.171	7.911	7.918	7.915	9.300	9.750
		9.750	9.750	10.400	12.150	12.350	100.000				
16	1305	225	205	215	174	90	66	60	55	35	35
		35	35	35	20	20	0				
15242	1305	7.950	7.978	7.980	7.964	8.171	7.985	7.992	7.977	9.300	9.750
		9.750	9.750	10.400	12.150	12.350	100.000				

FIGURE 4.30 DPSA ECONOMIC DISPATCH FOR CASE 2
(UNIT 5 IS VALVE POINT LOADED)

4.6 COMPUTATIONAL REQUIREMENTS

From the computational experience of executing the batch mode program on UNIVAC 1108, the following chart is obtained. The computational requirements will vary according to the array sizes which are determined by the number of units to be dispatched, the time horizon and the dispatch interval, the upper and lower bounds of economic generating limits of all units and the discretization size of the generation. The chart is obtained for the following conditions:

- Number of Units 16

  O.C.1 through 8, P.W.1 through 5, and Valley 1 and 2

- Number of Stages 16

Time started	6:00 a.m.
Time ended	7:20 a.m.
Time interval	5 minutes

- Number of discretizations 360

Upper Bound of Economic Generation	285 MW of O.C.8
Lower Bound of Economic Generation	-50 MW of artificial unit
Discretization size	1 MW
Actual number of Discretizations needed	335

- Number of pairs 30

  All three pairing schemes explained in the previous section consist of 30 pairs

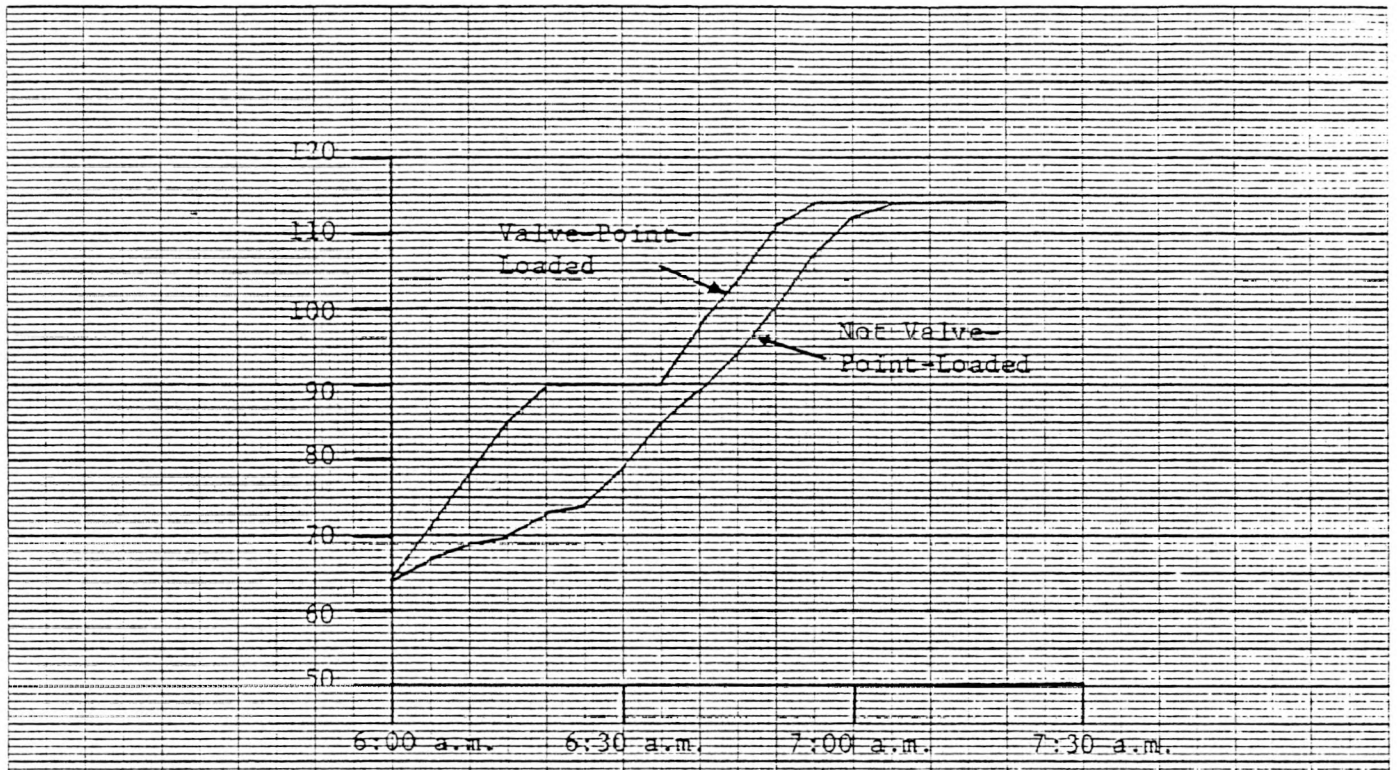

FIGURE 4.31 COMPARISON OF DISPATCHED OUTPUTS OF O.C.3 BETWEEN WHEN IT IS VALVE-POINT-LOADED AND WHEN IT IS NOT (CASE 1)

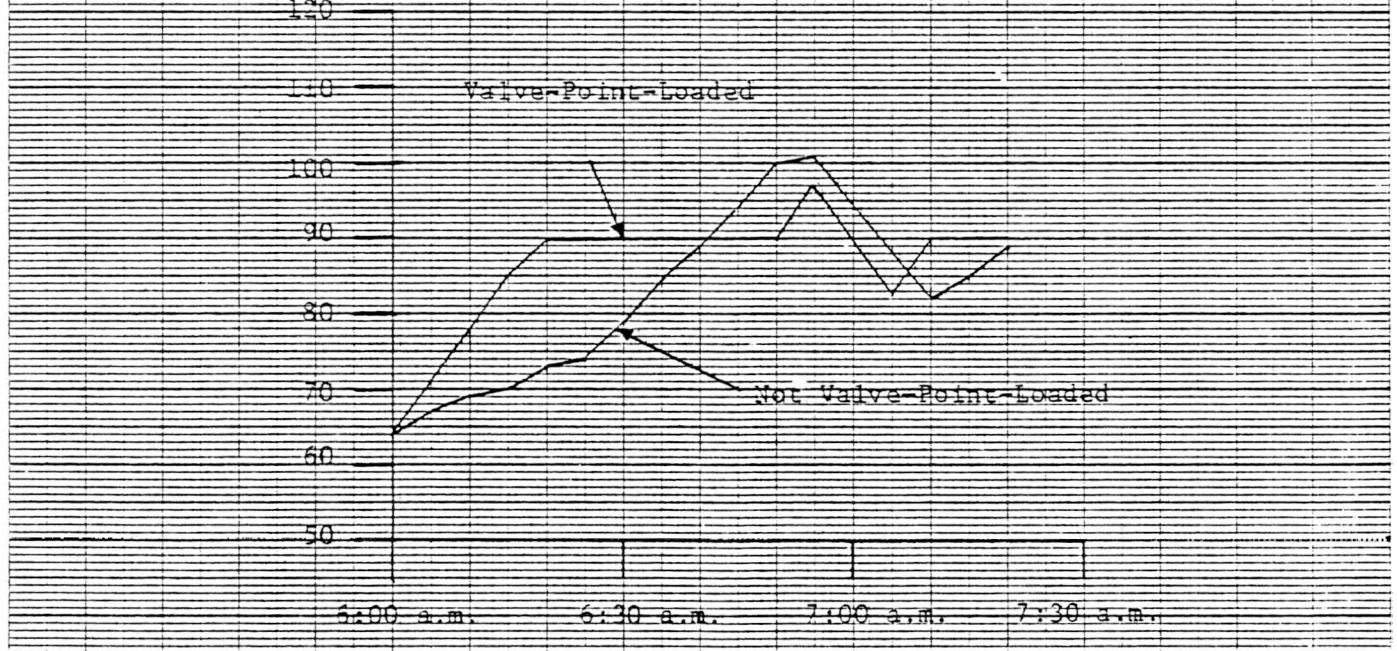

FIGURE 4.32 COMPARISON OF DISPATCHED OUTPUTS OF O.C.3 BETWEEN WHEN IT IS VALVE-POINT-LOADED AND WHEN IT IS NOT (CASE 2)

	MINMAR	DPSA	COMBINED
CORE REQUIREMENT	16.44 K	29.13 K	34.89 K
COMPUTATIONAL TIME REQUIREMENT	5.89	0.8 per pair per iteration	53.89*

* On average, it took two iterations to converge within the cost tolerance of $1

FIGURE 4.33 COMPUTATIONAL REQUIREMENT CHART

4.7 IMPACT OF CYBER FAILURE

The short-term load prediction, DPSA and MINMAR algorithms will be executed on the WEPCO CYBER computer, which is the background processor to the CDC 1700 foreground processor. The CDC 1700 issues raise/lower pulses to the units and performs the real-time functions of the AGC. Should the CYBER computer be subject to an outage, the AGC must continue to be performed by the CDC 1700. Accordingly, it is necessary to ensure that when the short-term load forecast and the dynamic economic dispatch cannot be done -- that at least a static economic dispatch can be performed on the CDC 1700. For these reasons, an abbreviated version of MINMAR will also be resident on the CDC 1700, for use when the CYBER is down. In this event, this version of MINMAR will be executed once each dispatch interval (tentatively each 5 minutes) to dispatch generation to the current estimate of the net generation requirement. This algorithm will be nearly identical to that discussed in Section 4.3; the principal difference will be that the data base will not provide for a multiple time-stages in the dispatch horizon and the program will not iterate over multiple time-steps. WEPCO has, in fact, recently coded such a minimum marginal cost algorithm. It is in use on the CDC 1700 for both economic dispatch computations and for power interchange buy-sell decisions.

References for Chapter 4

4-1 L.H. Fink, H.G. Kwatny, J.P. McDonald, "Economic Dispatch of Generation Via Valve-Point Loading", IEEE Trans on Power Apparatus and Systems, Vol. PAS-88, No. 6, pp 805-811, June 1969.

4-2 D. Ross, "Analysis of WEPCO Static Economic Dispatch and Unit Rate Limit Violations", SCI Project 5212 memo, January 13, 1978.

4-3 D. Ross, "Analysis of Actual WEPCO Unit Dispatch for January 31, 1978", SCI Project 5212 memo, February 14, 1978.

4-4 T.E. Bechert, H.G. Kwatny, "On the Optimal Dynamic Dispatching of Real Power", Paper 71TP 552-PWR, presented at IEEE Power Engineering Society Summer Meeting, Portland, Oregon, 1971.

4-5 T.E. Bechert, N. Chen, "Area Automatic Generation Control by Multi-Pass Dynamic Programming", IEEE Trans. on Power Apparatus and Systems, Vol. PAS-96, No. 5, Sept./Oct., 1977.

4-6 A.J. Korsak and R.E. Larson, "A Dynamic Programming Successive Approximations Technique with Convergence Proofs - Parts I & II", Automatica, Vol. 6, December 1969.

4-7 R.E. Bellman, Dynamic Programming, Princeton University Press, New Jersy, 1957.

4-8 R.E. Bellman, S.E. Dreyfus, Applied Dynamic Programming, Princeton University Press, New Jersey, 1962.

5. COORDINATING CONTROLLER

5.1 INTRODUCTION

The three major functions in the advanced AGC software package which is being developed are short-term load prediction, dynamic optimal dispatch and load-frequency control (LFC). In this chapter the LFC problem is defined and two major components of the prototype LFC structure are identified: the area coordinating controller and the individual unit controllers. The development and preliminary evaluation of the coordinating controller constitutes the major topic of this chapter while the unit controller design is reported in the succeeding chapter, 6.0.

5.1.1 Conventional AGC Structure

Four basic objectives of power system operation during normal operating conditions can be associated with automatic generation control:

1. Matching total system generation to total system load

2. Regulating system electrical frequency error to zero

3. Distributing system generation amongst control areas so that net area tie flows match net area tie flow schedules

4. Distributing area generation amongst area generation sources so that area operating costs are minimized

The first objective is conventionally associated with system primary or governor speed control; turbine speed governors respond proportionally to local frequency deviations and normally bring the rate-of-change of frequency to zero within a time-frame of several seconds.

The latter three objectives are accomplished by supplementary controls directed from area control centers. The second and third AGC objectives are classically associated with the regulation function, or load-frequency control, while the fourth objective is associated with the economic dispatch function of automatic generation control. The latter two functions typically operate in a time frame from several seconds to several minutes.

Introduced nearly 30 years ago, the tie-line bias control strategy [5.1] is utilized in most interconnected power systems to accomplish the regulation function of AGC. In this approach the second and third objectives are combined and each area attempts to regulate its area control error (ACE) to zero, where

$$ACE \triangleq M - S^{o} + B\,(f - f^{o}) \tag{5.1}$$

and

M = net tie flow out of the control area
S^{o} = scheduled tie flow out of the control area
B = area frequency bias constant (positive real)
f = actual frequency
f^{o} = scheduled frequency

A thorough discussion of the various aspects of tie-line bias control is provided in [5.1-5.2] and in other AGC literature. Very briefly, this strategy provides a steady-state target according to which each area meets its own load during normal conditions in the interconnection, contributes to frequency regulation and provides assistance to external areas when necessary. Although based on steady-state arguments, the tie-line bias control strategy has the important advantage that no inter-area communication is required, and it is on this basis that the decentralized automatic generation control of interconnected systems has been achieved.

The performance of conventional AGC has often been unsatisfactory however [5.3]. While some significant reasons for poor performance cannot be directly attributed to the control structure per se, not enough generating units on control for example, others can arise from the nature of the basic control algorithms as well as from the diverse data processing structures with which they are implemented. An important observation is that conventional AGC structures do not fully reflect the essential tracking nature of the problem. For example some are effectively pure integral controllers whose overall loop gain must be rather low to maintain stability. As a result tracking performance is limited, particularly during sustained, rapid load changes such as the morning load pickup. At such times manual operator intervention is generally required in order to maintain ACE within acceptable limits. Evidence of sustained fluctuations in frequency caused by inappropriate control has been reported [5.4]. In addition, a lack of coordination between the AGC regulation and economic dispatch functions can result in conflicting requirements on generating units and inefficient control.

5.1.2 Load-Frequency Control

Over the last few years numerous researchers have explored certain aspects of the load-frequency control problem in the context of modern control theory. One of the earliest studies was that of Fosha and Elgerd [5.6]. In employing the linear quadratic regulator theory, they introduced a significantly non-conventional approach which subsequently stimulated both an interest in the dynamic aspects of LFC as well as a lively and contructive dialogue between various control theorists and industry practitioners. One difficulty in this and other early studies is that they emphasized controlling synchronizing oscillations, whereas it is generally recognized that they are too fast for supplementary control to be either effective or desired [5.4]. Another weakness was recognized by Calovic [5.7], who made a clear distinction between the transient and steady state response aspects of LFC. A basic operating policy of interconnected control areas is that each area should attempt to regulate ACE to zero. While the relative gains applied to net interchange (M-S)

and frequency deviation by area load-frequency controllers could perhaps be adjusted independently in order to obtain a desired transient response during normal operating conditions, the tie-line bias control strategy sets this relative gain equal to the frequency bias coefficient (B) for each area. This strategy thus achieves an implicit coordination between areas, which is very important during an abnormal operating condition, by essentially defining mutually determined and consistent steady state targets for all areas in the interconnection.

In the paper [5.8] the problem of distinguishing dynamic and steady state behavior was more fully explored and in addition a third major difficulty of earlier optimal regulator designs for LFC was addressed, namely the often dominating effect of prime mover energy source dynamics on unit generation response capability. Load-frequency control is fundamentally a tracking problem, and in the frequency range of interest the response limitations imposed by thermal energy sources must be recognized in the LFC design.

Based on these considerations, four basic objectives of LFC will be used to define the control problem:

1. The total area generation should be controlled so as to track the area load plus schedule. This will be called the load tracking objective.

2. The individual unit generations should be controlled so as to track the desired unit economic trajectories. This will be called the economic tracking objective.

3. Load-frequency control should allow the area primary response to occur naturally.

4. Individual unit response rate limitations must not be violated.

- A natural parallel structure of LFC exists both in the mathematical description of the physical processes involved and in these basic objectives, and this structure is exploited by designing independent controllers for each generating unit and a coordinating controller for the control area. The resulting hierarchical control structure has important practical (i.e. implementation) advantages, and this is one reason that it is generally utilized in conventional LFC designs. The centralized component (supremal) of the LFC design, the coordinating controller, is of course the subject of this chapter while the decentralized components (infimals), the unit controllers, are developed in the succeeding chapter. A technical paper was prepared for, and presented at, the Sixteenth Annual Allerton Conference on Communication, Control and Computing (Allerton House, University of Illinois at Urbana-Champaign, October 4-6, 1978) which summarizes the basic objectives and structure of both components of the LFC design. While it will be published in the Allerton Conference Proceedings, this paper is contained in Appendix A of this volume for the convenience of those who may find useful the overview which it provides.

5.1.3 Two Coordinating Controller Structures

While the latter two LFC objectives defined previously must be considered at the coordinating controller level, they are primarily achieved at the individual unit level and the main purpose of the coordinating controller is to provide megawatt reference inputs to the unit control loops such that the load and economic tracking objectives are achieved in a coordinated manner. Two basic design structures have been developed for the coordinating controller which correspond to two alternative methodologies for the design of robust linear regulators which have disturbance rejection properties.

These two categories of available controller synthesis procedures are roughly distinguished by the fact that one is based on the feedback of states of a dynamic system driven by the error vector, and

the other is based on the feedback of estimates of (possibly artificial) disturbance states. The former category includes the robust servo-compensator design methodology developed by Davidson [5.10] while the latter category includes the methodology which has been developed by Kwatny [5.9]. There has been a considerable amount of development work in this general area of synthesis procedures for robust linear regulators and the above references are excellent examples taken from a rather large body of control literature.

In [5.17], Kwatny and Kalnitsky discuss the two major categories of the numerous methodologies which have been developed and make the interesting observation that the error augmentation and the disturbance estimation approaches lead to multivariable compensator structures which are analogous to the two principal compensator configurations of classical single-input single-output control theory. The former approach results in a feedback compensation structure of the common minor within a major loop configuration while the latter one results in a series compensation structure. As a result of this structural difference, these two design methodologies can in general lead to substantially different closed loop response characteristics. Due primarily to this fact, two coordinating controllers have been developed, with more or less equal emphasis, in order to determine which structure is preferable for LFC.

The design which will be referred to as Coordinating Controller One (CC1) is based on the error augmentation approach and is developed in Section 5.2. Coordinating Controller Two (CC2) is based on the disturbance estimation approach and is developed in Section 5.3. In the remainder of this section the model used for design purposes is discussed.

5.1.4 Model

The model used for developing the coordinating controller structure is a very simple representation of a control area connected to an external system. Tie-line synchronizing oscillations have been removed because, for the purposes of AGC simulation and design, it is reasonable to assume that the interconnection is at a common system frequency [5.11]. This assumption is consistent with the observation made earlier, that synchronizing oscillations are generally too fast for supplementary control to be effective, and roughly implies that the model is limited by this assumption to the low frequency range, approximately out to .01 hz.

Table 5.1 contains definitions of the variables and parameters employed, while a block diagram is given in Figure 5.1. The major assumption made in deriving the coordinating controller structure is reflected in the unit model employed. The closed-loop system consisting of the unit and its unit controller is represented by a unity transfer function and thus the model is useful in the very low frequency range only. One reason that such a simplistic representation has been used is that the coordinating controller does not, as a result, require estimates of unit internal state variables. The basic idea here is that each unit controller is designed to provide a certain bandwidth and tracking capability, which is consistent with the limitations of that particular unit, and that the coordinating controller must work within that closed-loop bandwidth. Expanding on this idea somewhat, suppose that the estimation problem is temporarily ignored and that two basic steps in the controller synthesis are identified: first, relatively simple compensators are designed to provide desired tracking/disturbance rejection capabilities and are adjoined to the plant (in the error augmentation approach this design step is clear, while in the disturbance estimation approach this step is practically tied to

TABLE 5.1

NOMENCLATURE

Δf, y_1	frequency deviation from nominal
ΔIC, y_2	net tie flow deviation from schedule
y_3	area electrical load (at prevailing frequency)
P_T^o, y_4	area mechanical power at 60 Hz
H	total system inertia
β_1	local area regulation $\beta_1 = D_1 + R_1^{-1}$
β_2	external area regulation $\beta_2 = (D_2 + R_1^{-1})$
β	total system regulation ($\beta_2 = \beta_1 + \beta_2$)
D_1	local area load characteristic
D_2	external area load characteristic
R_1	local area governor characteristic
R_2	external area governor characteristic
B	frequency bias (positive) constant used in definition of ACE
ACE	area control error, ACE $\triangleq \Delta IC + B\Delta f$
x_i	ith unit generation demand @ 60 Hz
x_{n+1}	state variable representing frequency under ideal conditions
ω_1	disturbance term representing frequency error due to imperfect knowledge of β
ω_2	disturbance term representing external area generation and load conditions
ω_3	disturbance representing local area electrical load at 60 Hz
ω_4	disturbance representing rate of change of local area load
u_i	ith unit control variable, rate of change of generation
Δ_1	local area excess generation at 60 Hz
Δ_2	external area excess generation at 60 Hz
S^o	local area net tie flow schedule

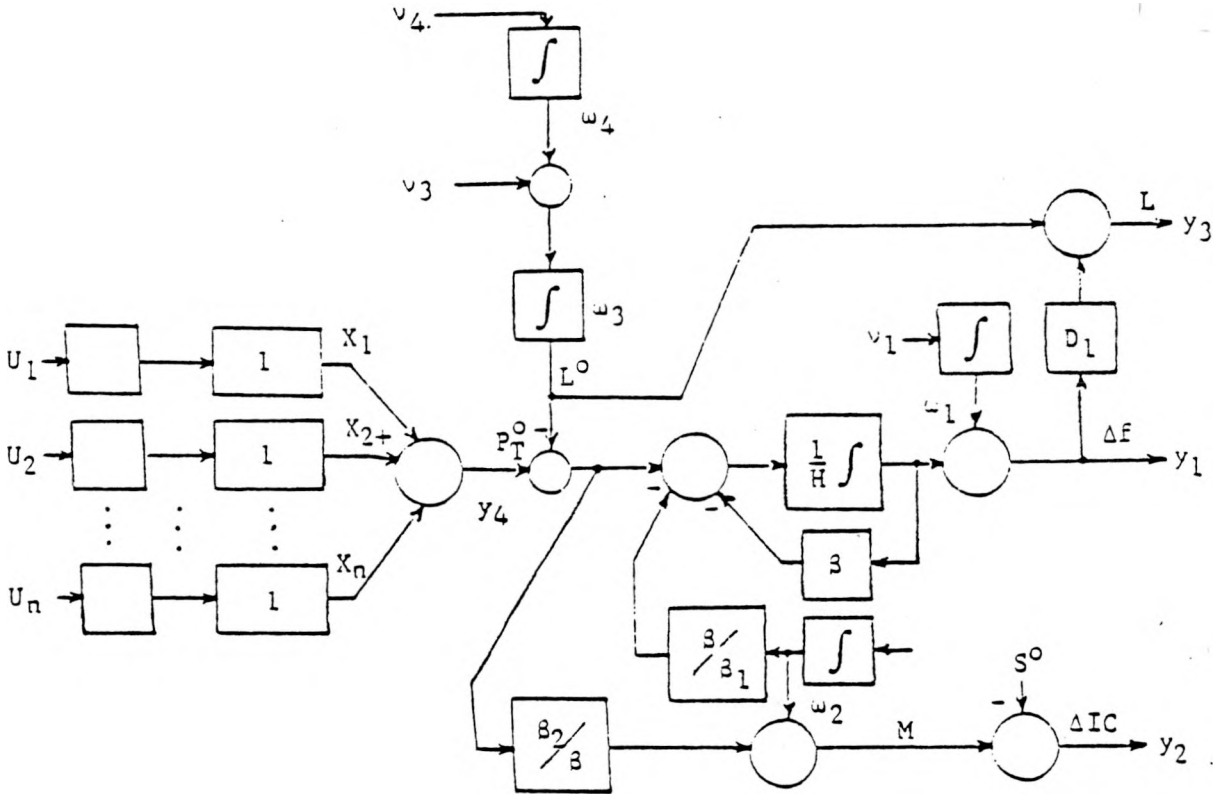

FIGURE 5.1 MODEL FOR COORDINATING CONTROLLER DESIGN

the observor design although it can be conceptually separated from the problem of estimating states of the plant) and second, a feedback gain matrix is designed to provide internal stability. The decomposition of the LFC structure into unit controllers and coordinating controllers, as well as the subsequent modeling assumptions employed in the latter design, has been motivated by the practical need to structure this stabilizing feedback gain matrix so that the resulting controller can be implemented at WEPCO. Of course, a centralized LFC design obtained from a straightforward application of either multivariable synthesis technique will result in full gain matrix. In particular, off-diagonal blocks associated with individual unit internal state variables will be full, although there is not a strong physical reason to expect that such cross-terms are needed for internal stabilization, e.g. a pressure deviation measurement from unit A can not be expected to critically affect the ability to stabilize unit B. In the context of these multivariable design methodologies, the design of individual unit MW control loops based on adequately detailed unit models, and the design of a coordinating controller based on a simple closed-loop unit model, is an effective way to avoid the complexity associated with a centralized solution.

5.2 COORDINATING CONTROLLER ONE

5.2.1 General Structure

Coordinating Controller One is based on the error augmentation approach mentioned previously and as a result the question of what error or errors should be continuously regulated by the LFC algorithm immediately arises. Of course the NAPSIC control performance criteria are for the most part stated in terms of certain measures on the area control error, and the continuous regulation of some function of ACE is standard practice during normal system operation. The "function of ACE" could for example be obtained using a low pass filter with dead-band logic or more sophisticated compensation such as that reported by

Ross in [5.13]. The ACE strategy is theoretically based on primarily steady state arguments however and some thought has been given in this project to the meaning of ACE as a continuous error, in the context of the basic objectives of LFC discussed previously. As a result a minor variation of the ACE strategy has been adopted for this coordinating controller design. Before discussing the general structure of the controller this variation is developed.

For simplicity at this point, consider the idealized steady state relations

$$G_T \triangleq G_T^o - 1/R_T\Delta f$$

$$L_T \triangleq L_T^o + \beta_L\Delta f \tag{5.1}$$

where:

G_T is total area electrical generation
L_T is total area electrical load
G_T^o is total area electrical generation at 60 Hz
L_T^o is total area load demand (electrical load at 60 Hz)

Now

$$ACE = \Delta IC + B\Delta f \tag{5.2}$$

but

$$\Delta IC = M - S^o = G_T - L_T - S^o \tag{5.3}$$

so

$$ACE = G_T^o - L_T^o - S^o + (-1/R_T - \beta_L + B)\Delta f \tag{5.4}$$

If we assume for the sake of argument that the area frequency bias (B) is equal to the area natural frequency response coefficient ($1/R_T + \beta_L$) then we see that ACE is a measure of area electrical generation/area load plus schedule mismatch referenced to 60 Hz. Presumably, if the relationships (5.1) are replaced with the appropriate dynamic relationships then a "dynamic ACE" can be defined which should be a measure of the LFC primary (load) tracking objective identified in Section 5.1.2. However, this approach leads (at least) to theoretical problems when the LFC problem is carefully formulated due to the fact that the electrical generation of a unit is not, strictly speaking, controllable from its speed-changer motor input. Because the electric power which flows from a unit depends on the current electrical state of the entire interconnected power system, defining an area control problem in terms of controlling electrical generation is in a sense an ill-posed problem. This (current) practice couples the various LFC area controllers through their objective functions, which can be seen by expressing ΔIC in the form (synchronizing oscillations have been removed)

$$\Delta IC = \frac{H_{EX}}{H_{SYS}} (P_T - L_T) - \frac{H_{AREA}}{H_{SYS}} (P_{EXT} - L_{EXT}) - S^o \qquad (5.5$$

where P_T (P_{EXT}) is the total area (system) mechanical power and $H_{SYS} = H_{AREA} + H_{EX}$ is the total system inertia. Because of this argument, and the fact that mechanical power is actually controlled from the governor speed-changer motor input, the load tracking objective of LFC is defined in terms of mechanical rather than electrical power for this coordinating controller. The difference between the two is simply a derivative of frquency term, so the steady state strategy of ACE control is not affected, but this term in ACE is destabilizing and hence it is removed by defining

$$\begin{aligned} ACEM &\triangleq P_T^o - L_T^o - S^o + (B - 1/R_T - \beta_L)\Delta f \\ &= ACE + 2H_{AREA} \cdot \dot{\Delta f} \end{aligned} \qquad (5.6)$$

as the (mechanical) area control error which is to be regulated to zero.

Numerous results can be obtained which provide insight into the effects of the negatively-signed derivative of system frequency term in ACE. A very simple but interesting one can be obtained using the static relationships (5.1) and comparing the variance of system frequency for a two area system for two cases. In each case we let $B = 1/R + \beta_L$ and assume that each area is able to achieve some ideal but comparable performance, in each case. Thus in case one each area maintains $G_T^o - L^o - S^o = W$ while in case two each area maintains $P_T^o - L^o - S^o = W$, where, for areas one and two, W_1 and W_2 are zero mean, independent random variables with variances σ_1^2 and σ_2^2 respectively. Then the variance of system frequency, $\sigma_{\Delta f}^2$ is

$$\begin{cases} \frac{1}{\beta^2}\,(\sigma_1^2 + \sigma_2^2) & \text{when electrical generation is controlled} \\ \\ \frac{1}{2H\beta}\,(\sigma_1^2 + \sigma_2^2) & \text{when mechanical power is controlled} \end{cases} \qquad (5.7)$$

Now H is the total system inertia constant and $\beta = 1/R_1 + 1/R_2 + \beta_{L1} + \beta_{L2}$ is the total system natural frequency characteristic. Comparing the two results in (5.7), it is clear that the variance of system frequency is considerably reduced when mechanical power is controlled. The reason for this difference is that the derivative of frequency term in ACE effectively reduces system frequency damping and is in this sense destabilizing. One way to see this is to do some manipulation of the block diagram of a simple two area model.

Consider the two area model illustrated in block diagram form in Figure 5.2 which shows ACE control and was analyzed, for example, in [5.4]. By sliding the derivative of frequency term in ACE through the speed-changer motor representation in Figure 5.2, the form illustrated in Figure 5.3 is obtained. The point here is that regulating ACE with this configuration is equivalent to regulating ACEM but with considerably

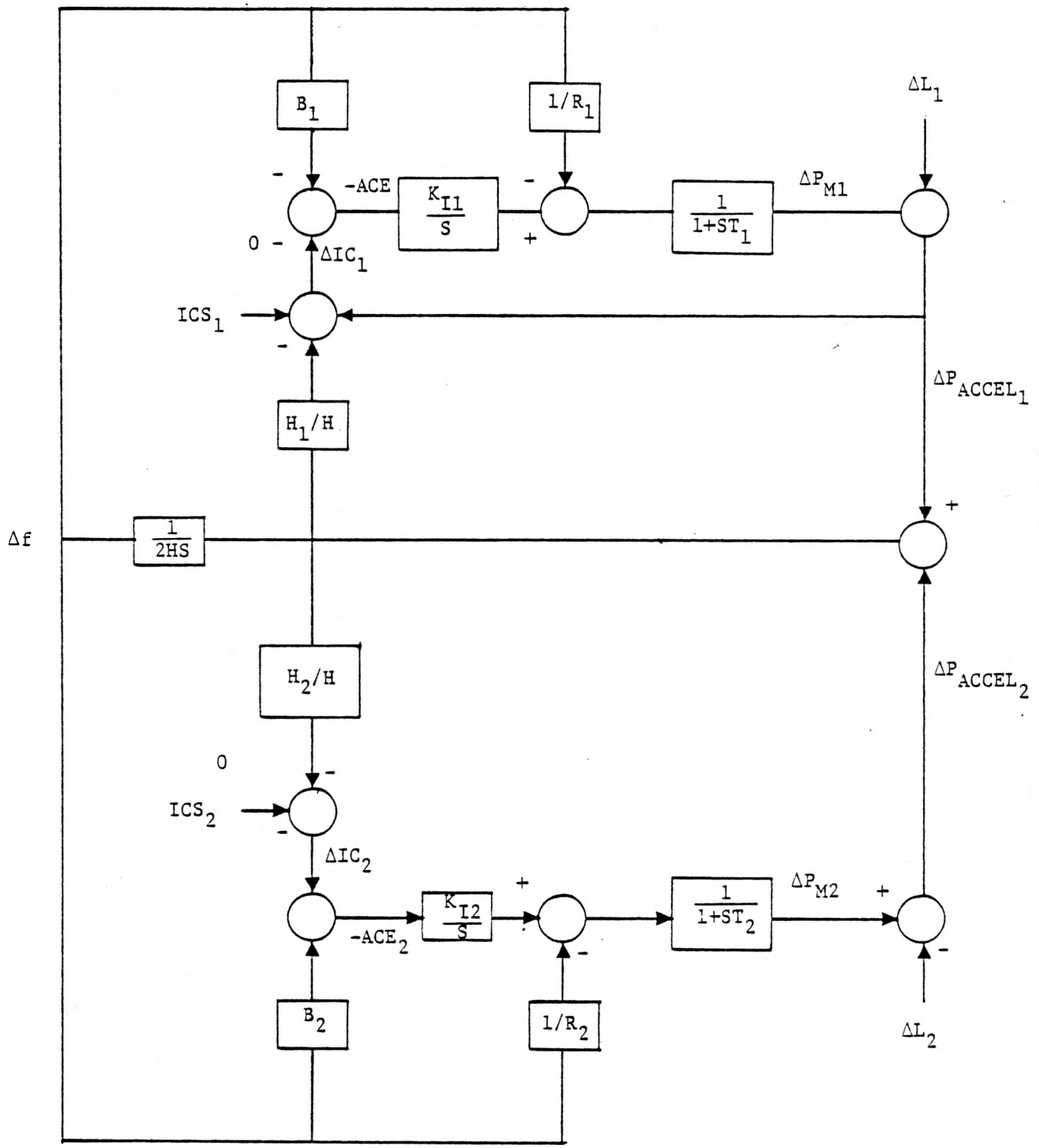

FIGURE 5.2 TWO AREA MODEL - ACE REGULATION

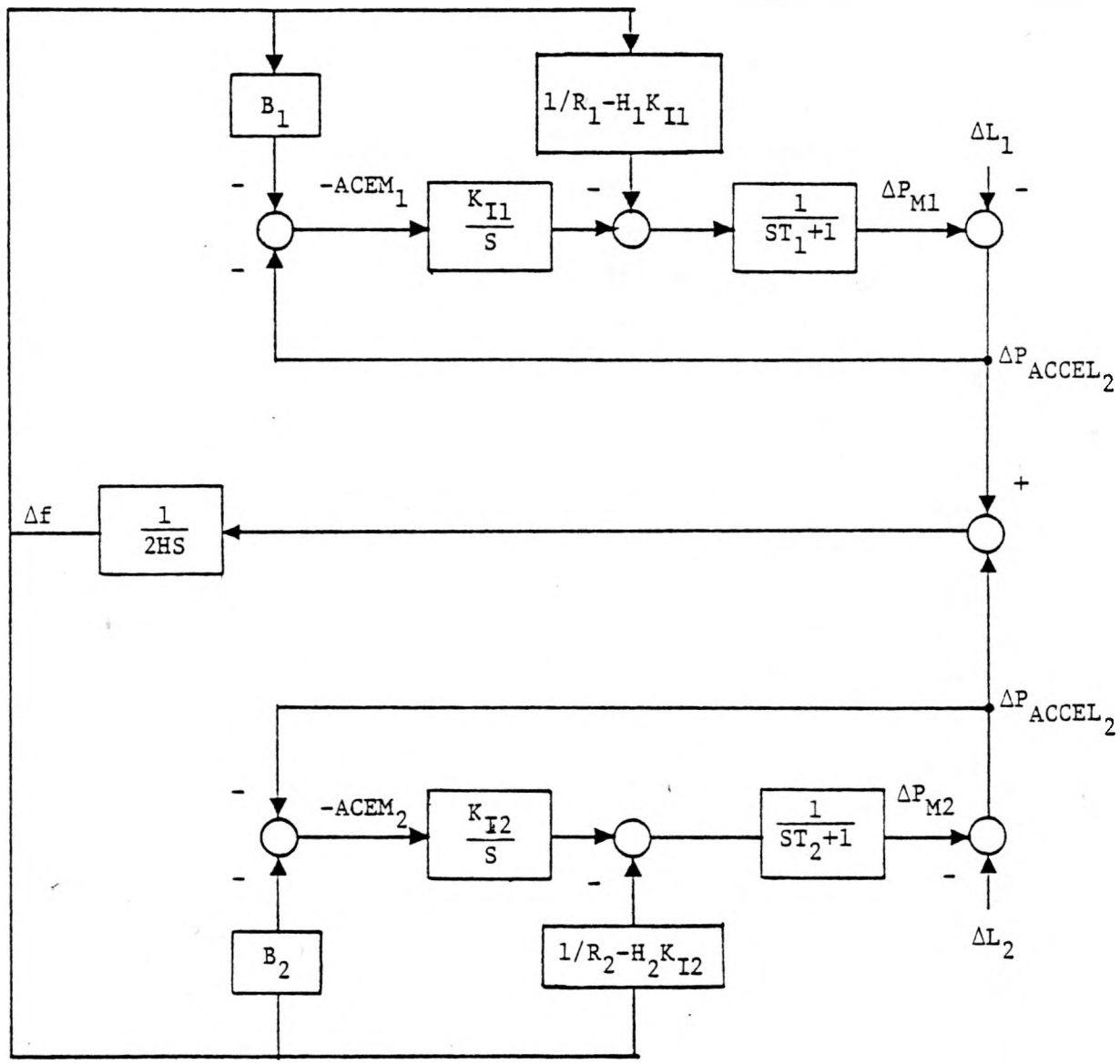

FIGURE 5.3 REARRANGED TWO AREA MODEL - ACE REGULATION REDUCES NET FREQUENCY DAMPING

reduced effective governor response characteristic, $1/R_1' = 1/R_1 - H_1 \cdot K_{I1}$ for area one, etc. If the control error is taken to be ACEM then this reduction does not occur, i.e., $1/R_1' = 1/R_1$ as shown in Figure 5.4. Notice that increasing the gain on ACE, in order to achieve better tracking performance for example, further reduces the effective damping. This would appear to represent a very significant limitation of the simple ACE controller in Figure 5.2 or 5.3.

The practical significance of this distinction between ACE and ACEM has not yet been determined, however. It is necessary to perform some comparative analyses, using the detailed non-linear AGC simulation program developed in Task 1, in order to more thoroughly evaluate some of the concepts which have been discussed in this subsection and to obtain some meaningful quantitative results. Certainly the relative magnitude of the derivative term and the performance of the filter designed to estimate mechanical power (Section 5.2.3) are important factors. Even if the practical differences are small however, it seems fair to conclude that a consistent statement of the load tracking objective is to control area 60 hz. mechanical power so as to track area 60 hz load plus schedule (note that any value of area frequency bias B can be easily accommodated in the filter for estimating 60 hz. load, for example, with a bias term $(B - 1/R_T - \beta_L)\Delta f$). In addition to the potential performance benefits of this modified ACE strategy, the area control problem can be more clearly defined, because the external area's accelerating power has been removed from the area control error, at the expense of slightly complicating the associated estimation problem.

Having identified ACEM as a consistent measure of the load tracking objective, the basic structure of coordinating controller one can be illustrated with the block diagram form of Figure 5.5. This control structure is based on the model illustrated in Figure 5.1 and, because a unity transfer function is used to represent the closed loop system of

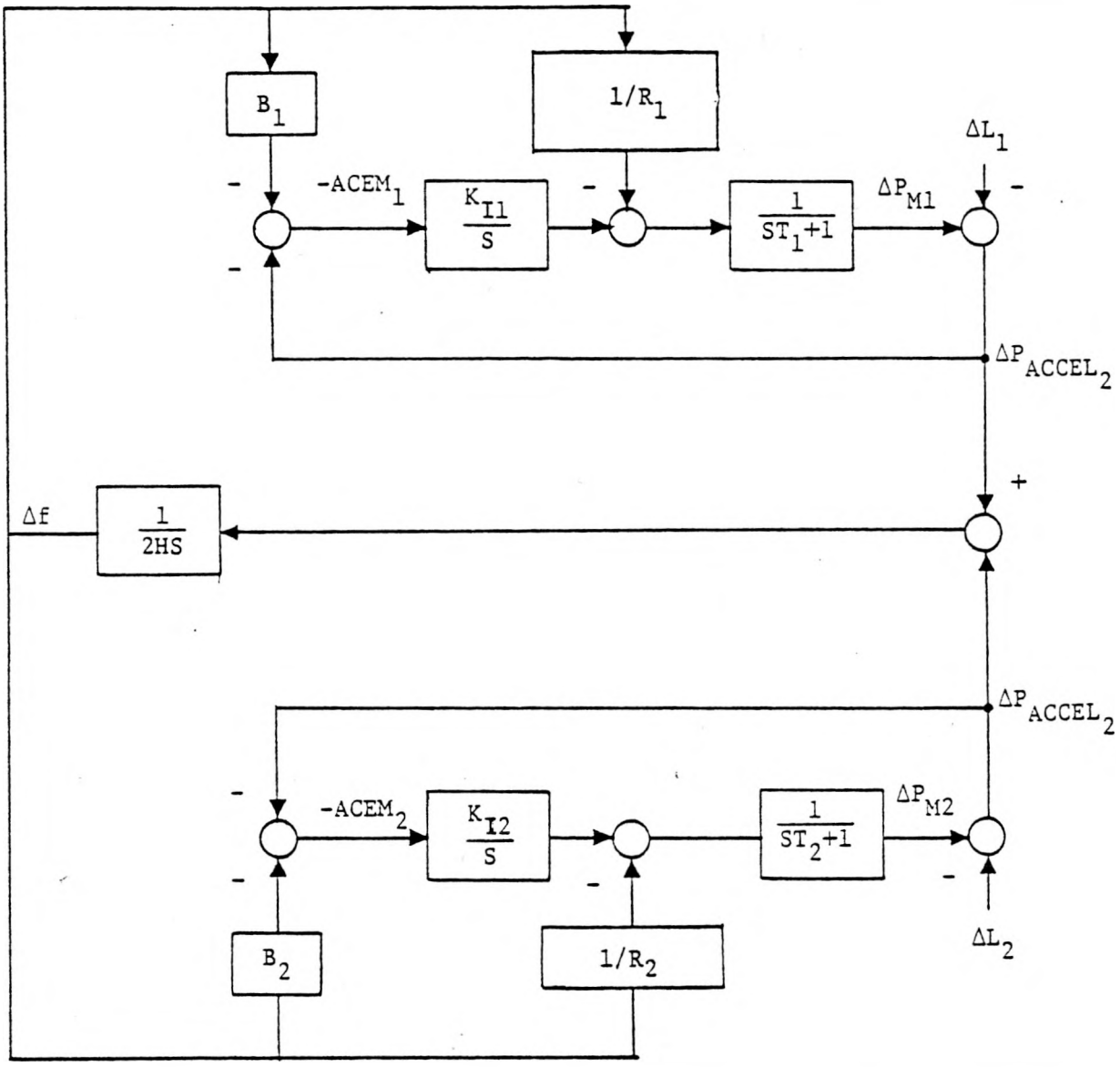

FIGURE 5.4 TWO AREA MODEL - ACEM REGULATION

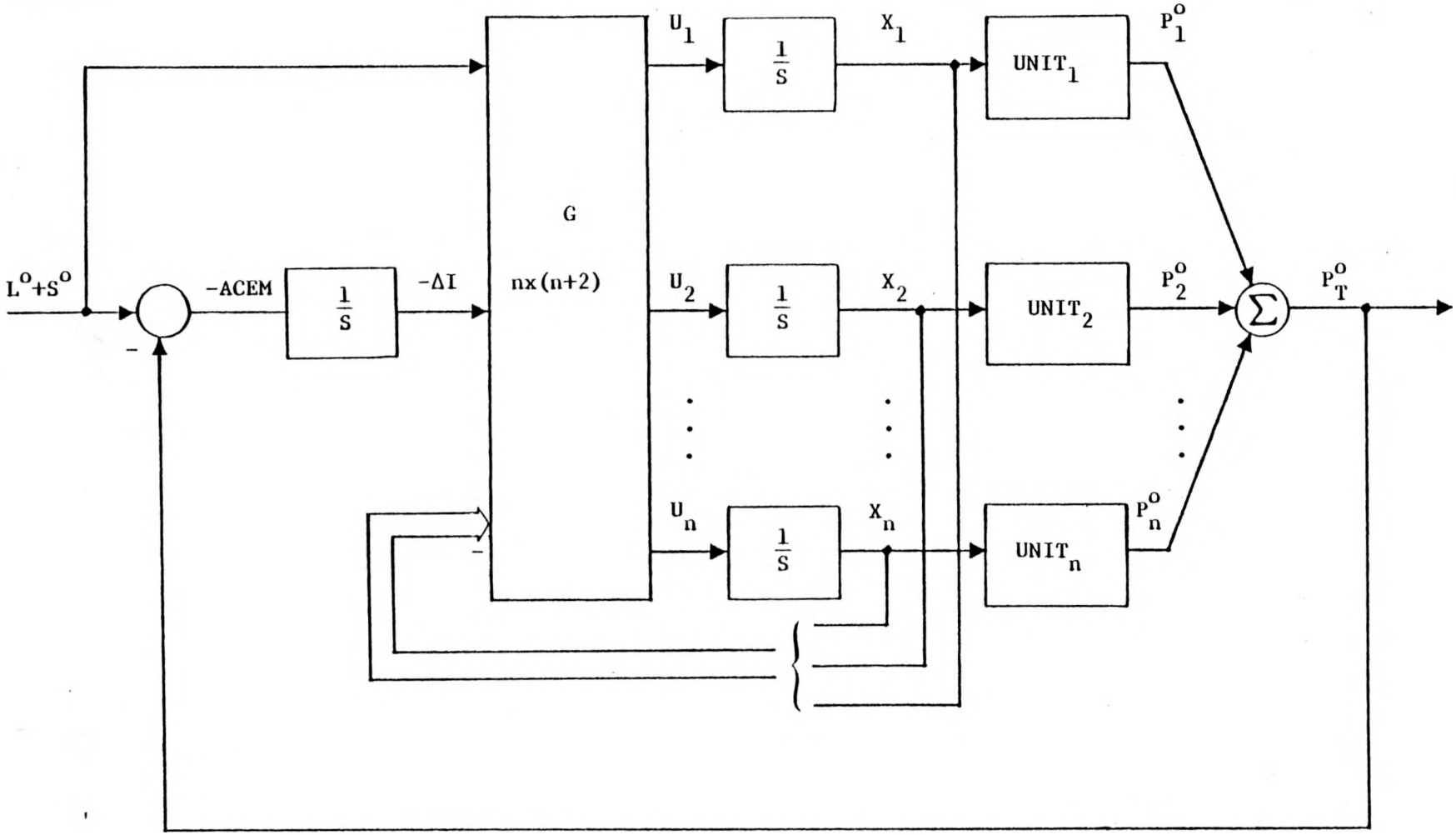

FIGURE 5.5 BASIC CONFIGURATION OF COORDINATING CONTROLLER ONE - UNIT INPUTS ARE INTERPRETED AS STATES

each unit in this model, the question immediately arises whether unit MW reference inputs or mechanical power outputs (at 60 hz.) should be interpreted as the states which are fed back through the gain matrix G. The former interpretation was illustrated in Figure 5.5 while the latter is illustrated in Figure 5.6. Of course both could be fed back, through different gains, and while this is the approach employed in the recommended design, a discussion of this issue is deferred to Section 5.2.4 because some of the results contained therein are useful for investigating this design freedom.

The feedforward of $L^o + S^o$ shown in the configurations of Figures 5.5 and 5.6 is not an immediate consequence of the robust servo-compensator design methodology. In fact the regulator design step in this approach employs the linear quadratic regulator theory for the determination of the feedback gain matrix, i.e., for the matrix G shown in these figures excluding the column of feedforward gains. The choice of the latter gains, which affect the closed loop response but not the absolute stability of the system, represents another design freedom which has been exercised in order to improve the load tracking performance of the basic servo-compensator.

The Dynamic Economic Dispatch component of the AGC software package provides smooth, rate-constrained economic trajectories for units in the appropriate control mode(s). These trajectories are based upon the short term load forecast which is in turn non-trivially based upon the past history of secular load demand and a number of important exogenous variables (indirectly via the existing WEPCO hourly load forecast) such as weather conditions, etc. These trajectories are incorporated into Coordinating Controller One as a simple feedforward term. For the basic configuration of Figure 5.6 for example, the addition of the dynamic economic dispatch feedforward term is illustrated in Figure 5.7. Several observations are appropriate at this point. First,

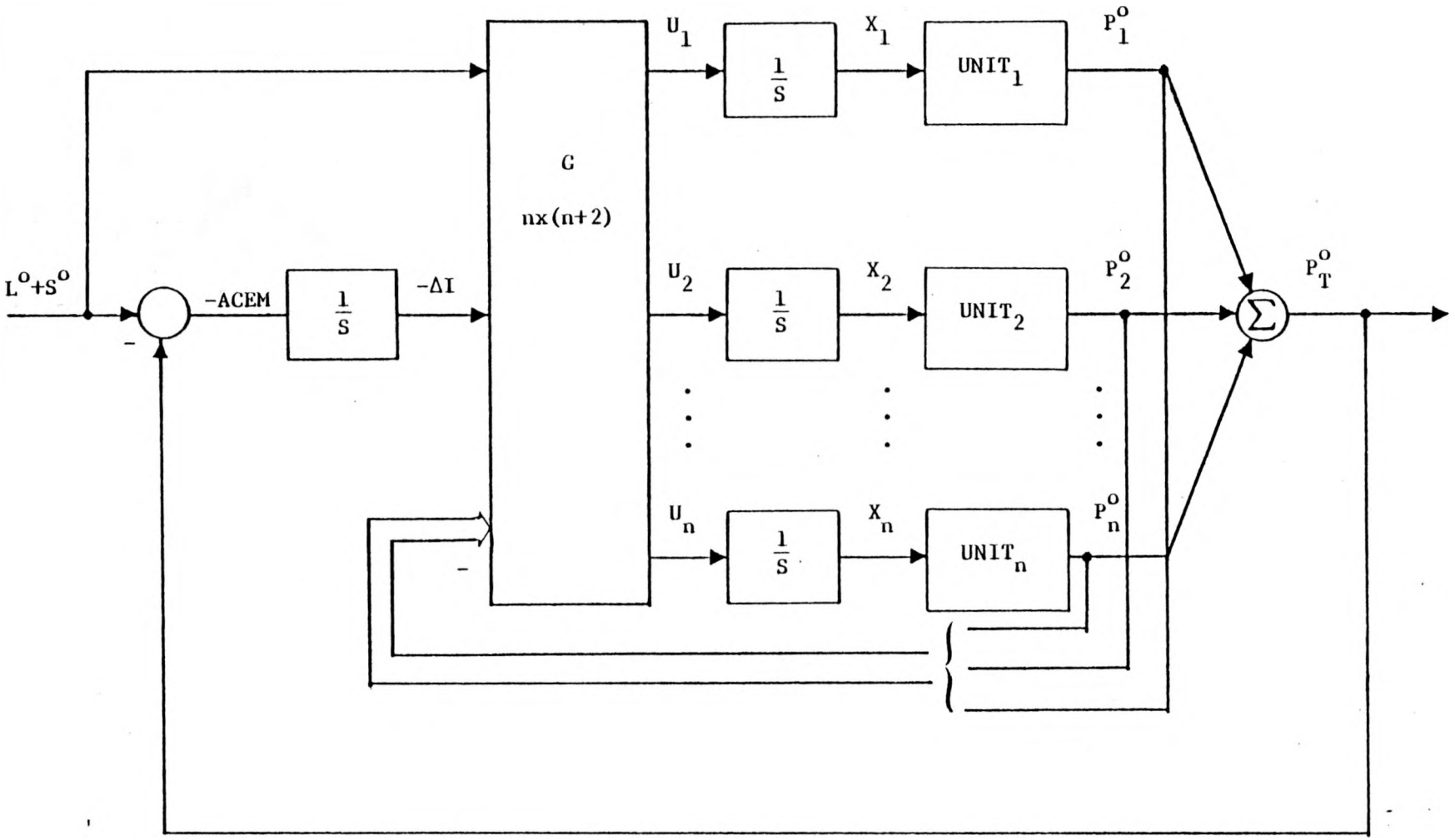

FIGURE 5.6 BASIC CONFIGURATION OF COORDINATING CONTROLLER ONE - UNIT OUTPUTS ARE INTERPRETED AS STATES

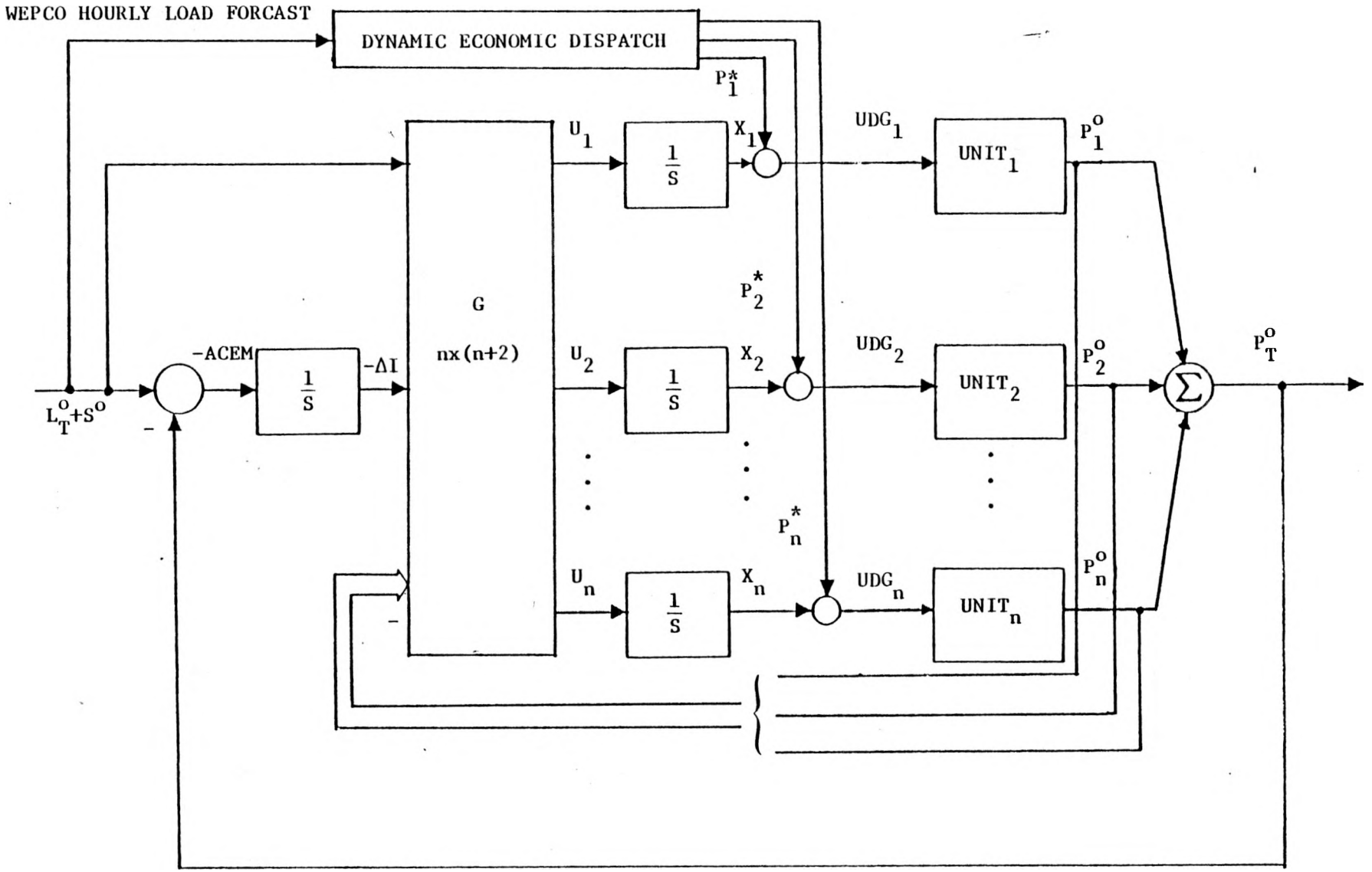

FIGURE 5.7 BASIC CONFIGURATION OF COORDINATING CONTROLLER ONE (UNIT OUTPUTS AS STATES) DYNAMIC ECONOMIC DISPATCH PROVIDES FEEDFORWARD

because these trajectories are smooth and rate-constrained, it is reasonable to feed them forward without additional processing in the coordinating controller. Second, because the economic trajectories P_i^*, i = 1,2,...n are determined based on the short-term load forecast, they can be advanced in time with respect to real-time. There are two advantages then of these feedforward signals; they are based on a forecast of secular load, hence the higher frequency components of load demand are effectively removed without the phase lag introduced by a low pass filter working in real-time and in addition a "pure" advance of ΔT seconds can be introduced to partially compensate for the lag associated with unit response in order to improve load tracking performance. Concomitant with these advantages is the disadvantage associated with forecast errors, but this problem is of course amenable to feedback control.

5.2.2 Regulator Design

A major step in the design procedure is the determination of the feedback gain matrix illustrated in Figures 5.5 - 5.7. The feedforward terms are neglected, disturbance inputs are set to zero, and a standard regulator design, based on the well-established linear quadratic regulator theory, is obtained for the resulting pertubational system given in Equation (5.8).

$$\dot{\Delta x}_i = \Delta u_i \qquad i = 1,2,...n \tag{5.8}$$

$$\dot{\Delta I} = \sum_{i=1}^{n} \Delta x_i$$

Defining the infinite-time quadratic cost function J,

$$J = \int_0^\infty [\bar{\Delta x}^T Q \bar{\Delta x} + \Delta u^T R \Delta u] dt \tag{5.9}$$

the solution to this standard regulator problem provides with certain minor technical restrictions on the matrices Q and R, the feedback gain matrix $\bar{G}$, where

$$\bar{G} = R^{-1}B^{T}K \tag{5.10}$$

K is the maximal solution to the Riccatti equation

$$KA + A^{T}K + Q - KBR^{-1}B^{T}K = 0 \tag{5.11}$$

where (5.8) is put into the standard state form

$$\dot{\overline{\Delta x}} = A\overline{\Delta x} + B\Delta u \tag{5.12}$$

$$\overline{\Delta x}^{T} \triangleq [\Delta x_1, \Delta x_2, \ldots \Delta x_n, \Delta I]$$

$$\Delta u^{T} \triangleq [\Delta u_1, \Delta u_2, \ldots \Delta u_n].$$

The nx(n+2) gain matrix G illustrated in Figures 5.5 - 5.7 is obtained from the nx(n+1) feedback gain matrix $\bar{G}$ given in (5.10) by augmenting the comumn vector of feedforward gains g_{ff}, where

$$g_{ff}^{T} \triangleq [g_{ff,1}\ g_{ff,2} \cdots g_{ff,n}]. \tag{5.13}$$

In both coordinating controller structures a regulator design based on the linear quadratic formulation is carried out. In both cases the pertubation states Δx_i, i = 1,...,n are part of the model used in this design step, but the two synthesis procedures differ with respect to the additional states which are involved in the regulator design. For example, the integral state ΔI in (5.8), which again has been introduced in order to provide reset and enhance robustness in this case, does not appear in the regulator problem formulation associated with Coordinating Controller Two. In both cases, however, a specific structure is imposed on the state deviation, quadratic cost term in (5.9) determined by the pertubation states Δx_i, i = 1,2,...n in order to explicitly define costs

which correspond to each of the LFC tracking objectives defined earlier, i.e., the load (primary) tracking and the economic (secondary) tracking objectives. This separation of the state deviation cost into two terms is common to both structures; in this section the basic concept involved is simply introduced and applied, while a more detailed mathematical approach is followed in Section 5.3.1.

Consider the sum Δx_T, where

$$\Delta x_T \triangleq \Delta x_1 + \Delta x_2 + \ldots + \Delta x_n \tag{5.14}$$

Regulation of Δx_T during the transient actually implies regulation of total generation to the value for which ACEM = 0. Thus the scalar quadratic cost term $q_1(\Delta x_T)^2$ is a measure of performance for the load tracking objective. Furthermore, a quadratic weighting on variations of the quantities $\Delta x_1, \ldots, \Delta x_n$ in the subspace defined by Δx_T = constant corresponds to a measure of performance for the economic tracking objective. Thus we can rewrite the general cost expression of (5.9) by separating these terms, i.e.,

$$J = \int_0^\infty [q_1 \Delta x^T C^T C \, \Delta x + \Delta x^T (I - C^* C)^T Q_2 (I - C^* C) \Delta x + q_3 (\Delta I)^2 + \Delta u^T R \Delta u] dt \tag{5.15}$$

where

$$C^T \in R^n, \; C = [11 \ldots 1], \; CC^* = I$$

and the first two terms in (5.15) correspond to the load and economic tracking objectives respectively. Figure 5.8 provides an illustration of the two orthogonal subspaces for the case of n = 3, i.e. for a three machine system. Defining different state deviation costs in each subspace

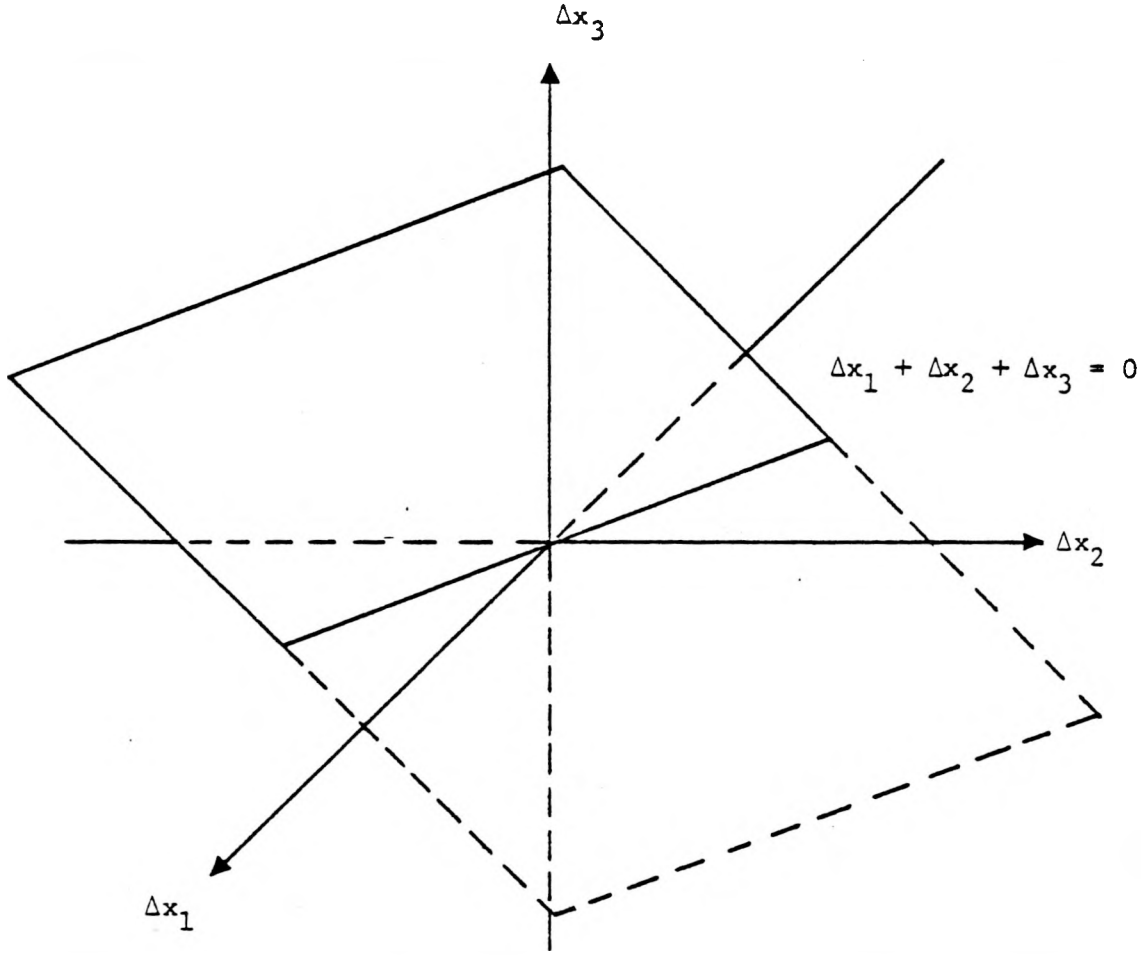

FIGURE 5.8 3 MACHINE EXAMPLE - SPACE DEFINED BY PERTUBATIONAL VARIATIONS Δx_1, Δx_2 AND Δx_3 IS DIVIDED INTO TWO ORTHOGONAL SUBSPACES

reflects the objective of shaping the closed loop response so that generation change will occur with different response times in each subspace. For example, for a step change in load ΔL, total generation could change with a relatively fast response time according to an allocation which is based upon unit regulating capacity and capability, while a redistribution of the total change amongst the available units, which may be based upon unit economics and current high and low limits, could occur with a slower response time. In terms of the geometrical illustration in Figure 5.8, the "first"response, which corresponds to the load tracking objective, is motion orthogonal to the $\Delta x_1+\Delta x_2+\Delta x_3 = 0$ plane while the "second" response, which corresponds to the economic tracking objective, is motion parallel to this plane.

In order to simplify the discussion at this point, suppose that the integral state ΔI is removed from the model and hence from the cost functional (5.15). Then it is shown in Section 5.3.1 that the solution to this standard regulator problem results in a closed loop eigensystem which has n-1 modes which lie in the subspace corresponding to ACEM = 0 and an additional mode in the direction of $R^{-1}C^T$. This last mode regulates ACEM to zero and its response time is determined by the scalar parameter q_1. The additional (n-1) modes are "redistribution" modes which allow for the redistribution of generation to (possibly economic) targets whcih lie in the ACEM = 0 subspace and which have response times that depend on the parameter matrix Q_2. Thus, response times corresponding to the load and economic tracking objectives can be separately specified. With the integral state included the modal structure is similar, but now there are two modes associated with ACEM and its integral which have response times that are determined by the scalar parameters q_1 and q_3. By applying a similarity transformation to the model description (5.8) and investigating the regulator problem solution in the new state space, this modal structure can not only be more easily recognized but a suboptimal regulator structure can be obtained.

- The similarity transformation of interest is defined in terms of the pseudo-inverse of C introduced in (5.15), C*. Let

$$(C^*)^T = (C_1^* \;\; C_2^* \;\; \ldots \;\; C_n^*), \text{ and}$$

define

$$\delta x_i \triangleq \Delta x_i - C_i^* \Delta x_T \qquad i = 1,2,\ldots n \tag{5.16}$$

Notice that $C\,\delta x = C\,\Delta x - CC^*\Delta x_T = 0$, because $CC^* = I$ and $C\Delta x = \Delta x_T$ by definition. The new states are obtained from (5.14) and (5.16) and can be written in matrix form

$$\begin{bmatrix} \delta x_1 \\ \delta x_2 \\ \cdot \\ \cdot \\ \cdot \\ \delta x_{n-1} \\ \Delta x_T \end{bmatrix} = \begin{bmatrix} 1-C_1^* & -C_1^* & \cdots & -C_1^* & -C_1^* \\ -C_2^* & 1-C_2^* & \cdots & -C_2^* & -C_2^* \\ \cdot & \cdot & & \cdot & \cdot \\ \cdot & \cdot & & \cdot & \cdot \\ \cdot & \cdot & & \cdot & \cdot \\ -C_{n-1}^* & \cdot & \cdots & 1-C_{n-1}^* & -C_{n-1}^* \\ 1 & 1 & \cdots & 1 & 1 \end{bmatrix} \begin{bmatrix} \Delta x_1 \\ \Delta x_2 \\ \cdot \\ \cdot \\ \cdot \\ \Delta x_{n-1} \\ \Delta x_n \end{bmatrix} \tag{5.17}$$

Denoting the (n-1) vector $\delta\hat{X}$ obtained by deleting the linearly dependent δX_n from the n vector δX, (5.17) can be more compactly written

$$\begin{bmatrix} \delta\hat{x} \\ \hline \Delta x_T \end{bmatrix} = \begin{bmatrix} T \\ \hline C \end{bmatrix} \begin{bmatrix} \Delta x \end{bmatrix}, \tag{5.18}$$

while the inverse transformation is

$$\begin{bmatrix} \Delta x \end{bmatrix} = \left[\begin{array}{c|c} I_{n-1} & C^* \\ \hline -1\,-1\,\cdots\,-1 & \end{array}\right] \begin{bmatrix} \delta\hat{x} \\ \hline \Delta x_T \end{bmatrix} \tag{5.19}$$

where I_{n-1} is the (n-1) x (n-1) identity matrix. Applying the transformation (5.18) to the model equations (5.8) yields the state equations (5.20)

$$\frac{d}{dt}\begin{bmatrix} \delta\hat{x} \\ \hline \Delta x_T \\ \Delta I \end{bmatrix} = \begin{bmatrix} 0 & 0 \\ \hline 0 & \begin{matrix} 0 & 0 \\ 1 & 0 \end{matrix} \end{bmatrix} \begin{bmatrix} \delta\hat{x} \\ \hline \Delta x_T \\ \Delta I \end{bmatrix} + \begin{bmatrix} \hat{T} \\ \hline \bar{C} \\ 0 \end{bmatrix} \begin{bmatrix} \Delta u \end{bmatrix} \qquad (5.20)$$

which are partitioned in order to separate terms associated with total generation change.

Now the quadratic costs (5.15) used in the regulator problem formulation can be written in terms of the new state variables in (5.20). Proceeding term by term,

$$q_1 \, \Delta x^T C^T \Delta x = q_1 \Delta x_T^2 \text{ , and} \qquad (5.21)$$

$$\Delta x^T (I - C^* C)^T \, Q_2 (I - C^* C) \Delta x = \delta\hat{x} \, \hat{Q}_2 \, \delta\hat{x} \qquad (5.22)$$

while the last two terms remain unchanged. The economic tracking costs (5.22) are obtained by noting that

$$\delta x = P \, \delta\hat{x} \qquad (5.23)$$

where P is the n x (n-1) matrix

$$P \triangleq \begin{bmatrix} & I_{n-1} & \\ \hline -1 & -1 \cdots & -1 \end{bmatrix} \qquad (5.24)$$

and the LHS of (5.22) is equal to

$$\delta x^T Q_2 \delta x = \delta \hat{x}^T P^T Q_2 \, P \, \delta \hat{x} \triangleq \delta \hat{x} \, \hat{Q}_2 \delta \hat{x} \tag{5.25}$$

Thus by defining the (n+1) x (n+1) matrix Q

$$Q = \left[\begin{array}{c|c} Q_2 & \\ \hline & q_1 \\ \hline & \\ & q_3 \end{array}\right] \tag{5.26}$$

the cost function J of (5.15) can be compactly written

$$J = \int_0^\infty (x^T Q x + \Delta u^T R \Delta u) dt, \tag{5.27}$$

where $x^T \triangleq (\delta \hat{x}^T, \Delta x_T, \Delta I)$, and the regulator design can be carried out in the new state space with (5.26) and the state equations (5.20). The Ricatti equation

$$KA + A^T K + Q - KBR^{-1}B^T K = 0 \tag{5.28}$$

has a special structure, when a particular choice is made for R, which provides insight into the closed loop eigensystem and allows a suboptimal regulator design to be obtained. Consider the term $BR^{-1}B^T$ in (5.28), where B is given in (5.20).

$$BR^{-1}B^T = \left[\begin{array}{c} \hat{T} \\ \hline C \\ 0 \end{array}\right] R^{-1} \left[\begin{array}{c|cc} \hat{T}^T & C^T & 0 \end{array}\right] \left[\begin{array}{c|cc} \hat{T}R^{-1}\hat{T}^T & \hat{T}R^{-1}C^T & 0 \\ \hline CR^{-1}\hat{T}^T & CR^{-1}C^T & 0 \\ 0 & 0 & 0 \end{array}\right] \tag{5.29}$$

Now the assumption is made that R is chosen such that

$$\hat{T}R^{-1}C^T = 0 \tag{5.30}$$

While this is a restrictive assumption, the meaningful case of $R = \text{diag}[r_i]$ is not excluded by (5.30). If this choice of R is made, for example, (5.30) yields the equations

$$1/r_i - C_i^* (1/r_1 + 1/r_2 + \ldots + 1/r_n) = 0 \quad i = 1,2,\ldots n-1 \tag{5.31}$$

which can be satisfied by choosing the particular pseudo inverse of $C(C^*)$

$$C_i^* = S/r_i \qquad i = 1,2,\ldots n \tag{5.32}$$

where

$$1/S \triangleq 1/r_1 + 1/r_2 + \ldots + 1/r_n$$

Thus in this case $R^{-1}C^T = \alpha C^*$, where α is the scalar $\alpha = CR^{-1}C^T$.

When R is chosen to satisfy (5.30), cross-terms in the Ricatti equation (5.28) are eliminated, i.e., with the solution K of (5.28) partitioned conformally with the partition of the state equations (5.20),

$$K = \begin{bmatrix} K_{11} & K_{12} \\ K_{21} & K_{22} \end{bmatrix} \qquad \begin{matrix} K_{11} & (n-1) \times (n-1) \\ K_{22} & 2 \times 2 \end{matrix}$$

then $K_{12} = K_{21}^T = 0$. As a result the Ricatti equation decouples into two Ricatti equations which are much easier to solve:

$$\hat{Q}_2 - K_{11}(\hat{T}R^{-1}\hat{T}^T)K_{11} = 0 \qquad \text{(a)}$$

$$K_{22}A_{22} + A_{22}^T K_{22} + \begin{bmatrix} q_1 & \\ & q_3 \end{bmatrix} - K_{22}\begin{bmatrix} CR^{-1}C^T & 0 \\ 0 & 0 \end{bmatrix}K_{22} = 0 \qquad \text{(b)} \qquad (5.33)$$

$$K_{12} = K_{21}^T = 0$$

where $A_{22} = \begin{bmatrix} 0 & 0 \\ 1 & 0 \end{bmatrix}$ from (5.20)

As one would expect, the decoupling of the Ricatti equation occurs because the problem of minimizing the quadratic cost (5.27), subject to the state equations (5.20) with the linear feedback controls $\Delta u = -G\Delta x$, where $G = R^{-1}B^T K$, has been decomposed into two independent minimization problems, one corresponding to the load tracking objective and the other to the economic tracking objective. The solution to the first problem determines the total control which will be applied, while the solution to the latter problem determines how the total control will be allocated amongst the n machines. The separation of the state deviation costs is clear from the block diagonal form of Q given in (5.26); the assumption mode previously on the form of the control effort quadratic weighting matrix R induces a similar separation of control costs. Applying the same transformation to the controls Δu_i, i = 1,2,...,n that was applied to the state deviations in (5.18) yields

$$\Delta u = \delta u + C^* \Delta u_T, \qquad (5.34)$$

$$\Delta u_T \triangleq C\Delta u$$

and

$$\Delta u^T R \Delta u = \delta u^T R \delta u + \delta u^T R C^* \Delta u_T + \Delta u_T (C^*)^T R \delta u + (C^*)^T R C^* \Delta u_T^2$$

$$= \delta u^T R \delta u + (C^*)^T R C^* \Delta u_T$$

because $R^{-1}C^T = \alpha C^*$ by assumption.

Having investigated the optimal regulator solution with the aid of a physically meaningful similarity transformation, the closed loop eigensystem which results can be characterized. The Ricatti solution (5.33) provides the control law

$$\Delta u = -R^{-1}B^T K x = -R^{-1} \left[\begin{array}{c|c|c} \hat{T}^T & C^T & 0 \end{array}\right] \left[\begin{array}{c|c} K_{11} & \\ \hline & K_{22} \end{array}\right] \left[\begin{array}{c} \delta\hat{x} \\ \hline \Delta x_T \\ \Delta I \end{array}\right] \qquad (5.35)$$

and hence the closed loop matrix A_{CL} for the transformed system (5.20) is

$$A_{CL} = A - BG = \left[\begin{array}{c|c} -\hat{T}R^{-1}\hat{T}^T K_{11} & 0 \\ \hline 0 & A_{22} - \left[\begin{array}{cc} CR^{-1}C^T & 0 \\ 0 & 0 \end{array}\right] K_{22} \end{array}\right] \begin{array}{l} \uparrow \\ n-1 \\ \downarrow \\ \uparrow \\ 2 \\ \downarrow \end{array} \qquad (5.36)$$

$$\leftarrow n-1 \rightarrow \quad \leftarrow \qquad 2 \qquad \rightarrow$$

It is easy to see from the block diagonal form of A_{CL} in (5.36) that the closed loop system will have n-1 modes which lie in the subspace corresponding to ACEM = 0 and two additional modes associated with the regulation of ACEM and its integral. Moreover from (5.33) we see that the former modes have time constants which are determined by the parameter matrix $\hat{Q}_2$ while the latter modes have time constants which are determined by the scalar parameters q_1 and q_3. Of course the closed loop system matrix associated with the original state variables Δx and ΔI is obtained by applying the similarity transformation defined previously in (5.18) and (5.19). The feedback gain matrix $\bar{G}$ (5.10), which provides the controls $\Delta u = -\bar{G}\Delta\bar{x}$, where again $\Delta\bar{x}^T = (\Delta x^T, \Delta I)$, can be obtained from the feedback gain matrix $R^{-1}B^T K$ defined in (5.35) by using the same transformation. That is, from (5.35)

$$\Delta u = -R^{-1}B^T K x, \text{ where } x^T = (\delta\hat{x}^T, \Delta x_T, \Delta I)$$

but from (5.18) $\delta\hat{x} = \hat{T}\Delta x$ and $\Delta x_T = C\Delta x$, so

$$\Delta u = -R^{-1}B^T K x = -R^{-1}B^T K P \Delta\bar{x} \triangleq -\bar{G}\Delta\bar{x} \tag{5.37}$$

where

$$P \triangleq \begin{array}{c} \left[\begin{array}{cc} \hat{T} & \\ C & \\ & 1 \end{array}\right] \\ \begin{array}{cc} n & 1 \end{array} \end{array} \quad \begin{array}{l} (n-1) \\ 1 \\ 1 \end{array} \tag{5.38}$$

5.2.3 Simplified Regulator Design

The previous subsection described the solution of a quadratic regulator problem which resulted in the nx(n+1) feedback gain matrix $\bar{G}$. While $\bar{G}$ could be obtained via the Ricatti equation (5.11), the similarity transformation introduced provided an alternative means which exploits the special structure of the problem. In this approach the relevant Ricatti equation, (5.32), actually consists of two uncoupled Ricatti equations. From a practical point of view the significance of this is that (5.32-b) can be solved analytically, while (5.32-a) is a very special Ricatti equation (no linear terms) which can be solved using very efficient and reliable Cholesky factorization algorithms [5.18]. This computational concern is important because the generating units on-line vary throughout the day and in addition the system dispatcher and/or plant operators often change the operating mode of the on-line units. Each such change necessitates a change in the feedback gain matrix $\bar{G}$, so either $\bar{G}$ must be computed on-line or a large number of gain matrices must be pre-computed and stored. Furthermore, a change in the control law may be

desirable for other reasons, such as, changes in unit high and low regulating limits. Due to the many possible combinations of regulating units and changing unit parameters, storing and retrieving pre-computed gain matrices is not an attractive alternative, but reducing the main computational requirement from that of an (n+1) dimensional Ricatti equation solution to that of an (n-1) dimensional symmetric factorization problem means that the on-line calculation of $\bar{G}$ is feasible. Nonetheless, this alternative still places a significant computational burden on the existing WEPCO control center computer system and for this reason further simplification of the regulator design is desirable.

The (n-1) redistribution modes represent (n-1) degrees of freedom for the regulator design in the sense that (n-1) eigenvalues can be assigned to the secondary tracking objective via the parameter matrix $\hat{Q}_2$. Due to the parallel structure of the problem, it is possible to trade-off these (n-1) degrees of freedom with the computational burden of obtaining the feedback gain matrix $\bar{G}$. While this interesting observation has not been fully explored in general, one particular case has been developed in detail. The special case in which the (n-1) secondary tracking modes have a common eigenvalue corresponds to a solution of the Ricatti equation which can be obtained analytically. This allows gains to be updated very easily when unit parameters and status change.

The simplified regulator design and associated coordinating controller structure is based on the cost-separation ideas developed in the previous section. A slightly different formulation is used to facilitate the analytical solution however. Again we define the transformed state variables

$$\Delta x_T \triangleq C\Delta x = \sum_{i=1}^{n} \Delta x_i \tag{5.39}$$

$$\delta x_i \triangleq \Delta x_i - C_i^* \Delta x_T \qquad i=1,2,\ldots n \tag{5.40}$$

where CC*=1. The control variables are similarily transformed, i.e.

$$\Delta U_T \triangleq C\ \Delta U = \sum_{i=1}^{n} \Delta U_i \tag{5.41}$$

$$\delta U_i \triangleq \Delta U_i - D_i^* \Delta U_T \qquad i=1,2,\ldots n \tag{5.42}$$

where CD*=1. The arrays C* and D*, whose elements will be called secondary and primary participation factors, are used to parameterize the design. In the early stages of the coordinating controller development it was thought that these participation factors could be chosen to reflect, among other things, unit economics and regulating capability respectively and could, for example, be manually entered into the LFC program by the power system supervisor at WEPCO as economic and regulation participation factors. The latter two sets of participation factors are used in the existing WEPCO LFC program to provide two useful degrees of freedom in the allocation of total generation response. In the later analysis and testing of this coordinating controller, which is summarized in the following subsection, the secondary and primary participation factors of (5.40) and (5.42) were found to be less useful than two related sets of participation factors for reflecting unit economics and regulating capability however. In this subsection (5.40) and (5.42) will nevertheless be used to simply derive a coordinating controller structure which is consistent with the LFC objectives identified previously and which has two degrees of freedom for the allocation of total generation response. Then in subsection 5.2.4 a more natural way of specifying these two degrees of freedom will become apparent from a frequency domain interpretation of the resulting structure.

The two modes associated with total generation response, which were determined by the parameters q_1 and q_3 of (5.26) in the previous

subsection, can alternatively be fixed by constraining the total input ΔU_T as

$$\Delta U_T = -K_p \Delta x_T - K_I \Delta I \tag{5.43}$$

This determines the quadratic state and control deviation costs associated with total generation change in the general cost expression (5.15). Substituting the relations (5.39 - 5.43) into the original state equations (5.8) yields the transformed system equations:

$$\begin{aligned} \delta\dot{x}_i &= \delta u_i - (D_i - C_i)(K_p \Delta x_T + K_I \Delta I) \\ &\triangleq \delta u_i + \beta_i^P \Delta x_T + \beta_i^I \Delta I \end{aligned} \qquad i=1,2,\ldots n \tag{5.44}$$

$$\Delta\dot{x}_T = -K_p \Delta x_T - K_I \Delta I \tag{5.45}$$

$$\Delta\dot{I} = \Delta x_T$$

Now define the quadratic cost $\hat{J}$,

$$\hat{J} = \int_0^\infty \left[\sum_{i=1}^n q_1 \delta x_i^2 + \sum_{i=1}^n r_i \, \delta u_i^2 \right] dt \tag{5.46}$$

If the constraint $\sum_{i=1}^n \delta u_i = 0$ is maintained in the minimization of (5.46), then the state deviation cost in (5.46) corresponds to the economic tracking objective. Thus, having constrained the total input in (5.43), the problem of minimizing (5.46) subject to the system equations (5.44, 5.45) and the constraint $C\delta u = 0$ has a solution which is directly related to the

factorization problem (5.33-a) in the previous subsection. In order to facilitate an analytic solution the constraint $C\delta u = 0$ will be temporarily ignored and then later imposed, however. With this temporary assumption (a "trick" which simplifies the necessary algebra) the solution to this minimization problem yields the gain matrix $G = R^{-1}B^TK$, where K is the solution of the Ricatti equation

$$KA + A^TK + Q - KBR^{-1}B^TK = 0 \tag{5.47}$$

where, from (5.44-5.45)

$$A = \left[\begin{array}{c|cc} & \beta_1^P & \beta_1^I \\ & \beta_2^P & \beta_2^I \\ 0 & \cdot & \cdot \\ & \cdot & \cdot \\ & \cdot & \cdot \\ & \beta_n^P & \beta_n^I \\ \hline & -K_P & -K_I \\ 0 & & \\ & 1 & 0 \end{array}\right] \tag{5.48}$$

$$BR^{-1}B^T = \begin{bmatrix} 1/r_1 & & & & 0 & 0 \\ & 1/r_2 & & & & \\ & & \ddots & & & \\ & & & 1/r_n & & \\ 0 & & & & 0 & 0 \\ & & & & 0 & 0 \end{bmatrix} \begin{matrix} \} n \\ \\ \\ \\ \} 2 \end{matrix} \qquad (5.49)$$

$$\begin{matrix} \underbrace{\qquad\qquad} & \underbrace{\qquad} \\ n & 2 \end{matrix}$$

The above problem is in the general form:

$$\frac{d}{dt}\begin{bmatrix} x_1 \\ x_2 \end{bmatrix} = \begin{bmatrix} 0 & A_{12} \\ 0 & A_{22} \end{bmatrix} \begin{bmatrix} x_1 \\ x_2 \end{bmatrix} + \begin{bmatrix} B_1 \\ 0 \end{bmatrix} u \quad , \qquad (5.50)$$

$$J = \int_0^\infty (x^T Q x + u^T R u)\,dt \qquad (5.51)$$

$$Q = \begin{bmatrix} Q_{11} & 0 \\ 0 & 0 \end{bmatrix} \quad , \quad R = \begin{bmatrix} R_{11} & 0 \\ 0 & 0 \end{bmatrix} \quad , \qquad (5.52)$$

By partitioning the matrix K, which is the solution of the Ricatti equation (5.47), conformally with (5.50) and (5.52) the Ricatti equation for this general problem yields the following three matrix equations:

$$Q_{11} - K_{11} B_1 R_{11}^{-1} B_1^T K_{11} = 0 \tag{5.53}$$

$$K_{11} A_{12} + K_{12} A_{22} - K_{11} B_1 R_{11}^{-1} B_1^T K_{12} = 0 \tag{5.54}$$

$$K_{21} A_{12} + A_{12}^T K_{11} + K_{22} A_{22} + A_{22}^T K_{22} - K_{21} B_1 R_{11}^{-1} B_1^T K_{22} = 0 \tag{5.55}$$

(The assumption, which is valid for the coordinating controller design, is made that the system is stabilizable, and detectable in the cost, so that the Ricatti equation solution is unique.) Note that, due to the form of B in (5.50), K_{22} is not needed and that by first solving (5.53) for K_{11}, (5.54) can be solved for K_{12}.

For the diagonal quadratic cost matrices in (5.46), the off-diagonal terms of K_{11} in (5.53) are zero. Denoting the diagonal elements of K_{11} by K_{ii}, i=1,2,...n, we then have the simple solution for the diagonal terms of K_{11},

$$k_{ii} = \sqrt{q_i r_i} \qquad i=1,2,...n \tag{5.56}$$

For our particular problem, equation (5.54) can now be solved for K_{12} and it has the form

$$\begin{bmatrix} k_{11} & & & \\ & k_{22} & & \\ & & \ddots & \\ & & & k_{nn} \end{bmatrix} \begin{bmatrix} \beta_1^P & \beta_1^I \\ \beta_2^P & \beta_2^I \\ \vdots & \vdots \\ \beta_n^P & \beta_n^I \end{bmatrix} + \begin{bmatrix} k_{1,n+1} & k_{1,n+2} \\ k_{2,n+1} & k_{2,n+2} \\ \vdots & \vdots \\ k_{n,n+1} & k_{n,n+2} \end{bmatrix} \begin{bmatrix} -K_p & -K_I \\ 1 & 0 \end{bmatrix} - \begin{bmatrix} k_{11}/r_1 & & & \\ & k_{22}/r_1 & & \\ & & \ddots & \\ & & & k_{nn}/r_n \end{bmatrix} \begin{bmatrix} k_{1,n+1} & k_{1,n+2} \\ k_{2,n+1} & k_{2,n+2} \\ \vdots & \vdots \\ k_{n,n+1} & k_{n,n+2} \end{bmatrix} = 0 \quad (5.57)$$

Equation (5.57) can be easily solved for $k_{i,n+1}$ and $k_{i,n+2}$, i.e.

$$\begin{aligned} (-K_p - \sqrt{q_i/r_i})k_{i,n+1} + k_{i,n+2} &= -\sqrt{q_i r_i}\ \beta_i^P \\ -K_I\, k_{i,n+1} - \sqrt{q_i/r_i}\, k_{i,n+2} &= -\sqrt{q_i r_i}\ \beta_i^I \end{aligned} \qquad i=1,2,\ldots n \quad (5.58)$$

Thus, from (5.56) and (5.58) the feedback controls are

$$\delta u_i = -g_i \delta x_i - \hat{g}_i^P \Delta x_T - \hat{g}_i^I \Delta I \qquad i=1,2,\ldots n \quad (5.59)$$

where

$$g_i = \sqrt{q_i/r_i} \qquad i=1,2,\ldots n \quad (5.60)$$

$$\begin{bmatrix} g_i^P \\ g_i^I \end{bmatrix} = (C_i^* - D_i^*)\ \frac{g_i}{K_p g_i + K_I + g_i^2} \begin{bmatrix} g_i K_p + K_I \\ K_I g_i \end{bmatrix} \qquad i=1,2,\ldots n \quad (5.61)$$

Now $\sum_{i=1}^{n} \hat{g}_i^P = \sum_{i=1}^{n} \hat{g}_i^I = 0$, because $CC^* = CD^* = 1$, but

we see from (5.59) that the constraint $C\delta u = 0$, which was ignored in the optimization of the quadratic cost $\hat{J}$ in (5.46), can in general only be met if $g_i = g$, $i=1,2,\ldots n$. Thus the analytic "suboptimal" solution is

$$\delta u_i = -g\delta x_i - g(C_i^* - D_i^*)\frac{K_p g + K_I}{K_p g + K_I + g^2}\,\Delta x_T - g(C_i^* - D_i^*)\frac{K_I g}{K_p g + K_I + g^2}\,\Delta I \qquad (5.62)$$

By using the relations $\delta x = \Delta x - C^*\Delta x_T$ and $\delta u = \Delta u - D^*\Delta u_T$, the feedback controls in (5.62) can be transformed back to the original variables, yielding the final result

$$\Delta u_i = -g\Delta x_i - g_i^P \Delta x_T - g_i^I \Delta I \qquad i=1,2,\ldots n \qquad (5.63)$$

where

$$g_i^P = \frac{D_i^* K_p(K_p g + K_I) - C_i^* g K_I - g^3 D_i^*}{g(K_p + g) + K_I}$$

$$g_i^I = \frac{D_i^* K_I(K_p g + K_I) + C_i^* K_I g^2}{g(K_p + g) + K_I}$$

5.2.4 Analytic and Linear Simulation Results

The simplified regulator design developed in the proceeding subsection provides the feedback gain matrix for either of the Coordinating Controller One configurations (Figures 5.5 and 5.6) in terms of the scalar parameters K_p, K_I, g and the two participation factor vectors C* and D*. In this subsection results which are relevant to the selection of a particular configuration and parameter set are described. A significant amount of work was performed on this step of the design, using primarily the classical design tools of root loci analysis and Nyquist gain and phase margin calculations. Step responses were also computed in the time domain, for a simple linearized three machine system, to aid the selection of a prototype design which can be implemented in the detailed AGC simulation program for further tuning and evaluation. The purpose of this subsection is to provide a few selected results which illustrate the basic characteristics of the prototype design for Coordinating Controller One.

In order to proceed with the parameter selection, a model for the closed-loop response of a unit with its unit controller must be assumed. The design of the unit controllers is covered in the next chapter, 6.0. For the purposes of the coordinating controller design, a simple model was constructed which approximates the closed-loop response of 60 hz unit generation to unit MW reference input that was obtained with the unit controller and unit model described in Chapter 6.0. While the assumption that each generating plant can be represented by a very simple model is not a very good one, it is perhaps worthwhile to emphasize that it is made with respect to the closed-loop feedback system consisting of the plant and unit controller. Thus an interpretation of the model is that it represents the idealized plant input-output relationship, in the low frequency range, which the unit controller is, by design, acting to maintain during normal conditions in the plant. With this in mind, the

second order model illustrated in Figure 5.9 was found to yield a reasonable approximation to closed-loop unit input-output behavior. The transfer function description corresponding to Figure 5.9 is given below:

$$(S^2 \tau_g + S + K_g)\ P^o = K_g \quad UDG, \tag{5.65}$$

or

$$P^o = \frac{K_g/\tau_g}{(S + \lambda_1)(S + \lambda_2)} \cdot UDG$$

where $\lambda_1 \cdot \lambda_2 = K_g/\tau_g$. Note that this representation maintains the type one characteristic of the actual unit controller. For the range of unit parameters investigated in the unit controller design, a conservative choice of model parameters in (5.65) is $K_g = .0069$, $\tau_g = 17.2414$ so that

$$\lambda_1 \cong .008, \quad \lambda_2 \cong .05, \quad K_g/\tau_g \cong 4 \times 10^{-4}$$

The dominant pole corresponds to a time constant of 125 seconds, so for a step change in UDG it is assumed that the unit output reaches the new desired generation in about 10 minutes. Of course whether or not this is a reasonable assumption depends, among other things, on actual plant conditions and on the magnitude of the presumed step change in unit desired generation (UDG). A consideration involved in this choice is that the major component of UDG will generally be P_i^*, the smooth and rate-constrained desired trajectory determined by the dynamic economic dispatch algorithm, and that the unit model used for coordinating controller design purposes is intended to represent unit response to Δx_i, which is essentially the i^{th} unit's share of the total tracking error. It is anticipated that the total tracking error will normally be small enough that this unit response model is reasonable. The primary affect of the assumed unit model on the Coordinating Controller parameter selection has been to

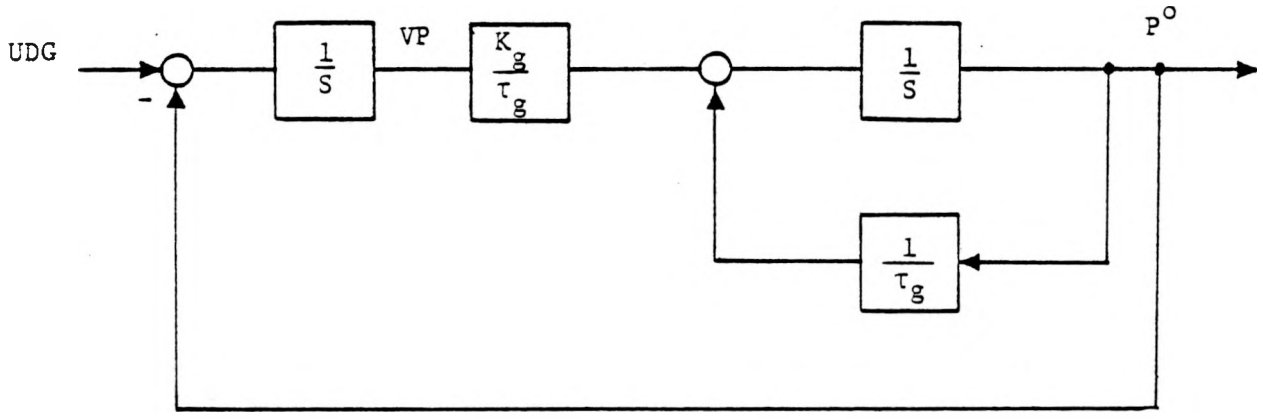

FIGURE 5.9 SECOND ORDER MODEL USED TO REPRESENT CLOSED-LOOP RESPONSE OF UNIT AND UNIT CONTROLLER

indirectly provide a bandwidth specification. Subsequently testing of the prototype design with the AGC simulation program will probably result in a modification of the desired bandwidth, but this can be easily accomplished.

The first configuration investigated was that corresponding to Figure 5.5, where unit inputs were interpreted as states in the regulator design. Although this is not the configuration of the recommended prototype design, a brief development of the first configuration will be made for comparative purposes. A number of the frequency domain analyses and linear simulation tests which will be illustrated below were used to choose the feedforward gains for the 60 hz load (estimate) and for the nominal (economic) trajectories provided by the dynamic dispatch algorithm. The resulting coordinating controller equations for this configuration are

$$\Delta u_i = s\Delta x_i = -g\Delta x_i - g_i^P(P_T^* + \Delta x_T - L_T^o - S^o) - g_i^I(P_T^o - L_T^o - S^o), \qquad (5.66)$$

with

$$UDG_i = \Delta x_i + P_i^*, \qquad i=1,2,\ldots n$$

This structure is illustrated in Figure 5.10. Essentially two scalar errors are formed, passed through a first order filter and distributed through two sets of gains. The first error is the integral of (-ACEM) while the proportional error is $-(P_T^* + \Delta x_T - L_T^o - S^o)$. Summing up the equations in (5.66) yields an expression for the total control,

$$UDG_T = P_T^* + \Delta x_T = P_T^* - \frac{G^I}{s(s+g)}(P_T^o - L_T^o - S^o) - \frac{G^P}{(s+g)}(P_T^* + \Delta x_T - L^o - S^o) \qquad (5.67)$$

The quantities P_T^o and L_T^o appearing in (5.67) are of course stochastic variables and in the actual implementation estimates of them are used to determine the control inputs. The estimation problem is discussed in subsection 5.2.5. At this point, for the purposes of obtaining

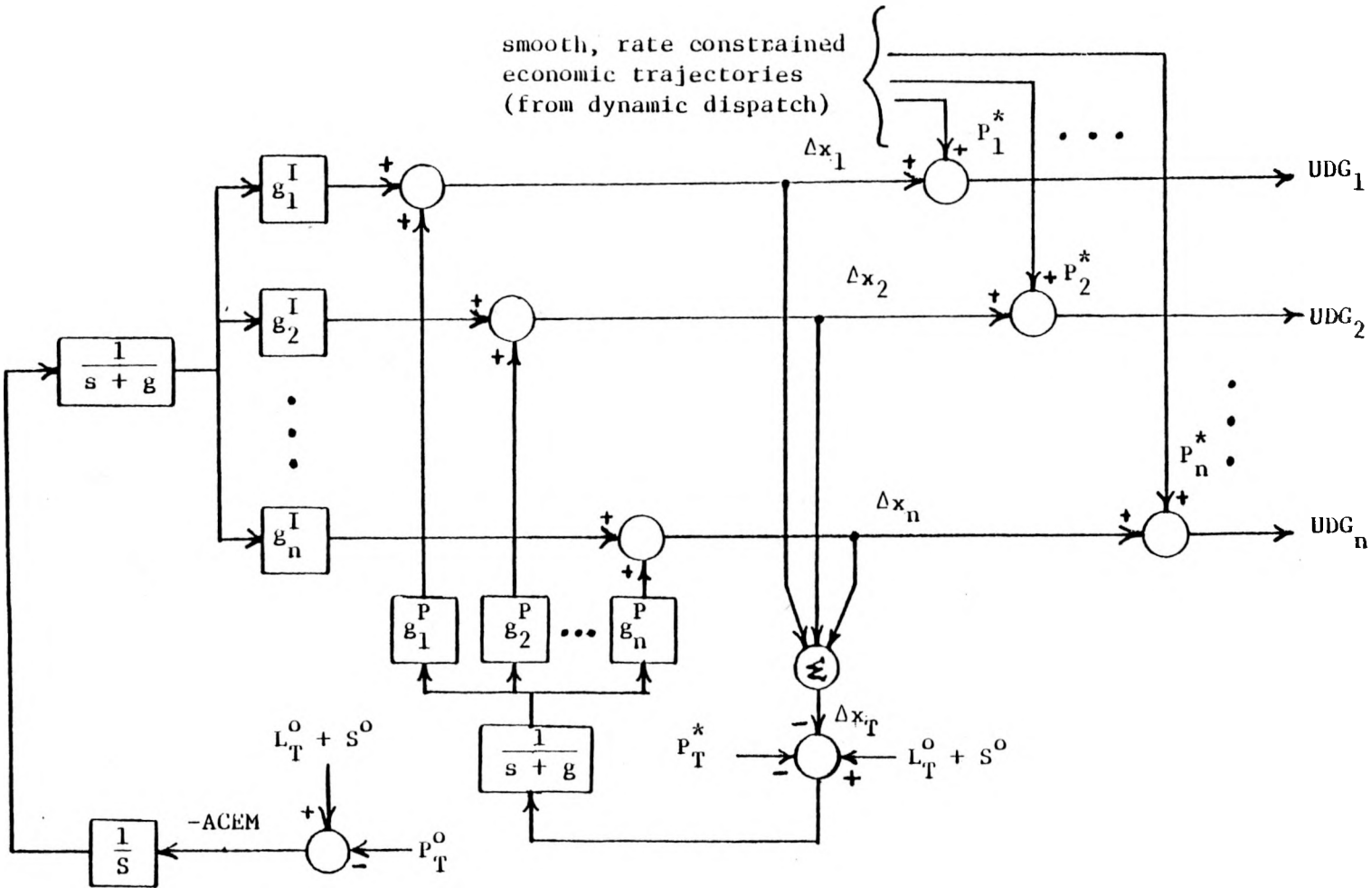

FIGURE 5.10 FIRST CONFIGURATION FOR COORDINATING CONTROLLER ONE

some frequency domain analytical results, a simple first order filter is assumed. That is, $\hat{P}_T^o = \frac{1}{s\tau_f + 1} \cdot P_T^o$ and $\hat{L}_T^o = \frac{1}{s\tau_f + 1} \cdot L_T^o$. The quantity P_T^*, the current value of the total generation demand determined by the Dynamic Dispatch algorithm, is much more difficult to represent in terms of the variables of the models used for the coordinating controller design because it is based on a forecast of the secular component of load demand. The feedforward of P_T^* has a significant effect on area tracking performance however and thus an assumed relationship between P_T^* and $L_T^o + S^o$ can be useful in analyzing the Coordinating Controller. The model which has been used is

$$P_T^* = \frac{a}{s\tau_D + 1} \quad (L_T^o + S^o) + \Delta L \tag{5.68}$$

where a is ideally 1.0, τ_D is choosen to roughly represent the affects of the slower execution rate of Dynamic Dispatch and ΔL is a generally non-zero mean random disturbance representing forecast errors, etc.

The system described by equations (5.56), (5.67) and (5.68) can then be put in the block diagram form of Figure 5.11, where

$$G_1(s) = \frac{G^I}{s(s+g)(s\tau_f+1)}$$

$$C_F(s) = \frac{s(a+G^P \cdot \tau_D)+G^P+a \cdot g}{(s\tau_D+1)(s+G^P+g)(s\tau_f+1)}$$

$$G_2(s) = \frac{s+g}{(s+g+G^P)}$$

$$T_G(s) = \frac{K_g}{s(s\tau_g+1)}$$

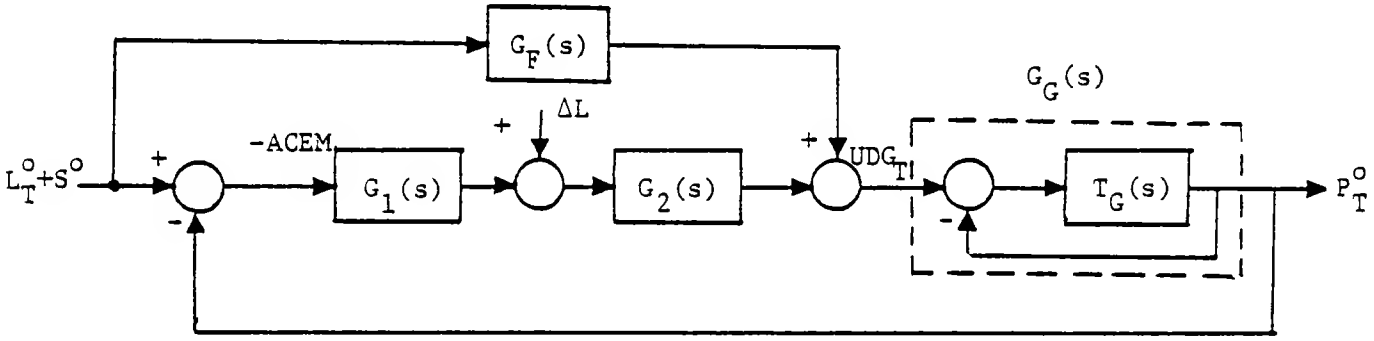

FIGURE 5.11 TOTAL RESPONSE MODEL OF FIRST CONFIGURATION IN BLOCK DIAGRAM FORM

$T_G(s)$ is the return ratio for the aggragate unit closed loop system;

$$T_G(s) \triangleq \frac{n(s)}{d(s)}, \quad P_T^o = T_G(s)(UDG_T - P_T^o),$$

so the closed loop transfer function $G_G(s)$ is given by

$$P_T^o = (1-T_G(s))^{-1}T_G(s)\cdot UDG_T = \frac{n(s)}{n(s)+d(s)} \cdot UDG_T \triangleq G_G(s)\cdot UDG_T \qquad (5.69)$$

With a little manipulation, the block diagram form of Figure 5.11 can be put into a standard unity feedback form without any feedforward, resulting in the relationship

$$P_T^o = T(s)(-ACEM) + W(s)\Delta L \qquad (5.70)$$

where the return ratio T(s) for the new feedback system is

$$T(s) = \frac{G_G(s)\,[G_F(s) + G_1(s)G_2(s)]}{[1 - G_G(s)G_F(s)]}, \text{ and}$$

$$W(s) = \frac{G_G(s)G_2(s)}{[1-G_G(s)G_F(s)]}$$

This form is illustrated in Figure 5.12.

Note that the closed loop response is given by

$$P_T^o = \frac{T(s)}{1+T(s)}\,(L_T^o + S^o) + \frac{W(s)}{1+T(s)}\,\Delta L$$

Thus the return ratio operator is central to the investigation of the stability properties and tracking performance of the closed-loop system. The absolute stability of the feedback system can be checked using the Nyquist stability criteria, and more importantly a quantitative measure of robustness can be obtained, the most familiar being gain and phase margins. At least for minimum phase systems, gain and phase margins can

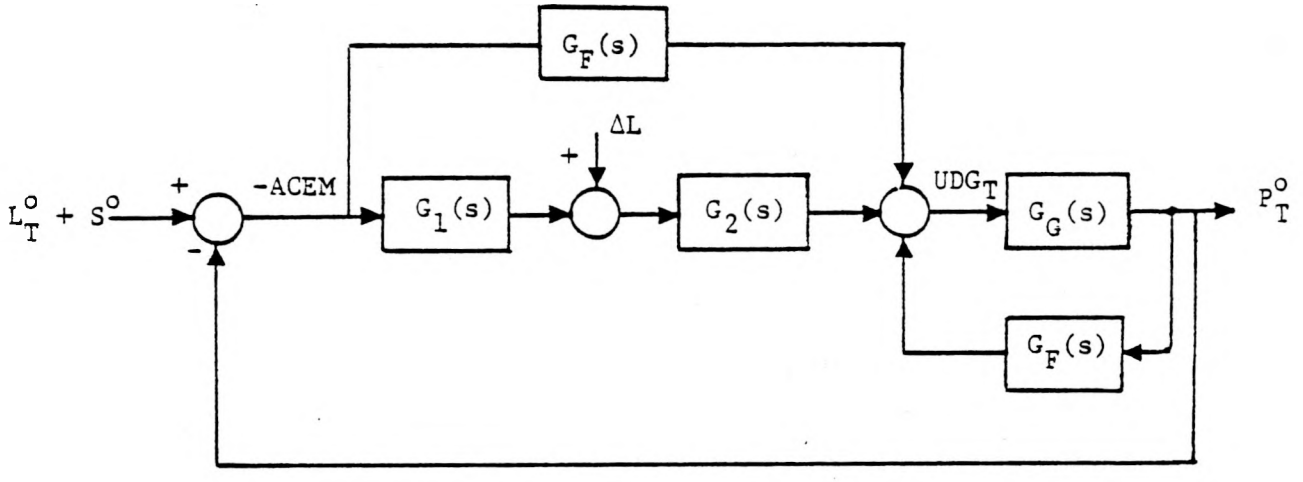

FIGURE 5.12 ALTERNATIVE BLOCK DIAGRAM FORM FOR TOTAL GENERATION RESPONSE

be equivalently obtained from Bode plots of T(s), i.e., plots of the magnitude and phase of T(s) for s = jw. Because we have put the system into a unity feedback form the critical point for stability is when T(s) = -1, or 0dB gain (gain of T(jw) in dB is 20 x Log|T(jw)|) and -180 degrees phase. Positive gain and phase margins guarantee closed-loop stability for respective variations in the gain and phase of the return ratio operator T(s); the gain margin is 0dB - 20 log$|T(jw_{c,p})|$, where $\angle T(jw_{c,p}) = -180$ (crossover) and the phase margin is $180 + \angle T(jw_{c,g})$, where $|T(jw_{c,g})| = 1$ (crossover).

Bode plots of T(s) are shown in Figure 5.13 for the first configuration (Figure 5.12) with a selected set of controller parameters g, G^I and G^P and two different values of τ_D, the time constant associated with Dynamic Dispatch. The gains were chosen to make the crossover at .004 radians and to provide lead compensation resulting in the indicated stability margins for plot B, where τ_D = 1200 seconds and τ_F = 20 seconds. It should be noted that the margins are significantly affected by the parameter τ_D and τ_F were affectively set to zero when plot A was made so the effect of τ_D was not isolated in this particular case. Based on a number of other results not repeated here however, one can conclude that τ_D is the parameter of major interest in this instance. The reason that a parameter of the feedforward operator $G_F(s)$ in Figure 5.11 affects T(s) is simply that T(s) corresponds to the block diagram form illustrated in Figure 5.12, where margins are with respect to the loop being broken at the point -ACEM. Thus Figures 5.11 and 5.12 are equivalent from an input-output point of view, but they are different feedback systems with accordingly different robustness properties. Generally the more complicated feedback system which results when the feedforward operator is brought inside the feedback loop was analyzed because this affords some insight into the effects of the Dynamic Dispatch. This distinction is particularly relevant for this first configuration because P_T^* is used

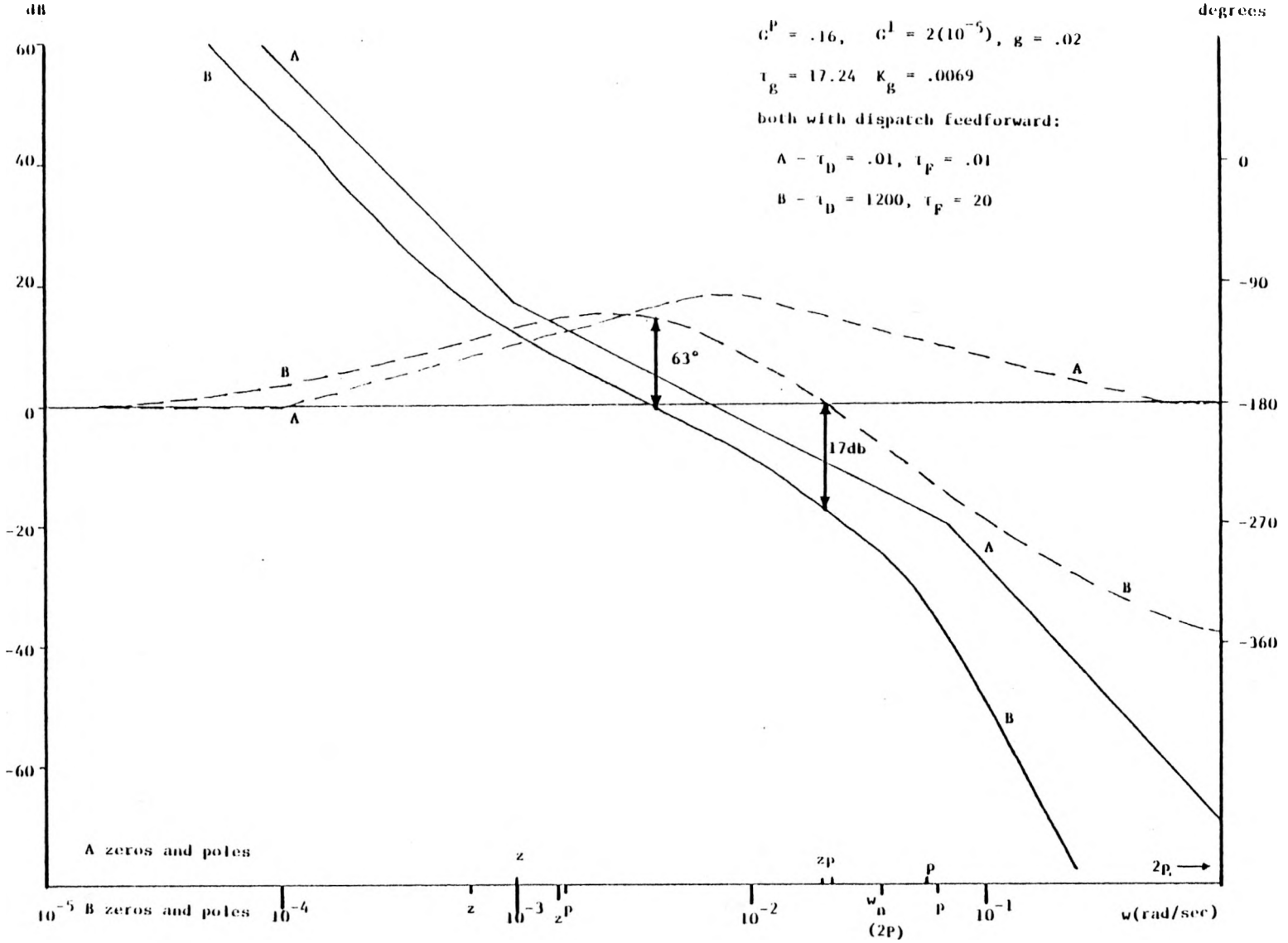

FIGURE 5.13 GAIN AND PHASE OF RETURN RATIO T(s) FOR FIRST CONFIGURATION

in the proportional error. That the stability margins are significantly affected by the parameters of the Dynamic Dispatch model has been interpreted as an undesirable characteristic of the first coordinating controller configuration, although the simple model of the Dispatch generation demand P^* used for the analysis is not very good because of the significant phase lag introduced as a result of representing the slower time scale of economic dispatch with a first order filter.

With the parameters g, G^P and G^I determined, a sample three machine system can be simulated to observe both the total response characteristics as well as the effects of different unit participation factors on each unit's contribution to the total response. Recall from (5.63) that the primary and secondary participation factors C^* and D^* determine, for a given g, G^P and G^I, the individual unit proportional and integral gains g_i^P and g_i^I. An alternative way is to define proportional and integral participation factors directly via

$$g_i^P \triangleq P_i * G^P \qquad (5.71)$$

$$g_i^I \triangleq I_i * G^I$$

where $\sum_i P_i = \sum_i I_i = 1$. The relationship between the primary/secondary and proportional/integral participation factor sets will be explored later, in conjuction with the more detailed investigation of the recommended coordinating controller configuration. In order to illustrate the time domain behavior of the first configuration, these new participation factor sets are simply introduced at this point.

Each unit and unit controller in the three machine system is represented with the model of (5.65). The nominal model parameters

indicated in (5.65) were used for the second machine; thus the eigenvalues for the second machine are $\lambda_1^2 = .008$, $\lambda_2^2 = .05$. The first and third machine were modelled as 50 percent slower and faster than the "average" machine respectively, so $\lambda_1^1 = .004$, $\lambda_2^1 = .025$ and $\lambda_1^3 = .012$, $\lambda_2^3 = .075$. For the gains indicated in Figure 5.13, the response of this three machine system to a 1 p.u. step change in load is illustrated in Figure 5.14. In Figure 5.14a the controller outputs Δx_i are plotted vs. time. For this case, the dispatch feedforward signals P_i^* were assumed to be based on a perfect forecast, so $a = 1.0$ and $\Delta L = 0$ in (5.68), where $P_i^* \triangleq F_i^* P_T^*$, $\Sigma F_i = 1$. Thus $\lim_{t\to\infty} P_T^*(t) = \Delta L$ and as a result the steady state targets for the reference inputs Δx_i is zero. The participation factors in this case were

$P_1 = .33$	$I_1 = .53$	$F_1 = .53$
$P_2 = .33$	$I_2 = .33$	$F_2 = .33$
$P_3 = .34$	$I_3 = .14$	$F_3 = .14$

In Figure 5.14b the unit 60 Hz mechanical power outputs are plotted vs. time, while in Figure 5.14c ACEM and its integral are shown.

The first configuration for Coordinating Controller One is somewhat unusual in that a proportional error is formed from the MW reference inputs to the units as a result of interpreting the inputs as states in the regulator design. This configuration was investigated because some early eigenanalysis studies indicated that plant poles are less affected by the proportional feedback of unit reference inputs than by the proportional feedback of unit outputs. This is an issue of some importance because the simple models used for the closed-loop system of each unit and its unit controller are assigned poles which in a sense represent the limitation of that unit's closed-loop response to MW reference inputs. The placement of those poles is determined by each

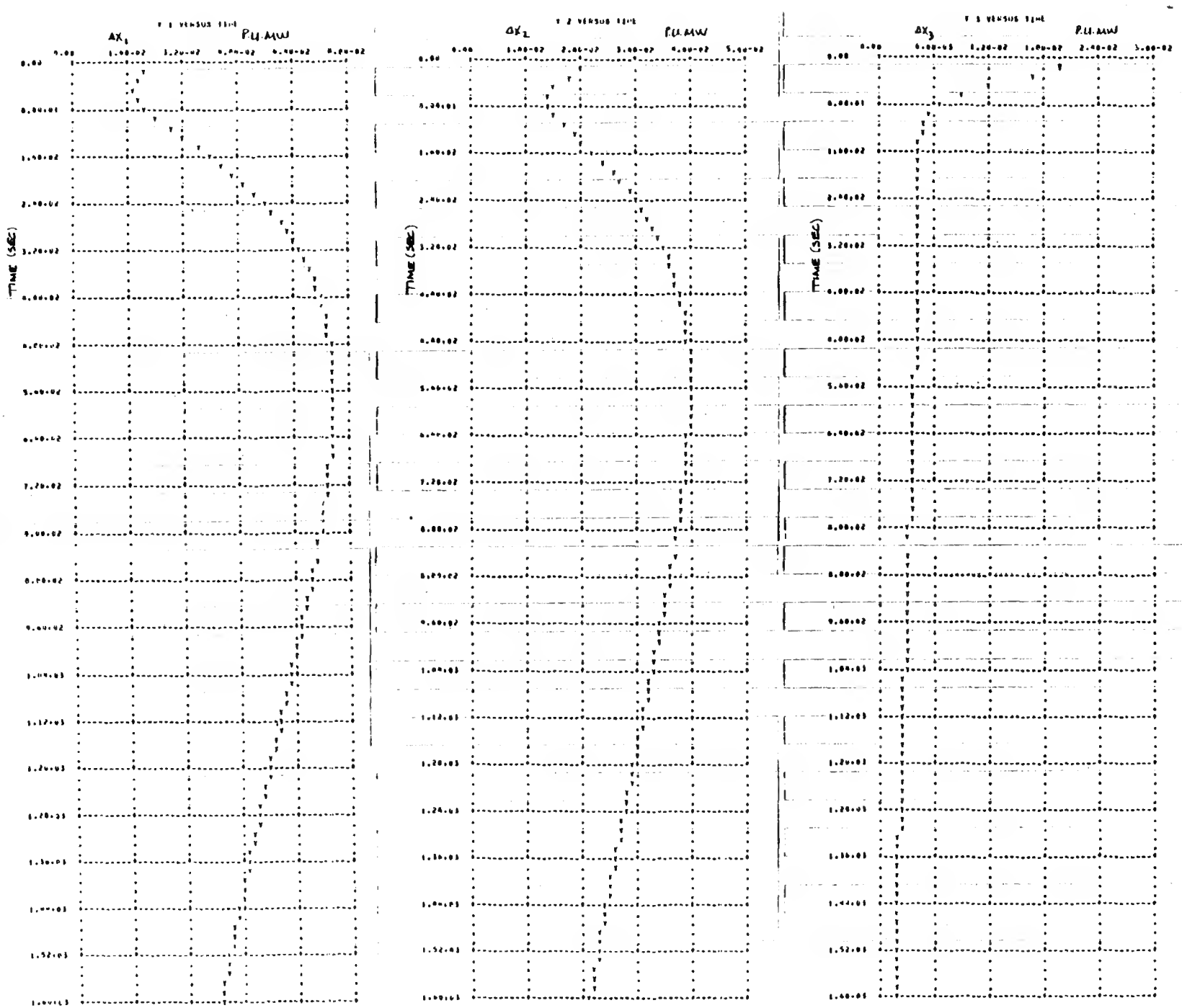

FIGURE 5.14*a* STEP RESPONSE OF THREE MACHINE SYSTEM WITH FIRST CONFIGURATION COORDINATING CONTROLLER OUTPUTS $\Delta\chi$

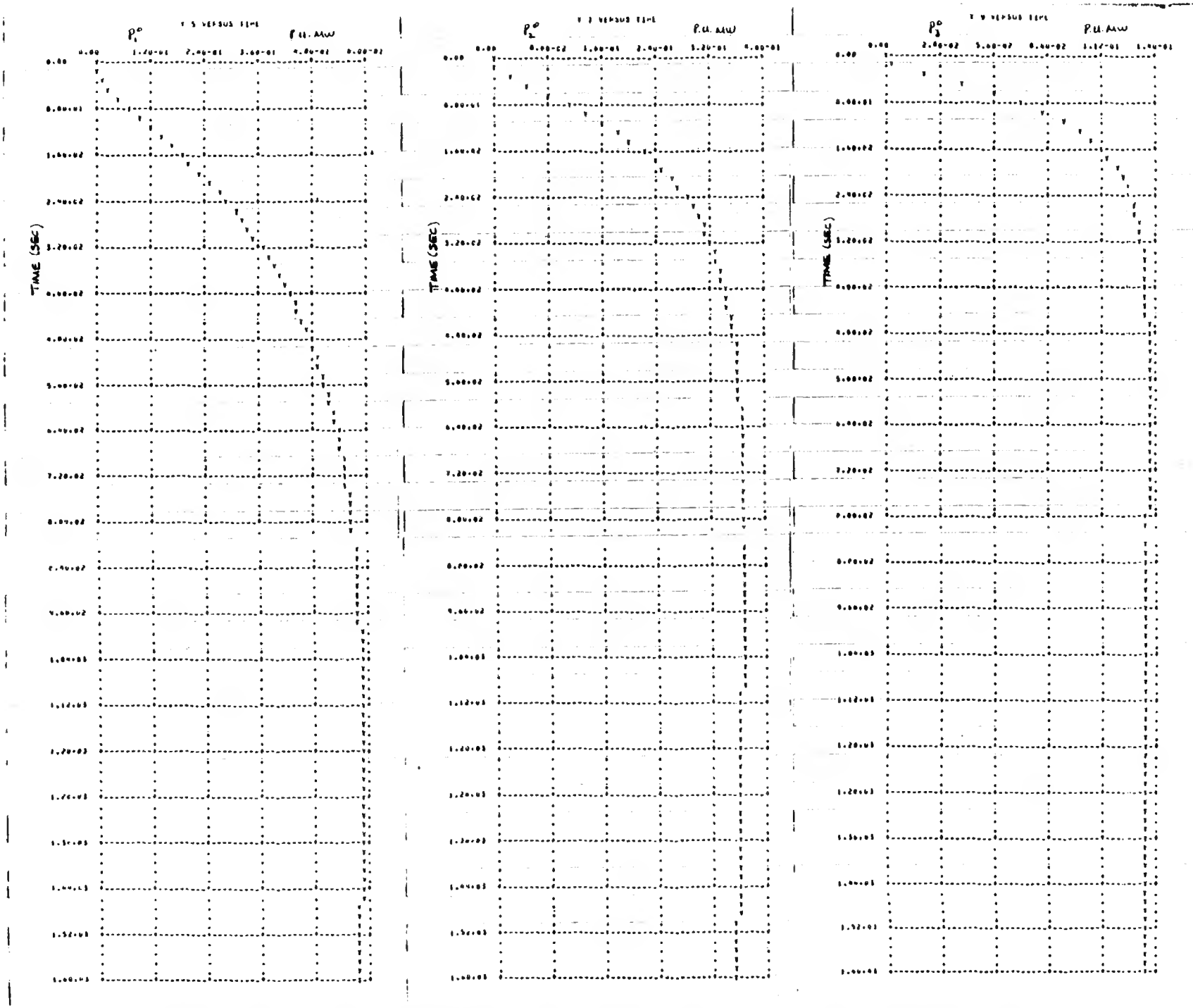

FIGURE 5.14b STEP RESPONSE OF THREE MACHINE SYSTEM WITH FIRST CONFIGURATION
UNIT OUTPUTS P^0

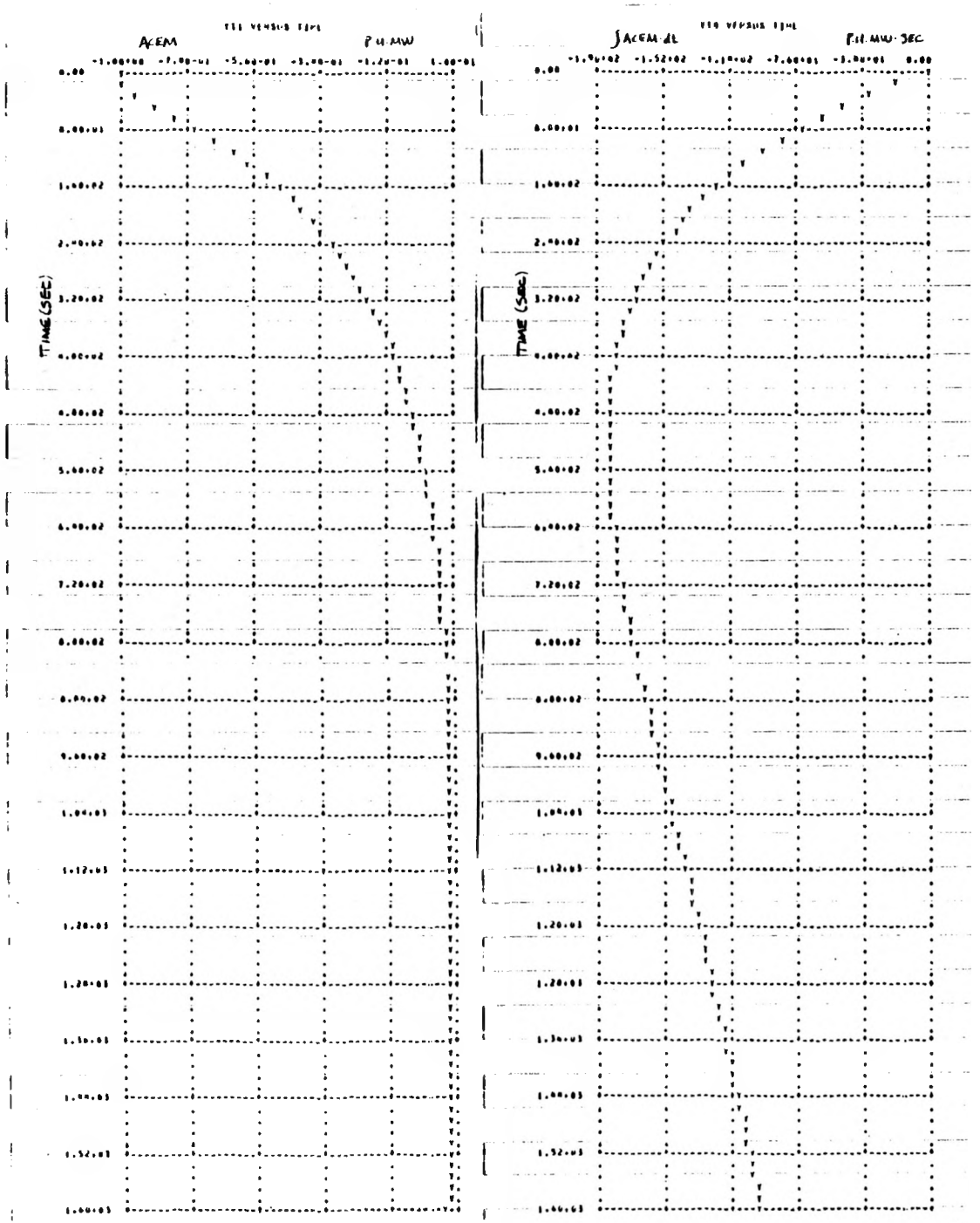

FIGURE 5.14c ACEM AND $\int ACEM \cdot dt$

unit controller design based on the capabilities of each particular unit. This is an over-simplification of course, but basically the LFC structure consists of n inner-loops, the unit controllers, and one outer-loop is designed to provide a unit tracking capability which is within the physical limitations of the plant. When the outer loop is closed then the closed-loop poles associated with each inner loop are changed and based on the above interpretation of those poles, it is desirable that closing the outer loop does not move them a great deal. Further work on the second configuration revealed however, that the two configurations are not significantly different in this regard, primarily because the integral feedback of ACEM; which they both utilize, itself has a strong effect on pole location.

In the second configuration for Coordinating Controller One ACEM replaces the quantity $P_T^* + \Delta x_T - L_T^o - S^o$ as the proportional feedback signal. Referring to Figure 5.10, this change can be made on the block diagram of the first configuration by taking the feedback points Δx_i, "sliding them through" the addition of the feedforward terms P_i^* (this then cancels the $-P_T^*$ term of the proportional error) and then transferring each point from unit MW reference input UDG_i to unit output P_i^o. As a result the second configuration has the block diagram form shown in Figure 5.15. During normal operating conditions the unit with its unit controller will tend to maintain, in the presence of unknown constant disturbances due to the reset capability provided by the unit controller, a unity transfer function in the low frequency range between MW reference input UDG_i and 60 Hz mechanical power output P_i^o. Thus in the low frequency range the two configurations result in similar closed-loop characteristics, which are dependant on the models used for units and dynamic dispatch, in the midfrequency range. A particular example of this difference will be illustrated later in this subsection.

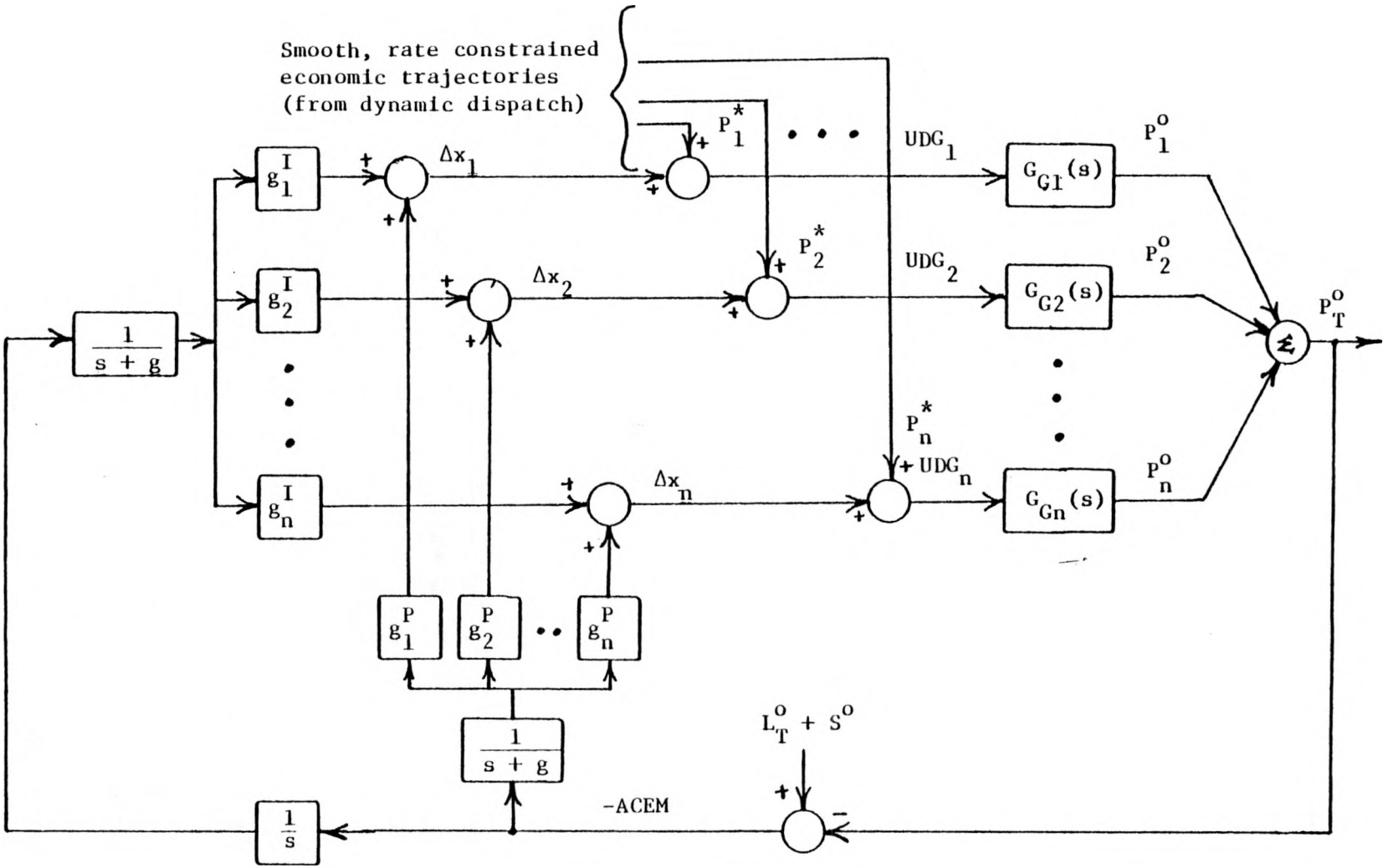

FIGURE 5.15 SECOND CONFIGURATION FOR COORDINATING CONTROLLER ONE

When an abnormal situation occurs at one (or more) of the plants so that the unit does not respond or is suddenly taken off control, either automatically or by the plant operator, then a major difference between the two configurations becomes apparent. Assume for the sake of argument that the abnormal occurance is some disturbance which results in the sudden loss of a unit which was in the automatic control mode. In the first configuration the resulting change in ACEM will not appear in the proportional error until an update of unit status is made in the LFC program and the participation factors are adjusted accordingly. Until this update is made, the additional generation needed from the other units will be obtained only due to the integral of ACEM feedback loop. This is undesirable because the response may be sluggish and possibly oscillatory, depending on the value of the integral loop gain and the response capability of the remaining units, due in a sense to the action of the proportional loop under such a disturbance. The problem in this case stems from the fact that the first configuration results in a significantly different response for disturbances in generation than for disturbances in load; for example, if a disturbance resulting in the loss of a unit is simulated as a step in load demand with the models used above, then the closed-loop system undergoes an effective structural change concomitant with the simulated change in load demand. In the second configuration these potential problems do not arise, however. The system response will be qualitatively the same for either disturbances in generation or disturbances in load. For the loss of a unit the total proportional and integral loop gains will change, but in a simple, non-conflicting manner and no undesirable effective structural changes occur.

The form of the second configuration for Coordinating Controller One shown in Figure 5.15 illustrates clearly its relation to the first configuration. Simple manipulation results in the more easily interpreted block diagram form shown in Figure 5.16. This is the recommended configuration

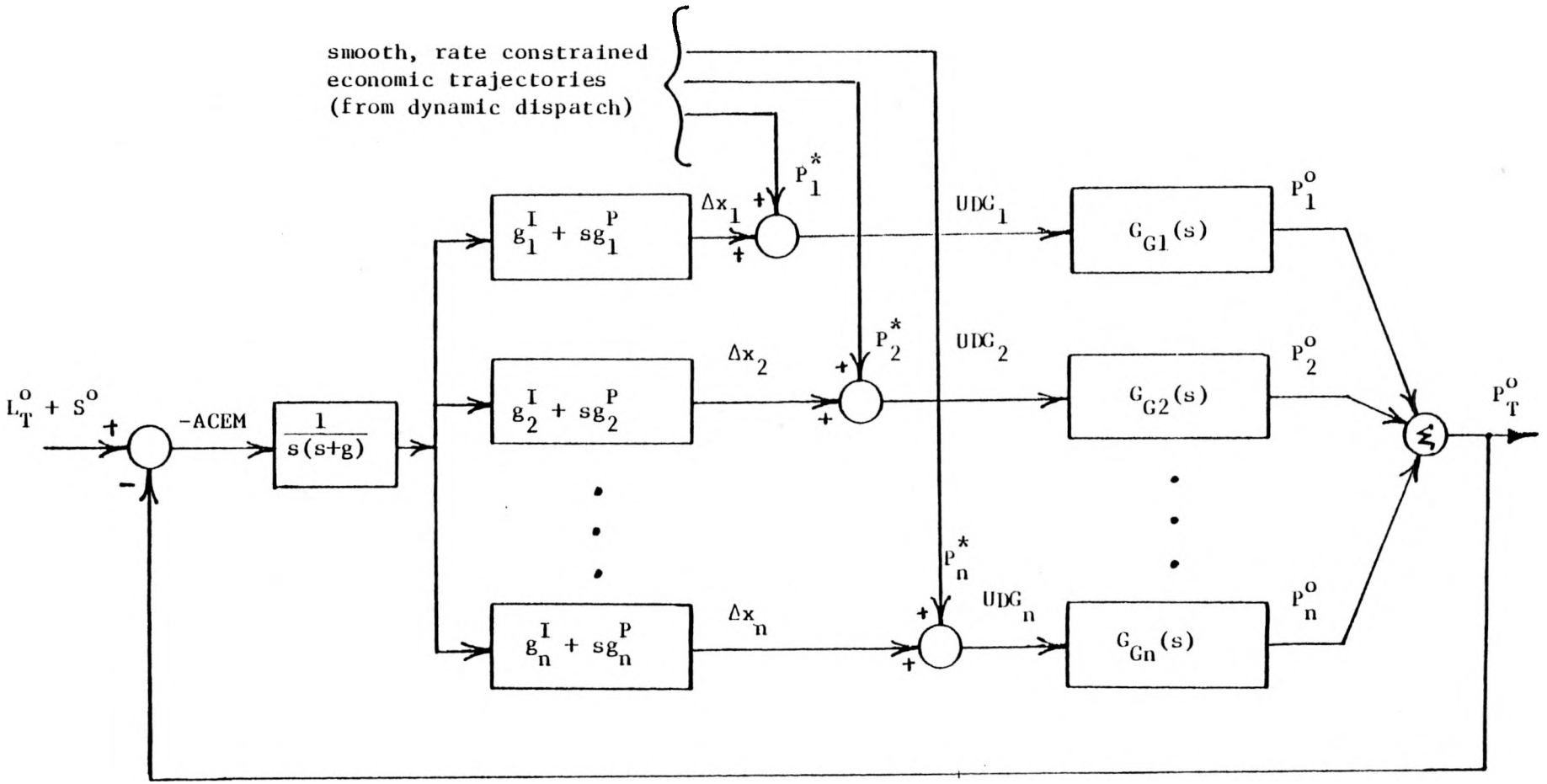

FIGURE 5.16 COORDINATING CONTOLLER ONE

for Coordinating Controller One and in the remainder of this section the term Coordinating Controller One will refer to this (the second) configuration. From Figure 5.16 the controller equations are

$$\Delta U_i = s\Delta x_i = -g\Delta x_i - g_i^P(P_T^o - L_T^o - S^o) - g_i^I/s\ (P_T^o - L_T^o - S^o) \qquad (5.72)$$

and

$$UDG_i = \Delta x_i + P_i^*, \qquad i=1,2,\ldots n$$

or

$$UDG_i = \Delta x_i + P_i^* = \frac{-(g_i^I + sg_i^P)}{s(s+g)}\ ACEM + P_i^* \qquad i=1,2,\ldots n \qquad (5.73)$$

Summing (5.73) over units yields the total control expression

$$UDG_T = \Delta x_T + P_T^* = \frac{-(G^I + sG^P)}{s(s+g)} \cdot ACEM + P_T^* \qquad (5.74)$$

Using the same first order measurement filter representation and Dynamic Dispatch representation as before, equation (5.68), the resulting total response model is illustrated in block diagram form in Figure 5.17, where

$$G_F(s) = \frac{a}{(s\tau_D + 1)(s\tau_F + 1)}\ ,$$

$$G_C(s) = \frac{G^I + S\ G^P}{s(s\tau_F + 1)(s+g)} \quad \text{and} \qquad (5.75)$$

$$G_G(s) = \frac{K_g/\tau_g}{s^2 + s/\tau_g + K_g/\tau_g} = \frac{1}{(s\lambda_1^{-1} + 1)(s\lambda_2^{-1} + 1)}$$

An alternative feedback form can be obtained by simple manipulation of Figure 5.17. As before, this manipulation results in a feedback system

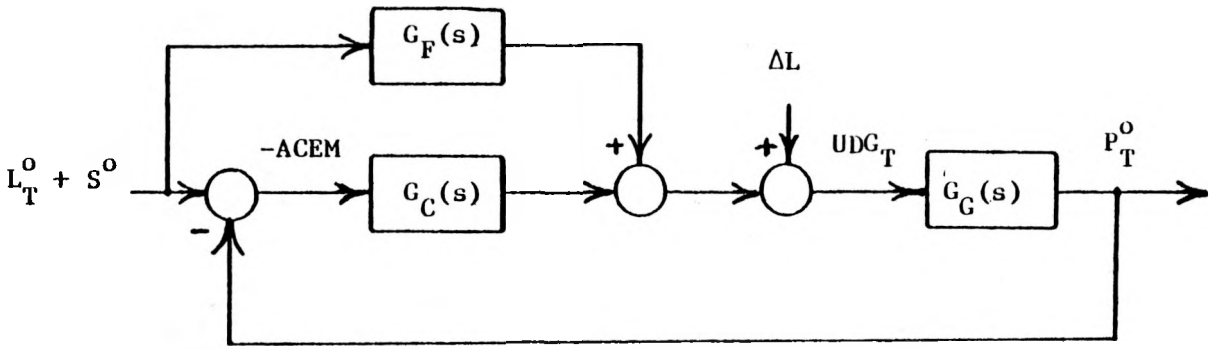

FIGURE 5.17 TOTAL RESPONSE MODEL IN BLOCK DIAGRAM FORM

which has a different return ratio operator (and hence different robustness properties) with respect to breaking the loop at the point (-ACEM), but has an identical input-output operator; this alternative feedback form is illustrated in Figure 5.18.

The return ratio operator for the system in Figure 5.18 relates total 60 Hz mechanical power to the error (-ACEM),

$$P_T^o = -T(s)\ \text{ACEM} = -T(s)(P_T^o - L_T^o - S^o) \tag{5.76}$$

where T(s) is given by

$$T(s) = \frac{[G_F(s) + G_C(s)]\cdot G_G(s)}{1 - G_G(s)G_F(s)} \tag{5.77}$$

Equation (5.77) can be rewritten using the relations (5.75) and simplified, yielding the expression

$$T(s) = G^I\, g^{-1}\ \frac{s^2(G^I)^{-1}\,[a+\tau_D\, G^P]+s[(G^I)^{-1}(ag+G^P)+\tau_D]+1}{s(sg^{-1}+1)[(s\lambda_1^{-1}+1)(s\lambda_2^{-1}+1)(s\tau_D+1)(s\tau_F+1)-a]} \tag{5.78}$$

Notice that for the parameter "a" equal to zero, the return ratio in (5.78) becomes equal to the return ratio for the feedback form of Figure 5.17, i.e.,

$$T(s)\Big|_{a=0} = G^I\, g^{-1}\cdot \frac{(s\, G^P/G^I + 1)}{s(sg^{-1}+1)(s\lambda_1^{-1}+1)(s\lambda_2^{-1}+1)(s\tau_F+1)} \tag{5.79}$$

so (5.78) is a more general expression which easily allows both feedback systems, i.e. Figures 5.17 and 5.18, to be analyzed.

Bode plots of T(s) for the Coordininating Controller is shown in Figure 5.19, with a a=1 and two widely separated values of dispatch

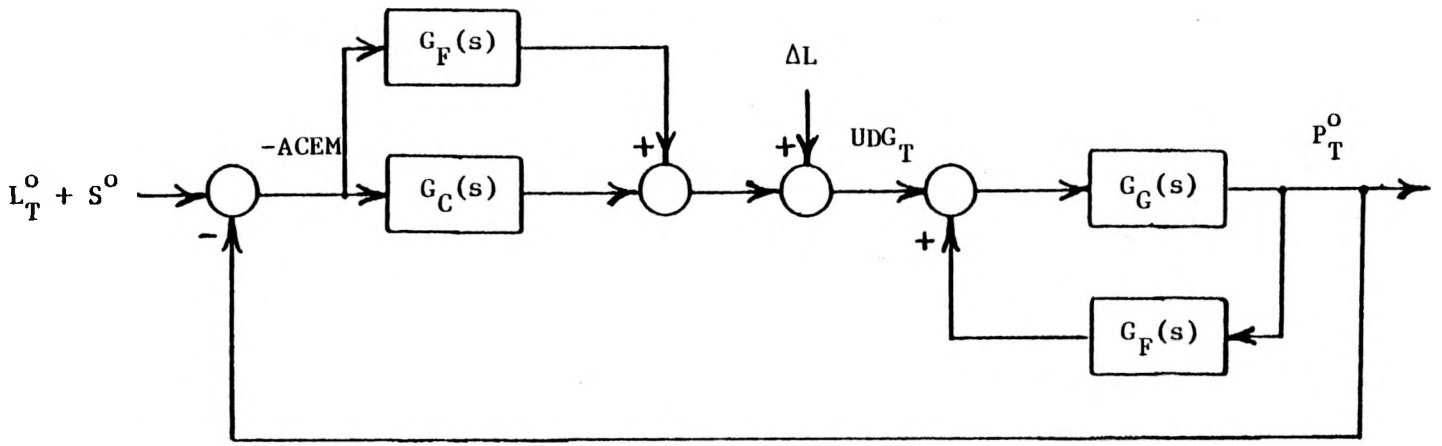

FIGURE 5.18 ALTERNATIVE BLOCK DIAGRAM FORM FOR TOTAL GENERATION RESPONSE

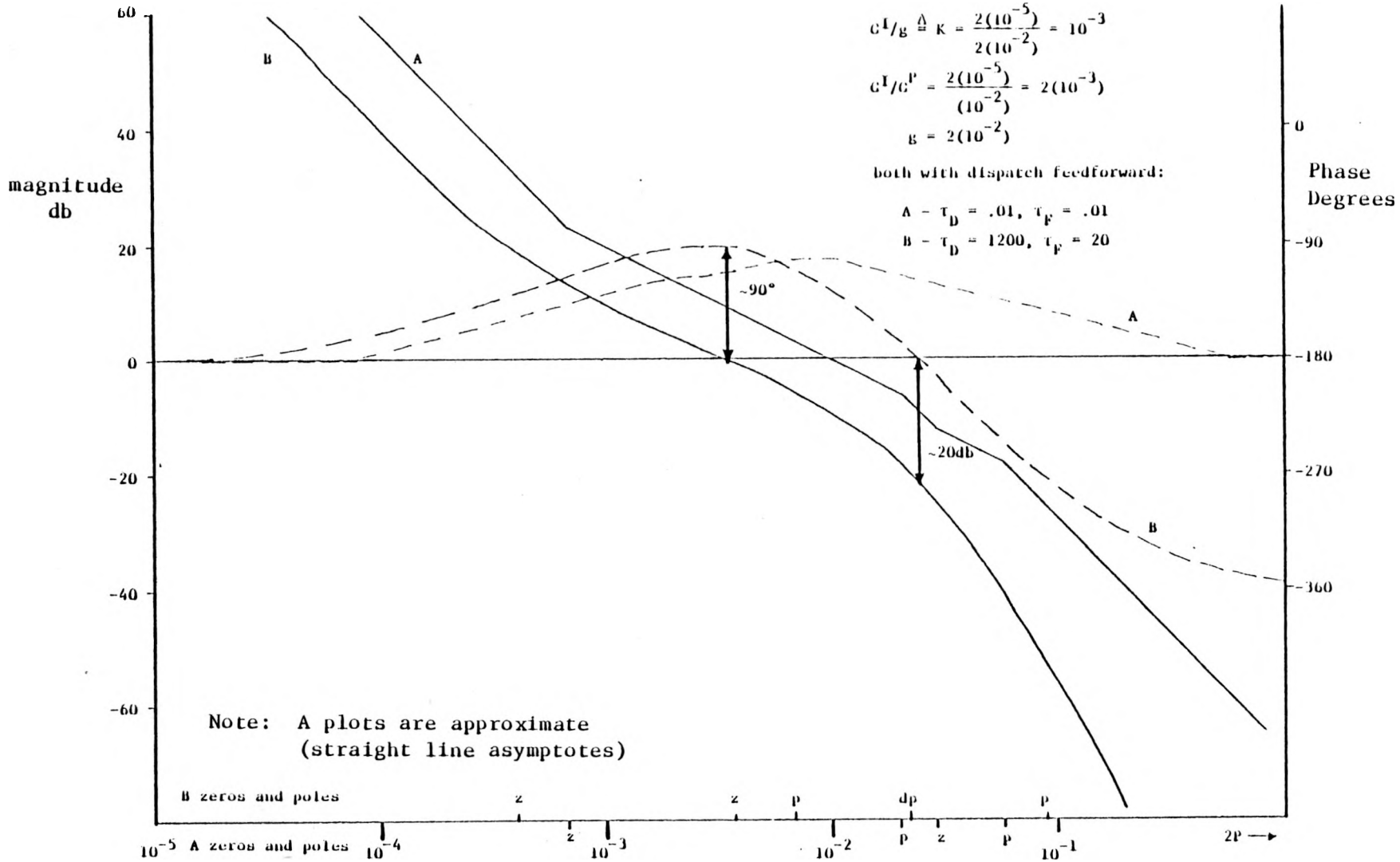

FIGURE 5.19 MAGNITUDE AND PHASE OF COORDINATING CONTROLLER RETURN RATIO

feedforward time constant τ_D. While the parameters are not quite identical, these plots can be compared to those shown previously for the first configuration in Figure 5.13. Notice the different affects of the change in τ_D (and τ_F, although the later is not as significant); with the second configuration the gain and phase margins remain essentially the same, while they change significantly with the first configuration. While the gain and phase characteristics of the Coordinating Controller shift with respect to frequency as time constant τ_D is varied, their basic shape and relation to each other are only moderately affected. A related time domain property is that the basic shape of the response (for example the amount of overshoot) is only moderately affected although response times become somewhat longer as τ_D increases.

It is interesting that, although derived from a multivariable, robust optimal linear regulator point of view, the Coordinating Controller illustrated in Figure 5.16 can be interpreted as a multi-loop integral controller with a first order compensation network in each loop. This interpretation, and the associated classical frequency domain design point of view, has been very helpful in understanding the basic properties and capabilities of the Coordinating Controller. Both lead and lag compensation were investigated, as each can be used to modify the uncompensated frequency domain characteristics in order to increase loop gains in the lower frequency range for better tracking as well as to provide adequate stability margins and concomitantly to help shape the time domain response characteristics. Based on this investigation it was concluded that lead compensation is preferable for several reasons. In terms of response, it is useful because it provides a form of anticipation which helps, for example, to get the units moving initially following a disturbance. While lead compensation is evident in the total system response return ratio plotted in Figure 5.19, it is even easier to see its effect on the feedback system which results when the dynamic dispatch feedforward is set to

zero, i.e., a = 0. The feedback system which results when a = 0 in (5.78) corresponds to a linearization about the unit responses to the dispatch signal, and while this point will be discussed in more detail below, it is worth having this physical interpretation in mind when analyzing the return ratio for the case a = 0. At any rate, a frequency plot of T(s) is shown in Figure 5.20 for the same parameters used in generating Figure 5.19 except that now a = 0 and hence T(s) is given by the simple expression (5.79). The various pole and zero locations are marked on the frequency axis in Figure 5.20, from which we can see that the lead compensation of the coordinating controller was chosen to have an attenuation factor of $\frac{G^I}{G^P \cdot g} = 1/10$. Clearly, from the aggregate area response point of view, the Coordinating Controller is basically a simple frequency-dependent gain operating on ACEM, with the lead compensation flattening the gain magnitude, and adding positive phase, in the midfrequency range in order to improve ACEM regulation. In the multiple-machine (multi-loop) context, each loop has its own frequency-dependent gain operating on ACEM and the two sets of participation factors allow the frequency characteristic of each loop to be adjusted corresponding to the relative economics and regulating capability of each unit.

The basic multi-loop frequency domain characteristic of the Coordinating Controller can be more easily explored by effectively re-linearizing the models about the Dynamic Dispatch trajectories. Referring to the block diagram in Figure 5.16, the controller equations are

$$UDG_i = \Delta x_i + P_i^* \triangleq G_{c,i}(s)\ (-ACEM) + P_i^*, \text{ i.e.,}$$

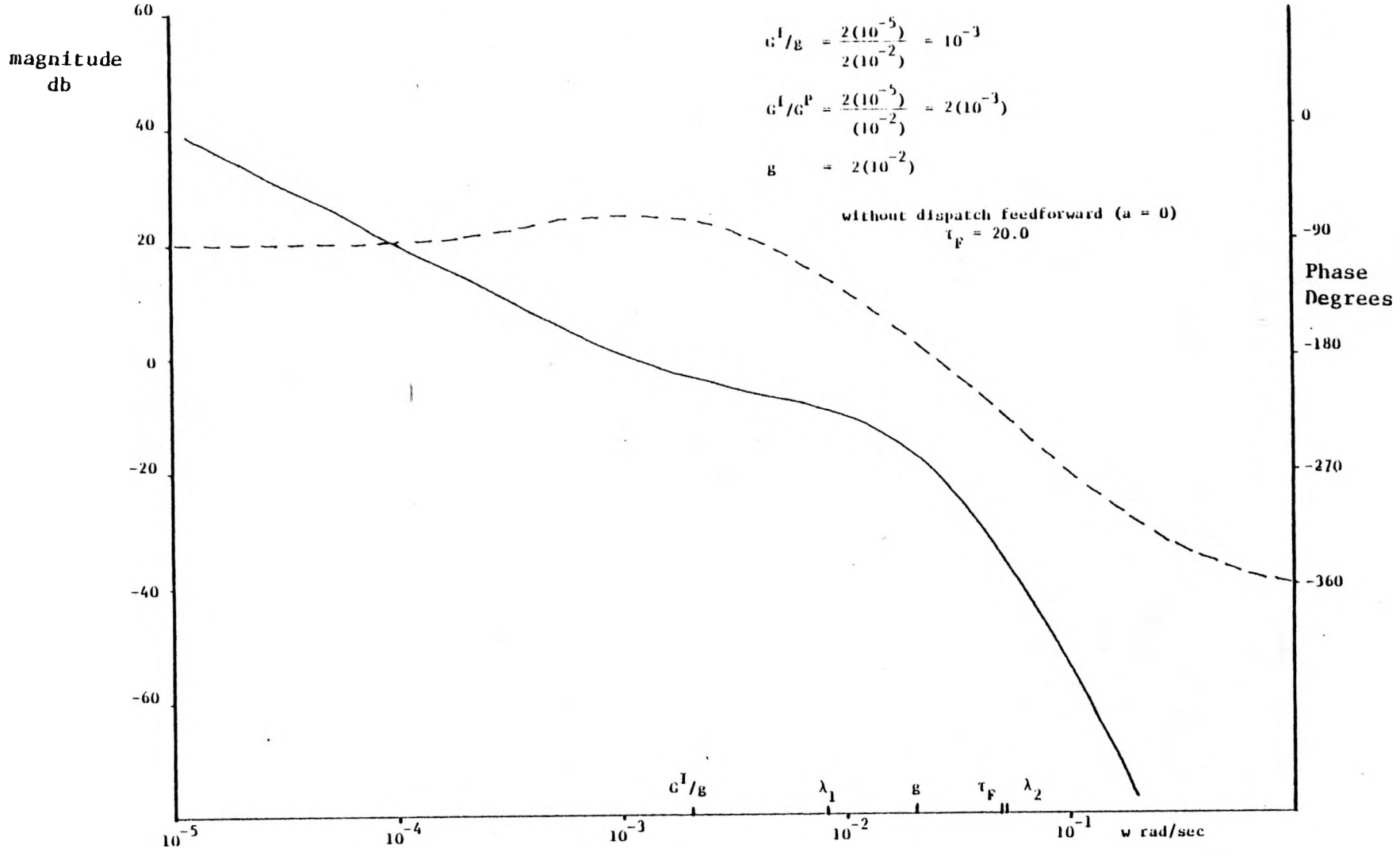

FIGURE 5.20 RETURN RATIO FOR SYSTEM WITHOUT DISPATCH FEEDFORWARD

$$UDG_i = \frac{g_i^I}{g} \frac{(s\, g_i^P/g_i^I + 1)}{s(sg^{-1}+1)} (-ACEM) + P_i^*, \qquad i = 1,2,\ldots n, \qquad (5.80)$$

while each unit, with its unit controller, is modeled by

$$P_i^o = G_{G,i}(s) \cdot UDG_i \qquad i = 1,2,\ldots n \qquad (5.81)$$

Suppose that we define

$$P_i^o \triangleq \bar{P}_i^o + \Delta P_i^o, \qquad i = 1,2,\ldots n \qquad (5.82)$$

where

$$\bar{P}_i^o \triangleq G_{G,i}(s)\, P_i^* \qquad i = 1,2,\ldots n \qquad (5.83)$$

The dynamical system representation for the "Δ" variables describes the system linearized about the solution corresponding to the inputs P_i^*, i.e., Equation (5.83) is a shorthand frequency domain expression which is intended to represent a decomposition of the differential equation solution corresponding to (5.80) and (5.81), where $\bar{P}_i^o(t)$ is the forced solution to the input $P_i^*(t)$ and $\Delta P_i^o(t)$ contains the rest of the forced solution plus the natural solution determined by initial conditions, so we have

$$P_i^o = G_{G,i}(s)\, \Delta x_i = G_{G,i}(s)\, G_{C,i}(s)\, (-ACEM), \quad i=1,2,\ldots n \qquad (5.84)$$

But

$$ACEM = \sum_{i=1}^{n} (\bar{P}_i^o + \Delta P_i^o) - L_T^o - S^o \triangleq \bar{P}_T^o + \Delta P_T^o - L_T^o - S^o$$

$$= \Delta P_T^o - (L_T^o - S^o - \bar{P}_T^o) \triangleq \Delta P_T^o - \Delta L_T^o \qquad (5.85)$$

so the block diagram representation of Figure 5.16 can be rearranged according to this new linearization to yield the form illustrated in Figure 5.21. Clearly the feedback system of Figure 5.21 has the total response return ratio characteristic shown in Figure 5.20 when a measurement filter representation is included, i.e., it corresponds to the case a = 0 discussed above. It is, however, important to note that the disturbance input to this system description is not the total 60 Hz load plus schedule, $L_T^o + S^o$, but the difference between total demand and the sum of the trajectories $\bar{P}_L^o$, $\Delta L_T^o = L_T^o + S^o - \bar{P}_T^o$. ACEM is not affected by this rearrangement, however, so the total area control error (mechanical) is a variable of the pertubational system representation.

Viewing Figure 5.21 as a single-input/multiple-output (SIMO) system, the open loop operators $G_{C,i}(s)\, G_{G,i}(s) \triangleq T_i(s)$ are return ratios, where the total return ratio T(s) is

$$T(s) = T_1(s) + T_2(s) + \cdots + T_n(s) \tag{5.86}$$

The T(s) plotted in Figure 5.20 was obtained from (5.86) by assuming that each unit is identical, $G_{G,i}(s) = G_G(s)$ for all i, and by adding the measurement filter model $(s\tau_F + 1)^{-1}$ to each $G_{C,i}(s)$. In order to illustrate the effects of the participation factors P_i and I_i, i=1,2,...n, consider a three machine system with the following participation factors:

$I_1 = .53$ $\qquad$ $P_1 = .14$

$I_2 = .33$ $\qquad$ $P_2 = .33$

$I_3 = .14$ $\qquad$ $P_3 = .53$

With the measurement filter included, the MW reference input supplied to each unit by the coordinating controller is

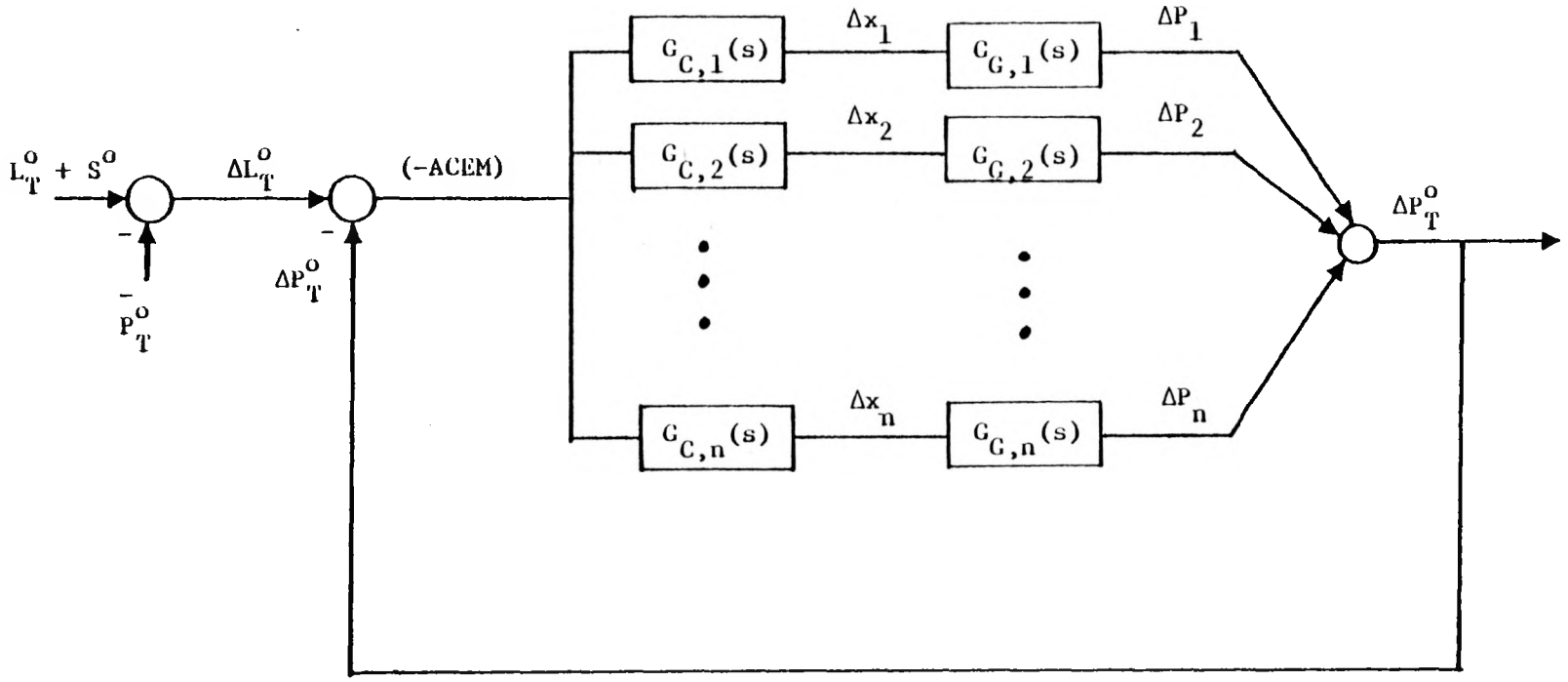

FIGURE 5.21 BLOCK DIAGRAM REPRESENTATION FOR LINEARIZATION ABOUT DYNAMIC DISPATCH FEEDFORWARD

$$\Delta x_i = G_{C,i}(s)\ (-ACEM) = \frac{G^I}{g}\ I_i \frac{\left(s\,\frac{G^P}{G^I}\,\frac{P_i}{I_i} + 1\right)}{s(sg^{-1}+1)(s\tau_F+1)}\ (-ACEM)\quad i=1,2,\ldots n \qquad (5.87)$$

The magnitudes of $G_{C,i}(s)$ for the three machine systems are plotted in Figure 5.22. Now it is easy to verify that the integral factors I_i determine the steady state allocation of the difference between load demand and the sum of the unit trajectories due to the Dynamic Dispatch feedforward, so for a step in ΔL_T^o the sample system will have the steady state MW reference inputs

$$\Delta x_1(ss) = I_1\ \Delta L_T^o$$
$$\Delta x_2(ss) = I_2\ \Delta L_T^o$$
$$\Delta x_3(ss) = I_3\ \Delta L_T^o.$$

However, unit one is considered to be a poor regulator, unit two an average regulator and unit three a good regulator and hence in the midfrequency range the participation of each unit is adjusted in Figure 5.22 to reflect this distinction. If you consider the straight-line asymptotes for the magnitude plots in Figure 5.22, and if all of the zeros of the $G_{C,i}(s)$ are less than g (each unit is lead compensated to some degree) then the participation factors I_i and P_i simply determine the relative gain magnitudes in the low and midfrequency ranges respectively. That is, the ith and jth gain magnitude asymptotes in the low frequency range, which are at -20 dB/decade, are separated by 20 log (I_i/I_j) and the ith and jth gain magnitude asymptotes in the midfrequency range, which are flat, are separated by 20 log (P_i/P_j). Each transfer function then has a pole at s = g as well as one at $s = \tau_F^{-1}$. The former corresponds to the key simplification made in the Coordinating Controller derivation, namely assigning a single eigenvalue to the n-1 redistribution modes, while the latter corresponds of course to the measurement filter pole. The different allocation of gain in the low and midfrequency ranges corresponds to the contribution of each unit to the secondary (realignment)

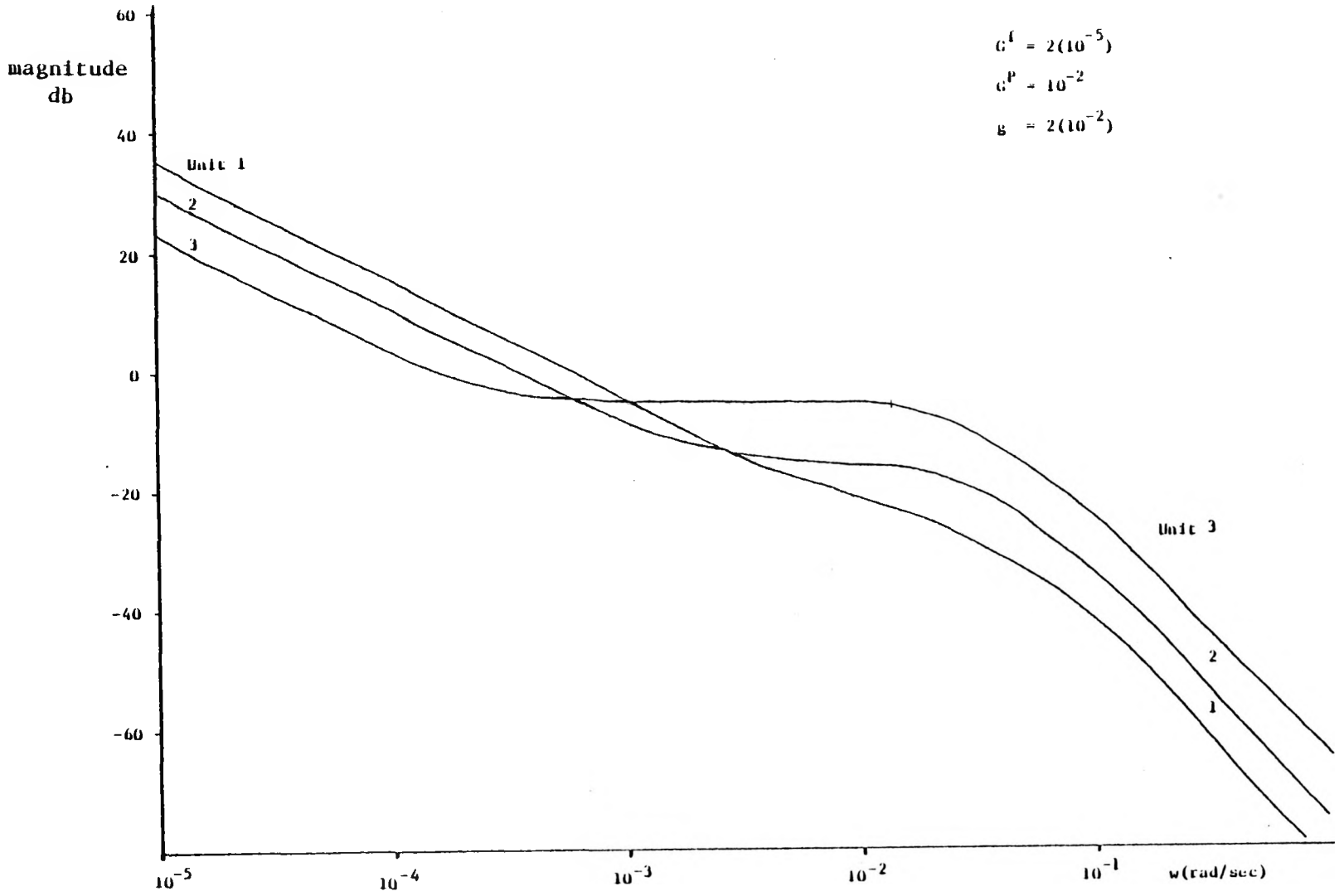

FIGURE 5.22 MAGNITUDE OF $G_{C,i}(s)$ FOR SAMPLE THREE MACHINE SYSTEM

and primary components of system response which were discussed in the previous Regulator Design subsection.

The first example of the time domain response of the sample three unit system provides another comparison between the recommended configuration and the first configuration. The same unit parameters which were used in obtaining the responses shown previously in Figure 5.14 were used in obtaining the responses with the recommended configuration in Figure 5.23. The controller parameters for this run were

$$G^I = 2(10^{-5}) \quad G^P = 1(10^{-3}) \quad g = 2(10^{-2})$$

$$a = 1.0 \qquad \tau_D = 10$$

$$I_1 = .53 \qquad P_1 = .33 \qquad F_1 = .53$$

$$I_2 = .33 \qquad P_2 = .33 \qquad F_2 = .33$$

$$I_3 = .14 \qquad P_3 = .33 \qquad F_3 = .14$$

Thus a "perfect" (and unrealistically fast) dynamic dispatch feedforward was chosen, for illustrative purposes. In comparing Figure 5.23 with Figure 5.14, it is apparent that the selected configuration provides a somewhat smoother response. The main reason for including these responses however is to note that the system in this particular case is evidently Type 2 with respect to load. That is, for a step change in 60 Hz demain, we see that the integral of ACEM is driven to zero in the steady state. Or for a sustained ramp in 60 Hz demand, ACEM would be driven to zero in the steady state.

With the particular model being used for the Dynamic Dispatch however, the type of the system is dependent on the value of a. It is easy to see from Equation (5.78) that for a $\neq$ 1.0 the system is Type 1

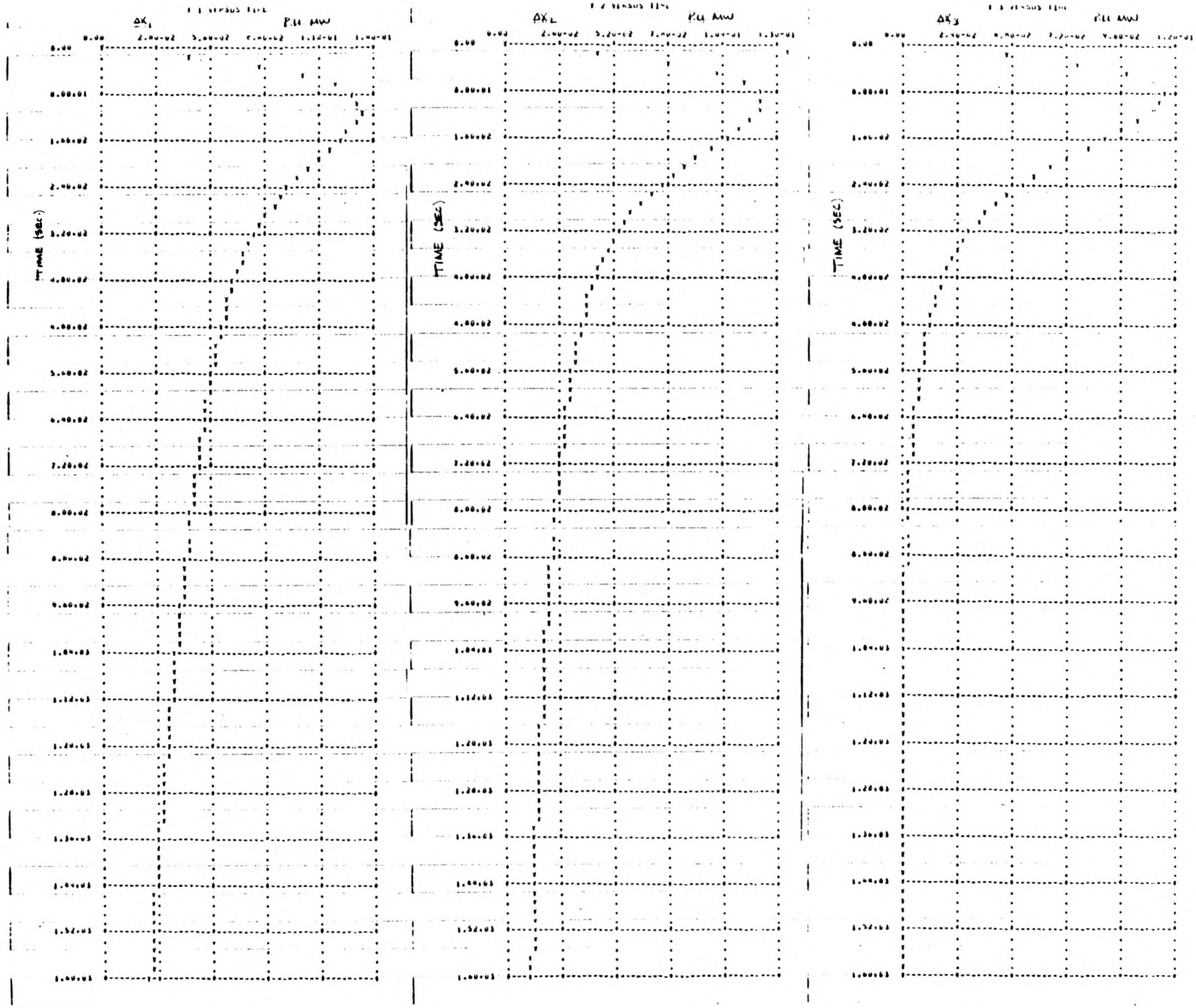

FIGURE 5.23a CONTROLLER REFERENCE INPUTS

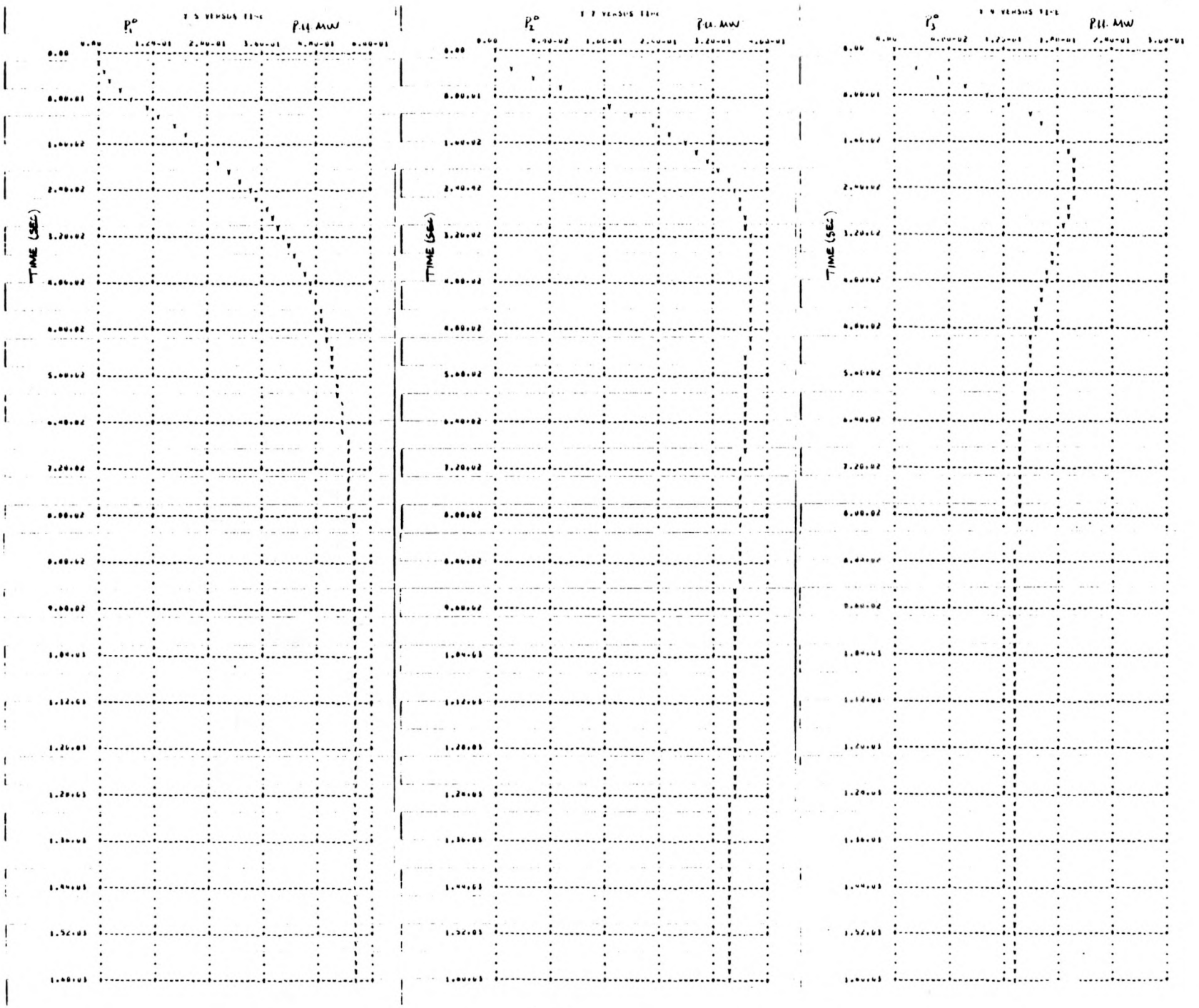

FIGURE 5.23b UNIT 60 Hz OUTPUTS

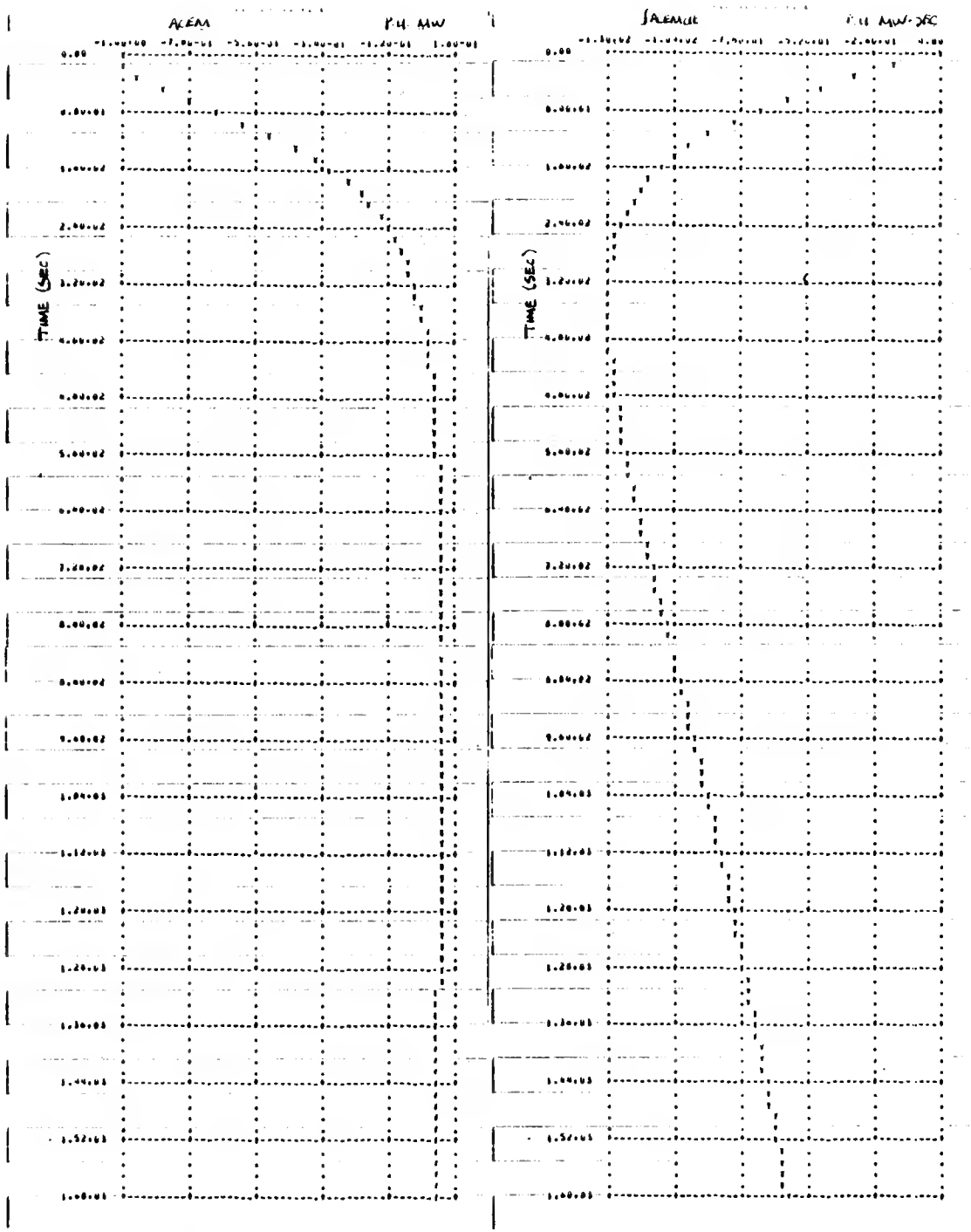

FIGURE 5.23c ACEM AND ∫ACEM dt, 1.0 pu STEP LOAD CHANGE

with respect to the total load demand disturbance ($L_T^o + S^o$). To illustrate this with a simulation, the same 1.0 pu step change in load demand was applied to the three machine system whose responses were shown in Figure 5.23. The only change was in the participation factors, which were changed to:

$$I_1 = .53 \qquad P_1 = .14 \qquad F_1 = .3$$
$$I_2 = .33 \qquad P_2 = .33 \qquad F_2 = .2$$
$$I_3 = .14 \qquad P_3 = .53 \qquad F_3 = .1$$

Now $F_1 + F_2 + F_3 = a = .6$, so the dispatch feedforward now only supplies a fraction (.6) of the total load demand change. The resulting responses are shown in Figure 5.24. Notice that in this case the integral of ACEM, Figure 5.24c, does not go to zero. This example also illustrates the steady state allocation of the difference between the load demand change and the sum of the dispatch feedforward targets; from Figure 5.24a we see as expected that the reference inputs Δx_i approach the steady state values of

$$\Delta x_1(ss) = I_1 * (1.0 - 0.6) = 0.21 \text{ pu MW},$$
$$\Delta x_2(ss) = I_2 * (1.0 - 0.6) = 0.13 \text{ pu MW, and}$$
$$\Delta x_3(ss) = I_3 * (1.0 - 0.6) = 0.05 \text{ pu MW}$$

The participation factors used in this example were also chosen to have a very large spread, the ratio P_i/I_i varying between 0.26 and 3.79. This is the reason for the significant overshoot of P_3^o shown in Figure 5.24. For a given set of total controller gains and unit response models, this ratio determines the amount of unit output overshoot (or lack thereof).

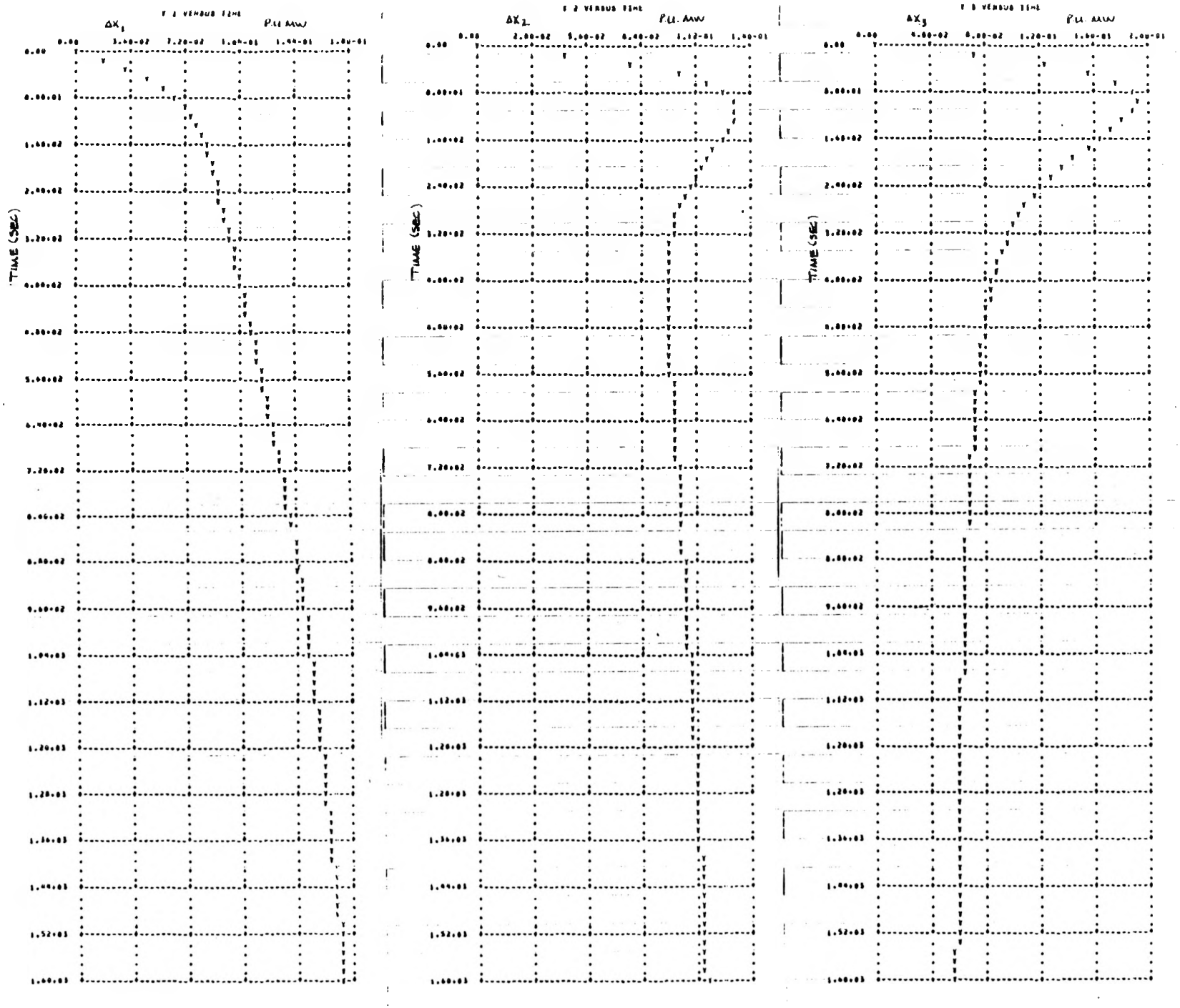

FIGURE 5.24a CONTROLLER REFERENCE INPUTS

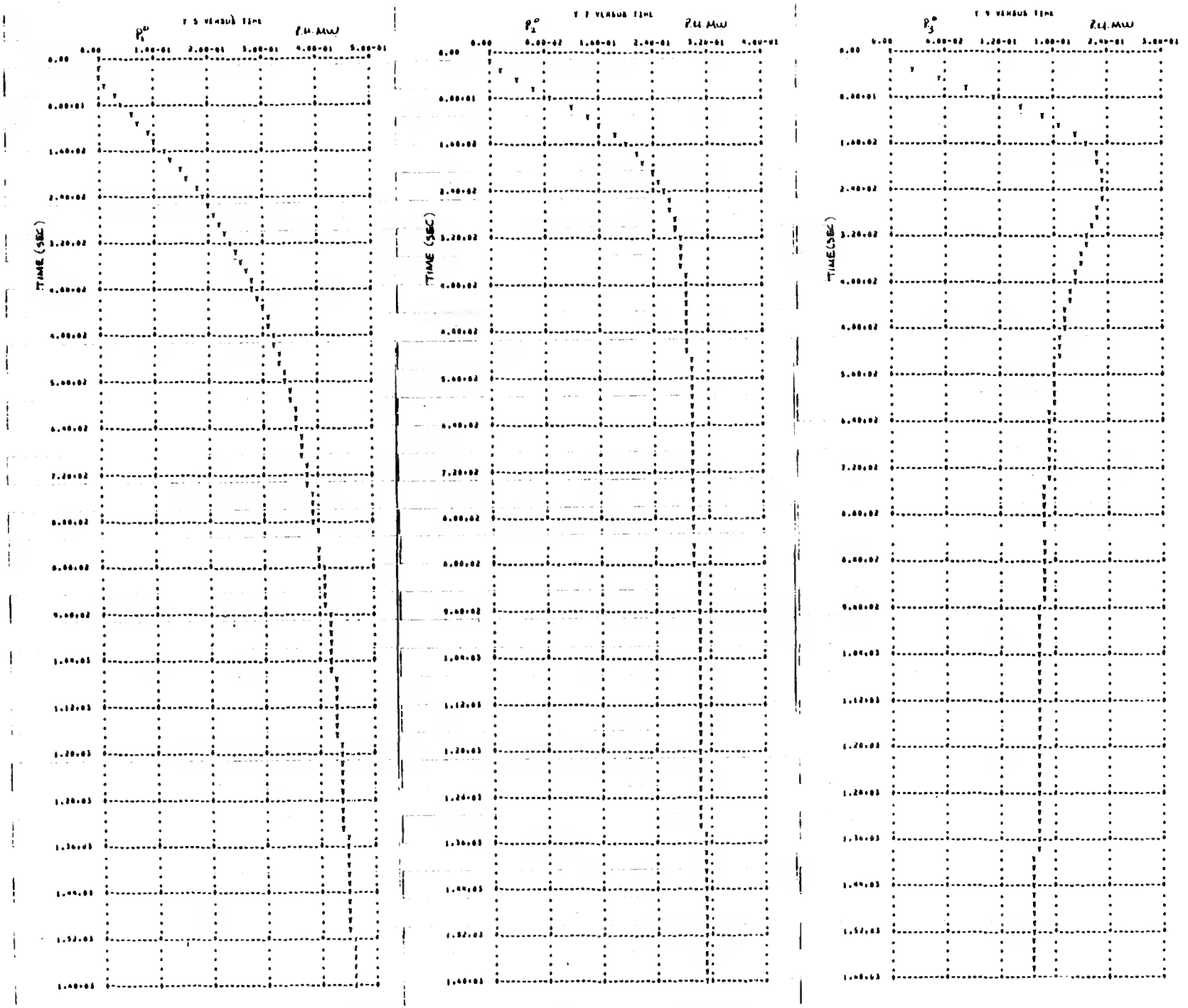

FIGURE 5.24b UNIT 60 Hz OUTPUTS

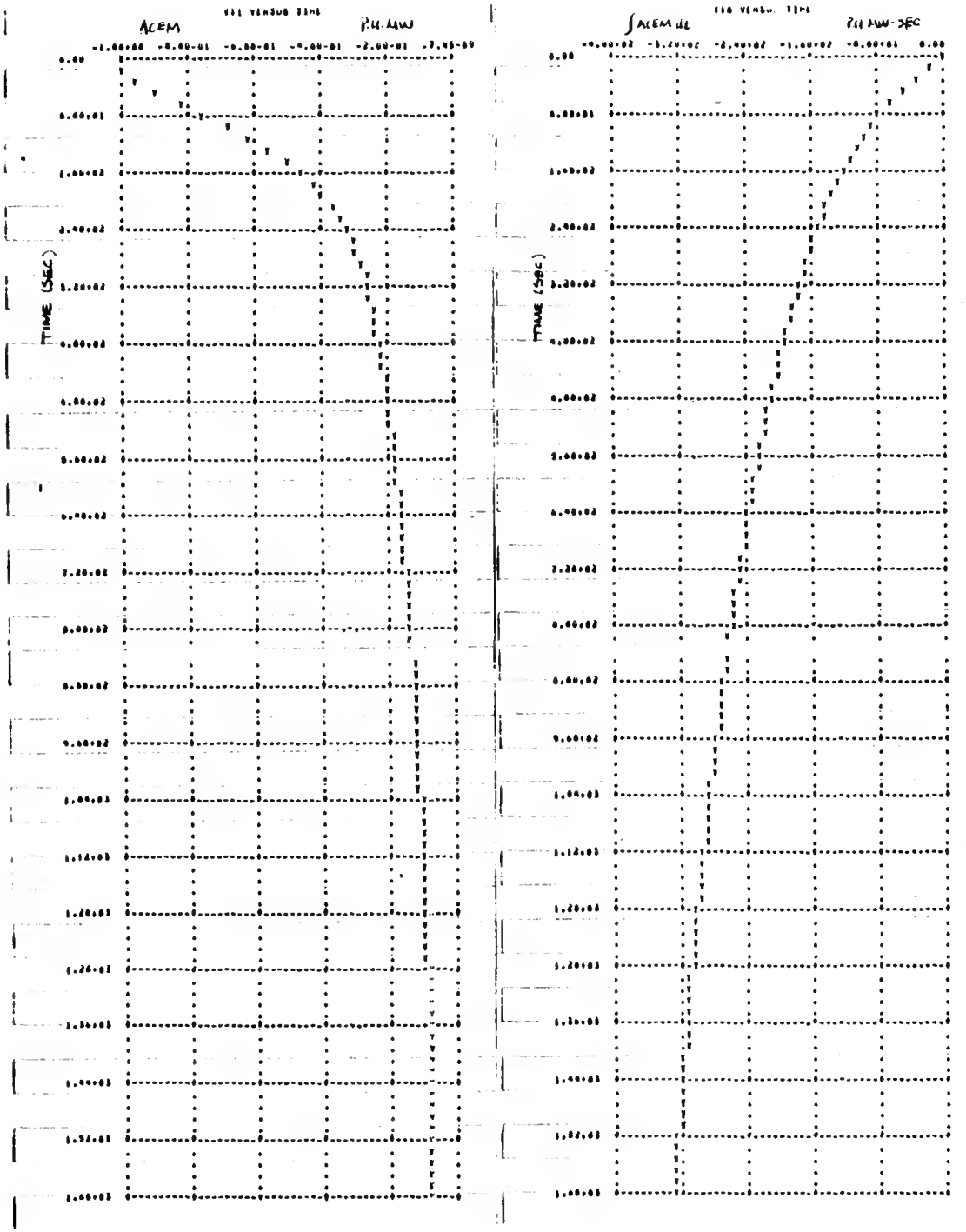

FIGURE 5.24c ACEM AND IACEM, 1.0 pu STEP LOAD CHANGE

Before the issue of system type is investigated in more detail, the issue of overshoot, raised by the previous example, should perhaps be addressed because it is neither uncommon nor unsurprising that unit reversal is often considered to be a characteristic of bad control. In general, it is clear that unit reversal is a natural tendancy when a unit has an available amount of fast responding capacity and is considered to be a good regulator but is at the same time, whether for economic or other reasons such as regulating limit constraints, considered to be less favorable for absorbing sustained load changes. If this distinction is to be exploited by the LFC algorithms, then as the relative weighting of the ACEM regulation performance measure vs. the control effort performance measure is increased the amount of unit reversal which occurs will tend to increase concomittantly. Unit reversal is a part of the broader issue of regulation and from this point of view the question is not really whether a unit reversal should occur but rather with what magnitude and over what period of time should reversals occur. No serious attempt was made to quantitatively analyze the Coordinating Controller along these lines during the prototype design stage, as the AGC simulation program provides a much more realistic test environment for such an investigation. The more qualitative analyses performed using the simple three machine system do show however, that the controller structure can be parameterized to provide a wide range of responses for each unit, and that it is easy to tune the Coordinating Controller to reflect a particular area regulation objective. Some of the basic tradeoffs are also clear; for example, in the case illustrated in Figure 5.24, we notice the essentially two-mode response of ACEM to the step load change. The relative contribution of the initial, primary response mode is a strong function of the amount of lead compensation. Figure 5.24b shows that this component of the total response is distributed so as to take advantage of the better regulating unit(s), but that a reversal of unit three occurs due to the relative weighting used for the steady-state allocation, which is dominated by the secondary, realignment mode.

The issue of system type with respect to total demand, which is of considerable importance since it involves the control area operating policy regarding area inadvertent interchange, is somewhat obscured by analyzing the system linearized about a constant operating point, i.e., by analyzing the block diagram representation of Figure 5.16. This is the case because the model assumed for the Dynamic Dispatch,

$$P_i^* = F_i \cdot \frac{a}{s\tau_D+1} (\hat{L}_T^o + \hat{S}^o) + \Delta L \qquad i=1,2,\ldots n \qquad (5.88)$$

leads to the conclusion mentioned previously, that the system type with respect to total demand (the number of zeros, in the transfer function relating ACEM to $L_T^o + S^o$) is two if a = 1.0 and one otherwise. This in turn raises questions about the interpretation of the dispatch model suggested by (5.88); for example, ΔL is certainly correlated with L_T^o so how should this correlation be accounted for in determining system type? A more useful viewpoint is provided by the pertubational system defined in (5.80 - 5.84) and illustrated in Figure 5.21. This system is clearly type one from the disturbance ΔL_T^o, ACEM will be driven to zero while for a sustained ramp in ΔL_T^o, ACEM will approach a finite value determined by the rate of change of ΔL_T^o and the total loop gain. Complete agreement has not been reached on this issue however, as one can argue that the pertubational system should be type two. In fact, Coordinating Controller Two has been designed to have the higher type and this issue will as a result arise again in the next section, which describes this second controller structure. It is relatively straightforward to provide either controller with either type, so the question is simply which type will best allow the control area to meet its operating objectives.

The main reasons for tentatively providing the Coordinating Controller One with the lower type will be summarized. It is useful to first recall that the desired generation trajectories are calculated in the Dynamic Dispatch by performing an optimization over a moving window

of 1 to 1.5 hours duration. The Dynamic Dispatch is designed to run in a tracking mode, updating the desired trajectories based on the latest 5 minute load forecasts. For the sake of argument, suppose that the Dynamic Dispatch is decomposed into a two step procedure; an optimization over the moving window using only the spline fit to the short term load forecast, and an "immediate-term" correction based on the five minute load forecast and sensitivity factors provided by the dynamic optimization procedure. Interpolation is used between these five minute points so that the desired generation trajectories P_i^* are smooth and defined on the LFC execution rate (4 second) basis. This decomposition is not equivalent from an economic point of view, but is equivalent from a load tracking point of view. The reason for making it is to attempt to conceptually illustrate that the system is in fact "nearly" type two, and then to interpret the meaning of this in the context of unintentional inadvertent accumulation.

The second step in this procedure, which essentially corrects for forecast errors of the slower-running short term load forecast and trims the desired generation feedforward trajectories accordingly, can of course be viewed as a part of the Coordinating Controller. Then if, for the sake of argument, the predictive element of this step is removed and the correction is made on a 4 second basis, it is easy to verify that this corrective procedure amounts to a unity feedforward in Figure 5.21 from ΔL_T^o to total reference input Δx_T. This conceptual rearrangement results in a type two relationship between ACEM and the disturbance ΔL_T^o, where the second zero comes from the reset integrators which are a part of each unit controller. Thus if ΔL_T^o is a step input disturbance, then both ACEM and its integral IACEM will be driven to zero. It seems reasonable to assume that no significant sustained ramp in ΔL_T^o will occur and if so unintentional inadvertent could not, in theory, accumulate. From a different point of view, the controller would in this case be "paying back" inadvertant on

a continuous basis. Allowing for the occasional perversity of nature and taking each viewpoint towards its extreme, the former becomes optimistic, representing a version of ideal control, while the latter raises several questions regarding the appropriateness of maintaining a type two relationship between ACEM and ΔL_T^o at the LFC level.

The first question is whether or not it is a control area's objective to maintain zero unintentional inadvertant on a "continuous" (LFC execution rate time scale) basis. A control area's objective may instead be to maintain zero unintentional inadvertant over a time interval greater than the LFC interval; as this time interval is increased, the interconnection can be exploited and economic considerations may become involved, e.g., "peak shaving", etc. The second question centers around the fact that a control area, acting independently to reduce its accumulated inadvertant energy, will cause other interconnected control areas to experience a net opposite change in their own accumulated inadvertents. Such an action is somewhat contrary to current practice, in which pairwise agreements are made between control areas to each reduce the magnitude of their oppositely-signed accumulated inadvertents, of the same kind (peak, etc.). Accomplished via simultaneous (pseudo) tie schedule changes, this practice does not cause other interconnected areas to experience a change in their own inadvertents. Thus there are two aspects to the second question: the paying back of inadvertent at (very) roughly the same cost level, and the possible creation of inadvertent in other control areas. The former aspect would certainly be satisfied most of the time if a policy of continuous inadvertent reduction was adopted, while the significance of the latter concern seems to mostly depend on the magnitude of the accumulated inadvertent itself and hence is difficult to predict.

With these considerations in mind, there does not seem to be a compelling reason to add an additional integrator to Coordinating Controller One and hence increase by one the type of the relationship between ACEM and ΔL_T^o. In fact, the discussion of the second, corrective step in the calculation of the feedforward terms P_i^* suggested that the pertubational system is in a sense nearly type two already, when the corrective step is speeded up and considered to be a part of the Coordinating Controller. The latter observation is interesting because the concept of "nearly type two" can be related to the first question raised above, namely over what interval is it the objective to accumulate a zero net unintentional inadvertant?

Referring again to Figure 5.21, suppose that ΔL_T^o is some disturbance which is zero mean over some interval of time T. Suppose further for simplicity that all initial conditions for the pertubational system are zero prior to the beginning of the disturbance interval (t = 0 say) and that ΔL_T^o goes to zero at t = T for ΔT seconds, where ΔT is sufficiently long for transients to settle. Under these assumptions for the model of Figure 5.21, the unintentional inadvertant at $t = T + \Delta T$ will be zero. Thus an area objective of maintaining, on the average, a zero net change in unintentional inadvertant over an arbitrary interval T can be achieved by forcing ΔL_T^o to be, on the average, a zero mean disturbance over the same interval. The potential benefit of this approach is the flexibility it provides in controlling inadvertent. This flexibility is essentially lost if an exact type two relationship is maintained between ACEM and ΔL_T^o by the Coordinating Controller although the latter structure theoretically provides more capability for achieving ideal performance. As an aside, it is worth mentioning that several controls are available for affecting ΔL_T^o so as to achieve the desired first order (mean) statistical properties. Perhaps the most important one is the variable amount of pure lead which can be introduced to the feedforward terms P^* due to the fact that the latter terms are in part based on a prediction of future load demand.

The magnitudes of $G_{C,i}(s)$ (Equation 5.87) plotted in Figure 5.22 show how the participation factors I_i and P_i determine the relative gain magnitudes for each loop in the low and midfrequency ranges respectively. The total gain parameters shift these individual characteristics with respect to absolute gain and frequency but preserve the relative scaling determined by the participation factors. The total response return ratio provides one approach for selecting the total gain parameters. This frequency domain approach is straightforward when the pertubational system of Figure 5.21 is analyzed and has the advantage of a clear physical interpretation as well as providing important robustness measures. An alternative approach for selecting the total gain parameters is to simply go back to the linear quadratic regulator formulation and parameterize the design in terms of the quadratic cost weightings. This approach would certainly be required if the simplifications introduced had not been made, but for the prototype structure for WEPCO either approach can be easily used. With either approach the closed-loop eigensystem is of interest, and in Task 2 numerous eigenanalyses were performed on both the aggregate total response system and the sample three machine system, particularly in the early design stages. Examples of the latter have not been included because the frequency domain analyses and the step response examples pretty much provide the same information. Root loci plots for the total system response model do provide a useful picture of the effect of the total gain parameters on the closed-loop poles however. For example, Figure 5.25 shows a root loci plot parameterized by the total loop gain G^I/g as well as the fixed parameter values used. The ratio G^I/G^P was held constant in order to maintain in this case a compensation attenuation factor of 1/10 as G^I was varied. The basic features illustrated in Figure 5.25 are typical of a range of parameter values. The corresponding eigenvectors are not shown, but essentially these loci can be interpreted as follows. The open loop unit pole at $s = 5(10^{-2})$, which is intended to roughly represent the initial response of the unit (with its unit controller)

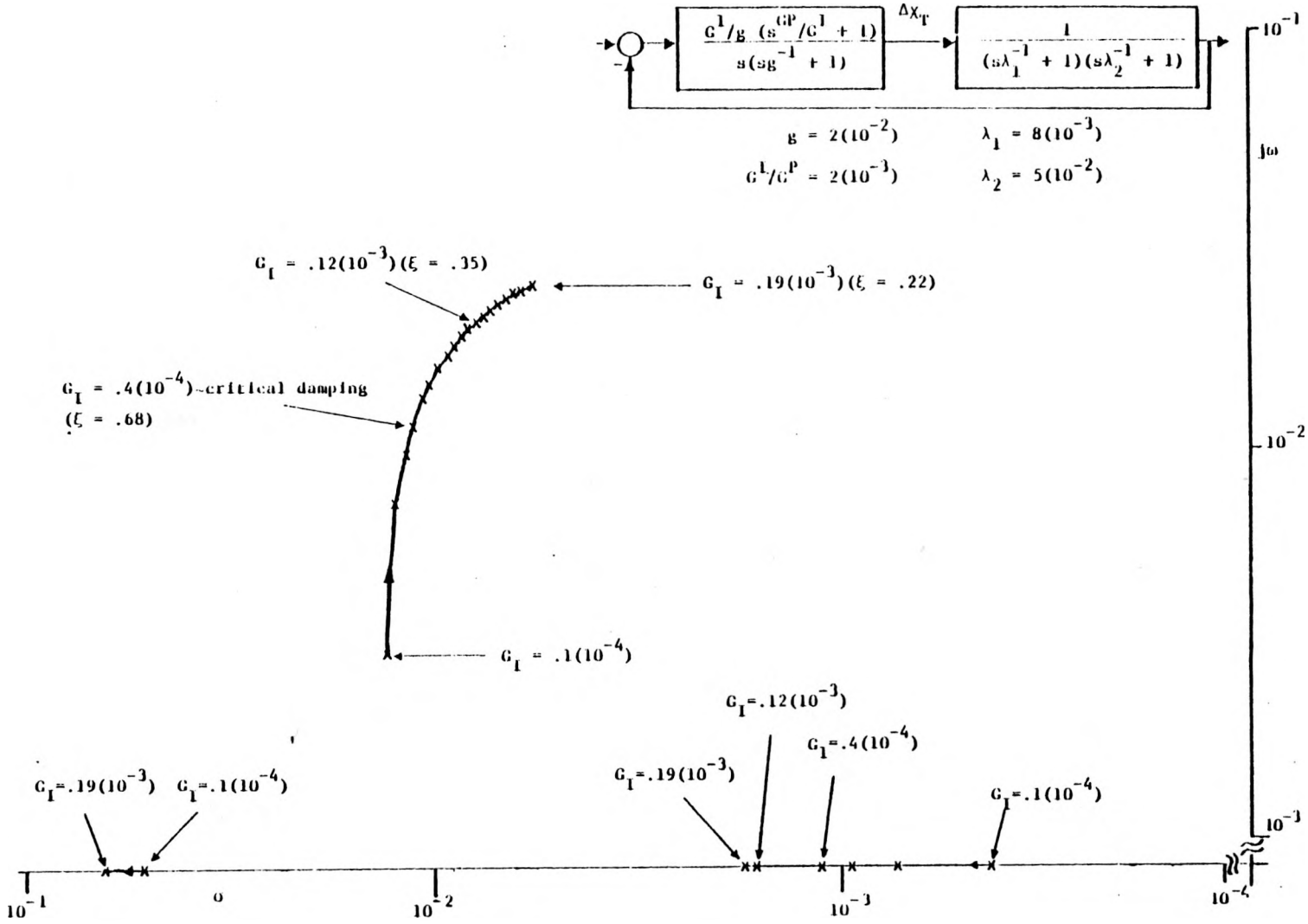

FIGURE 5.25 CLOSED-LOOP POLES AS A FUNCTION OF TOTAL LOOP GAIN

due to change in boiler stored energy when the turbine valve area is changed, is shifted to the left when the loop is closed but is then relatively insensitive to the loop gain in the practical range shown. The other open-loop unit pole, at $s = 8(10^{-3})$, is intended to roughly represent the limitation of the unit fuel/pressure system. As the loop gain is increased, this mode interacts with what was called the controller primary response mode in the regulator design subsection, resulting in the complex conjugate closed loop poles shown. These poles dominate the initial period of the step responses shown previously and their location is closely related to the midfrequency or regulating range characteristic of the return ratio operator T(s). The slower pole in Figure 5.25 is basically that of the realignment mode, and hence it dominates the slow settling to ultimate steady state targets evident in the previous step responses.

If we take the parameters values shown in Figure 5.25 when critical damping occurs, the total response return ratio has the characteristic shown in Figure 5.26. For interest, T(s) is shown both with and without feedforward, where the latter again corresponds to the pertubational system of Figure 5.21. In contrast to the first configuration, there is a nice smooth transition from one to the other. These parameter values seem to be a reasonable starting point for further testing and tuning using the AGC simulation program. Figure 5.27 shows the response of the pertubational form (no feedforward) of the three machine system to a 1.0 pu step change in ΔL_T^o with the same total gain values.

$$G^I = 4(10^{-3}) \qquad G^P = 2(10^{-2}) \qquad g = 2(10^{-2})$$

$$I_1 = .53 \qquad P_1 = .40$$

$$I_2 = .33 \qquad P_2 = .40$$

$$I_3 = .14 \qquad P_3 = .20$$

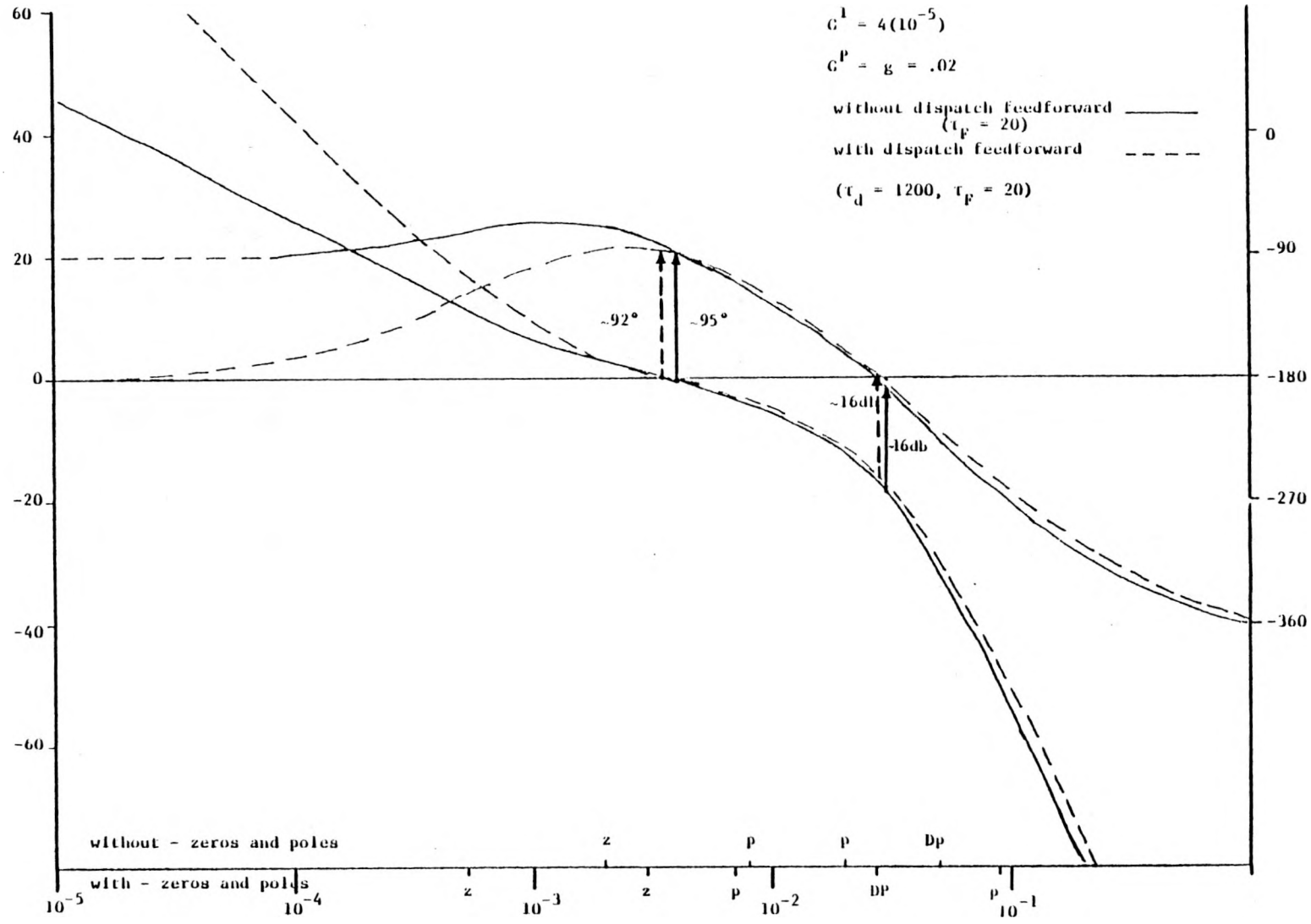

FIGURE 5.26 MAGNITUDE AND PHASE OF TOTAL RESPONSE RETURN RATIO

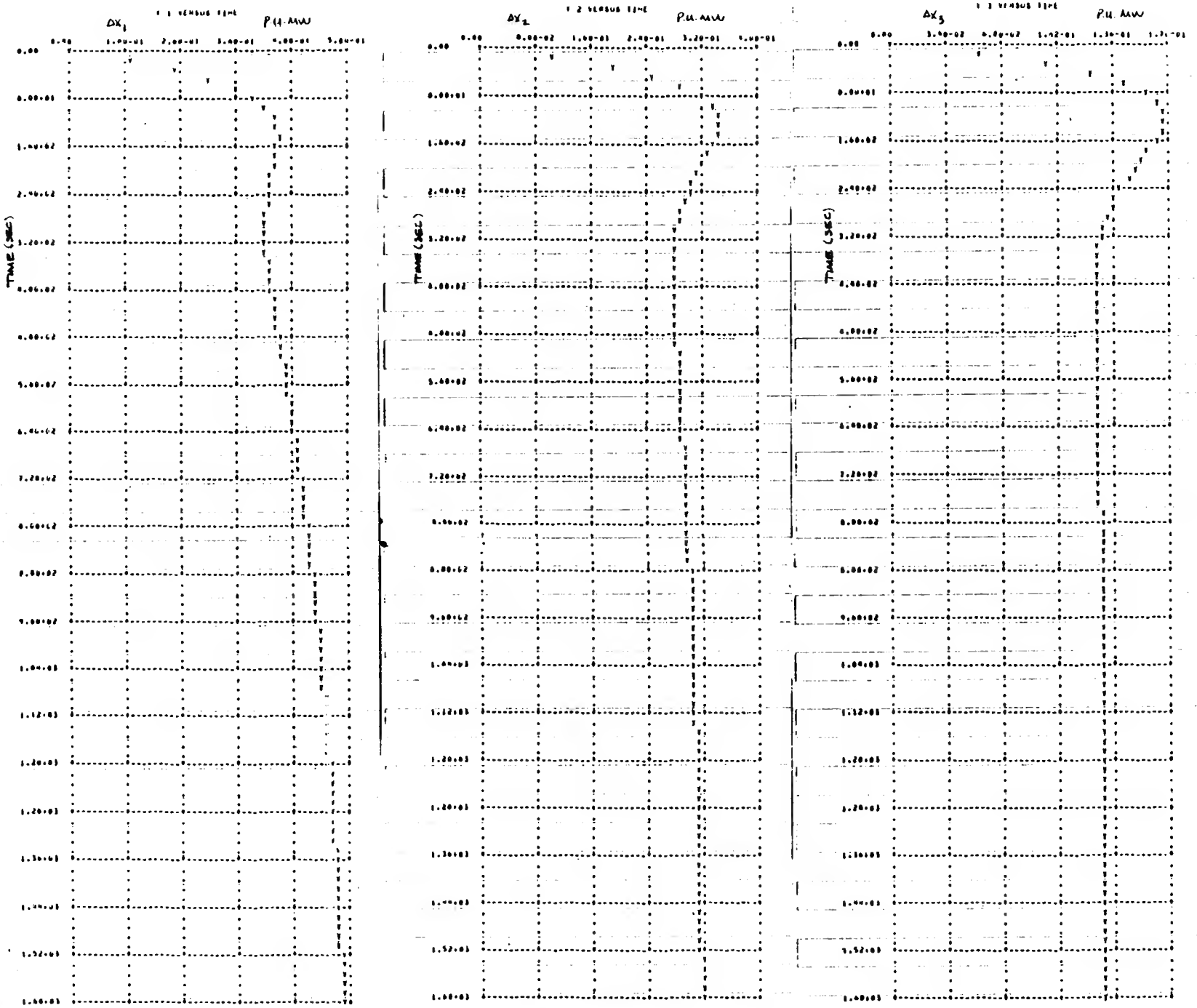

FIGURE 5.27a CONTROLLER REFERENCE INPUTS FOR PERTUBATIONAL SYSTEM NO I FOR)

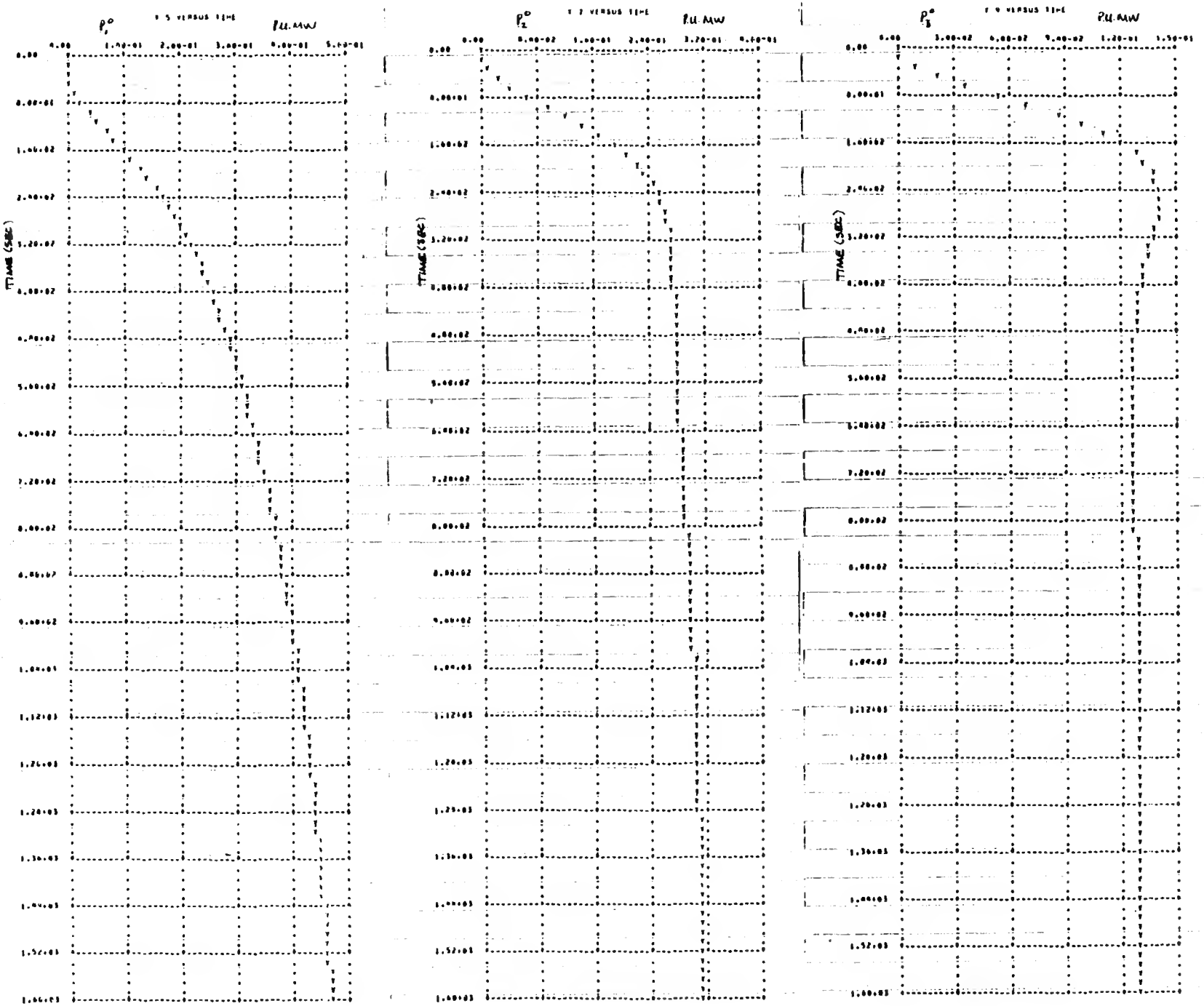

FIGURE 5.27b UNIT OUTPUTS FOR PERTUBATIONAL SYSTEM

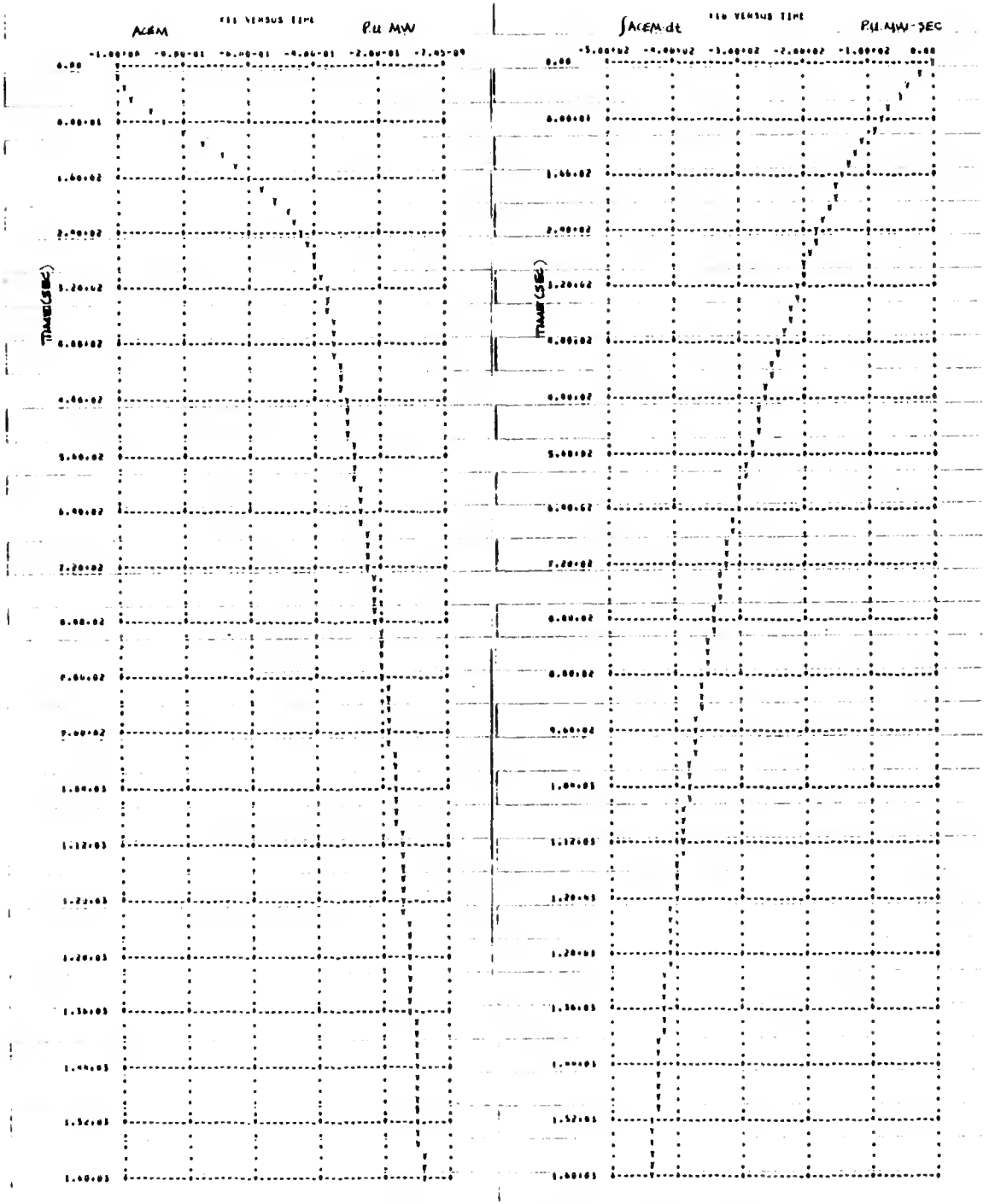

FIGURE 5.27c ACEM AND IACEM, PERTUBATIONAL SYSTEM

The participation factors were adjusted to cut back on the overshoot of the better regulating unit from the previous examples and in Figure 5.27b the outputs again illustrate the different sorts of responses which can be obtained with the Coordinating Controller and the simple unit closed-loop response models. The essentially two-mode response of ACEM is evident in Figure 5.27c, unencumbered by the effects of feedforward in this case.

5.2.5 ACEM Filter

The only variable which needs to be estimated for Coordinating Controller One is the area control error (mechanical) ACEM, where

$$\text{ACEM} = P_T^o - L_T^o - S^o \tag{5.89}$$

Methods for estimating ACE in conventional LFC designs evidently span a wide spectrum, ranging from simple first or second order low pass filters operating on the measurement samples of tie flows and system frequency to relatively sophisticated digital filters based on more complicated models of these stochastic processes [e.g. 13]. Now ACEM was derived in Section 5.2.1 by removing the external area's accelerating power component from ACE and as a result the estimation problem is perhaps more complicated because the only term in (5.89) which is directly measurable is the net tie schedule S^o. As a result of this difference, and the fact that the estimation of 60 Hz load and 60 Hz mechanical power are treated as separate problems in this subsection, the estimator for ACEM has a form which differs significantly from the simple filter for ACE. It is helpful to keep in mind that despite such differences in appearance, ACE and ACEM themselves differ by an accelerating power term which may or may not be significant in the upper range of the LFC bandwidth and hence their estimates will agree in the low frequency range if their design is based on comparable statistical models.

Area electrical power balance implies

$$L_T(t) = G_T(t) - M(t), \tag{5.90}$$

where $G_T(t)$ is the total area electrical generation and $M(t)$ is the net tie flow. Denoting the LFC execution rate by Δt (presently 4.0 sec. at WEPCO) and letting K index this discretization of time (i.e., sample times at $K \cdot \Delta t$, $K = 0,1,\ldots$), then the quantities $G_T(K)$ and $M(K)$ are obtained in summing up the individual unit electrical generation and tie flow values provided by the WEPCO Data Acquisition System (DAS) at the time $K \cdot \Delta t$. The analysis of the DAS made in Section 4.2 of the Task 1 Final Report indicated that significant errors could potentially result when $M(K)$, and to a lesser extent when $G_T(K)$, are computed. As was indicated in the conclusion of that analysis, a useful quantitative estimate of these errors would require a considerable effort in both data gathering and analysis, however. Such information would be useful in designing a filter for the 60 Hz load demand estimate required by the Coordinating Controller, and this is one reason that this particular part of the LFC algorithm development was originally planned for the later stages of the Task 2 work and/or the first stage of Task 3. The most important question of course is whether the existing measurement system constrains the LFC bandwidth or whether this specification can be determined primarily by the desired tradeoff between the performance objectives of control effort and load tracking. While a few doubts raised by the DAS analysis performed to date may remain in the minds of some people, a simple filter is proposed here which is based, among other things, on the assumption that all measurement errors can be represented by a white noise which is not significant enough to constrain the desired LFC bandwidth. Then, using the static model for 60 Hz load demand

$$L_T^o(t) \cong L_T(t)[1 - \bar{\beta}_L(f(t) - f_o)] \tag{5.91}$$

the measurement equation is

$$y^1(K) = L_T^o(K) + V(K) = [G_T(K) - M(K)][1 - \bar{\beta}_L(f(K) - f_o)] \qquad (5.92)$$

where V(K) is a white sequence with covariance r(K).

Referring to Section 5.2, ACEM was defined as the difference between the total area mechanical power referenced to 60 Hz. and the total area load demand plus schedule at 60 Hz. In the context of the steady state arguments which illustrate the conventional ACE strategy for LFC, the assistance which the control area will provide to the interconnection in the event of a sustained system frequency deviation $f - f_o$, when the control error ACEM as defined in Equation (5.89) is employed, is $\beta \cdot (f - f_o)$ (MW) where β is the current best estimate of the actual (real-time) natural area frequency characteristic. So defined, β of course a function of the area load and the combined droop characteristics of the units on-line at a particular time. At least partly due to this fact and to the uncertainty in β at any load level itself, the current practice recommended by NAPSIC is to use the constant-valued area frequency bias B in defining ACE, where B is chosen to be, in theory, slightly greater than the area's natural frequency bias β at a mutually agreed upon measure of area peak load or capacity. In order to be consistent with the ACE strategy in this regard, it is necessary to add a bias term $(B - \beta)(f - f_o)$ to ACEM, i.e.

$$ACEM = P_T^o - L_T^o - S^o + (B - \beta)(f - f_o) \qquad (5.93)$$

It is convenient to include this correction term, which has a small numerical magnitude, with L_T^o and hence to add this bias correction term

to the measurement equation (5.92). Thus the corrected measurement equation is:

$$y(K) \triangleq L_T^o(K) + V(K) = [G_T(K) - M(K)][1 - \bar{\beta}_L(f(K)-f_o)]-(B-\beta)(f(K)-f_o) \quad (5.94)$$

The control error ACEM, formed from an unbiased estimate $\hat{L}_T^o(K)$ based on the measurement (5.94) and the estimate $\hat{P}_T^o$ to be discussed below, is identical to conventional ACE in the low frequency range.

A simple Kalman filter is used to obtain the estimates $\hat{L}_T^o(K)$. For notational simplicity, $L(K) = L_T^o(K)$ and $\hat{L}(K) = \hat{L}_T^o(K)$ are used in the remainder of this development. Consider the model

$$\begin{aligned} L(K) &= L(K-1) + e(K-1) + (\bar{L}(K) - \bar{L}(K-1)) \\ e(K) &= \phi(K-1)\, e(K-1) + w(K-1) \end{aligned} \qquad K = 1,2,... \quad (5.95)$$

with the observation model equation

$$y(K) = L(K) + V(K) \quad (5.96)$$

$w(K)$ is a white sequence, uncorrelated with $V(K)$, with covariance $q(K)$. $\bar{L}(K)$ is treated as a deterministic input to (5.95); it is based on a prediction of the secular component of the 60 Hz load demand. In this project, $\bar{L}(K)$ is obtained from the 5 minute forecast algorithm by sampling a quadratic interpolation between the lastest 5 minute load estimate and the current one and two step-ahead 5 minuts forecasts. Equation (5.95) really just models the residual $r(K) \triangleq L(K)-\bar{L}(K)$, where

$$\begin{aligned} r(K) &= r(K-1) + e(K-1) \\ e(K) &+ \phi(K-1)\, e(K-1) + w(K-1) \end{aligned} \qquad K = 1,2,... \quad (5.97)$$

For $\phi(K) = 0$ for all K, $r(K)$ is a random walk; otherwise it is a random constant bias plus a first order Markov process. Note that $\hat{L}(K) = \hat{r}(K) + \bar{L}(K)$. The Kalman filter equations for the model (5.95) and observation (5.96) are well-known (e.g. [5.16]) and hence are not repeated here. The key feature of this filter formulation is the use of the secular load trend estimate provided by the 5 minute load forecasting algorithm. The form of the residual model in (5.97) appears to be appropriate at this time, although work is in progress for confirming this hypothesis. The same methodology employed in developing the short term and 5 minute load forecasting algorithms can be used for identifying a different model if necessary.

Unit mechanical power referenced to 60Hz, P_i^o is considered to be the unit mechanical power output which would result if the governor was disconnected and the transient due to this disturbance has settled out. The purpose of defining this referenced quantity, which is of course not directly measurable, is to satisfy the third area LFC objective identified in Section 5.2, i.e., to allow the unit primary response to occur naturally and hence to contribute to the system objective of frequency regulation. The aim then, is to make the LFC controller blind, as it were, to the natural behavior of the primary response loop. Because individual unit 60 Hz mechanical powers are used to define the area control error ACEM it is clear that each Unit Controller should act to maintain a zero error between the MW reference input UDG_i provided by the Coordinating Controller and P_i^o. (This issue of biasing the unit control loop set points so that they are consistent with the area frequency bias term of ACE in conventional LFC structures was raised, for example, by Cohn in [5.1], although it is not clear that this is always done in actual implementations, perhaps due to the view that this bias term is normally very small in absolute value and may get lost in the discretization of the unit pulsing logic anyway.) Thus the filter associated with each unit

controller generates an estimate of unit 60 Hz mechanical power, $\hat{P}_i^o$ and hence

$$\hat{P}_T^o = \sum_{i=1}^{N} \hat{P}_i^o \tag{5.98}$$

Currently each unit filter is based on a similar linear model; their design is covered in Section 6 and hence is not repeated here. It should be noted that the summation in (5.98) is over all on-line units. Although the unit filter and unit controller are more or less developed in Section 6 as a single algorithm, they are separated in implementation so that a unit filter is formed for each on-line unit while a unit controller is formed for each unit on automatic control.

It is perhaps worthwhile to add a few comments on estimating P_T^o. First, if the turbine-governor was a linear system, then it is easy to construct a model which is consistent with the above definition of unit 60 Hz mechanical power. In order to focus on the basic idea, the very simple model shown in Figure 5.28 is used as an example. Many governors have a significant backlash however, and this complicates the estimation problem considerably. The governor-turbine representation with this nonlinearity included which corresponds to Figure 5.28 is shown in Figure 5.29. Using the definition of P_i^o given above, a decomposition similar to that in Figure 5.28 can only be obtained for very specific assumptions. It is fairly easy to show however, that as more and more governors are placed in parallel, the equivalent governor characteristic approaches the form shown in Figure 5.30 when it is assumed that frequency deviations are zero mean and that the initial position of the unit operating points are uniformly distributed in an equivalent deadband at $\Delta f = 0$. Thus these aggregate governor deadband assumptions provide the same hypothetical separation of unit mechanical power into two components

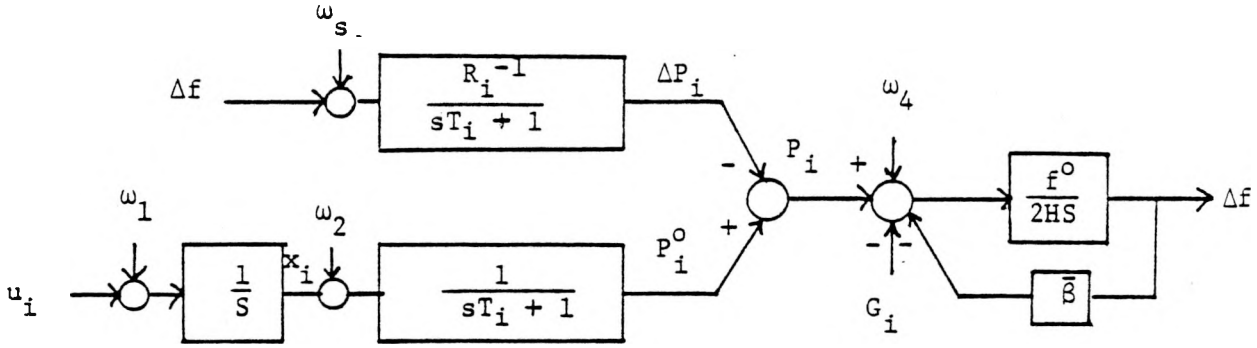

FIGURE 5.28

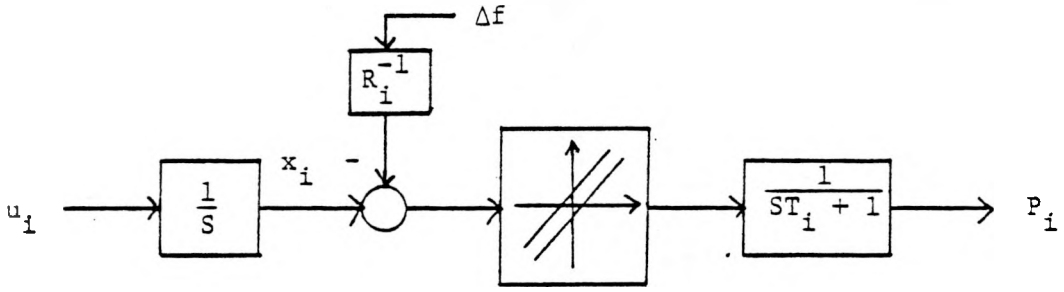

FIGURE 5.29

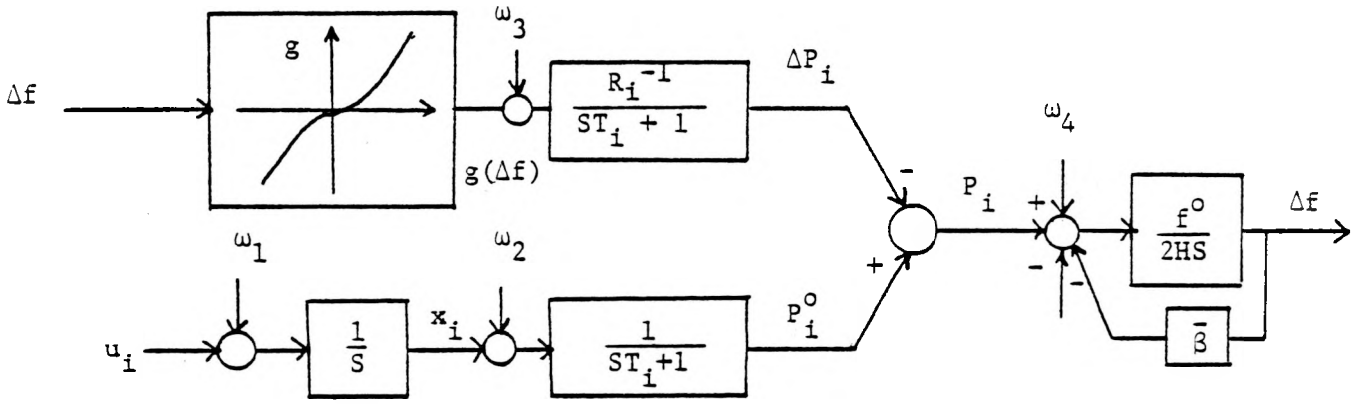

FIGURE 5.30

as the linear model. A filter can be designed based on a model of the same form as that in Figure 5.30 and some preliminary work was performed on this in Task 2. While an extended Kalman filter is one possible approach to incorporating the aggregate effects of unit deadbands, the technique of statistical linearization [5.16] appears to be very well-suited for this particular problem. This is because the non-linearity is an odd function whose input (Δf) has statistics which are fairly well known a priori. This approach was looked at and is promising, although it does have significantly higher computational requirements than the linear filter however. As the measurements are fairly certain relative to the model uncertainty, an observor is a possible alternative approach.

The main feature of an estimator for P_T^o which is based on a nonlinear stochastic model like that in Figure 5.30, is that it provides a potentially meaningful way to obtain a nonlinear frequency bias. This is mentioned because the latter idea has recently received some attention by researchers and industry practitioners alike. It was suggested, for example, by Kennedy [5.15] as a possible means for reducing unnecessary control action. Ewart has reported some interesting results and observations which suggest that unnecessary and even destabilizing control action may result due to the current practice in frequency bias setting [5.4], and based on that analysis it would appear that a nonlinear estimator for P_T^o could help the problem. On the other hand some detailed simulation results (including the above aggregate deadband representation) and system frequency spectral analyses provided in [5.14] indicate that the aggregate governor deadband affects on system frequency are relatively small. At least small enough that no limit cycle instability phenomena were detected although it was concluded that they are significant enough that nonlinear frequency biasing may be expected to reduce unnecessary control action.

Evidently, the nonlinear frequency bias idea raises both difficult technical questions and AGC objective issues. In both regards it is a problem which encompasses more than just the single area point of view, and as a result it lies somewhat outside of this project's scope. While both of the prototype LFC structures can provide such a characteristic, the current plan for the project software implementation stage is to use a linear frequency bias in the estimation of P_T^o. By analyzing the estimation error $\hat{P}_T^o - P_T^o$ during the simulation testing, it is hoped that some further insight into the frequency bias issue can be gained however, and based on these results a modification of this plan may be considered.

5.3 COORDINATING CONTROLLER TWO

5.3.1 General Structure

As was mentioned in Section 5.1.3, the second Coordinating Controller structure is based on a different robust linear multivariable regulator design methodology than the structure developed in the last section. In the first structure the dynamic error ACEM was formed and a servo-compensator was designed to provide desired disturbance rejection properties and transient response characteristics. In the second structure, estimates of the disturbance states of the model illustrated in Figure 5.1 are formed, and the controller feeds these back in such a way that ACE will be driven, in the face of these disturbances, to zero in the steady state as well as shapes the transient which leads to this equilibrium. In this subsection the general structure of Coordininating Controller Two is developed and a number of its theoretical properties are investigated. The material in this subsection was provided by project consultant H.G. Kwatny (Professor of Systems Engineering, Drexel University) in the early stages of the Task 2 work; it not only specifies the proposed

structure for Coordinating Controller Two but contains several ideas which have had a significant impact on the Coordinating Controller One design as well. The most important idea is that of the primary and secondary state deviation costs which in turn induce the particular feedback regulator structure which has been exploited in both designs. Now a considerable amount of qualitative material and discussion was included in the previous section describing the first controller structure, a great deal of which is relevant to the second controller structure as well. Many of these interpretative comments are therefore not repeated here and the emphasis in this section is primarily on the technical details of the second coordinating controller structure.

The same simplified dynamic model of the principle (local) control area connected to an external system is used and the reader is referred to the discussion made previously in the last section. A block diagram is given in Figure 5.1 and Table 5.1 contains definitions of the variables and parameters employed. The equations are listed below:

$$\dot{x}_i = u_i \qquad i = 1,\ldots n \tag{5.99}$$

$$\dot{x}_{n+1} = -(\beta/H)\, x_{n+1} + H^{-1}\{\sum_{i=1}^{n} x_i - \omega_3 - \beta/\beta_1 \cdot \omega_2\}$$

$$\dot{\omega}_1 = \nu_1 \tag{5.100}$$

$$\dot{\omega}_2 = \nu_2$$

$$\dot{\omega}_3 = \omega_4 + \nu_3$$

$$\dot{\omega}_4 = \nu_4$$

$$y_1 = x_{n+1} + \omega_1 \tag{5.101}$$

$$y_2 = (\beta_2/\beta) \left(\sum_{i=1}^{n} x_i - \omega_3\right) + \omega_2 - S^o$$

$$y_3 = D_1(x_{n+1} + \omega_1) + \omega_3$$

The first step in this design procedure is the characterization the ultimate state trajectory. With ν_1, ν_2, ν_3 and ν_4 set to zero in (5.100) it is desired to determine state and control trajectories $\bar{x}$ and $\bar{n}$ such that (5.99) and (5.101) are satisfied for all initial states and in addition that

$$ACE \triangleq y_2 + By_1 = 0 \tag{5.102}$$

These trajectories can generally be obtained as linear functions of ω_1, ω_2, ω_3, ω_4. In fact, this possibility is a necessary condition for the existence of a solution to the regulator problem. It is easily verified that any solution $\bar{x}$, $\bar{u}$ which satisfies

$$\bar{x}_1 + \bar{x}_2 + \ldots + \bar{x}_n = -\left[\frac{B\beta}{B+\beta_2}\right] \omega_1 - \left[\frac{(\beta_1 - B)\beta}{\beta_1(B+\beta_2)}\right] \omega_2 + \omega_3 + \frac{\beta}{B+\beta_2} S^o \tag{5.103}$$

$$\bar{x}_{n+1} = \left[\frac{B}{B+\beta_2}\right] \omega_1 - \left[\frac{\beta}{\beta_1(B+\beta_2)}\right] \omega_2 \tag{5.104}$$

$$\bar{u}_1 + \bar{u}_2 + \ldots + \bar{u}_n = \omega_4 \tag{5.105}$$

$$\dot{\bar{x}}_1 = \bar{u}_1, \ \dot{\bar{x}}_2 = \bar{u}_2, \ \ldots, \ \dot{\bar{x}}_n = \bar{u}_n \tag{5.106}$$

also satisfies the required equations.

Thus, one obvious choice from the many possible solutions is

$$\bar{x} = \gamma[-\phi_1 - \phi_2 \quad 1 \quad 0]\omega + \gamma\, \phi_s\, s^o \tag{5.107}$$

$$\bar{u} = \gamma\omega_4$$

where

$$\phi_1 = \left[\frac{B\beta}{B + \beta_2}\right], \quad \phi_2 = \left[\frac{(\beta_1 - B)\beta}{\beta_1(B + \beta_2)}\right], \quad \phi_s = \frac{\beta}{B+\beta_2} \tag{5.108}$$

and γ is any set of participation factors such that

$$\sum_1^n \gamma_i = 1 \tag{5.109}$$

Another possibility is the following. If x^*, u^* is any solution of the ultimate state problem for any particular disturbance trajectory, say ω^*, then a solution for arbitrary ω is

$$\bar{x} = x^* + \gamma[-\phi_1\omega_1 - \phi_2\omega_2 + (\omega_3 - \chi_T^*) + \phi_s\, s^o] \tag{5.110}$$

$$\bar{u} = u^* + \gamma[\omega_4 - u_T^*] \tag{5.111}$$

where

$$\chi_T^* = \sum_1^n \chi_i^* \quad \text{and} \quad u_T^* = \sum_1^n u_i^*$$

The contoller configuration corresponding to this solution is illustrated in Figure 5.31.

The second step of the design methodology is to formulate the feedback control problem. The state variable feedback gain matrix K is

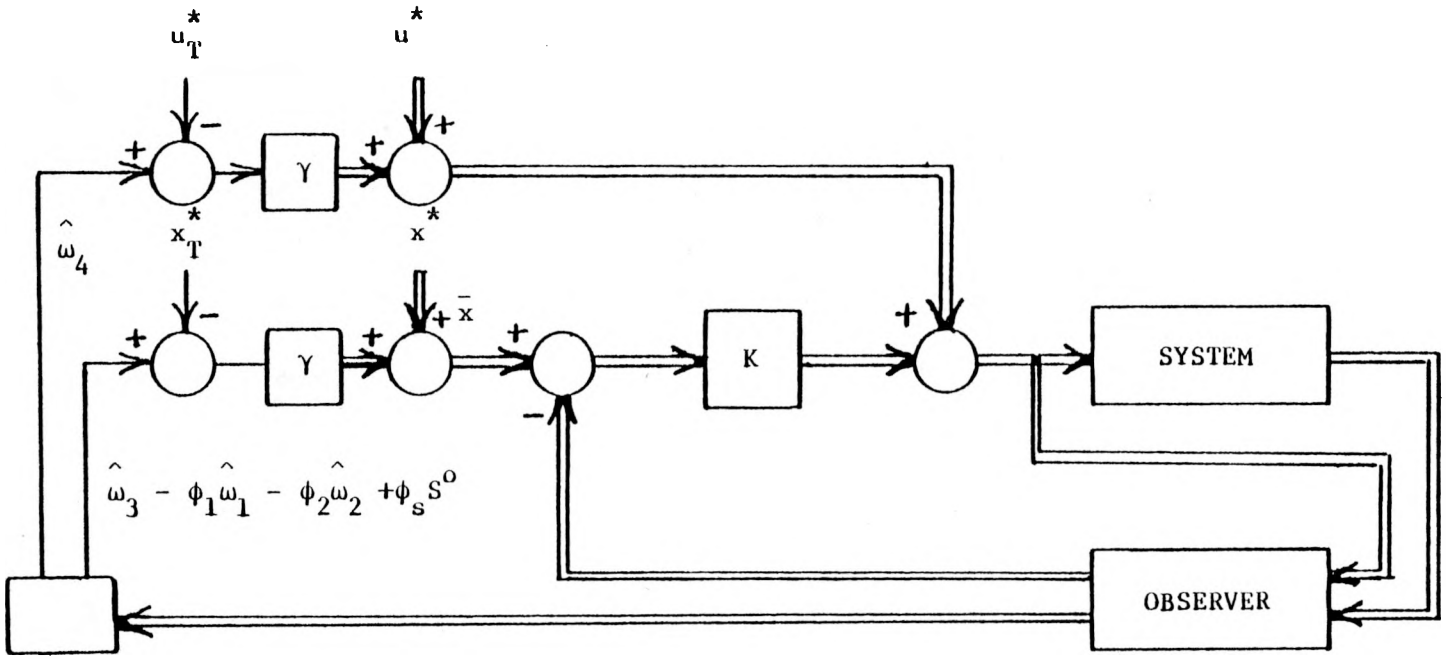

FIGURE 5.31 CONTROL SYSTEM STRUCTURE

obtained by solving the purely deterministic optimal regulator problem defined below. Ignoring all stochastic variables in the model described above leads to the model illustrated in Figure 5.32, which characterizes the perturbations about the nominal trajectories defined by $\bar{u}$, $\bar{x}$. It is desired to find the matrix K of the control law

$$\Delta u = -K\Delta x \tag{5.112}$$

which minimizes a penalty function of the type J given above for a specific choice of output variables y. As noted, the available possibilities include ACE, net tie flow, and frequency as well as any other linear combination of the state variables. Moreover, these can be utilized either individually, or in pairs, or as triplets of variables, etc. The outputs need not be measurable. In selecting an output set at this stage it is necessary to keep in mind that only the transient response will be affected. The ultimate state values will in no way be altered, nor will the observer-estimator.

In view of this, the sum $\Delta G = \Delta x + \ldots + \Delta x_n$ is a meaningful and convenient choice. It is meaningful because regulation of ΔG during the transient actually implies regulation of total generation to its utlimate state value as established by the specification that ACE = 0. Also, it is proportional to the net tie flow deviation. It is convenient because there is no need to alter the time constant associated with frequency and the "frequency mode" is not observable in ΔG. Indeed, it has been repeatedly pointed out that it is undesirable to attempt to use AGC to regulate with a bandwidth wide enough to encompass this mode.

In this case, the performance index becomes

$$J = \int_0^\infty (\Delta x' C' Q_1 C \Delta x + \Delta x' [I - C^* C]\, Q_2 [I - C^* C]\Delta x + \Delta u' R \Delta u) dt \tag{5.113}$$

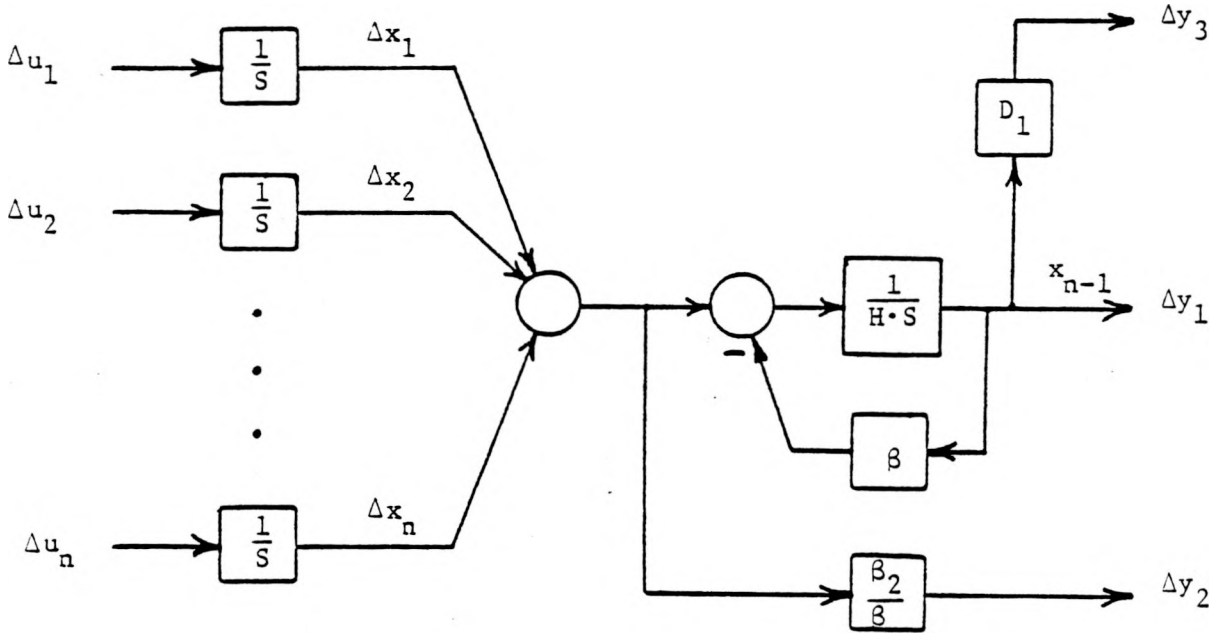

FIGURE 5.32 MODEL FOR STATE FEEDBACK CONTROLLER DESIGN

where

$$C = [\overbrace{1 \ldots 1}^{n} \overbrace{0}^{1}]$$

Note, one choice for C^* is:

$$C^* = \begin{bmatrix} \bar{C}^* \\ 0 \end{bmatrix}, \quad \text{where} \quad \bar{C}\,\bar{C}^* = I \text{ and } \bar{C} = [\overbrace{1 \ldots\ldots 1}^{n}]$$

The matrix Q_1 is a scalar whereas the matrix Q_2 is (n+1) x (n+1). In what follows Q_2 will be specified to be block diagonal, of the form

$$Q_2 = \text{diag}\,(\bar{Q}_2, 0)$$

where $\bar{Q}_2$ is an nxn, symmetric, positive semidefinite matrix. This insures that the frequency mode is not observable in the cost functional.

The well known solution to the standard regulator problem reduces to

$$K = [\overbrace{R^{-1}\bar{P}}^{n} : \overbrace{0}^{1}] \updownarrow n \tag{5.114}$$

where $\bar{P}$ is the maximal solution of the nxn Riccati equation:

$$-\bar{P}R^{-1}\bar{P} + \bar{Q} = 0 \tag{5.115}$$

and

$$\bar{Q} = \bar{C}'Q_1\bar{C} + [I-\bar{C}^*\bar{C}]'\ \bar{Q}_2\ [I - \bar{C}^*\bar{C}]$$

The extremely simple form of these relationships are due to the special structure of the problem. Note that the closed loop eigenvalues of the system of Figure 5.33 with state variable feedback are the n eigenvalues

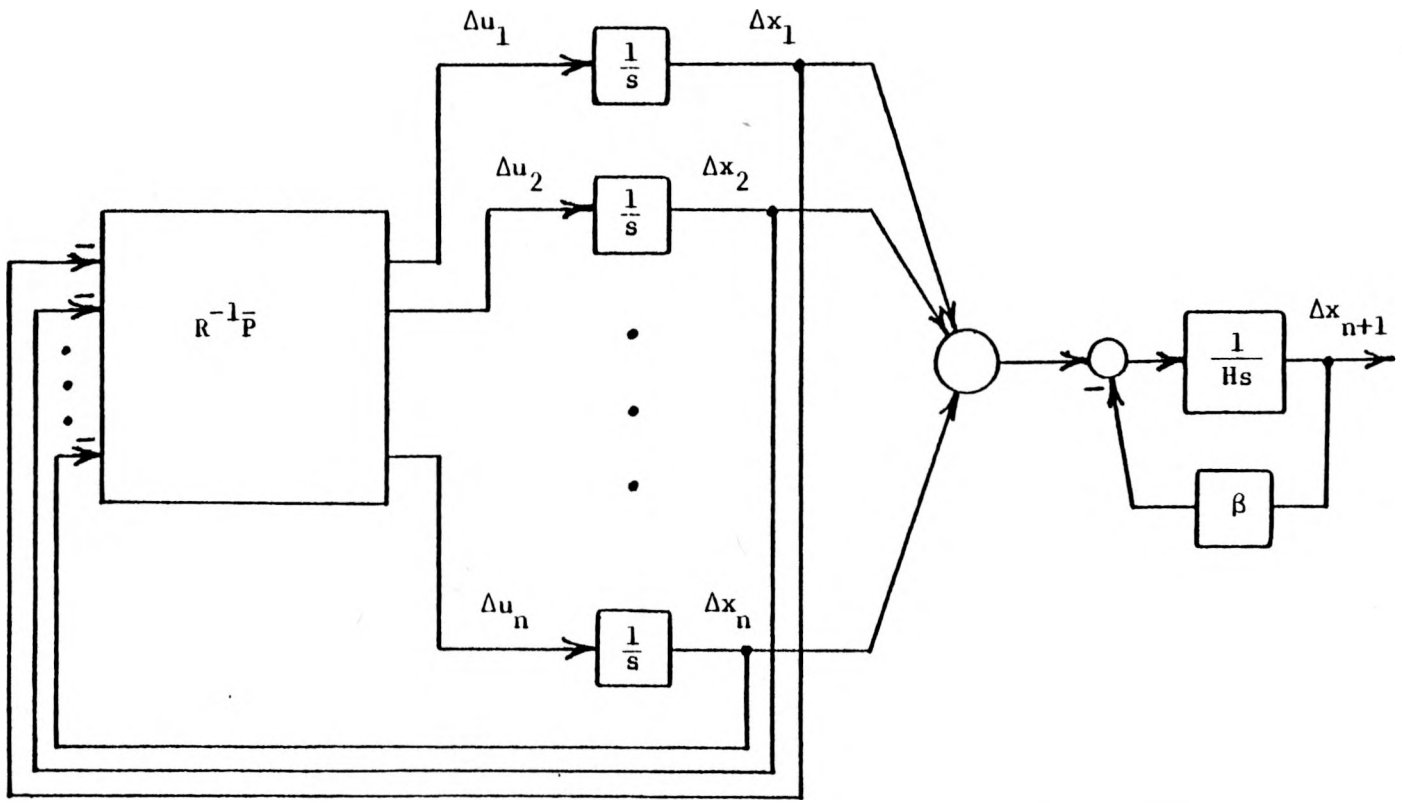

FIGURE 5.33 PERTUBATIONAL SYSTEM WITH STATE FEEDBACK

of $R^{-1}\bar{P}$ and $-\beta/H$. If the eigenvector of $R^{-1}\bar{P}$ corresponding to the eigenvalue λ_i is denoted e_i, then the eigenvectors of the system are

$$\begin{matrix} n \\ 1 \end{matrix}\begin{bmatrix} e_i \\ \hline e_i'\bar{C} & \beta \end{bmatrix} \qquad i = 1,\ldots n \quad \text{and} \quad \begin{bmatrix} 0 \\ 1 \end{bmatrix}\begin{matrix} n \\ 1 \end{matrix} \tag{5.116}$$

The eigenvalues and eigenvectors of $R^{-1}\bar{P}$ can be conveniently characterized in terms of the weighting matrices R and $\bar{Q}$. This can be accomplished by using certain well-known ideas pertaining to the simultaneous reduction of two matrices to an appropriate canonical form.

Since R^{-1} is a symmetric positive definite matrix there exists a nonsimgular matrix T such that

$$R^{-1} = TT' \tag{5.117}$$

from which it immediately follows that

$$T^{-1}R^{-1}(T^{-1})' = I \tag{5.118}$$

Upon pre- and post-multiplying equation (5.115) by T' and T, respectively it is determined that

$$T'\bar{P}R^{-1}\bar{P}T = T'\bar{Q}T, \tag{5.119}$$

or

$$\tilde{P}\tilde{P} = \tilde{Q}, \tag{5.120}$$

where

$$\tilde{P} = T'\bar{P}T, \quad \tilde{Q} = T'\bar{Q}T. \tag{5.121}$$

Since $\tilde{Q}$ is a non-negative symmetric matrix there exists an orthogonal transformation defined by a matrix S whose columns are the eigenvectors of $\tilde{Q}$ such that equation (5.120) can be transformed into

$$(S'\tilde{P}S)\ (S'\tilde{P}S) = S'\tilde{Q}S \tag{5.122}$$

or

$$\hat{P}\hat{P} = \text{diag}(q_1^2, \ldots, q_n^2) \tag{5.123}$$

where

$$\hat{P} = S'\tilde{P}S \tag{5.124}$$

and $q_1^2, \ldots, q_n^2$ are the (non-negative) eigenvalues of $\tilde{Q}$. Note that they are also the eigenvalues of the similar matrix

$$\tilde{T}\tilde{Q}T^{-1} = T(T'\bar{Q}T)T^{-1} = TT'\bar{Q} = R^{-1}\bar{Q}$$

Moreover, a necessary and sufficient condition that all of these eigenvalues be positive is the $\bar{Q}$ (as well as R^{-1}) be positive definite.

Also, note that from (5.123)

$$\hat{P} = \text{diag}\ (q_1, \ldots, q_n) \tag{5.126}$$

so that

$$\tilde{P} = S\ \text{diag}\ (q_1, \ldots, q_n)S', \tag{5.127}$$

and

$$\bar{P} = (T')^{-1}\ S\ \text{diag}\ (q_1, \ldots, q_n)\ S'T^{-1} \tag{5.128}$$

Premultiply this last expression by R^{-1} to obtain

$$R^{-1}\bar{P} = TS \text{ diag } (q_1, \ldots, q_n)\ S'T^{-1} \tag{5.129}$$

$$= TS \text{ diag } (q_1, \ldots, q_n)\ (TS)^{-1}$$

This implies that the eigenvalues of $R^{-1}\bar{P}$ are $q_1, \ldots, q_n$ and the eigenvectors of $R^{-1}\bar{P}$ are the columns of TS.

Useful information can be obtained about the structure of the solution to the control problem by examining the eigenvectors of the unitary transformation S which diagonalizes $\tilde{Q}$. Consider transformation of variables.

$$x = Ty \tag{5.130}$$

which transforms the quadratic form $x'\bar{Q}x$ into

$$y'T'\bar{Q}Ty = y'\tilde{Q}y.$$

The matrix Q can be expressed

$$\tilde{Q} = T'\bar{C}'Q_1\bar{C}T + [I - T^{-1}\bar{C}^*\bar{C}T]'T\bar{Q}_2T[I - T^{-1}\bar{C}^*\bar{C}T] \tag{5.131}$$

$$= H'Q_1H + [I - H^*H]'\ T'\bar{Q}_2T[I - H^*H]$$

where $H = \bar{C}T$ and $H^* = T^{-1}\bar{C}^*$ is a right inverse of H.

Note that $Hy = 0$ implies $Cx = 0$ so that the null space of C maps into the null space of H under the transformation defined by (5.130). Also observe that the range of $[I - H^*H]'$ is orthogonal to the null space of $[I - H^*H]$ and

the latter is precisely the range of H^*. If H^* happens to be the particular right inverse $H'(HH')^{-1}$ then the range of $[I - H^*H]'$ is orthogonal to the rnage of H' and is therefore precisely the null space of H. In this special case, then, the eigenvectors of $\tilde{Q}$ divide into two orthogonal groups. One of which contains vectors in the null space of H and the other with vectors in the range of H'.

The closed loop eigenvectors are, in fact, the eigenvectors of $\tilde{Q}$ transformed into the coordinate system of the x variables according to the transformation (5.130). Thus, the system eigenvectors are composed of two (non-orthogonal) groups, one of which consists of vectors in the null space of $\bar{C}$ and the other in the range of the matrix $TH' = TT'\bar{C}' = R^{-1}\bar{C}'$. Moreover, the eigenvectors of the first group are influenced only by the weighting matrix $\bar{Q}_2$ and the second group only by the weighting matrix Q_1.

With respect to the problem at hand, these observations mean that n-1 of the modes of the closed loop system will lie in the plane corresponding to ACE = 0 and an additional mode will be in the direction of $R^{-1}\bar{C}'$. Moreover, it is this last mode which regulates ACE to zero and the speed of this mode is controlled by the scalar paramter Q_1. The additional modes are "redistribution" modes which allow for the redistribution of generation to target which lies in the ACE = 0 plane. Moreover, the redistribution motion takes place within that plane, and the response times depend on the parameter matrix $\bar{Q}_2$.

This advantageous choice of H^* is achieved by specifying $\bar{C}^*$ so that

$$T^{-1}\bar{C}^* = H^* = H'(HH')^{-1} \tag{5.132}$$

or

$$\bar{C}^* = T(T'\bar{C}')(\bar{C}TT'\bar{C}')^{-1} = R^{-1}\bar{C}'(\bar{C}R^{-1}\bar{C}')^{-1}.$$

$\bar{C}^*$ is clearly a right inverse of $\bar{C}$.

With R and $\bar{Q}$ positive definite $q_i^2 > 0$ for i = 1, ..., n and consequently all of the eigenvalues of $R^{-1}\bar{P}$ are real and positive. Thus, the closed loop is stable and all of the responses are non-oscillatory. Additional quantitative information can be obtained. Consider the scaler function of the vector u

$$\rho(u) = \frac{u'\tilde{Q}u}{u'u}$$

If $u = u_i$ is an eigenvector of $\tilde{Q}$, and since $\tilde{Q}$ is self adjoint, then $\rho(u_i) = q_i^2$, the corresponding eigenvalue. Furthermore, $\rho(u)$ has a stationary value whenever u is an eigenvector u_i.

Since H' is an eigenvector of $\tilde{Q}$, say u_1, it follows that

$$q_1^2 = \rho(u_i) = \frac{\tilde{HQH'}}{HH'} = \frac{HH'Q_1HH'}{HH'} = Q_1\bar{C}R^{-1}\bar{C}' \tag{5.133}$$

Suppose

$$R = \text{diag}\left(\frac{1}{U_1^2}, \ldots, \frac{1}{U_n^2}\right), \tag{5.134}$$

then,

$$q_1^2 = Q_1 \sum_1^n U_i^2 \tag{5.135}$$

and

$$q_1 = \sqrt{Q_1}\sqrt{\sum_1^n U_i^2} \tag{5.136}$$

5.3.2 Suboptimal Regulator Design

The previous subsection described the characterization of the ultimate state and control trajectories, and the solution of the quadratic regulator problem which resulted in an nxm feedback gain matrix $R^{-1}\bar{P}$ that shapes the transient response of deviations about these ultimate state trajectories. The detailed analysis of the closed-loop eigensystem provides considerable insight into the nature of the closed-loop response in relation to the separation of quadratic state variation costs corresponding to the primary and secondary tracking objectives. The same ideas were discussed in the process of the feedback regulator design for Coordinating Controller One in Section 5.2.2, and additional insight was obtained there by using the simple transformation introduced in (5.17). Then in Section 5.2.3 this transformation was utilized in developing a simplified regulator design which has significant advantages from an implementation point of view. All of those results, developed ostensibly in Sections 5.2.2 and 5.2.3 for Coordinating Controller One, are directly applicable to the second controller structure provided the integral state is simply deleted where necessary. The special case of interest here is, again that in which the n-1 secondary tracking modes have a common eigenvalue; it corresponds to a solution of the Ricatti equation which can be obtained analytically, and this allows gains to be updated very easily when the set of regulating units changes. For this special case the feedback gain matrix $R^{-1}\bar{P}$ has the form

$$R^{-1}\bar{P} = \begin{bmatrix} g+g_1 & g_1 & g_1 & \cdots & g_1 \\ g_2 & g+g_2 & g_2 & \cdots & g_2 \\ \cdot & \cdot & & & \\ \cdot & & \cdot & & \\ \cdot & & & \cdot & \\ g_n & g_n & \cdots & & g+g_n \end{bmatrix} \tag{5.137}$$

With this feedback gain matrix the closed-loop system has the form illustrated in Figure 5.34. The issue of state interpretation again arises and in Figure 5.34 the unit 60 Hz mechanical power outputs are considered to be the states to be fed back. Also, the star component of $\bar{u}$, $u^* - \gamma u_T^*$ from Equation 5.111, has been moved through the controller integrators in Figure 5.34. Thus the Dynamic Dispatch trajectories x^* (these were labeled P^* in the Coordinating Controller One section, 5.2) need not be differentiated. Now for Coordinating Controller One a mixed interpretation of state in the regulator design was ultimately employed; that is, for the feedback controls

$$\Delta u_i = -g\Delta x_i - g_i \Delta x_T \tag{5.138}$$

the first term was interpreted as a unit MW reference input while the second term was interpreted as the total area 60 Hz mechanical power output. Among other things, this choice was found to provide more control over the stability margins as the parameters of the assumed unit model(s) were varied. Whether or not the same interpretation is preferable for Coordinating Controller Two has not yet been determined, but this is mentioned here because the latter (mixed) interpretation yields the structure which is illustrated in Figure 2 of the Allerton Conference paper contained in Appendix A of this report. In the remainder of this section the interpretation that just unit outputs are fed back, as in Figure 3.34, will be used however.

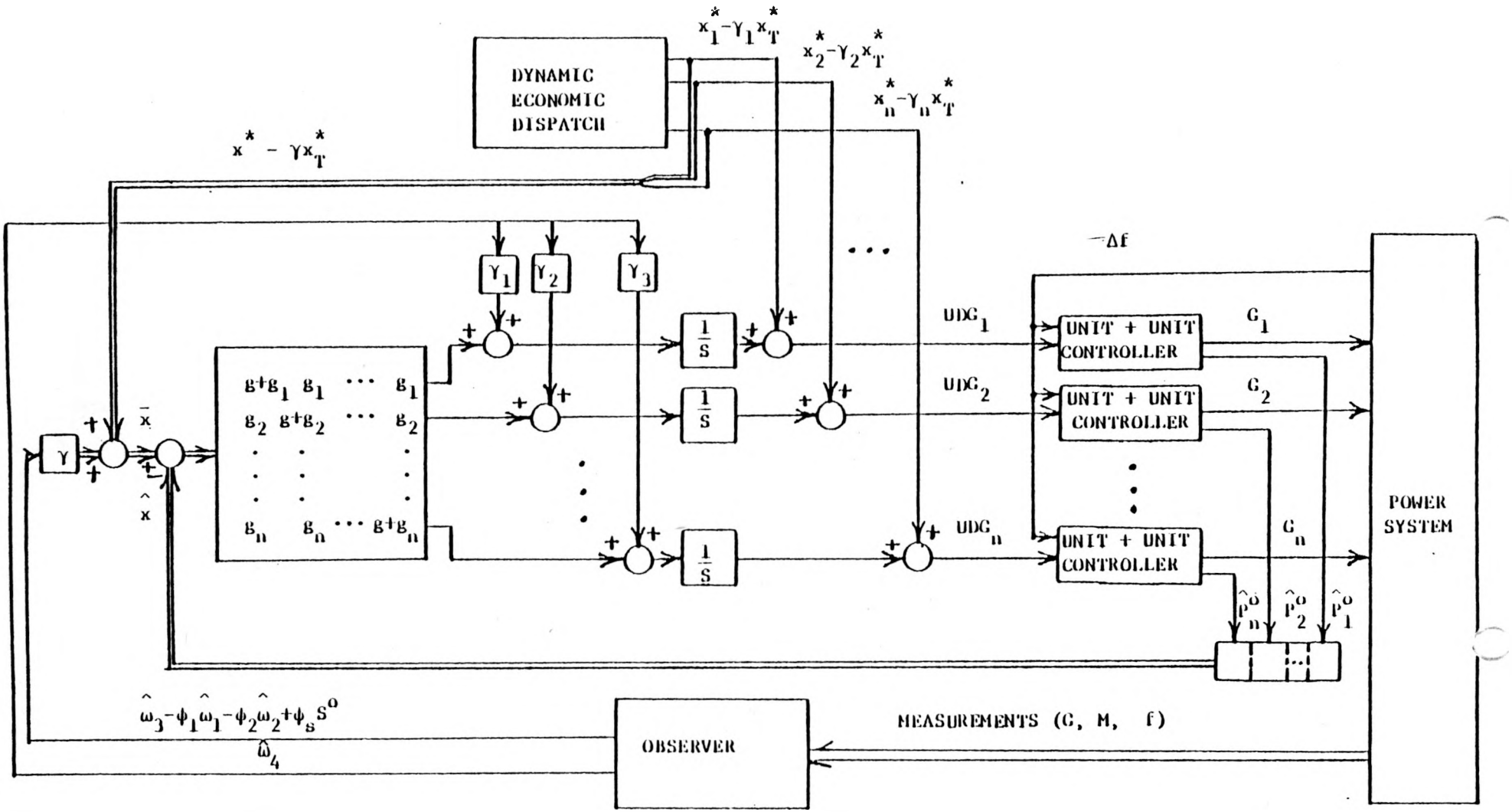

FIGURE 5.34 CLOSED LOOP SYSTEM

5.3.3 Observer Design

It is necessary to design an observer for the variables $x_1, x_2, \ldots x_{n+1}, \omega_1, \omega_2, \omega_3$ and ω_4 which are required for the feedback control law of Coordinating Controller Two to be implemented. If unit MW reference inputs are interpreted as states in the regulator design then $x_1, x_2, \ldots x_n$ are generated by the control computer and this results in a simplification of the observer design. If unit outputs are interpreted as states, then $\omega_1, \omega_2, \ldots \omega_n$ correspond to unit 60 Hz mechanical power outputs. For the latter case the relevant material in Section 5.2.5 is applicable, and it will be assumed without further comment that estimates generated by the unit controller filters will be used as required. As an aside, it is mentioned that the non-linear frequency bias idea has not been investigated in the context of the second Coordination Controller structure, however, and hence such an extension, which at least initially appears to be more complicated for Coordinating Controller Two, will not be considered. At any rate, for either case of the regulator-state interpretation, it is necessary at this point to generate estimates only of $x_{n+1}, \omega_1, \omega_2, \omega_3$ and ω_4.

Treating for the moment $y_4 = \sum_{i}^{n} x_i$ as a known input, the system model equations can be written:

$$\dot{x}_{n+1} = (-\beta/H)\, x_{n+1} + \left[0 - \frac{\beta}{H\beta_1} - \frac{1}{H} \quad 0\right] \omega + (1/H) y_4 \qquad (5.139)$$

$$\dot{\omega}_1 = \nu_1$$

$$\dot{\omega}_2 = \nu_2$$

$$\dot{\omega}_3 = \omega_4 + \nu_3$$

$$\dot{\omega}_4 = \nu_4$$

$$y_1 = x_{n+1} + \omega_1 \tag{5.140}$$

$$y_2 = \beta_2/\beta\ (y_4 - \omega_3) + \omega_2$$

$$y_3 = D_1(x_{n+1} + \omega_1) + \omega_3$$

Project consultant H.G. Kwatny applied the methodology described in [5.12] to the above formulation and an analytic solution was obtained. It was found to be convenient to reorder the equation (5.139) by defining

$$W^T \triangleq (\omega_4, \omega_3, \omega_2, \omega_1), \quad \eta^T \triangleq (\nu_4, \nu_3, \nu_2, \nu_1) \tag{5.141}$$

so that (5.139) and (5.140) become, in terms of the new variables in (5.141)

$$\begin{bmatrix} \dot{x}_{n+1} \\ W \end{bmatrix} = A_1 \begin{bmatrix} x_{n+1} \\ W \end{bmatrix} + B_1 y_4 + G\eta \tag{5.142}$$

$$\begin{bmatrix} y_1 \\ y_2 \\ y_3 \end{bmatrix} = H \begin{bmatrix} x_{n+1} \\ W \end{bmatrix} + Dy_4 \tag{5.143}$$

The construction of the observer design matrices H^*, Λ and θ_2 is straightforward but somewhat involved and as a result the details are omitted. The solution is

$$\begin{bmatrix} \hat{\chi}_{n+1} \\ \hat{W}_1 \\ \hat{W}_2 \\ \hat{W}_3 \\ \hat{W}_4 \end{bmatrix} \underbrace{\begin{bmatrix} -\phi H/\beta & 0 & 0 \\ -\phi D_1 & 0 & \phi \\ -D_1 & 0 & 1 \\ -D_1\beta_2/\beta & 1 & \beta_2/\beta \\ 1+\phi H/\beta & 0 & 0 \end{bmatrix}}_{H^*} \begin{bmatrix} y_1 \\ y_2 \\ y_3 \end{bmatrix} - \underbrace{\begin{bmatrix} 0 \\ 0 \\ 0 \\ \beta_2/\beta \\ 0 \end{bmatrix}}_{H^*D} y_4 + \underbrace{\begin{bmatrix} 1 & 0 \\ 0 & 1 \\ 0 & 0 \\ 0 & 0 \\ -1 & 0 \end{bmatrix}}_{\theta_2} \begin{bmatrix} \xi_1 \\ \xi_2 \end{bmatrix} \tag{5.144}$$

$$\frac{d}{dt} \begin{bmatrix} \xi_1 \\ \xi_2 \end{bmatrix} = \underbrace{\begin{bmatrix} -\phi & \\ & -\phi \end{bmatrix}}_{\Lambda A_1\theta_2} \begin{bmatrix} \xi_1 \\ \xi_2 \end{bmatrix} + \underbrace{\begin{bmatrix} \phi/\beta \\ 0 \end{bmatrix}}_{\Lambda B_1} y_4 + \underbrace{\left[\begin{array}{cc|c|cc|c} -\phi & 0 & -\phi/\beta & -\phi/\beta_1 & 0 \\ 0 & -\phi & 0 & 0 & 0 \end{array}\right]}_{\Lambda A_1} \left\{ H^*y - \underbrace{\begin{bmatrix} 0 \\ 0 \\ 0 \\ \beta_2/\beta \\ 0 \end{bmatrix}}_{H^*D} y_4 \right\} \tag{5.145}$$

where the eigenvalue $-\phi$ was doubly assigned to this second order observer. Equations (5.144) and (5.145) can be put in transfer function form; the result, in terms of the original variables of (5.139) is given below. The expression for $\hat{x}_{n+1}$ is not given because it is not explicitly used in the feedback design due to the fact that the frequency mode was appropriately made unobservable in the cost functional of the regulator design step.

$$\hat{\omega}_1 = \left[\frac{s(\phi^{-1}+H/\beta)+1}{s\phi^{-1}+1}\right] y_1 + \frac{1}{\beta_1} \cdot \frac{1}{(s\phi^{-1}+1)} \left[(-D_1y_1+y_3)+y_2-y_4\right] \tag{5.146}$$

$$\hat{\omega}_2 = y_2 + \beta_2/\beta\ (-D_1y_1+y_3) - \beta_2/\beta \cdot y_4$$

$$\hat{\omega}_3 = (-D_1y_1 + y_3)$$

$$\hat{\omega}_4 = \frac{s}{s\phi^{-1}+1} \quad (-D_1 y_1 + y_3)$$

5.3.4 Analytical Results

Summing up equations (5.110), the total ultimate state trajectory $\bar{x}_T$ is

$$\bar{x}_T = \hat{\omega}_3 - \phi_1\hat{\omega}_1 - \phi_2\hat{\omega}_2 + \phi_s S^o \tag{5.147}$$

From (5.146),

$$\hat{\omega}_3 = y_3 - D_1 y_1 = G - M - D_1\Delta f \triangleq L_T^o \tag{5.148}$$

and using (5.148) and the disturbance estimates from (5.146), (5.147) can be put in the form

$$(s\phi^{-1}+1)\bar{x}_T = s\phi^{-1}\frac{\phi_1}{\beta_1}(L_T^o+S^o) - \phi_1[s(\phi^{-1}+\frac{H}{\beta})+1]y_1 - \frac{\phi_1}{B}[s\phi^{-1}(\beta_1-B)+1]y_2 \tag{5.149}$$

$$+ [s\phi^{-1}\phi_2\frac{\beta_2}{\beta}+1]y_4$$

The area control error ACE is however

$$ACE \triangleq y_2 + By_1 \tag{5.150}$$

and hence substituting ACE into (5.149) yields

$$(s\phi^{-1}+1)\bar{x}_T = s\phi^{-1}\frac{\phi_1}{\beta_1}(L_T^o+S^o) - s\phi_1(\phi^{-1}+\frac{H}{\beta}-\phi^{-1}\beta_1+\phi^{-1}B)y_1 \tag{5.151}$$

$$- \frac{\phi_1}{B}[s\phi^{-1}(\beta_1-B)+1]ACE + [s\phi^{-1}\phi_2\frac{\beta_2}{\beta}+1]y_4$$

Before proceeding, an approximate result can be simply obtained from (5.151) which is quite insightful. While several approaches are viable, the easiest is to first let the observer become very fast, so that in the limit $\phi^{-1} \to 0$ and (5.151 becomes

$$\bar{x}_T \approx -s\phi_1 \frac{H}{\beta} \cdot \Delta f - \frac{\phi_1}{B} \cdot ACE + P_T^o \tag{5.152}$$

where the physical variables represented by y_1 and y_4 have been substituted for clarity. Now with the exception of the derivative of system frequency, (5.152) is familiar in the context of conventional LFC structures because the desired generation referred to 60 Hz, $\bar{x}_T$, is just actual generation referred to 60 Hz minus the area control error

($\phi_1/B = \frac{\beta_1+\beta_2}{B+\beta_2}$ is 1.0 for all practical purposes). The derivative of system frequency term is a very interesting term entering into the ultimate total state trajectory however. Recall from Section 5.2.1 the definition of the area control error (mechanical) ACEM, which was derived from the basic LFC objectives previously, quite independently from the derivation leading up to (5.152). From that previous development it was found that

$$ACE = ACEM - H_1 \cdot s\Delta f \tag{5.153}$$

Substituting (5.153) into (5.152) yields

$$\bar{x}_T \approx -s\phi_1 (\frac{H}{\beta} - \frac{H_1}{B})\Delta f - \frac{\phi_1}{B} \cdot ACEM + P_T^o \tag{5.154}$$

and it is clear that the second control structure is effectively cancelling out the potentially destabilizing derivative of system frequency

component of ACE. It is again emphasized that this is a relatively high frequency component which may or may not have some significance in the context of a practical LFC bandwidth, but it is nonetheless very interesting that the second control structure, which is designed to drive ACE to zero in the steady state, attempts to climinate this component of ACE in a transient sense. Furthermore, while this property was intentionally (and exactly) provided for Coordinating Controller One as a consequence of the fact that a consistent, instantaneous area control error had to be defined, in this case it is an unanticipated consequence of the design methodology itself.

If the closed-loop system representation corresponding to the simplified regulator design which was illustrated in Figure 5.34 is reduced to the total response representation, and the relationship for $\bar{x}_T$ derived in (5.151) is used to relate the total ultimate state trajectory to the physical system outputs, then the block diagram form illustrated in Figure 5.35 results. For simplicity, the estimator for total 60 Hz mechanical power P_T^o is modeled in Figure 5.35 with a first order filter whose time constant is the same as that assigned to the two observer states in the previous subsection. This is a convenient representation for the closed-loop, total response system. For example, a return ratio can be defined by breaking the loop at the point of the ACE feedback and stability margins can be computed which are analogous to those obtained for the first controller structure previously. However, a problem was encountered in the analysis of this system which casts doubt on the original formulation and/or the succeeding steps which led to this compact representation, and this difficulty can be best demonstrated by deriving the closed loop transfer functions which relate ACE to the disturbance inputs. This derivation is lengthy but straightforward; the basic steps are summarized below.

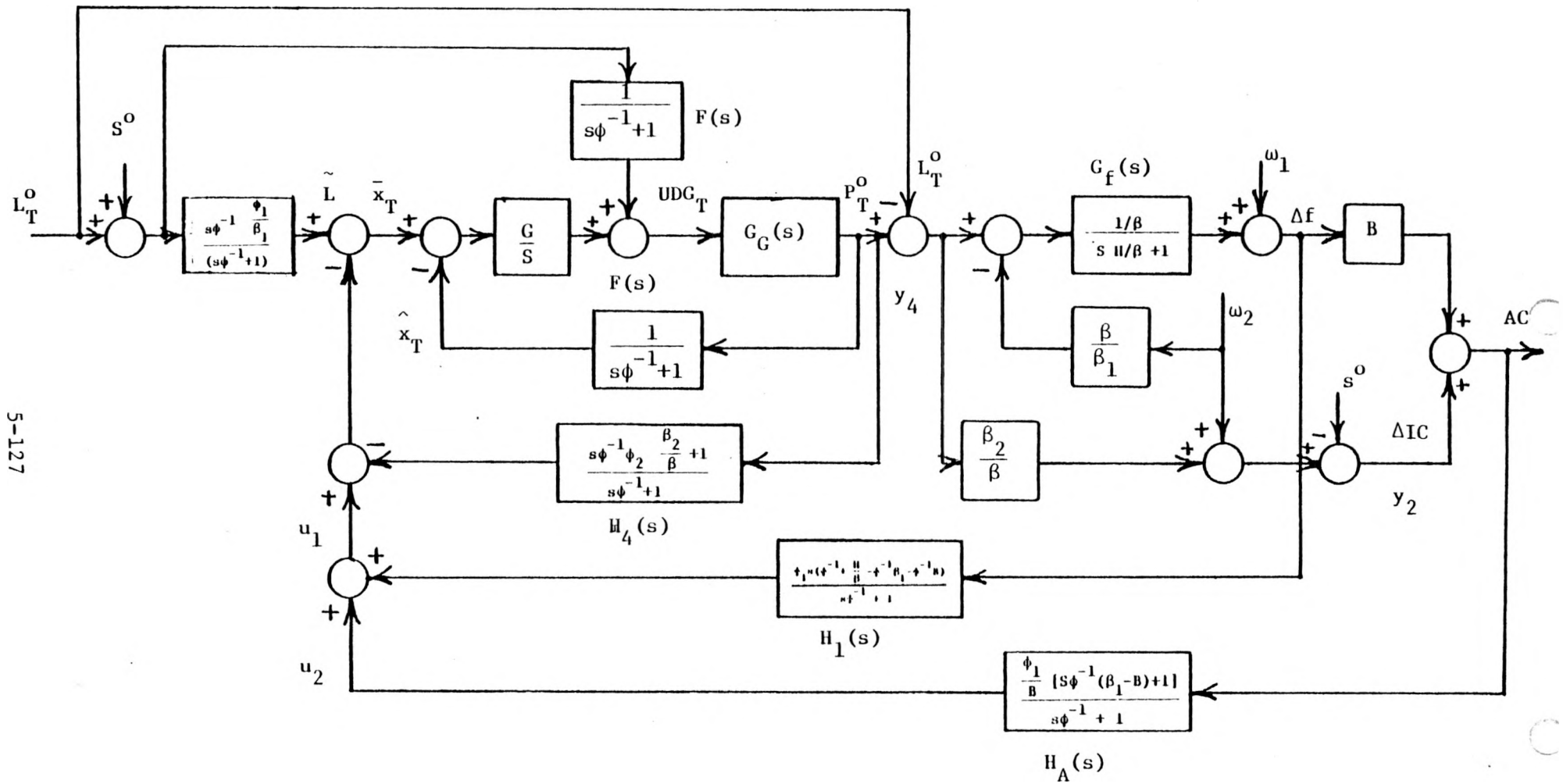

FIGURE 5.35 CLOSED LOOP TOTAL RESPONSE SYSTEM

From Figure 5.35,

$$P_T^o = G_G(s)[F(s)(L^o + S^o) + G/s\ (\bar{x}_T - F(s)P_T^o)] \tag{5.155}$$

where, referring to (5.137), $G \triangleq g + g_1 + g_2 + \ldots + g_n$, and $G_G(s)$ is the transfer function relating total area unit desired generation to total area 60 Hz mechanical power. It can be the same $G_G(s)$ used in the previous section for example. Now

$$\bar{x}_T = \tilde{L} - u_1 + H_4(s)\ P_T^o \tag{5.156}$$

and substituting (5.156) into (5.155) yields

$$P_T^o(1-G_G(s)\ G\ \phi^{-1}\phi_2\ \frac{\beta_2}{\beta} \cdot F(s)) = G_G(s)[(F(s) + \frac{G}{s} \cdot H_3(s))(L^o+S^o)-\frac{G}{s} \cdot u_1] \tag{5.157}$$

Also from Figure 5.35 we have that

$$\Delta f = \omega_1 + G_f(s)\ [P_T^o - L_T^o - \frac{\beta}{\beta_1}\ \omega_2], \tag{5.158}$$

and thus

$$u_1 = u_2 + H_1(s)\ [\omega_1 + G_f(s)(P_T^o - L_T^o - \frac{\beta}{\beta_1}\ \omega_2] \tag{5.159}$$

Substituting (5.159) into (5.151) and collecting terms,

$$[1-G_G(s)G\phi^{-1}\phi_2\ \frac{\beta_2}{\beta} \cdot F(s)+G_G(s)\ \frac{G}{s}\ H_1(s)G_f(s)]\ P_T^o = \tag{5.160}$$

$$G_G(s)[F(s)+\frac{G}{s}\ H_3(s)+\frac{G}{s}\ H_1(s) \cdot G_f(s)]L^o+G_G(s)[F(s)+\frac{G}{s} \cdot H_3(s)]s^o$$

$$- G_G(s)\ \frac{G}{s}\ H_1(s)\omega_1 + G_G(s)\ \frac{G}{s} \cdot H_1(s)G_f(s)\omega_2-G_G(s)\ \frac{G}{s} \cdot u_2$$

But ACE is given by

$$ACE = \left(\frac{\beta_2}{\beta} + BG_f(s)\right)(P_T^o - L_T^o) + \left(1 - BG_f(s)\,\frac{\beta}{\beta_1}\right)_2 - S^o \qquad (5.161)$$

so

$$P_T^o = \left(\frac{\beta_2}{\beta} + BG_f(s)\right)^{-1}\,[ACE - (1-B\cdot G_f(s)\,\frac{\beta}{\beta_2})\omega_2 + S^o] + L^o \qquad (5.162)$$

Substituting (5.162) into (5.160), using $u_2 = H_A(s)\,ACE$ and collecting terms,

$$\begin{aligned}
&[N(s) + \left(\frac{\beta_2}{\beta} + BG_f(s)\right)G_G(s)H_A(s)\,\frac{G}{s}]\,ACE \qquad (5.163)\\
&= \left(\frac{\beta_2}{\beta} + BG_f(s)\right)[G_G(s)(F(s) + \frac{G}{s}\cdot H_3(s) + \frac{G}{s}\,H_1(s)\cdot G_f(s)) - N(s)]L_o\\
&+ [\left(\frac{\beta_2}{\beta} + BG_f(s)\right)G_G(s)(F(s) + \frac{G}{s}\cdot H_3(s)) - N(s)]S^o\\
&- \left(\frac{\beta_2}{\beta} + BG_f(s)\right)G_G(s)\,\frac{G}{s}\cdot H_1(s)\,\omega_1\\
&+ [\left(\frac{\beta_2}{\beta} + BG_f(s)\right)\,\frac{G}{s}\cdot H_1(s)G_f(s) + (1-BG_f(s)\,\frac{\beta}{\beta_1})N(s)]\omega_2,
\end{aligned}$$

where

$$N(s) \triangleq [1 - G_G(s)\cdot G\cdot F(s)\,\phi^{-1}\phi_2\,\frac{\beta_2}{\beta} + G_G(s)\,\frac{G}{s}\,H_1(s)\cdot G_f(s)] \qquad (5.164)$$

It is necessary to reduce the rational functions on each side of (5.163) to polynomials in s, i.e. to clear the denominators. Thus, referring to Figure 5.35, a symbol is assigned to the numerator and denominator of each transfer function:

$$H_1(s) \triangleq \frac{n_1(s)}{d_F(s)} \qquad (5.165)$$

$$H_3(s) \triangleq \frac{n_3(s)}{d_F(s)}$$

$$H_4(s) \triangleq \frac{n_4(s)}{d_F(s)}$$

$$H_A(s) \triangleq \frac{n_A(s)}{d_F(s)}$$

$$G_G(s) \triangleq \frac{1}{d_G(s)}$$

$$G_f(s) \triangleq \frac{1}{d_f(s)}$$

After substituting (5.165) into (5.163) the denominators of (5.163) can be cleared by formally multiplying through by $d_G(s)d_f^2(s)d_F(s)s$. Doing this and collecting terms and simplifying yields

(5.166)

$$d_f(s)[d_G(s)d_F(s)d_f(s)s - d_f(s)\cdot s\cdot G\phi^{-1}\phi_2 \frac{\beta_2}{\beta} + Gn_1(s) + \frac{\beta_2}{\beta} d_f(s)n_A(s)G + Bn_A(s)\cdot G]ACE$$

$$= s\cdot d_f(s)(\frac{\beta_2}{\beta}d_f(s)+B)(1+G\phi^{-1}\frac{\phi_1}{\beta_1} - d_G(s)d_F(s)+\phi^{-1}\phi_2 \frac{\beta_2}{\beta}\cdot G)L^o$$

$$+ d_f(s)(\frac{\beta_2}{\beta}d_f(s)\cdot s + \frac{\beta_2}{\beta} Gn_3(s)d_f(s) + s\cdot B + B\cdot Gn_3(s) - d_G(s)d_F(s)d_f(s)\cdot s -$$

$$\phi^{-1}\phi_2 \frac{\beta_2}{\beta} G\cdot s\cdot d_f(s) - Gn_1(s))S^o$$

$$- d_f(s)(\frac{\beta_2}{\beta} d_f(s)\, Gn_1(s) + BGn_1(s))\omega_1$$

$$+ [n_1(s)(\frac{\beta_2}{\beta} Gd_f(s) + BG + Gd_f(s) - BG\frac{\beta}{\beta_1}) + d_f^2(s)d_G(s)d_F(s)s$$

$$- \phi^{-1}\phi_2 \frac{\beta_2}{\beta} G\cdot s\cdot d_f^2(s) - B\frac{\beta}{\beta_\perp} d_G(s)d_F(s)d_f(s)\cdot s + B\frac{\beta_2}{\beta_1}\phi^{-1}\phi_2 Gd_f(s)\cdot s]\omega_2$$

The polynomial operating ACE in (5.166) is of course the closed loop characteristic polynomial for the system illustrated in Figure 5.35. Its order is as expected: 4 plus the order of $d_G(s)$ (recall that the observer is second order). We see that the system frequency mode has not been altered by the feedback controller, which is also correct due to the fact that system frequency was unobservable in the cost function used to determine the feedback law. Now $n_1(s)$ and $n_3(s)$ each have a single zero at the origin, and it is clear that reset of ACE is assured for unknown constant values of the disturbances S^o, ω_1 and ω_2, i.e., there is a type one relationship between ACE and each of these disturbances as expected. There is also a type one relationship between ACE and L^o however, and this contradicts the original problem formulation which was intended to assure a type two relationship between these variables. This surprising result appears to be in conflict with theoretically derived properties of the general design methodology used in the development of Coordinating Controller Two. It is felt that an explanation of this result is required in order to provide assurance that the second controller structure is indeed free of some subtle error.

5.4 COMPARATIVE EVALUATION

While the two Coordinating Controller structures developed in Task 2 share a number of common features, they were derived from two alternative design methodologies which can, in general, lead to significant differences in closed loop response and disturbance rejection characteristics. Because of this, the Task 2 plan for this component of the AGC algorithms was to develop each structure on a more or less equal basis and to make a preliminary comparative evaluation using the simplified design models. A more comprehensive and realistic evaluation would then be performed in

Task 3 using primarily the detailed AGC simulation program. Unfortunately, although the Coordinating Controller One prototype design has been completed and implemented in the AGC simulation program, the Coordinating Controller Two prototype has not been implemented due primarily to the unresolved technical issue described above. The current thinking is to continue with the original plan for comparative evaluation of the two coordinating controller designs during Task 3. This implies that implementation of the second structure must be accomplished during the first stage of Task 3. It is anticipated that an explanation of the noted anomoly will be forthcoming and the implementation can be easily accomplished in view of the fact that much of the work done on the first controller, particularly, in the areas of gain and parameter selection, is directly transferable. Thus, despite the fact that a number of interesting comparisons between the two structures can be made based on the work performed in Task 2, the comparative evaluation of the two Coordinating Controllers is deferred to Task 3.

REFERENCES FOR CHAPTER 5

5-1 N. Cohn, Control of Generation and Power Flow of Interconnected Systems, John Wiley and Sons, New York, 1966.

5-2 N. Cohn, "Some Aspects of Tie-Line Bias Control on Interconnected Power Systems", Trans. AIEE (Power Apparatus and Systems), Vol. 75, 00 1415-1428, February, 1957.

5-3 L.H. Fink, "Concerning Power System Control Structure", Advances in Instrumentation, ISA, Vol. 26, Part 1, 1971.

5-4 D.N. Ewart, "Automatic Generation Control - Performance Under Normal Conditions", Final Report for ERDA Contract E(49-18)-2147.

5-5 J.C. Russel and W.P. Rades, "The Wisconsin Electric Power Company Energy Control System", Proc. 1973 PICA Conference, Minneapolis, Minnesota, pp. 135-141, June 4-6, 1973.

5-6 C.E. Fosha and O.J. Elgerd, "The Megawatt - Frequency Control Problem: A New Approach Via Optimal Control Theory", IEEE Transactions, Vol. PAS-89, pp 563-578, April, 1970.

5-7 M.S. Calovic, "Linear Regulator Design for a Load and Frequency Control", IEEE Transactions, Vol. PAS-91, No. 6, pp 2271-2285, 1972.

5-8 H.G. Kwatny, K.G. Kalnitsky and A. Bhatt, "An Optimal Tracking Approach to Load-Frequency Control", IEEE Transaction, Vol. PAS-94, No. 5, pp 1635-1643, 1975.

5-9 H.G. Kwatny, "Optimal Linear Control Theory and a Class of PI Controllers for Process Control", Proceedings 13th JACC, pp 274-281, 1972.

5-10 E.J. Davidson, "The Output Control of Linear Time-Invariant Multi-variable Systems with Unmeasurable Arbitrary Disturbances", IEEE Transactions, Vol. AC-17, pp 621-629, 1972.

5-11 C.W. Taylor and R.L. Cresap, "Real-Time Power System Simulation for Automatic Generation Control", presented at the IEEE PES Summer Meeting, San Francisco, CA, 1975.

5-12 H.G. Kwatny, "Minimal Order Observors and Certain Singular Problems of Optimal Estimation and Control", IEEE Transactions, Vol. AC-19, No. 3, pp 274-276, 1974.

5-13 C.W. Ross, "Error Adaptive Control Computer for Interconnected Power Systems", IEEE Transactions on Power Apparatus and Systems, Vol PAS-85, pp 742-749, 1966.

5-14 K.Y. Lee, D.P. Dave, and C.W. Taylor, "Automatic Generation Control Analysis with Aggregate Governor Deadband Effects", presented at the IEEE PES Summer Meeting, Los Angeles, CA., 1978.

5-15 Current Operational Problems Working Group, "Current Operating Problems Associated with Automatic Generation Control", presented at the IEEE/ASME/ASCE Joint Power Generation Conference, Los Angeles, CA., September 18-21, 1977.

5-16 Applied Optimal Estimation, Arthur Gelb, editor, The M.I.T. Press, Cambridge, Massachusetts, 1974.

5-17 H.G. Kwatny and K.C. Kalnitsky, "On Alternative Methodologies for the Design of Robust Linear Multivariable Regulators", IEEE Transactions on Automatic Control, Vol. AC-23, No. 5, October, 1978.

5-18 J.H. Wilkenson, The Algebraic Eigenvalue Problem, Clarendon Press, Oxford, 1965.

6. UNIT CONTROLLER

The unit controller portion of the overall AGC package functions as a servo control algorithm. A unit's power output demand is given to the unit controller which then determines the control signal necessary to move this unit's actual output to match demand. The controller's main design goal was to track changes in demand as closely as possible without excessive control activity. A secondary objective was to avoid undue upsets to the unit's internal process variables as a result of the tracking activity.

The principle design technique employed was the Linear Quadratic Gaussian (LQG) method of modern state space control. In addition, various logic strategies involving hard constraints on selected variables and rates are also included in the final design. The material that follows describes the design procedure and the rationale for the procedure. An example using WEPCO Units demonstrates the controller's closed loop response and the robustness of the design.

6.1 MODEL

A model to serve as the basis for design was derived from the detailed unit model presented in the AGC proposal. Figure 6.1 is a block diagram of the simplified, physically based model. The features of this model are:

- Linearized throttle pressure/steam flow relationship
- Two dynamic physical states for the boiler, the drum and the fuel system

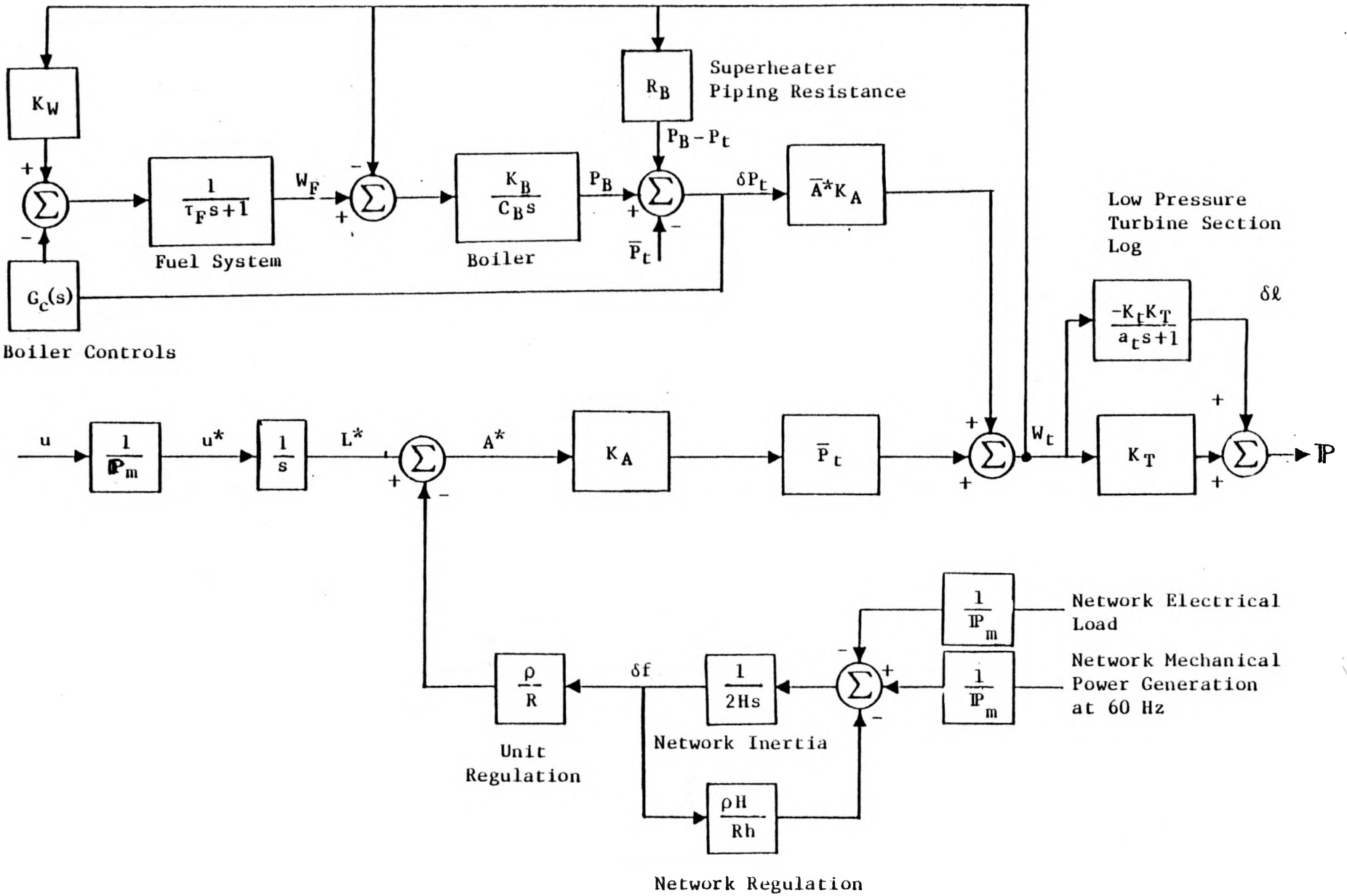

FIGURE 6.1 PHYSICALLY BASED, LINEARIZED UNIT MODEL

Figure 6.1 (Continued)

PROCESS VARIABLES

A^*	turbine valve opening, % of full open
a_t	time lag of the low pressure section of the turbine's power output, sec
δf	frequency deviation, Hz
L^*	generation demand, % of maximum unit rating
$\delta \ell$	lagging part of the turbine power output, MW
P_B	boiler drum pressure, psi
P_t	throttle pressure, psi
$\bar{P}_t$	throttle pressure at linearized operating point, psi
δP_t	throttle pressure deviation from linearized operating point, psi
$\mathbb{P}$	mechanical power output, MW
u	generation rate of change demand, MW/sec
u^*	generation rate of change demand, % of maximum unit rating/sec
W_F	boiler steam generation mass flow rate, lbm/sec
W_t	turbine first stage steam flow rate, lbm/sec

PARAMETERS

$\bar{A}^*$	turbine valve opening at linearized operating point, %
C_B	boiler time constant (drum & superheaters), sec
$G_c(s)$	boiler control transfer function, lbm/sec·psi
H	interconnected system inertia, $\frac{\%\text{ of maximum network rating} \cdot \text{sec}}{\text{Hz}}$

Figure 6.1 (Continued)

PARAMETERS (Continued)

h	unit inertia
K_A	turbine valve gain, lbm/% full open · sec · psi
K_B	boiler gain, psi · sec/lbm
K_W	switch for steam flow feed forward, dimensionless
K_T	turbine gain, MW · sec/lbm
K_t	low pressure section of the turbine's output as a fraction of total output, dimensionless
P_m	unit power rating, MW
R	regulation constant, Hz/% of maximum unit rating
R_B	superheater piping resistance, psi · sec/lbm
s	Laplace operator, 1/sec
ρ	attenuation factor on the regulation constant, dimensionless
τ_F	fuel system time constant (first order lag + transport delay), sec

- Turbine lags neglected because they are much faster than the boiler dynamics
- A simplified representation of the network frequency regulation dynamics (one state)

Boiler response is the principle dynamic element of this model that affects the AGC demand tracking objective. The influence of the boiler occurs through the variation in throttle pressure when changes in unit output are demanded. Changing throttle pressure causes a variation in turbine steam flow and hence unit power output for a constant turbine valve opening.

PID characterization of the boiler control transfer function yields

$$G_s(S) = K_p + \frac{K_I}{s} + K_d s \tag{6.1}$$

Then, with K_W representing the presence or absence (1.0 or 0.0) of steam flow feedforward, the transfer function between valve position and steam flow is

$$\frac{\delta W_t}{\delta A} = \frac{K_A \bar{P}_t \left[\tau_F C_B \frac{\bar{P}_t}{\bar{P}_B} s^3 + \left(C_B \frac{\bar{P}_t}{\bar{P}_B} + K_d \right) s^2 + K_p s + K_I \right]}{\bar{A}^* \left[\tau_F C_B s^3 + \left(C_B + \tau_F + K_d \right) s^2 + \left(K_p - K_w + 1 \right) s + K_I \right] + (1 - \bar{A}^*) \left[\tau_F C_B \frac{\bar{P}_t}{\bar{P}_B} s^3 + \left(C_B \frac{\bar{P}_t}{\bar{P}_B} + K_d \right) s^2 + K_p s + K_I \right]} \tag{6.2}$$

For design purposes, the following assumptions are made.

1. K_I is small and may be neglected
2. K_w is 1.0 or K_p is large relative to 1.0 so that $\frac{K_p}{K_p + (1 - K_w)}$ is nearly unity
3. $\bar{A}^*$ is the full open valve position and therefore equals 1.0

4. $\frac{\bar{P}_B^*}{\bar{P}_t^*}$ is at 100% load

5. Only first order dynamics are considered

Therefore, the model reduces to

$$\frac{\delta W_t^*}{\delta A^*} = \frac{\frac{1}{K_p}\left(C_B \frac{\bar{P}_B}{\bar{P}_t} + K_d\right)s + 1}{\frac{1}{K_p}\left(C_B + \tau_F + K_d\right)s + 1} \tag{6.3}$$

where the * refers to normalized values (δW_t and δA vary between zero and one). Figure 6.2 shows the comparison between a first order model and a critically damped second order model ($K_I = 0$) for a step change in valve postion. The first order is an acceptable representation provided the closed loop controller's frequency response range is designed slow enough to not interact with the higher frequency response states of the real unit. Note that the effective time constant in the denominator of Equation (6.3) could also be calculated from the s^3 term of Equation (6.2) for a critically damped second order response. Therefore, for the design model the time constant, a_1, in the demoninator of Equation (6.3) is calculated as

$$a_1 = \text{the larger of} \begin{cases} \frac{1}{K_p}\left(C_B + \tau_F + K_d\right) \\ \text{OR} \\ 2\left(\frac{\tau_F C_B}{K_p}\right)^{1/2} \end{cases} \tag{6.4}$$

Since the control objective centers around following power demand at 60 Hz and <u>not</u> the unit's response to frequency deviation, the

First Order $\quad \frac{\delta W_t^*}{\delta A} = \frac{\tau s+1}{2\tau s+1}$

Second Order $\quad \frac{\delta W_t^*}{\delta A} = \frac{0.8\tau^2 s^2 + \tau s+1}{\tau^2 s^2+2\tau s + 1}$

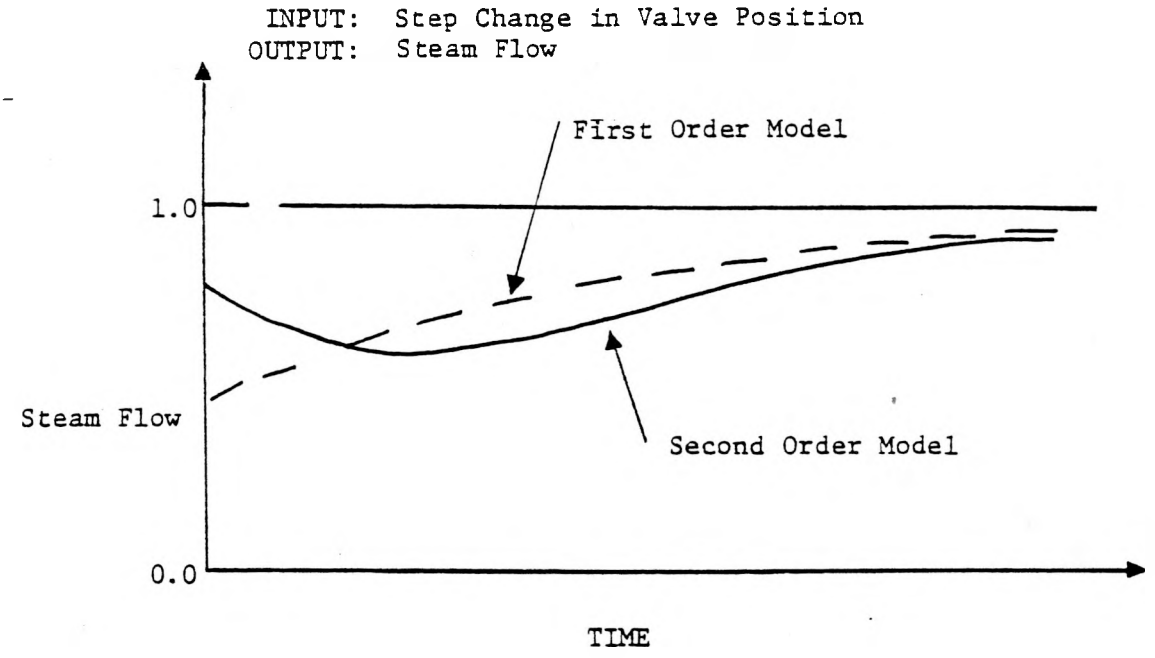

FIGURE 6.2 UNIT MODEL RESPONSE COMPARISON

model construct of Figure 6.3 must be employed for design. This model enables the unit controller to separate unit power into that portion due to frequency regulation, P_f, and that part that would be the unit's output at 60 Hz, P_{60}.

Since the typical time constants associated with frequency regulation are fast (i.e., under 20 seconds) the boiler dynamics (time constants of 90 to 180 seconds) are not incorporated into the P_f model. Also, for the same reason of differences in time scale, only the slow boiler/fuel system dynamics are included in the P_{60} model and not the fast turbine dynamics. These model simplifications considerably reduce the amount of real-time compuation necessary to operate the unit controller algorithm. Examples of the controller operating with a more complex model than used for the design show well behaved closed loop response.

A useful device for the unit design model involves normalizing state variables. Normalized variagles are:

δf^* = $\delta f/R'$ frequency deviation, % of effective regulation range

u^* = demand rate of change, % of maximum unit rating per minute

δP_t^* = throttle pressure deviation, % of full pressure

$\delta \ell^*$ = low pressure turbine section lag, % of maximum unit rating

Using these variables, the state equations are:

$$\frac{d}{dt}\begin{bmatrix} \delta\ell^* \\ \delta f^* \\ A^* \\ \delta P_t \end{bmatrix} = \begin{bmatrix} -\frac{1}{a_t} & \frac{k_t}{2R'h} & 0 & 0 \\ & -\frac{1}{2R'h} & 0 & 0 \\ 0 & 0 & 0 & 0 \\ 0 & 0 & 0 & -\frac{1}{a_1} \end{bmatrix} \begin{bmatrix} \delta\ell^* \\ \delta f^* \\ A^* \\ \delta P_t \end{bmatrix} \begin{bmatrix} 0 \\ 0 \\ m \\ -K_1 m \end{bmatrix} u^* \quad (6.5)$$

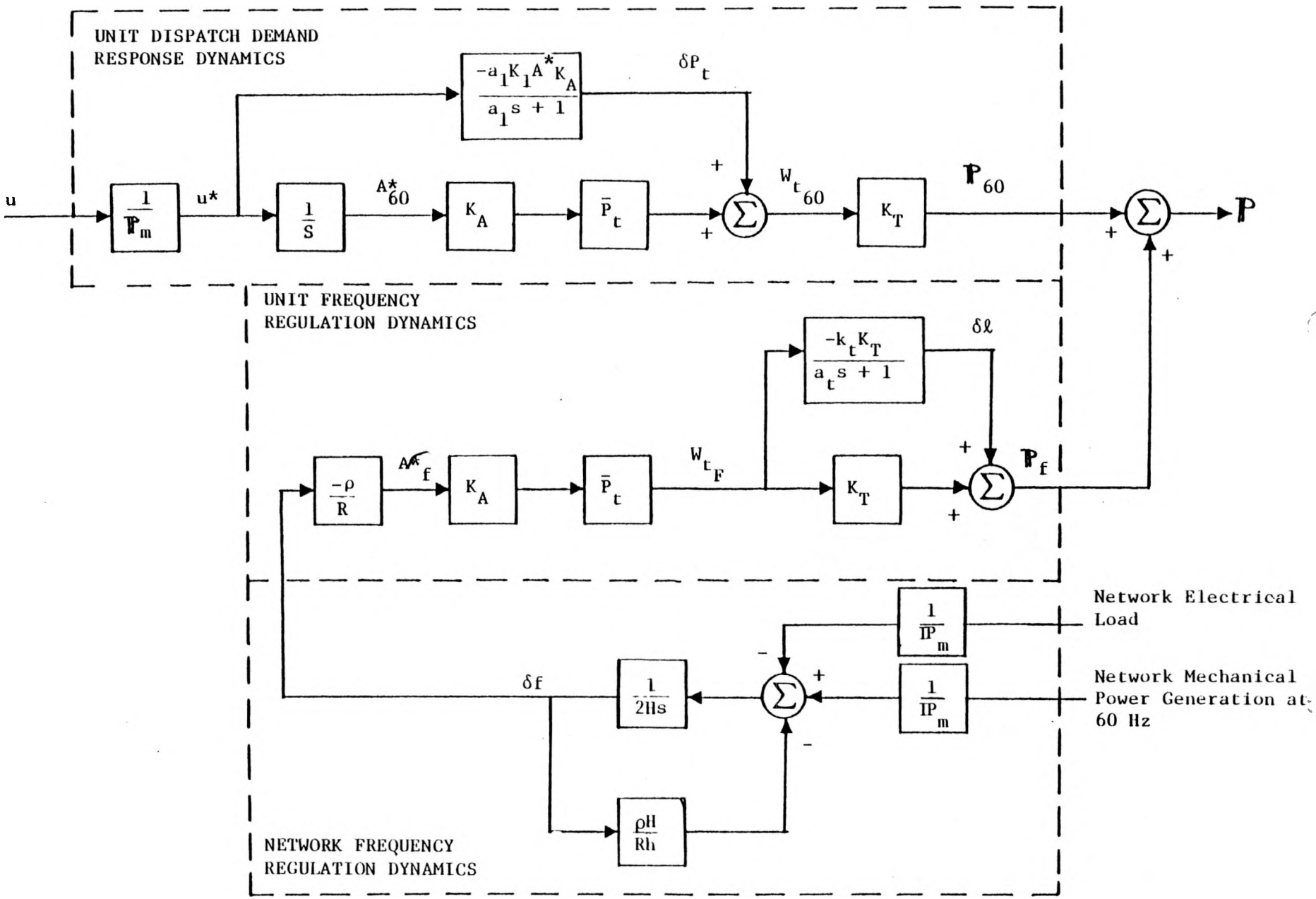

FIGURE 6.3 CONTROLLER DESIGN MODEL

The boiler/fuel system time constant, a_1, is defined in Equation (6.4). The other new parameters are defined as follows:

$$R' = \frac{R}{\rho} = \text{effective network regulation factor after accounting for such things as dead-bands} \tag{6.6}$$

$$1 - \frac{C_B \frac{\bar{P}_B}{\bar{P}_t} + K_d}{C_B + \tau_F + K_d} \tag{6.7}$$

Measurement variables that are not states that could be available include:

$$P_e^* = \mathbb{P}_{60} + \mathbb{P}_f - 2hR' \frac{d\delta f^*}{dt} \tag{6.8}$$

(Gross electrical power, % of maximum unit output)

$$W_t^* = W_{t_{60}}^* + W_f^* \tag{6.9}$$

(First stage steam flow, % of maximum)

6.2 CONTROLLER

Designing the controller amounts to using the model specified by Equations (6.5) and (6.8) in conjunction with appropriate performance index weights in a Linear-Quadradic-Gaussian design procedure. One minor modification to the model involves adding an integral state to give type 1 control response. The state equation is:

$$\frac{d}{dt} \int \delta P_{60}^* = A^* + \delta P^* - d^* \tag{6.10}$$

where d* is the desired unit 60 Hz power output as a percent of maximum unit output.

Gains are calculated by using the Steady State Linear Analysis Package (SLAP program). The program requires the following system equations as input.

$$\frac{d\underline{x}}{dt} = \underline{A}\,\underline{x} + \underline{B}\,\underline{u} + \underline{E}\,\underline{w} \tag{6.11}$$

$$\underline{y} = \underline{C}\,\underline{x} + \underline{D}\,\underline{u} + \underline{v} \tag{6.12}$$

Also required are the controller cost functional weightings;

$\underline{q}x$ = weightings on the states

$\underline{q}y$ = weightings on the measurements

$\underline{q}u$ = weightings on the control

and the noise statistics for the process noise sources, $\underline{w}$, and measurement noise sources, $\underline{v}$;

Expected Value $\{\underline{w}\,\underline{w}^T\} = \underline{Q}$ ($\underline{Q}$ may only have diagonal elements)

Expected Value $\{\underline{v}\,\underline{v}^T\} = \underline{R}$ ($\underline{R}$ may have only diagonal elements)

For the unit controller, various matrices in the above equations are detailed below. See previous memos for definition of terms

$\underline{x}$ = state variables $\begin{bmatrix} \ell_t^* \\ \delta f^* \\ A^* \\ \delta p_t^* \\ \int \delta P_{60}^* \end{bmatrix}$

$\underline{u}$ = control = u*

$\underline{w}$ = process noise = w_1 = unit process noise; w_2 = power network noise; w_3 = noise due to units pressure control system

$$\underline{A} = \begin{bmatrix} -\frac{1}{a_t} & \frac{K_t}{2R'h} & 0 & 0 & 0 \\ 0 & -\frac{1}{2R'h} & 0 & 0 & 0 \\ 0 & 0 & -\varepsilon & 0 & 0 \\ 0 & 0 & 0 & -\frac{1}{a_1} & 0 \\ 0 & 0 & 1 & 1 & -\varepsilon \end{bmatrix} \qquad \underline{B} = \begin{bmatrix} 0 \\ 0 \\ m \\ -K_1 m \\ 0 \end{bmatrix}$$

$$\underline{E} = \begin{bmatrix} 0 & \frac{-K_t}{2R'h} & 0 \\ 0 & \frac{1}{2R'h} & 0 \\ m & 0 & 0 \\ -K_1 m & 0 & -K_1 m \\ 0 & 0 & 0 \end{bmatrix}$$

$$\underline{y} = \text{measurements} \begin{bmatrix} \delta f^* \\ P_e^* \\ \delta \underline{p}_t^* \\ W_t^* \\ \mathbb{P}_{60}^* \end{bmatrix} \qquad \underline{v} = \begin{bmatrix} v_1 \\ v_2 \\ v_3 \\ v_4 \\ v_5 \end{bmatrix}$$

$$\underline{C} = \begin{bmatrix} 0 & 1 & 0 & 0 & 0 \\ 1 & 0 & 1 & 1 & 0 \\ 0 & 0 & 0 & 1 & 0 \\ 0 & -1 & 1 & 1 & 0 \\ 0 & 0 & 1 & 1 & 0 \end{bmatrix}$$

$\underline{D} = 0$

$$\underline{q}x = \begin{bmatrix} 0 & 0 & 0 & 0 & q_{\int \delta I P_{60}} \end{bmatrix}$$

$$\underline{q}y = \begin{bmatrix} 0 & 0 & q_{\delta p_t^*} & 0 & q_{I P_{60}} \end{bmatrix}$$

$\underline{q}u = q_u^*$

diagonal of $\underline{Q} = [q_1 \quad q_2 \quad q_3]$

diagonal of $\underline{R} = [r_1 \quad r_2 + q_2 \quad r_3 \quad r_4]$

The SLAP program produces the negative of controller gains, $-\underline{G}$, and Kalman Filter gains, $\underline{K}'$. The actual filter gains used, $\underline{K}$, have to be calculated as shown on the next page.

$$\underline{G} = [0 \quad 0 \quad g_1 \quad g_2 \quad g_3] \qquad \underline{K} = \underline{K}' + \frac{1}{1+\frac{r_2}{q_2}} \begin{bmatrix} 0 & \frac{K_t}{2hR'} & 0 & 0 & 0 \\ 0 & -\frac{1}{2hR'} & 0 & 0 & 0 \\ 0 & 0 & 0 & 0 & 0 \\ 0 & 0 & 0 & 0 & 0 \\ 0 & 0 & 0 & 0 & 0 \end{bmatrix}$$

The controller is implemented as

$$\tilde{u}^* = \underline{G}\,(\hat{\underline{x}} - \underline{H}d) \tag{6.13}$$

where $\tilde{u}^*$ is the continuous control, $\tilde{\underline{x}}$ are the state <u>estimates</u>, d is the 60 Hz power demand for the unit, and

$$\underline{H} = \begin{bmatrix} 0 \\ 0 \\ 1 \\ 0 \\ 0 \end{bmatrix}$$

The actual control applied, u*, is developed from $\tilde{u}^*$ after applying limits and discretization. The limits invoked include the following items.

1. Power Output - If the units total power output exceeds specified high or low limits, the control is set to zero unless the control is acting to move the unit away from the limit.

2. Rate of Change - Control action outside high or low rate of change limits is not allowed.

3. Throttle Pressure - If throttle pressure exceeds specified high or low limits, the control is set to zero unless the control is acting to move the pressure away from the limit.

Also, whenever the control has exceeded one of these limits, the power error integral state, $\int \delta P_{60}$, is frozen in order to prevent reset wind-up. Discretization of the control occurs after all limit checks. The discrete levels correspond to the available unit pulse widths that may be set.

6.3 KALMAN FILTER

The filter produces the state estimates, $\hat{\underline{x}}$. Since the LFC implementation is for discrete time steps, the filter requires two parts, the prediction and the correction. The prediction equations at step i are

$$\tilde{\underline{x}}_{i+1} = \underline{\Phi}\ \hat{\underline{x}}_i + \Psi \begin{bmatrix} u_i^* \\ d_i \end{bmatrix} \tag{6.14}$$

where

$$\underline{\Phi} = \text{exponential } \{\underline{A}\delta t\} \tag{6.15}$$

$$\Psi = -A^{-1}\ [\underline{I} - \underline{\Phi}]\ [\underline{B}\ \ \underline{F}] \tag{6.16}$$

δt = the time between steps

$\underline{F}$ = (a matrix needed to produce $\int \delta P_{60}$) $= \begin{bmatrix} 0 \\ 0 \\ 0 \\ 0 \\ -1 \end{bmatrix}$

The update equations at time step i+1 are

$$\hat{\underline{x}}_{i+1} = \tilde{\underline{x}}_{i+1} + \underline{K}_{\delta} \left[\underline{y} - \underline{C}\, \tilde{\underline{x}}_{i+1}\right] \tag{6.17}$$

where

$$\underline{K}_{\delta} = \delta t\, \underline{K} \left[\underline{I} + \delta t \underline{C}\, \underline{K}\right]^{-1} \tag{6.18}$$

6.4 RESULTS FOR THE WEPCO UNITS

Controller/filter designs for the WEPCO units have the following parameter values in common.

Cost Functional Weightings

$q_{\int \delta P_{60}}$	$(1/(1\%)(200\text{sec}))^2$	=	$0.25\ \text{sec}^{-2}$
$q_{\delta Pt}$	$(1/2.5\%)^2$	=	1600
$q_{P_{60}}$	$(1/1\%)^2$	=	10,000
qu*	$(1/3.33\%)^2$	=	900

Noise Statistics

q_1	$(50\%\ \text{min}^{-1})^2$	=	$0.25\ \text{min}^{-2}$
q_2	$(0.2\%)^2$	=	0.000004
q_3	$(25\%)^2$	=	0.0625
r_1	$(0.1\%)^2$	=	0.000001
r_2	$(1\%)^2$	=	0.0001
r_3	$(1\%)^2$	=	0.0001
r_4	$(2\%)^2$	=	0.0004
r_5	$(1000\%)^2$	=	100

(Note that measurement 5, 60 Hz power, is not a real measurement. It is only used in the controller gain design procedure. By setting a very high measurement noise $(1000\%)^2$, the Kalman Gains are effectively eliminated for this measurement).

Other Common Parameters

R	3.0 Hz/per unit output
ε	0.0001
2Rh	15 sec
K_d	0

Parameters unique to each unit are tabulated in Table 6.1. Table 6.2 lists the controller gains, $\underline{G}$, and Kalman filter gains, $\underline{K}$, that go into the unit control subroutine.

Figures 6.4 to 6.7 show the response of the unit controller design for WEPCO Unit 1. The response is to a step decrease in power demand from the unit. Note that the controller/filter represents a design based on the simplified, fifth order model. The results presented, however, are for the unit controller operating with the detailed, sixth order linearized unit model illustrated in Figure 6.1.

TABLE 6.1

WEPCO UNITS' PARAMETERS

Unit	1	2	3	4	5	6	7	8	9	10	11	12	13	14	15
τ_F, sec	60	60	60	60	90	90	90	90	60	60	60	60	60	60	60
$\frac{P_B}{P_t}$	1.08	1.08	1.08	1.08	1.08	1.08	1.08	1.08	1.08	1.08	1.08	1.08	1.08	1.08	1.08
C_B, sec	120	120	120	120	180	180	180	180	120	120	120	120	120	120	120
K_p	1	1	1	1	1	1	1	1	1	1					
a_1, sec	180	180	180	180	260	260	260	260	180	180	180	180	180	180	180
K_1	0.37	0.37	0.37	0.37	0.37	0.37	0.37	0.37	0.37	0.37	0.37	0.37	0.37	0.37	0.37
a_t, sec	7	7	7	7	7	7	7	7	2	2				7	7
K_t	0.7	0.7	0.7	0.7	0.7	0.7	0.7	0.7	0.7	0.7				0.7	0.7

TABLE 6.2

CONTROLLER AND FILTER GAINS FOR THE WEPCO UNITS

UNITS		1 THRU 4					5 THRU 8	9 AND 10				
CONTROLLER, GAINS, $\underline{G}$		0	0	3.77	3.22	0.0161	0 0 3.79 3.37 0.0161	0	0	3.77	3.22	0.0161
Kalman Gains, $\underline{K}$												
MEASUREMENTS AVAILABLE	Frequency Deviation	-.0295	.00180	0	0	0		-.0133	.00180	0	0	0
	Electrical Power	.0824	-.00256	0	0	0		.0824	-.00256	0	0	0
	Throttle Pressure	0	.605	-.464	.157	0	Same as Units 1 thru 4	0	.605	-.464	.157	0
	Steam Flow	0	-.154	.304	0	0		0	-.154	.304	0	0
		0	.793	0	.206	0		0	.794	0	.206	0
	Frequency Deviation	-.2095	.00180	0	0	0		-.0133	.00180	0	0	0
	Electrical Power	.0824	-.00256	0	0	0		.0824	-.00256	0	0	0
	Throttle Pressure	0	.668	-.480	0	0	Same as Units 1 thru 4	0	.668	-.480	0	0
		0	-.165	.308	0	0		0	-.165	.308	0	0
		0	1.00	0	0	0		0	1.00	0	0	0
	Frequency Deviation	-.0295	.00180	0	0	0		-.0133	.00180	0	0	0
	Electrical Power	.0824	-.00256	0	0	0		.0824	-.00256	0	0	0
		0	.817	0	0	0	Same as Units 1 thru 4	0	.668	0	0	0
		0	-.286	0	0	0		0	-.286	0	0	0
		0	1.00	0	0	0		0	1.00	0	0	0

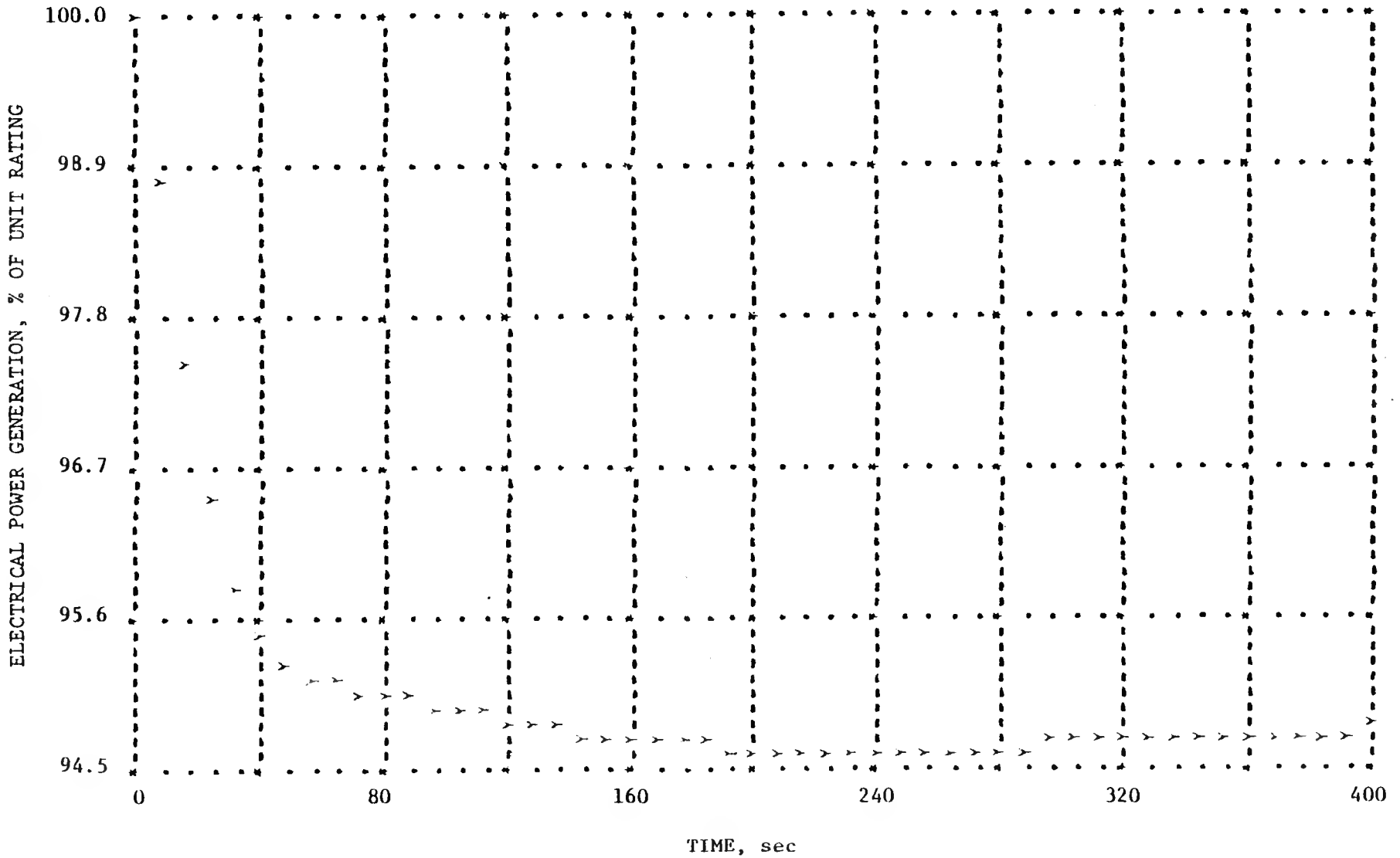

FIGURE 6.4 ELECTRICAL GENERATION RESPONSE TO A
5% STEP DECREASE IN POWER DEMAND

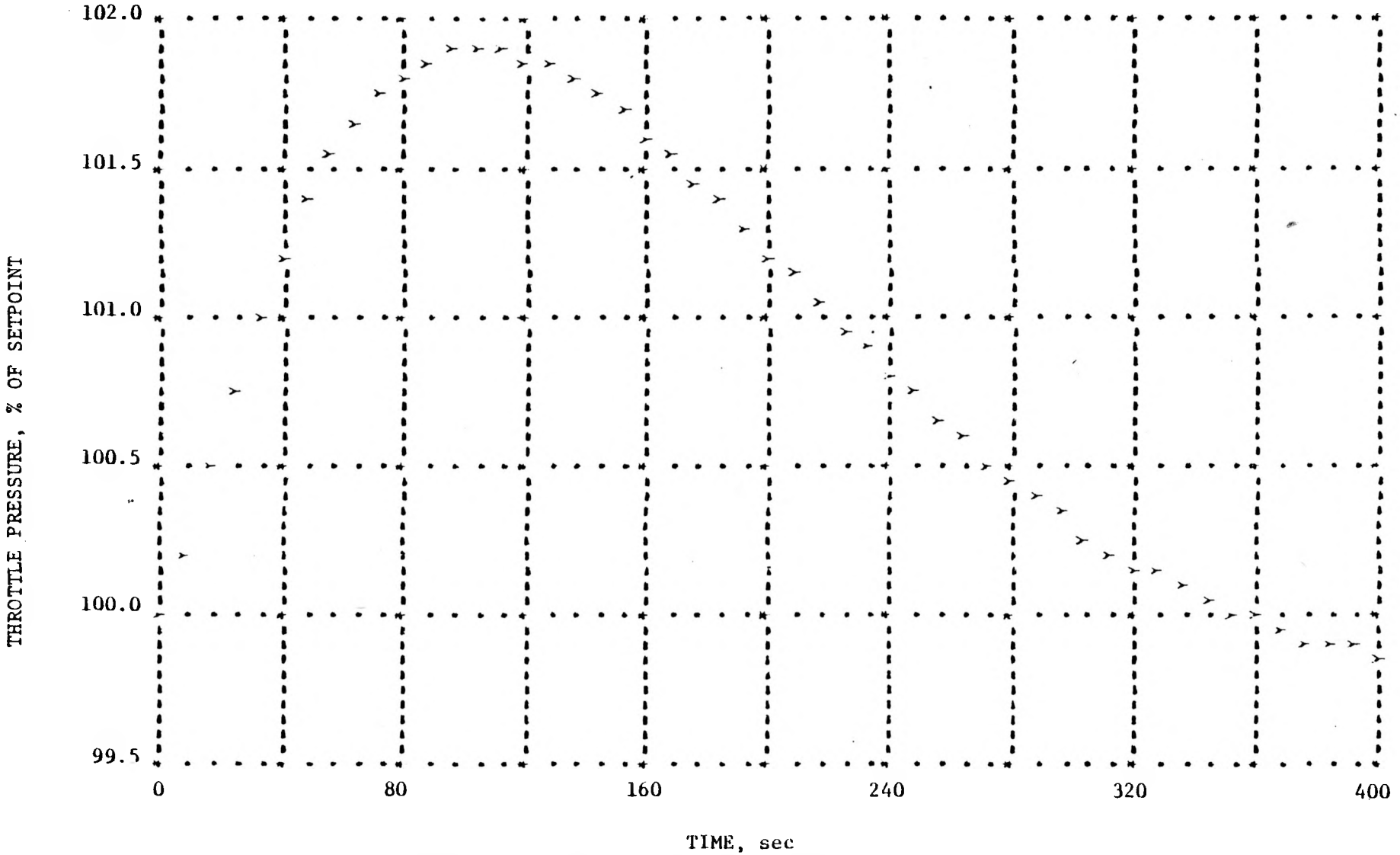

FIGURE 6.5 THROTTLE PRESSURE RESPONSE TO A 5% STEP DECREASE IN POWER DEMAND

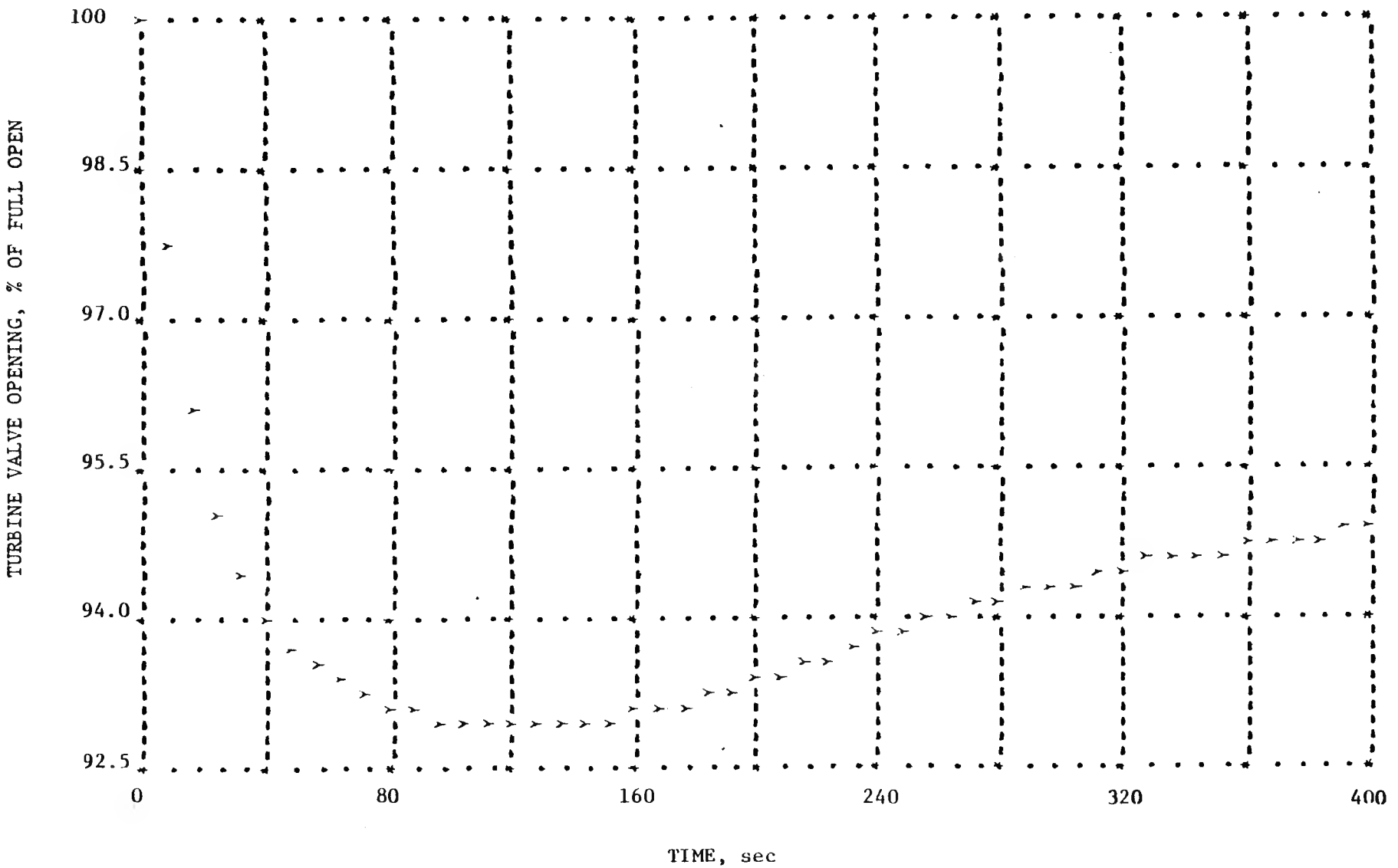

FIGURE 6.6 TURBINE VALVE RESPONSE TO A
5% STEP DECREASE IN POWER DEMAND

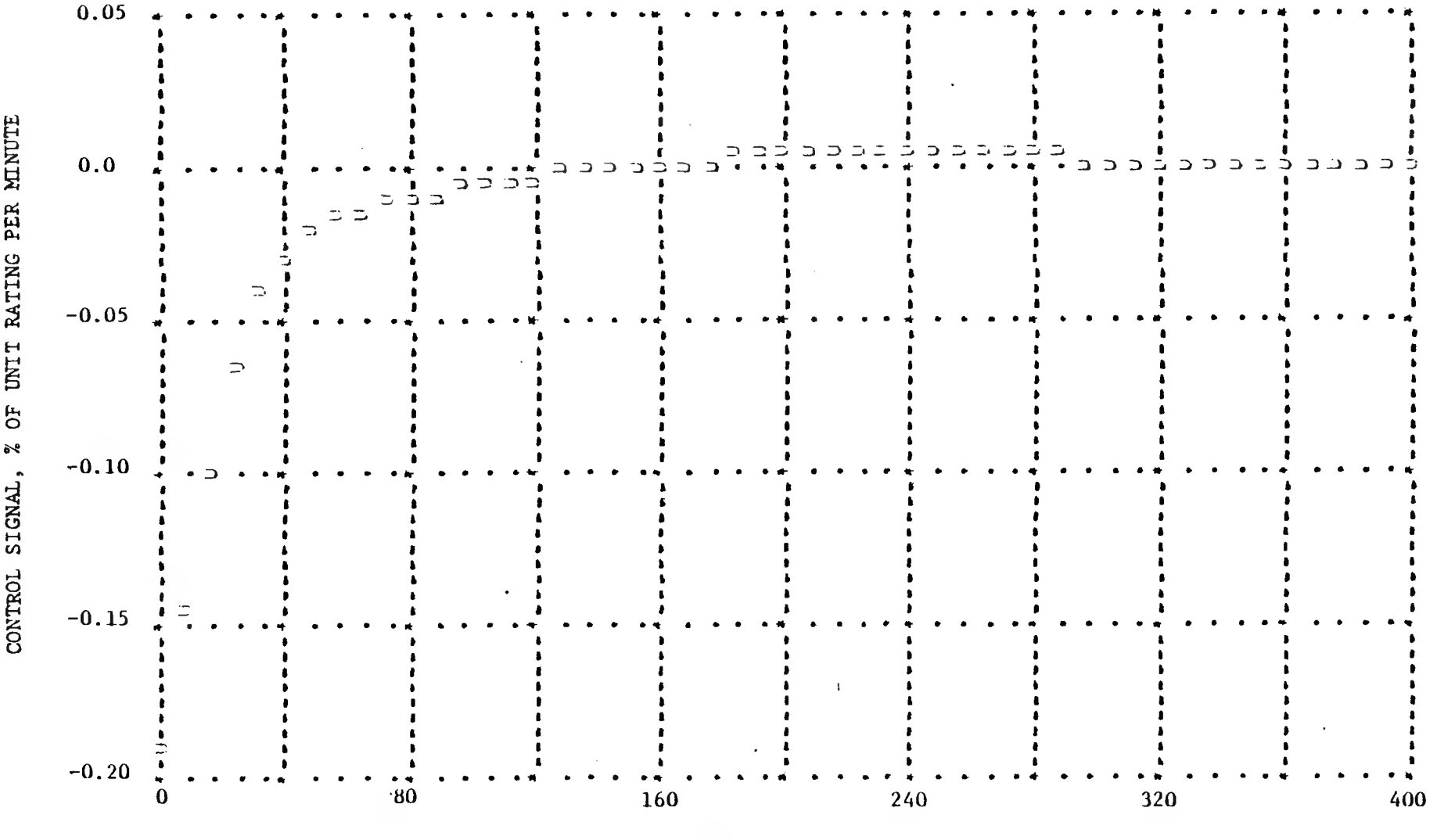

FIGURE 6.7 CONTROL SIGNAL FOR A 5% STEP DECREASE IN POWER DEMAND

APPENDIX A

AREA LOAD-FREQUENCY CONTROL

T.M. Athay
Systems Control, Inc.
Palo Alto, California

H.G. Kwatny
Drexel University
Philadelphia, PA

R.G. Smith
Systems Control, Inc.
Palo Alto, California

1.0 INTRODUCTION

An advanced Automatic Generation Control (AGC) software package is currently being developed in a U.S. Department of Energy demonstration project. The scope of this project includes the design, implementation and testing of an integrated and coordinated set of algorithms for AGC. A major function in the overall structure is that of Load-Frequency Control (LFC) and this paper summarizes the current stage of design of the LFC algorithms. The emphasis of the paper is on a discussion of LFC objectives and on the use of some ideas from modern control theory to derive basic control structures which reflect those objectives.

2.0 AUTOMATIC GENERATION CONTROL

2.1 Conventional AGC Structure

Four basic objectives of power system operation during normal operating conditions can be associated with automatic generation control:

1. Matching total system generation to total system load
2. Regulating system electrical frequency error to zero
3. Distributing system generation amongst control areas so that net area tie flows match net area tie flow schedules
4. Distributing area generation amongst area generation sources so that area operating costs are minimized.

The first objective is conventionally associated with system primary or governor speed control; turbine speed governors respond proportionally to local frequency deviations and normally bring the rate-of-change of frequency to zero within a time-frame of several seconds. The latter three objectives are accomplished by supplementary controls directed from area control centers. The second and third AGC objectives are classically associated with the regulation function, or load-frequency control, while the fourth objective is associated with the economic dispatch function of automatic generation control. The latter two functions typically operate in a time frame from several seconds to several minutes.

Introduced nearly 30 years ago, the tie-line bias control strategy [1] is utilized in most interconnected power systems to accomplish the regulation function of AGC. In this approach the second and third objectives are combined and each area attempts to regulate its area control error (ACE) to zero, where

$$ACE \triangleq M - S^o + B\,(f - f^o) \qquad (1)$$

and

M = net tie flow out of the control area
S^o = scheduled tie flow out of the control area

B = area frequency bias constant (positive real)
f = actual frequency
f^o = scheduled frequency

A thorough discussion of the various aspects of tie-line bias control is provided in [1,2] and in other AGC literature. Very briefly, this strategy provides a steady-state target according to which each area meets its own load during normal conditions in the interconnection, contributes to frequency regulation and provides assistance to external areas when necessary. Although based on steady-state arguments, the tie-line bias control strategy has the important advantage that no inter-area communication is required, and it is on this basis that the decentralized automatic generation control of interconnected systems has been achieved.

The performance of conventional AGC has often been unsatisfactory however [3]. While some significant reasons for poor performance cannot be directly attributed to the control structure per se, not enough generating units on control for example, others can arise from the nature of the basic control algorithms as well as from the diverse data processing structures with which they are implemented. An important observation is that conventional AGC structures do not fully reflect the essential tracking nature of the problem. For example some are effectively pure integral controllers whose overall loop gain must be rather low to maintain stability. As a result tracking performance is limited, particularly during sustained, rapid load changes such as the morning load pickup. At such times manual operator intervention is generally required in order to maintain ACE within acceptable limits. Evidence of sustained fluctuations in frequency caused by inappropriate control has been reported [4]. In addition, a lack of coordination between the AGC regulation and economic dispatch functions can result in conflicting requirements on generating units and inefficient control.

2.2 Advanced Automatic Generation Control

The overall objective of this development and implementation project is to demonstrate that significant improvements in AGC performance can be obtained by better utilization of existing control center hardware capability and more extensive application of current control system knowledge. The improved AGC software package, which is currently in an early stage of development, will be implemented and demonstrated at the Wisconsin Electric Power Company (WE) Control Center. The WE energy control center is representative of the current state-of-the-art, utilizing a hierarchical system of dual CDC Cyber and quad CDC 1700 computers [5].

An integrated and coordinated set of algorithms is being developed for AGC. Three respective functions will be performed: short-term load prediction, dynamic optimal dispatch and load-frequency control. Before reporting on the current status of the prototype design structures for the LFC function, a brief description of the first two functions is provided.

A short-term load predictor produces a forecast of the secular component of the daily load curve at five minute intervals for 1-2 hours into the future. The dynamic optimal dispatch then determines unit trajectories which track the secular load so that production costs are minimized in a time-integrated manner, rather than on an instant-by-instant basis as in conventional economic dispatch. The dispatch algorithm is based on the combined use of a minimum marginal cost method and a dynamic programming successive approximations method. Among other things, the combination of short-term load forecasting and dynamic dispatch provides the capability for valve point

loading (which will be demonstrated on two WE coal-fired units) and provides the plant operators with an advanced knowledge of future generation demand.

2.3 Load-Frequency Control

Over the last few years numerous researchers have explored certain aspects of the load-frequency control problem in the context of modern control theory. One of the earliest studies was that of Fosha and Elgerd [6]. In employing the linear quadratic regulator theory, they introduced a significantly non-conventional approach which subsequently stimulated both an interest in the dynamic aspects of LFC as well as a lively and constructive dialogue between various control theorists and industry practitioners. One difficulty in this and other early studies is that they emphasized controlling synchronizing oscillations, whereas it is generally recognized that they are too fast for supplementary control to be either effective or desired [4]. Another weakness was recognized by Calovic [7], who made a clear distinction between the transient and steady state response aspects of LFC. A basic operating policy of interconnected control areas is that each area should attempt to regulate ACE to zero. While the relative gains applied to net interchange (M - S) and frequency deviation by area load-frequency controllers could perhaps be adjusted independently in order to obtain a desired transient response during normal operating conditions, the tie-line bias control strategy sets this relative gain equal to the frequency bias coefficient (B) for each area. This strategy thus achieves an implicit coordination between areas, which is very important during an abnormal operating condition, by essentially defining mutually determined and consistent steady state targets for all areas in the interconnection.

In the paper [8] the problem of distinguishing dynamic and steady state behavior was more fully explored and in addition a third major difficulty of earlier optimal regulator designs for LFC was addressed, namely the often dominating effect of prime mover energy source dynamics on unit generation response capability. Load-frequency control is fundamentally a tracking problem, and in the frequency range of interest the response limitations imposed by thermal energy sources must be recognized in the LFC design.

Based on these considerations, four basic objectives of LFC will be used to define the control problem:

1. The total area generation should be controlled so as to track the area load plus schedule. This will be called the load tracking objective.

2. The individual unit generations should be controlled so as to track the desired unit economic trajectories. This will be called the economic tracking objective.

3. Load-frequency control should allow the area primary response to occur naturally.

4. Individual unit response rate limitations must not be violated.

The parallel structure of LFC is exploited by designing independent controllers for each generating unit and a coordinating controller for the control area. These two components of the LFC structure are separately discussed in the next two sections.

3.0 COORDINATING CONTROLLER

The purpose of the coordinating controller is to provide megawatt reference inputs to the unit control loops such that the load and economic tracking objectives are achieved in a coordinated manner. Two basic design structures have been developed for the coordinating controller which correspond to two alternative methodologies for the design of robust linear multivariable regulators which have disturbance rejection properties. The first, which will be developed here in more detail, corresponds to the approach based on the feedback of estimates of (possibly artificial) disturbance states [9]. The second is based on the robust servo-compensator design methodology [10].

3.1 Model

The model used for developing the coordinating controller structure is a very simple representation of a control area connected to an external system. Tie-line synchronizing oscillations have been removed because, for the purposes of AGC simulation and design, it is reasonable to assume that the interconnection is at a common system frequency [11]. Table 1 contains definitions of the variables and parameters employed, while a block diagram is given in Figure 1. The closed loop system consisting of the unit and its unit controller is represented by a unity transfer function and thus the model is useful in the very low frequency range only.

3.2 Control Problem

With the white noise inputs v_1, v_2, v_3 and v_4 set to zero in Figure 1 it is necessary to determine state and control trajectories $\bar{x}$ and $\bar{u}$ which characterize the ultimate steady state. We require that the trajectories satisfy the equations corresponding to the model of Figure 1 and in addition that

$$ACE = y_2 + By_1 = 0 \tag{2}$$

These trajectories can be obtained as linear functions of the disturbances ω_1, ω_2, ω_3 and ω_4 and in fact many solutions are possible. Let γ be a set of participation factors such that $\gamma_1 + \gamma_2 + \ldots + \gamma_n = 1$, let x^* be the desired economic unit trajectories determined by the dynamic dispatch functions, and denote the sum of the unit ultimate state trajectories by $\bar{x}_T$, i.e., $\bar{x}_T = \bar{x}_1 + \bar{x}_2 + \ldots + \bar{x}_n$. Then the ultimate state and control trajectories are given by (3) and (4):

$$\bar{x} = x^* + \gamma \bar{x}_T \tag{3}$$

$$\bar{u} = \gamma \bar{\omega}_4 \tag{4}$$

where:

$$\bar{x}_T = \frac{\beta}{B+\beta_2} S^o - \phi_1 \omega_1 - \phi_2 \omega_2 + \omega_3 \tag{5}$$

$$\phi_1 = \frac{B\beta}{B+\beta_2}, \quad \phi_2 = \frac{\beta_1 - B}{B+\beta_2} \tag{6}$$

A state variable gain matrix is obtained by next solving the deterministic optimal regulator problem corresponding to the pertubational system $\Delta x = x - \bar{x}$, $\Delta u = u - \bar{u}$. Consider the sum $\Delta x_T = \Delta x_1 + \Delta x_2 + \ldots + \Delta x_n$. Regulation of Δx_T during the transient actually implies regulation of total generation to its ultimate state value as established by the specification that ACE = 0.

Thus the scalar quadratic cost term $q_1(\Delta x_T)^2$ is a measure of performance for the load tracking objective of LFC defined previously. Furthermore, a quadratic weighting on variations of the quantities $\Delta x_1, \ldots, \Delta x_n$ in the subspace defined by $\Delta x_T = 0$ corresponds to a measure of performance for the economic tracking objective. Thus the state deviation costs in the performance index are separated into two terms which correspond to these two LFC tracking objectives:

$$J = \int_0^\infty [q_1 \Delta x^T C^T C \Delta x + \Delta x^T (I - C^* C)^T Q_2 (I - C^* C) \Delta x + \Delta u^T \bar{R} \Delta u] dt \qquad (7)$$

where

$$\bar{C} \in R^n, \quad \bar{C}^T = [11 \ldots 1]$$

$$C \in R^{n+1}, \quad C^T = [\bar{C}^T, 0]$$

and one choice for $C^* \in R^{n+1}$ is $(C^*)^T = [\bar{C}^*, 0]$, where $\bar{C}\,\bar{C}^* = I$. The $(n+1) \times (n+1)$ matrix Q_2 is chosen to be block diagonal of the form. $Q_2 = \text{diagonal}(\bar{Q}_2, 0)$ where $\bar{Q}_2$ is $n \times n$, in order to insure that the frequency mode, which is uncontrollable in a practical sense by a single area, is not observable in the cost functional.

The well-known solution to the standard regulator problem which provides the feedback gain matrix $\Delta u = -K\Delta x$ reduces to $K = [\bar{R}^{-1}\bar{P} : 0]$ where $\bar{P}$ $(n \times n)$ is the solution of the relevant Ricatti equation. One interesting result of this solution is that the closed loop eigen-system can be shown to have $n-1$ modes which lie in the subspace corresponding to $ACE = 0$ and an additional mode in the direction of $\bar{R}\bar{C}^T$. Moreover, it is this last mode which regulates ACE to zero and its response time is controlled by the scalar parameter q_1. The additional modes are "redistribution" modes which allow for the redistribution of generation to (possibly economic) targets which lie in the $ACE = 0$ subspace and which have response times that depend on the parameter matrix $\bar{Q}_2$.

3.3 Simplified Regulator Design

The previous subsection described the characterization of ultimate state and control trajectories and the solution of a quadratic regulator problem which resulted in an $n \times n$ feedback gain matrix $R^{-1}\bar{P}$ that shapes the transient response of deviations about the ultimate state trajectories. Several practical problems remain, however. An important one is that the generating units on-line vary throughout the day and in addition, the system dispatcher and/or plant operators often change the operating mode of the on-line units. For the existing WE control center computer system it is considered infeasible to solve the Ricatti equation for the matrix $\bar{P}$ on-line when the set of units assigned to regulating duty changes, and there are in addition several practical problems associated with storing and retrieving $n \times n$ gain matrices for all possible combinations of regulating units.

The $n-1$ redistribution modes represent $n-1$ degrees of freedom for the regulator design in the sense that $n-1$ eigenvalues can be assigned to the secondary tracking objective (indirectly), via the parameter matrix $\bar{Q}_2$. Due to the parallel structure of the problem, it is possible to trade-off these $n-1$ degrees of freedom with the compuational burden of obtaining the feedback gain matrix K. While this interesting observation has not been fully explored in general, one particular case has been developed in detail. The special case in which the $n-1$ secondary tracking modes have a common eigenvalue corresponds to a solution of the Ricatti equation which can be

obtained analytically. This allows gains to be updated very easily when the set of regulating units changes. For this special case the feedback gain matrix has the form

$$r_i = g_i\ g_i \cdots (g+g_i)\ g_i \cdots g_i \tag{8}$$

where r_i is the ith row of K and the term $(g+g_i)$ is in the ith column. Because off-diagonal terms are identical for each row, the resulting coordinating controller can be put into the very simple block diagram form of Figure 2.

3.4 Observor Design

The robustness and disturbance rejection properties of this coordinating controller arise from the feedback of the unmeasurable disturbance variables ω. The observor design used to provide estimates of these quantities is based on the methodology reported in [12]. Assigning a single time constraint ϕ^{-1} to the second order design, the resulting estimates are given in transfer function form below.

$$\hat{\omega}_1 = \left[\frac{1}{s\phi^{-1}+1}\right] \{[s(\phi^{-1}+H/\beta)+1]\ y_1 + 1/\beta_1\ [(-D_1 y_1+y_3)+y_2+S^o-y_4]\}$$

$$\hat{\omega}_2 = \beta_2/\beta\ \ [(-Dy_1+y_3) - y_4] + y_2 + S^o$$

$$\hat{\omega}_3 = -D_1 y_1 + y_3$$

$$\hat{\omega}_4 = \frac{s}{s\phi^{-1}+1}\ \ (-D_1 y_1 + y_3) \tag{9}$$

3.5 Alternative Coordinating Controller Structure

An alternative to the coordinating controller structure discussed previously has been developed which is based on the robust servocompensator design approach [10]. Because these two design methodologies can in general lead to substantially different closed loop response characteristics, both are being developed with more or less equal emphasis in order to determine which structure is preferable for LFC.

A slightly different viewpoint is taken for this design which can be illustrated by defining the steady state relationships.

$$G_T \triangleq G_T^o - 1/R_T \Delta f, \quad L_T \triangleq L_T^o + \beta_L \Delta f \tag{10}$$

where G_T is the total area electrical generation, L_T is the total area electrical load at the prevailing frequency, G_T^o is the total area electrical generation at 60 Hz and L_T^o is the total area load demand. Now

$$ACE = \Delta IC + B\Delta f = G_T^o - L_T^o - S^o + (B - 1/R_T - \beta_L)\Delta f \tag{11}$$

and if for the sake of argument we assume that $B = 1/R_T + \beta_L$, then we see that ACE is a measure of the area electrical generation-load mismatch referenced to 60 Hz. Because the electric power which flows from a unit depends on the current electrical state of the entire system we can see from

(11) that the continuous regulation of ACE couples the various LFC area controllers through their objective functions. This can also be seen by expressing the net tie flow deviation in the form

$$\Delta IC = \frac{H_{EX}}{H_{SYS}} (P_T - L_T) - \frac{H_{AREA}}{H_{SYS}} (P_{EXT} - L_{EXT}) - S^o \qquad (12)$$

where P_T (P_{EXT}) is the total area (system) mechanical power and $H_{SYS}=H_{AREA}+H_{EX}$ is the total system inertia. Because of this argument, and the fact that mechanical power is actually controlled from the governor speed changer motor input, the load tracking objective of LFC is defined in terms of mechanical rather than electrical power for the alternative coordinating controller. The difference between the two is simply a derivative of frequency term, so the steady state strategy of ACE control is not affected, but this term in ACE is destabilizing and hence it is removed by defining

$$ACEM = P_T^o - L_T^o - S^o = ACE + 2H_{AREA}\,\dot{\Delta f} \qquad (13)$$

as the (mechanical) area control error which is to be regulated to zero. Whether or not this is a practical distinction is yet to be determined, but the relative magnitude of the derivative term and the performance of the filter designed (but not yet tested) to estimate mechanical power are the main factors.

In a manner similar to that described previously, the linear quadratic regulator design associated with the robust servocompensator design approach has been formulated, and again the special case which corresponds to an analytic solution of the relevant Ricatti equation has been obtained. A block diagram of the resulting coordinating controller is shown in Figure 3. It is interesting to note that, although designed using a modern control methodology, the resulting structure can be interpreted as a classical multi-loop integral controller with lead compensation.

4.0 UNIT CONTROLLER

The predominant dynamics of the load-frequency control problem reside in the low frequency domain associated with unit energy sources. Thus the response capability of a unit is a major factor in AGC performance and unit control is an important component of the LFC structure. The objectives of the unit controller are two-fold: regulate unit actual 60 Hz generation to track the unit desired generation as provided by the coordinating controller, and ensure that the unit's internal process variables are not unduly upset as a result of the tracking activity.

4.1 Control Problem

Reasonably detailed nonlinear models of the WE units have been developed for an AGC simulation program which will be used for further development and testing of the new AGC algorithms. A simplified and linearized model has been derived from these models for the purpose of design which is shown in Figure 4. It corresponds to a coal-fired drum unit whose controls are of the boiler-follower type.

An important observation concerns the interaction of the generation control loop, which is to be designed, and the pressure-fuel control loop. It can be shown that the transfer function from the speed-changer input to the generator power output may have a pair of non-minimum phase zeros for reasonable values of plant parameters. This would explain why increasing

the generation control loop gain beyond some limit generally results in oscillatory behavior. It also would explain why it is practically impossible to improve performance by generation loop compensation methods alone. Thus, modern unit control systems employ coordination between these two strongly interacting control loops. Because throttle pressure is upstream of the possibly non-minimum phase zeros, one apparently effective solution to this problem is to use throttle pressure feedback.

The unit controllers have been designed using the linear quadratic gaussian method. Outputs of unit power output, throttle pressure deviation, frequency deviation and (for some units) first stage pressure are used by a Kalman filter for obtaining state variable estimates. The filter is designed to reference the estimate of unit output to 60 Hz in order to allow the unit's primary response to occur naturally. The controller contains a bias variable state in order to provide reset action and improve robustness. The feedback gain vector was obtained using standard optimal regulator techniques. In addition, various logic strategies involving hard constraints on selected variables and rates are also included.

The major difference between the LQG and conventional unit controller designs is in the incorporation of closed loop state variable estimates based on multiple measurements. The previous discussion emphasized the significance of measuring throttle pressure. Conventional designs often employ open loop estimation of a variable that represents boiler stored energy, which is a function of throttle pressure, and restrict control action when the estimated stored energy becomes too low. There is evidence that such an open loop estimate can be significantly in error, resulting in either an unnecessary restriction on unit response when the pressure is actually fine or unrealistic (and possibly destabilizing) control when the pressure is actually too low.

5.0 SUMMARY

The primary objectives of LFC have been briefly discussed in this paper, and a basic control structure derived in accordance with those objectives has been described. Some apparently reasonable assumptions have been used in order to derive, via methods of modern control theory, a control structure which is feasible for implementation on the existing WE control center computer system. Although similar in many respects to conventional designs, the resulting structure has several capabilities which, it is felt, can contribute to an improved AGC performance. A considerable amount of additional work is needed before a meaningful evaluation of the designs can be made, however.

Presently, the unit controller and the two coordinating controllers have been designed and partially evaluated using a combination of the LQG synthesis techniques, linear simulation and frequency domain analysis. Further development and evaluation of the LFC algorithms will in addition make extensive use of the detailed, non-linear AGC simulation program recently completed as a part of the project. In order to focus on LFC objectives and control structure, many design details and preliminary results have regretfully been omitted in this brief paper. Future reporting is intended however, that will discuss several interesting theoretical issues and important design details as well as provide results from the rather extensive evaluation which is planned.

6.0 ACKNOWLEDGEMENT

The advanced AGC development and implementation project is supported by the U.S. Department of Energy under contract number EC-77-01-2118. The direction and assistance provided by Lester H. Fink of DOE is gratefully acknowledged.

7.0 REFERENCES

1. N. Cohn, Control of Generation and Power Flow on Interconnected Systems, John Wiley and Sons, New York, 1966.

2. N. Cohn, "Some Aspects of Tie-Line Bias Control on Interconnected Power Systems", Trans. AIEE (Power Apparatus and Systems), Vol. 75, pp 1415-1428, February, 1957.

3. L.H. Fink, "Concerning Power System Control Structure", Advances in Instrumentation, ISA, Vol. 26, Part 1, 1971.

4. D.N. Ewart, "Automatic Generation Control - Performance Under Normal Conditions", Final Report for ERDA Contract E(49-18)-2147.

5. J.C. Russel and W.P. Rades, "The Wisconsin Electric Power Company Energy Control System", Proc. 1973 PICA Conference, Minneapolis, Minnesota, pp. 135-141, June 4-6, 1973.

6. C.E. Fosha and O.J. Elgerd, "The Megawatt - Frequency Control Problem: A New Approach Via Optimal Control Theory", IEEE Transactions, Vol. PAS-89, pp 563-578, April, 1970.

7. M.S. Calovic, "Linear Regulator Design for a Load and Frequency Control", IEEE Transactions, Vol. PAS-91, No. 6, pp 2271-2285, 1972.

8. H.G. Kwatny, K.G. Kalnitsky and A. Bhatt, "An Optimal Tracking Approach to Load-Frequency Control", IEEE Transaction, Vol. PAS-94, No. 5, pp 1635-1643, 1975.

9. H.G. Kwatny, "Optimal Linear Control Theory and a Class of PI Controllers for Process Control", Proceedings 13th JACC, pp 274-281, 1972.

10. E.J. Davidson, "The Output Control of Linear Time-Invariant Multivariable Systems with Unmeasurable Arbitrary Disturbances", IEEE Transactions, Vo. AC-17, pp 621-629, 1972.

11. C.W. Taylor and R.L. Cresap, "Real-Time Power System Simulation for Automatic Generation Control", presented at the IEEE PES Summer Meeting, San Francisco, CA, 1975.

12. H.G. Kwatny, "Minimal Order Observors and Certain Singular Problems of Optimal Estimation and Control", IEEE Transactions, Vol. AC-19, No. 3, pp 274-276, 1974.

TABLE 1
NOMENCLATURE

Δf, y_1	frequency deviation from nominal
ΔIC, y_2	net tie flow deviation from schedule
y_3	area electrical load (at prevailing frequency)
P_T^o , y_4	area mechanical power at 60 Hz
H	total system inertia
β_1	local area regulation $\beta_1 = D_1 + R_1^{-1}$
β_2	external area regulation $_2 = (D_2 + R_1^{-1})$
β	total system regulation ($\beta_2 = \beta_1 + \beta_2$)
D_1	local area load characteristic
D_2	external area load characteristic
R_1	local area governor characteristic
R_2	external area governor characteristic
B	frequency bias (positive) constant used in definition of ACE
ACE	area control error, ACE $\triangleq \Delta IC + B\Delta f$
x_i	ith unit generation demand @ 60 Hz
x_{n+1}	state variable representing frequency under ideal conditions
ω_1	disturbance term representing frequency error due to imperfect knowledge of β
ω_2	disturbance term representing external area generation and load conditions
ω_3	disturbance representing local area electrical load at 60 Hz
ω_4	disturbance representing rate of change of local area load
u_i	ith unit control variable, rate of change of generation
Δ_1	local area excess generation at 60 Hz
Δ_2	external area excess generation at 60 Hz
S^o	local area net tie flow schedule

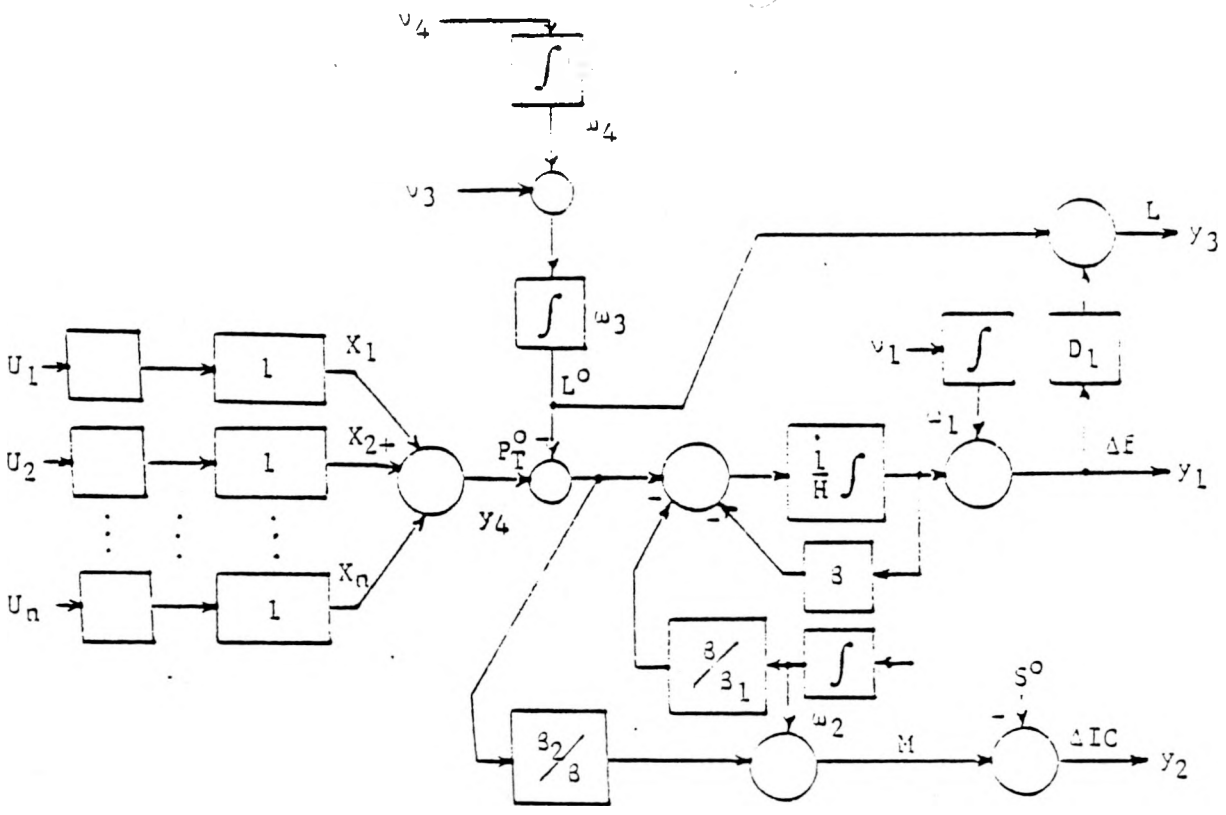

FIGURE 1: MODEL FOR COORDINATING CONTROLLER DESIGN

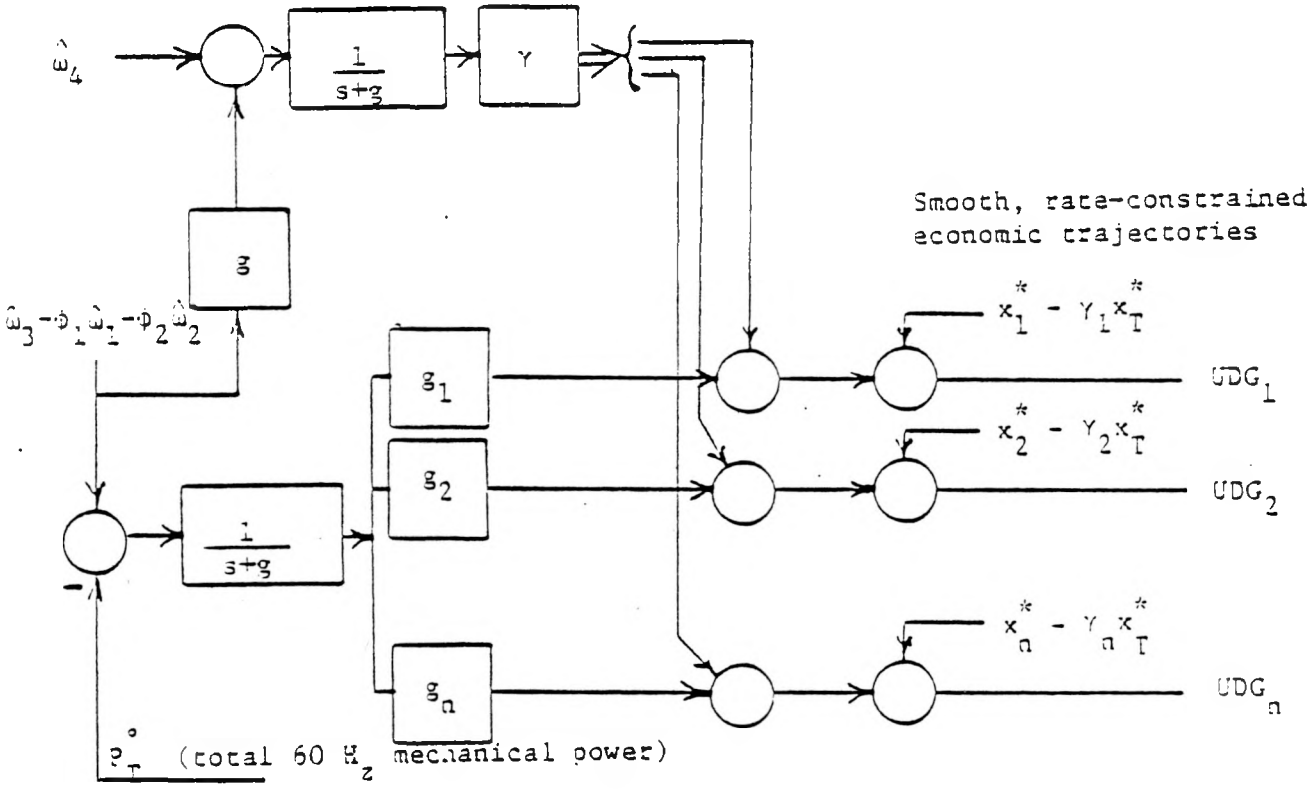

FIGURE 2: SIMPLIFIED COORDINATING CONTROLLER

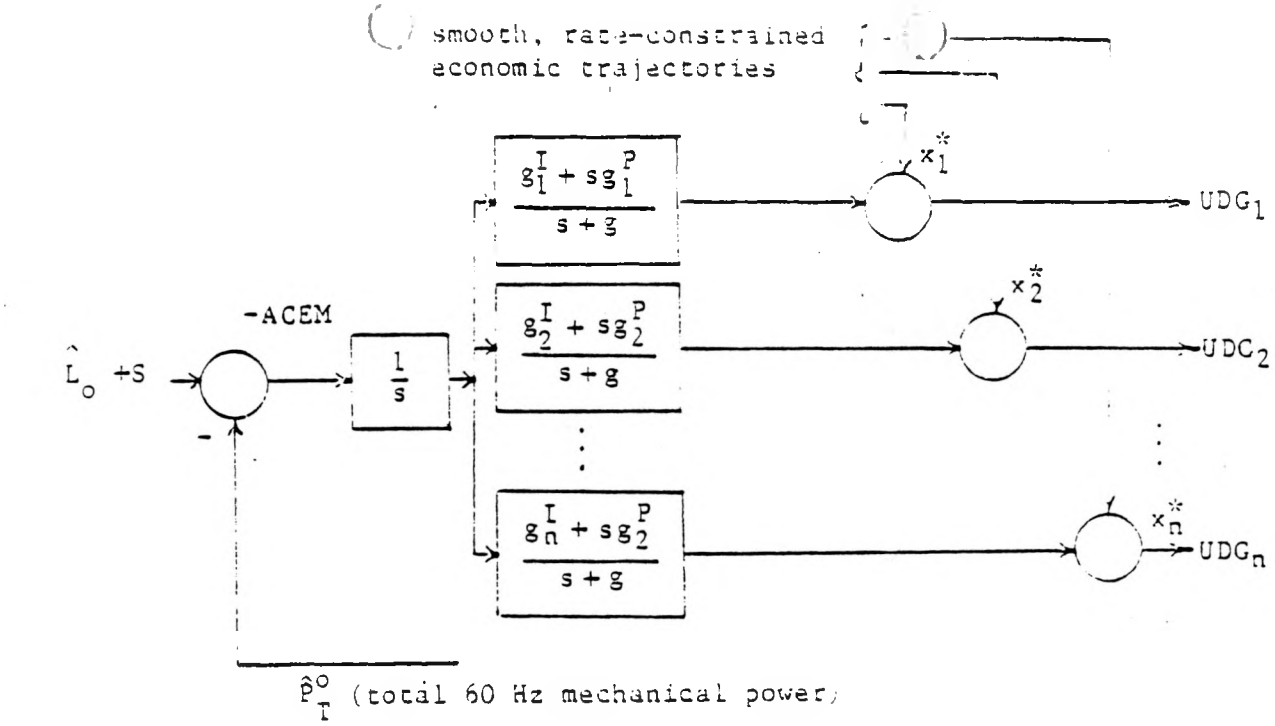

FIGURE 3: ALTERNATIVE COORDINATING CONTROLLER

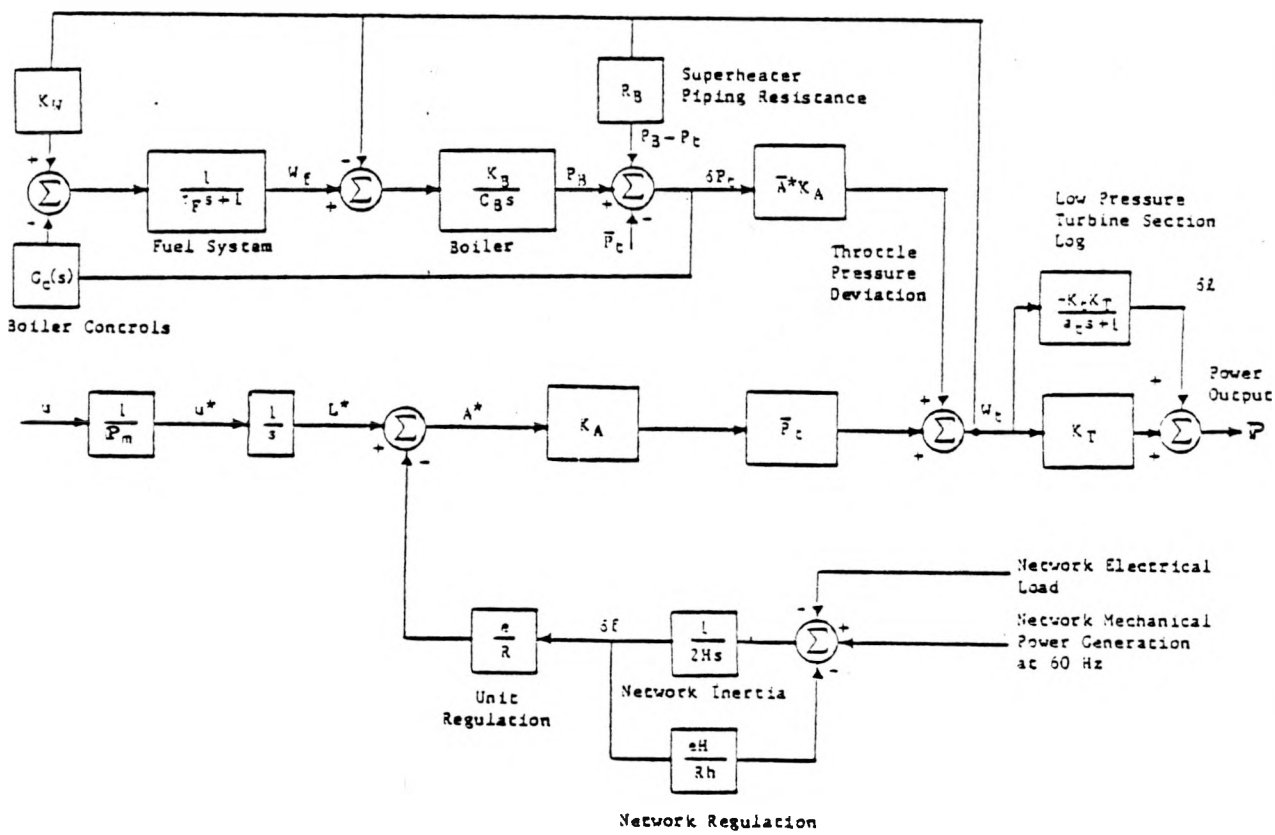

FIGURE 4: MODEL FOR UNIT CONTROLLER DESIGN

APPENDIX B

SHORT-TERM L[illegible] PREDICTION FOR ECONOMIC DISPATCH OF GEN[illegible]TION

Dale W. Ross
Systems Control, Inc.
Palo Alto, California

Gary B. Ackerman
Systems Control, Inc.
Palo Alto, California

Robert Bischke
Wisconsin Electric Power Company
Milwaukee, Wisconsin

Robin Podmore
Systems Control, Inc.
Palo Alto, California

Kent D. Wall
University of Virginia
Charlottesville, Virginia

ABSTRACT

A set of procedures and algorithms are developed for short-term (1-3 hours) electric power system load prediction. The short-term load predictors provide "look ahead" capability for an economic dispatch that coordinates predicted load changes with the rate-of-response capability of generation units. The short-term load prediction also enables valve-point loading of generation units. The predictor models are estimated empirically. Test results are given for the predictor models applied to actual loads of an electric utility.

INTRODUCTION

Benefits of Short-Term Load Prediction

Automatic Generation Control (AGC) is a prime example of a control problem where future information is vital to successful control. A power generating system must fulfill a tracking function; specifically, the generation must track the secular load component economically. Anticipatory control is beneficial, and short-term load predictions are needed to achieve such anticipation. Construction of these predictions, in general, is a challenging problem since electrical load is affected by many exogenous disturbances including weather. There is, however, a wealth of statistical information available in the form of system load time series, from which information can be extracted to provide an accurate load prediction that enhances the performance of an AGC system.

Short-term load prediction has direct application to the economic dispatch of generation units. State-of-the-art methods for economic dispatch are "static" in that they do not use, as input load data, anything more than the estimated current load. They do not "look ahead" over the future time horizon, using predicted load trends (say, of 1-3 hours ahead) to determine the economic allocation of generation to the load. Predictive or "look ahead" capability on the economic dispatch would be beneficial for several reasons:

- Economic dispatch is to track the secular load component. In state-of-the-art AGC, the secular load is determined by filtering or smoothing the actual load. Such smoothing introduces a large time lag in the economic dispatch. Short-term load prediction overcomes this lag, and hence can improve generation economics.
- The "look ahead" capability enables a better allocation of regulating margin in the near future. For instance, it can aid in reserving rate-of-response capability so that the generation can match rapidly changing load.
- Advance knowledge of load changes is useful to operating personnel. For instance, it can be used by plant operators in deciding when to commission plant auxiliaries. Also, dispatching personnel can use it in making timely adjustments to scheduled power transactions, to spinning reserve, and to other system elements to ensure a high degree of security.
- The potential benefits of valve-point loading cannot be obtained without having load prediction capability, and using it to dynamically dispatch generation (some units being dispatched to valve-points). As discussed in [1], one basic requirement for successful implementation of valve-point loading is that the amount of regulating capacity necessary to take up the difference between block-loaded generation and actual load is a function, among other things, of the amount of time required to pick up or drop one or more blocks of generation. Furthermore, some minimum amount of time, say 10 minutes, must be provided during which a unit remains at a given valve position without a reversal of load, otherwise the economic benefit of the valve-point loading will not be achieved. These considerations mean that successful valve point loading requires foreknowledge of the load trend.

In summary, short-term load prediction, operating over a time horizon of a few hours, has potential for improving automatic generation control. This paper discusses an approach taken in developing a short-term load prediction methodology for use in an automatic generation control system. The prediction methodology employs two models, an Hourly Predictor Model and a Five-Minute Predictor Model. Their development is discussed at length in this paper. While the emphasis of this paper is upon short-term load prediction, the work reported is part of a broader effort to develop an advanced automatic generation control (AGC) software package. This development, a U.S. Department of Energy demonstration project [15], includes the design, implementation and testing of an integrated and coordinated set of AGC algorithms. A major function in the overall structure is that of short-term load prediction and its use in the economic dispatch of generation units. Other functions are reported in [16], and other publications on the project work will be forthcoming.

PREVIOUS LOAD PREDICTION WORK

Over the last twelve years there has been considerable research on forecasting hourly electricity loads. The earliest work includes two noteworthy studies --

Chen and Winters [5], and F~ mer and Potton [8]. Both studies combined historical ta with climatic conditions (weather variables) in their respective models. The former study looked at peak loads while the latter modeled hourly system loads. All the work that followed basically included information of historical system loads in combination with weather data. There were, however, many variations in the model specifications.

Two of the subsequent studies were relatively more sophisticated than the others. Toyoda, Chen and Inoue [12] applied "State Estimation" to estimate the status of power systems for on-line real-time control. The authors split the forecast horizon into short-term (ten minutes to one hour) and medium-term (one hour to twenty-four hours). The effects of weather were included in the medium-term analysis, only. Gupta and Yamada [10] constructed a procedure for probabilistic forecasting of hourly power-system loads with a twenty-four hour horizon. The approach was "additive time-series" in that system loads were modeled as the sum of a trend component, a periodic cycle component and residual component. By modeling each of the three components, the authors introduced a method to forecast hourly loads that combined information on previous loads with weather data.

References [4] through [12] represent the relevant work in the area of short-term load forecasting. The modeling work for the Hourly Predictor and Five-Minute Predictor reported here combine historical load information with weather data, as the literature suggests. However, as will be shown in the following sections, the method used to incorporate prior load data into the forecasts is unlike that used in most other studies.

SPECIFICATION AND EMPIRICAL DETERMINATION OF THE LOAD PREDICTORS

General Model for Time Behavior of Load

A short-term electrical load predictor follows from the structure of the model used to represent the actual load evolution over time, and, in general, is given by a nonlinear function.

$$y_t = f(y^t, \chi^t, t, \varepsilon_t) \qquad (1)$$

where

y_t = actual system load in megawatts (expressed as integrated hourly load in the case of the hourly predictor; and as instantaneous 5-minute load in the case of the 5-minute predictor).

y^t = $\{y_\tau;\ -\infty < \tau \leq t-1\}$; i.e., all past observed actual system loads

χ^t = $\{\chi_\tau;\ -\infty < \tau \leq t-1\}$, i.e., all past observed exogenous variables

t = time index

ε_t = additive random disturbances representing all unobserved effects on the system load

Attempting to develop a precise representation for $f(\cdot)$ can be very costly and although a very accurate predictor would result, it is an open question whether the improvement in accuracy over a more simple representation would justify the extra modeling effort. It may be possible to obtain sufficient accuracy with a quite simple representation. Therefore, it is advisable to begin with a simplified form for $f(\cdot)$ and elaborate upon it only as required in order to meet performance requirements. Such an approach leads one to the trivial representation:

$$y_t = \chi_t + e_t \qquad (2)$$

where χ_t is now a scalar variable representing the value of the load at t as predicted by a regression of the load on all observed exogenous factors. The new additive random (unobserved) error, e_t, now represents both the truly random disturbances and the modeling errors inherent in replacing $f(\cdot)$ with χ_t. For the purposes of the Hourly Predictor and the chosen test site of this project, Wisconsin Electric Power Company (WEPCO), χ_t is taken as the WEPCO hourly integrated load forecast and is computed as an aggregate of all causal effects, including weather. More specifically, the WEPCO hourly load forecasting algorithm forecasts a base component and a weather-sensitive component of the load. The base component is updated by exponentially smoothing the actual loads for like hours of the week. The weather-sensitive component is produced by a stochastic model whose inputs are temperature and dewpoint forecast data from two weather stations.

The basic model of Equation (2) has been used for development of both an Hourly Load Predictor and a Five-Minute Load Predictor. We have already described how the WEPCO hourly integrated load forecast provides the exogenous input, χ_t, to the Hourly Load Predictor. In a similar manner, the Hourly Predictor provides an exogenous input, χ_t, to the Five-Minute Predictor -- as will be discussed in detail later. Hence, three distinct models have been combined in a hierarchy. This hierarchical relationship, depicted in Figure 1, separates the load prediction into the three time-frames of (a) a day, (b) a few hours, and (c) 5-minute intervals within the next hour. The advantage of the hierarchical approach is that it simplifies the load modeling by decomposing the relevant time-frames and the relevant exogenous factors.

FIGURE 1

HIERARCHICAL STRUCTURE OF LOAD PREDICTION METHODS

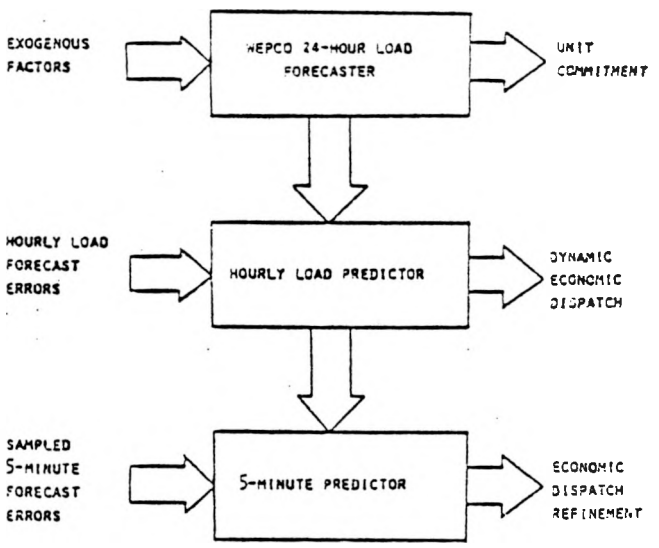

The optimal predictor for y_t can be obtained by formally taking conditional expectations across Equation (2).

$$y_{t+k|t-1} = \chi_{t+k} + e_{t+k|t-1} \qquad (3)$$

where $y_{t+k|t-1}$ denotes $E\{y_{t+k}|I^{t-1}\}$ and I^{t-1} symbolizes all the information available at time t-1. Likewise for $e_{t+k|t-1}$. The conditional expectation on χ_{t+k} reduces to χ_{t+k} itself since it is assumed that this value is always known into the future. From (2) it is seen that the structure inposed by (1) reduces the development of the optimal predictor to the development of an optimal predictor for e_t.

Similar arguments may be applied to the 5-minute predictor. The only difference being in the time scale and forecast horizon; i.e., replace t by τ to indicate time in units of 5-minutes instead of hours, and k=1 since we are only interested in one-step-ahead forecasts. The resulting predictor is then given by:

$$y'_{\tau+1|\tau} = \chi'_{\tau+1} + e'_{\tau+1|\tau} \qquad (4)$$

where

y'_τ = actual instantaneous system load at time τ

χ'_τ = some forecast of actual instantaneous load at time τ (derived from χ_t)

The primes are employed merely to differentiate the 5-minute sampled instantaneous load variables from the hourly integrated load variables.

All the known structure, representing all a priori information concerning observed cause-and-effect relationships is captured in the χ_t and χ'_τ variables. All the unknown structure, representing all the additional information which may be extracted from empirical data, is contained in the e_t and e'_τ variables. If systematic (serial correlation, for example) variation exists in these error terms then it can be employed to devise additional structure which will yield a more accurate forecast. The examination of e_t and e'_τ is a problem in statistical time series analysis and is discussed below.

Empirical Structure Determination

The analysis of the error term in Equation (2) and the estimation of a model for prediction of the error terms constitutes a problem in statistical time series analysis. The details of the methodology employed here are given in [13] and will not be presented. Only a summary of the relevant steps comprising the methodology is given to facilitate an understanding of the rationale behind the predictors selected for implementation in the AGC system.

In short, the Box-Jenkins methodology is an iterative procedure by which a model is constructed. The process proceeds from the most simple structure, with the least number of parameters, to as complex a structure as is required to obtain an "adequate" model -- "adequate" in the sense of yielding white residuals. This process of building increasingly complex models embodies its own philosophy of parsimony: "include only as many parameters as you really need". A schematic of the procedure is given in Figure 2. The first step is an identification of structure and employs sample autocorrelation patterns. After a structure has been chosen the next step involves an estimation of the coefficients inherent in the structure description. Next the optimal parameter estimates are inserted into the model to generate its estimated residuals. These are then subjected to diagnostic procedures to determine if they are indeed "white". If not, their sample correlogram is used to hypothesize a new structure and the cycle is begun anew. If the model satisfies all diagnostic tests it may then be implemented for on-line testing. The benefits of such a methodology are many, but primarily one will always be assured of a model which has the fewest possible parameters while still explaining all the systematic variation in the random errors.

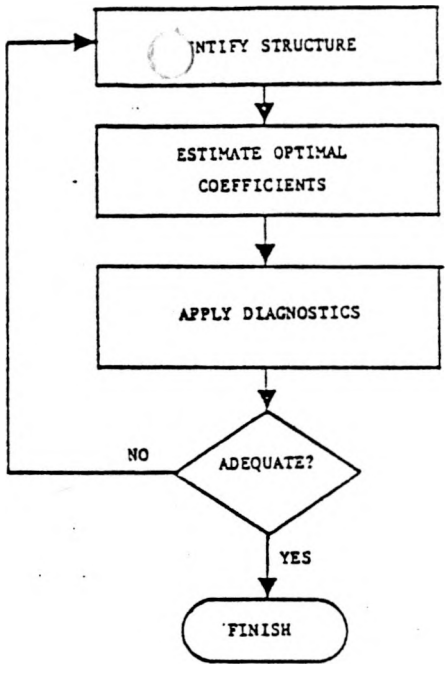

FIGURE 2

THE BOX-JENKINS METHODOLOGY

The particular form for e_t and e'_τ assumed by the Box-Jenkins methodology is the rational form:

$$e_t = \frac{c(L)}{d(L)}\,\eta_t \qquad (5)$$

where

$$c(L) = 1 + c_1 L + .. + c_q L^q \qquad (6)$$

$$d(L) = 1 + d_1 L + .. + d_p L^p \qquad (7)$$

where L is a shift (or lag) operator, i.e., $L^k \chi_t = \chi_{t-k}$, and η_t is a white noise process with the same normal distribution for every value of t. Thus by structure identification we mean specification of the integers p and q. In the econometric terminology (5) represents an autoregressive/moving-average ARMA(p,q) model. By examining the autocorrelation function for e_t it is possible to gain information regarding the values of p and q. This is the first step in the procedure.

Estimation of a set of coefficients $\{c_i, d_i\}$ is effected with the aid of maximum likelihood estimation algorithm described in [14].

THE HOURLY LOAD PREDICTOR: EVOLUTION OF THE TIME SERIES MODEL

Three different specifications of an hourly load predictor model were examined. The specifications were as follows:

- Specification I: Based on preliminary hourly load data for January and March, a twenty-fourth order differencing of the raw data was modeled as a first order autoregressive (AR) process.

- Specification II: The data were consecutively differenced, i.e., $e_t - e_{t-1}$, and modeled as a 24th order autoregressive process combined with a first order moving average (MA) of the residual error terms.

- Specification III: A different set of raw data were constructed to eliminate the input of the load dispatcher in the hourly forecast. A simple autoregressive (AR) model was identified as being robust across different data sets.

The different specifications were due to subsequent attempts to improve the hourly load predictor from the initial specification. Note that the third specification required a change in the raw data series since it was felt that the prior specifications exhibited residual error terms that were non-stationary. This is to say, estimation of the models exhibited wide variations in the parameters.

The maximum likelihood results for the three specifications can be found on Table 1. All six data sets are consecutive weekdays. The June and August sets are accompanied by dates since there were two samples taken from each month, respectively.

What appeared to be an attractive specification for January and March data with Specification I, failed to satisfy two requirements. First, application of the 24th order differencing to later data sets from June and August 1978 weekdays exhibited non-stationary properties in the sample autocorrelation functions. This indicated either that 24th order differencing might be appropriate for some but not all data sets, or that an alternative specification was required. Second, estimation of the AR(1) model on the 24th order differences exhibited parameter estimates for the autoregressive coefficient which were significantly different from the estimates made on January and March data (see left-most portion of Table 1, below)

TABLE 1
FULL INFORMATION MAXIMUM LIKELIHOOD ESTIMATION OF TIME SERIES SPECIFICATIONS ON WEPCO HOURLY LOADS

SPECIFICATION I

$$e_t - e_{t-24} = \frac{1}{1+d_1 L}\,\eta_t$$

Data Set	No. of Obs.	d_1	$\hat{\sigma}d_1$	$\hat{\sigma}_\eta$	R^2
January	96	-.76	.06	26.51	48.34
March	72	-.66	.09	30.76	43.16
June 5-9	120	-.32	.09	72.52	21.21
June 12-16	120	-.40	.09	75.47	14.67
August 7-10	96	-.87	.05	53.80	75.09
August 14-17	95	-.85	.05	42.73	72.65

SPECIFICATION II

$$e_t - e_{t-1} = d_1 L^{24}\,(e_t - e_{t-1}) + (1+c_1 L^1)\,\eta_t$$

Data Set	d_1	$\hat{\sigma}d_1$	c_1	$\hat{\sigma}c_1$	$\hat{\sigma}_\eta$	R^2
January	.54	.10	-.28	.13	24.01	31.92
March	.39	.12	-.35	.16	31.16	15.07
June 5-9	.16	.10	-.79	.07	59.12	21.20
June 12-16	.04	.10	-.73	.09	58.45	24.57
August 7-10	.23	.12	-.29	.10	49.02	0.0
August 14-17	.66	.10	.07	.10	48.70	29.98

SPECIFICATION III

$$e_t = \frac{1}{1 + d_1 L}\,\eta_t$$

Data Set	d_1	$\hat{\sigma}d_1$	$\hat{\sigma}_\eta$	R^2
January	-.78	.05	12.49	89.91
June 5-9	-.78	.06	40.20	60.75
June 12-16	-.82	.05	41.79	66.42
August 7-10	-.86	.05	41.33	73.47
August 14-17	-.76	.07	63.37	55.89

Notes:

d_1 is an autoregressive parameter

c_1 is a moving average parameter

$\hat{\sigma}$ is the estimated standard error

L^n is a polynomial lag operator of order n such that $L^n e_t = e_{t-n}$.

R^2 is the percent of variation in the dependent variable explained by the model.

Specification II exhibited widely varying parameter estimates for the autoregressive term. The range of values for the parameter labeled c_1, the moving average term, ranged from -.79 to .07. This implied that for some data sets the model might be ARMA(24,1) (e.g., January), AR(24) (e.g., August 14-17), or MA(1) (e.g., June 12-16).

Specification III was more robust across different data sets then the other two specifications. It should be noted that the sample autocorrelations of the noise process, η_t, indicated that greater complexity could be added to the AR(1) model. However, experimentation with more complex models never reduced the residual standard error by more than 5%, thus, the AR(1) model was selected to represent the hourly load predictor error process. In order to confirm the conclusion presented above, one additional data set for August 17-22 was subject to all three specifications. This data set was slightly different in that the third and fourth days were a Saturday and Sunday; respectively. All other data sets only considered weekdays. The results which can be found on Table 2 indicated that the AR(1) model's parameter estimates were similar to the processes estimated for the other five data sets. Specification I had an estimated AR parameter value of -.92, significantly larger than any previous estimate. Specification II estimation shows a significant (at rough a 95% confidence interval) AR(24) parameter value of .49, but the MA parameter is barely significant with 95% confidence for the August 17-22 data set. As discussed

TABLE 2

ESTIMATION OF THREE COMPETING SPECIFICATIONS ON WEPCO UNADJUSTED HOURLY LOAD ERROR: AUGUST 17-22

	d_1	$\hat{\sigma}d_1$	c_1	$\hat{\sigma}c_1$	$\hat{\sigma}_\eta$
SPECIFICATION I:					
$e'_t - e'_{t-24} = \frac{1}{1 + d_1 L'} \eta_t$	-.92	.03	--	--	42.99
SPECIFICATION II:					
$e'_t - e'_{t-1} = d_1 L^{24}(e'_t - e'_{t-1}) + 1 + c_1 L') \eta_t$	.49	.08	.19	.09	40.38
SPECIFICATION III:					
$e'_t = \frac{1}{1 + d_1 L'} \eta_t$	-.87	.04	--	--	44.51

Note: e'_t represents the error in the unadjusted 24 hour load predictor.

earlier, estimation of Specification II on different WEPCO data sets supported different structural forms; AR(24), MA(1) or ARMA(24,1).

It is our contention that an AR(1) model of the unadjusted hourly load error data is a simple and fruitful model to help predict hourly loads on the WEPCO system. The strength of the AR(1) model is the consistency of its parameter estimates for different types of days (e.g., weekdays vs. weekend) over different times of the year, and the model's ease in implementation.

EVOLUTION OF THE FIVE-MINUTE PREDICTOR

The formulation of a general model for a Five-Minute Predictor follows basically the same arguments as those developed above for the Hourly Predictor. The only difference being in the time scale and forecast horizon; i.e., replace t by τ to indicate time in units of 5-minutes instead of hours. The resulting predictor is then given by:

$$y'_{\tau+k|\tau} = \chi'_{\tau+k} + e'_{\tau+k|\tau} \qquad (8)$$

where:

y'_τ = actual instantaneous system load at time τ

χ'_τ = some forecast of actual instantaneous load at time τ (derived from χ_t); in particular, the spline interpolation derived from the Hourly Predictor Execution

e'_τ = error between actual load and forecasted load

All the known structure, representing all a priori information concerning observed cause-and-effect relationships is captured in the χ'_τ variable. All the unknown structure, representing all the additional information which may be extracted from empirical data, is contained in the e'_τ variable. If systematic (serial correlation for example) variation exists in these error terms then it can be employed to devise additional structure which will yield a more accurate forecast. As before, the examination of e'_τ is a problem in statistical time series analysis and is discussed below.

Generation of the e'_τ series was carried out in a manner consistent with the way in which the predictor would actually be implemented. First χ'_τ was computed by sampling a cubic spline interpolation [2], [3] on the predictions of hourly integrated load when they were fixed at the half-hour of each hour. Next the actual instantaneous minute-by-minute load was passed through a simple filter to compensate for any aliasing which might arise due to the 5-minute sampling process. Finally, these two sampled series were differenced to obtain e'_τ.

The sample autocorrelation of e_τ using WEPCO data for December 7, 1977 revealed significant serial correlation and at least first-order autoregression appeared likely. In fact, higher orders were called for, but an ARMA(1,0) was initially fit to illustrate the use of the autocorrelation diagnostic. Estimation of the ARMA(1,0) model produced autocorrelations in the residuals that appeared to be significantly different from zero. Thus, an ARMA(2,0) model was estimated. Its residuals produced a satisfactory autocorrelation function that indicated random behavior of the residuals. The second order model is all that is necessary to adequately describe all of the systematic variation in e'_τ. Similar results were obtained for WEPCO data taken over March 7, 1978 and March 8, 1978. The results of the maximum likelihood estimation for the three models are presented in Table 3 (variable m is the mean of the error, e'_τ).

TABLE 3

MAXIMUM LIKELIHOOD ESTIMATION OF ARMA(2,0) MODEL ON WEPCO 5-MINUTE LOADS

$$e'_\tau - m = \frac{1}{1 + d_1 L + d_2 L^2} \eta_t$$

Data Set	d_1	d_2	$\hat{\sigma}d_1$	$\hat{\sigma}d_2$	$\hat{\sigma}_\eta$	R^2
Dec. 7	-1.537	+0.579	.057	.057	4.71	97
March 7	-1.537	+0.564	.058	.057	3.86	98
March 8	-1.474	+0.551	.059	.059	4.11	93

From results given in Table 3, it appears that the ARMA(2,0) model has consistent parameter estimates for different days over a few different times of the year. The model is also quite simple to implement. Spline interpolation to the outputs of the Hourly Predictor to obtain the χ'_T variable in Equation (8) has some benefits. Namely, a priori knowledge about the daily load shape can be used to obtain a spline interpolation that not only passes through the hourly predictor points, but also has the desired daily load shape. This improves the capture of all a priori information in the variable χ'_T. One aspect of the model that requires some improvment is that the smoothing of instantaneous load (to prevent aliasing) causes variable e'_t to lag the actual load error. Work is underway to modify the smoothing to reduce this lag. Altogether, the results for the Five-Minute Predictor have to be considered tentative. While much on-line testing has been conducted on the Hourly Predictor at WEPCO (as discussed in the next section), testing of the Five-Minute Predictor against actual WEPCO load has, at this time, not been completed. There is preliminary evidence from the tests that the ARMA(2,0) model structure is valid -- but that the model parameters vary slightly with day-of-week and time-of-day.

WEPCO IMPLEMENTATION AND TESTING OF THE HOURLY LOAD PREDICTOR

The new Hourly Load Predictor was tested over six days (November 6-9, 13-14, 1978). Comparisons were made between the existing WEPCO System (24-hour) Load Forecast (SLF) program and the first and second hour-ahead outputs of the Hourly Predictor. The observed standard deviation of the load predictions are shown in Table 4.

TABLE 4

STANDARD ERRORS OF HOURLY LOAD PREDICTORS -- SIX DAY PERIOD

PREDICTION	STANDARD ERRORS (MW)					
	MONDAY Nov. 6	TUESDAY Nov. 7	WEDNESDAY Nov. 8	THURSDAY Nov. 9	MONDAY Nov. 13	TUESDAY Nov. 14
System Load Forecast (SLF)	60.45	37.59	27.3	21.65	103.66	100.45
Hourly Predictor (One hour ahead)	36.00	25.84	22.9	24.24	29.12	32.49
Hourly Predictor (Two hours ahead)	38.73	32.97	26.75	28.19	38.04	37.90

It is interesting to note from Table 4 that when the SLF program error is small (as on November 9) with near-zero mean value, the Hourly Predictor's performance is not much different than that of the System Load Forecast. This implies that the principal function performed by the Hourly Load Predictor is the elimination of bias in the System Load Forecast.

An hour-by-hour comparison of the Hourly Predictor with actual WEPCO load on November 13, 1978 is given in Table 5.

Abbreviations used in Table 5 are:

- SLF = System Load Forecast value for given hour
- HP1 = Hourly Predictor value, predicted one hour ago, for a given hour
- HP2 = Hourly Predictor value, predicted two hours ago, for a given hour
- E_S = Error of the SLF value
- E_1 = Error of the HP1 value
- E_2 = Error of the HP2 value

TABLE 5

WEPCO SYSTEM LOAD FORECAST AND HOURLY PREDICTOR OUTPUTS FOR NOVEMBER 13, 1978

HOUR	LOAD AND PREDICTIONS (MW)				PREDICTION ERRORS (MW)		
	ACTUAL	SLF	HP1	HP2	E_S	E_1	E_2
1	1493	1434	1524.2	1514.0	59	-31.2	-21.0
2	1430	1394	1454.0	1483.5	36	-24	-53.5
3	1422	1383	1420.6	1443.8	39	1.4	-21.8
4	1431	1371	1425.4	1430.9	60	5.6	0.1
5	1477	1424	1483.5	1477.9	53	- 6.5	- 0.9
6	1630	1583	1636.3	1642.2	47	- 6.3	-12.2
7	2019	1930	1977.4	1983.5	89	41.6	35.5
8	2447	2341	2427.7	2388.8	106	19.3	58.2
9	2638	2537	2641.4	2621.9	101	- 3.4	16.1
10	2713	2602	2702.8	2705.0	111	10.2	8.0
11	2769	2646	2757.3	2748.6	123	11.7	20.4
12	2786	2617	2739.2	2727.8	169	46.8	58.2
13	2675	2531	2697.1	2652.5	144	-22.1	22.5
14	2690	2546	2690.6	2709.8	144	- .6	-19.8
15	2627	2478	2622.2	2623.0	149	4.8	4.0
16	2576	2462	2610.8	2606.3	114	-34.8	-30.3
17	2687	2505	2620.9	2653.6	182	66.1	33.4
18	2804	2672	2850.7	2789.5	132	-46.7	14.5
19	2732	2659	2792.9	2835.0	73	-60.9	-103.0
20	2662	2603	2679.9	2738.4	59	-17.9	-76.4
21	2596	2526	2587.0	2606.1	70	9	-10.1
22	2399	2358	2429.0	2420.6	41	-29	-21.6
23	2169	2118	2160.6	2187.9	51	8.4	-18.9
24	1929	1878	1928.9	1922.0	51	0.1	7.0

CONCLUSIONS

A set of procedures and algorithms for the short-term prediction of electric power system load have been developed empirically and tested on an actual power system. The primary conclusions of the study are:

- The feasibility of short-term load prediction based on models derived from the Box-Jenkins time series methodology has been demonstrated.
- The resulting predictor models are simple in structure and (at least in the WEPCO application) have consistent parameter estimates for different types of days (e.g., weekdays vs. weekends) over different times of the year.
- The short-term load prediction methodology requires minimal software additions to an existing automatic generation control system; however, it depends upon the prior existence of a 24-hour integrated hourly load forecasting method. The prior existence of a 24-hour integrated hourly load forecasting method is, however, quite common -- as such load forecasts are normally needed for daily unit commitment decision-making.
- For the WEPCO tests, the Hourly Load Predictor was successful in explaining from 55 to 90 percent of the random errors between the actual integrated hourly load and the 24-hour forecast of integrated hourly loads. The 5-Minute Predictor was successful in explaining from 93 to 98 percent of the random errors between actual load and the spline interpolation of the hourly load predictions.

Significant benefits are foreseen for utilities that are faced with the problems of either (a) fully

utilizing the rate-of-response capability of the generation units in tracking system load, (b) making on-line adjustments to the unit commitment schedule and spinning reserve, or (c) implementing valve-point loading of units. For all of these problems, a basic requirement is foreknowledge of the load trend.

ACKNOWLEDGEMENT

The work reported in this paper is part of a current effort to develop an advanced AGC software package. This demonstration project, sponsored by the U.S. Department of Energy, includes the design, implementation and testing of an integrated and coordinated set of algorithms for AGC. Systems Control, Inc., Wisconsin Electric Power Company (WEPCO), and Control Data Corporation are jointly conducting the effort. The individual assistance and guidance of Lester H. Fink, U.S. DOE Project Manager, is gratefully acknowledged.

REFERENCES

1. L.H. Fink, H.G. Kwatny, J.P. McDonald, "Economic Dispatch of Generation Via Valve-Point Loading", IEEE Trans. on Power Apparatus and Systems, Vol. PAS-88, No. 6, pp 805-811, June 1969.

2. A.K. Cline, "Scalar-and Planar-Valued Curve Fitting Using Splines Under Tension", Communications of the ACM, Vol. 17, No. 4, April 1974, pp 218-220.

3. A.K. Cline, "Algorithm 475, Six Subprograms for Curve Fitting Using Splines Under Tension [E2]", Communications of the ACM, Vol. 17, No. 4, April 1974, pp 220-223.

4. D.H. Budenaers, "Sequential Short-Term Electric Power Demand Forecasting", Proc. American Statistical Assoc., 1973.

5. K.C. Chen and P.R. Winters, "Forecasting Peak Demand For An Electric Utility With a Hybrid Exponential Model", Management Science, Vol. 12, No. 12, August 1966.

6. W.R.Christiaanse, "Short-Term Load Forecasting Using General Exponential Smoothing", Trans. IEEE, July 1970.

7. S.L. Corpensing, N.D. Reppen and R.J. Ringles, "Experience With Weather Sensitive Load Models For Short and Long-Term Forecasting", Trans. IEEE, November, 1973.

8. E.D. Farmer and M.J. Potton, "Development of On-Line Load-Prediction Techniques With Results From Trials in the South-West Region of the CEGB", Proc. IEEE, Vol. 115, No. 10, October, 1968.

9. F.D. Galiana and F.C. Schweppe, "A Weather Dependent Probabilistic Model For Short Term Load Forecasting", Trans. IEEE, December 1971.

10. P.C. Gupta and K. Yanada, "Adaptive Short-Term Forecasting of Hourly Loads Using Weather Information", Trans. IEEE, February 1972.

11. R. Pyne, "Bus Load Forecasting and Its Intended Use in System Security Analysis", prepared for Engineering Foundation Conference at BPA in Portland, Oregon, July 1972.

12. J. Toyoda, et.al., "An Application of State Estimation to Short Term Load Forecasting", Trans. IEEE Vol. PAS-89, No. 7, September-October 1970, pp 1678-1686.

13. G.E.P, Box and Jenkin, Time Series Analysis: Forecasting and Control, San Francisco, Holden-Day, 1970.

14. K.D. Wall, "Estimation of Rational Distributed Lag Structural Form Models", Annals Econ. Social Meas., Vol. 5, No. 2, pp 53-63, 1976.

15. "Development and Implementation of Advanced Automatic Generation Control Software Package", U.S. Department of Energy Contract EC-77-01-2118, Systems Control, Inc. Palo Alto, California, (L.H. Fink, U.S. Department of Energy Project Manager).

16. T.M. Athay, H.G. Kwatny, R.G. Smith, "Area Load-Frequency Control", Proceedings of Sixteenth Annual Allerton Conference, Monticello, Illinois, October 4-6, 1978.

APPENDIX C

DYNAMIC ECONOMIC DISPATCH OF GENERATION

Dale W. Ross

Sungkook Kim

Systems Control, Inc.
1801 Page Mill Road
Palo Alto, California

ABSTRACT

A set of procedures and algorithms are developed for dynamic economic dispatch of generation units. When coupled with a short-term load predictor, "look-ahead" capability is provided by the dynamic economic dispatch that coordinates predicted load changes with the rate-of-response capability of generation units. Dynamic economic dispatch also enables valve-point loading of generation units. Two examples are provided which demonstrate that our approach overcomes the severe limits on the number of units that could be dynamically dispatched in past approaches.

INTRODUCTION

The basic purpose of the economic dispatch function is to schedule the outputs of the on-line power generators serving a particular area so as to meet the net area load at least cost. Most present day methods for economic dispatch are "static" optimization techniques that do not use, as input load data, anything more than a smoothed estimate of present load. They do not "look ahead" over the future time horizon, using predicted load trends (say, of 1-2 hours ahead) to determine the economic allocation of generation to the load. Such predictive or dynamic economic dispatch, as we shall call it, would be beneficial for several reasons:

- Economic dispatch is to track the secular load component. In state-of-the-art AGC, the secular load is determined by filtering or smoothing the actual load. Such smoothing introduces a large time lag in the economic dispatch. Short-term load prediction, combined with dynamic economic dispatch, overcomes this lag, and hence improves generation economics.

- A static dispatch, unlike a dynamic dispatch, cannot foresee that the present loading of units can affect the total generation rate-of-response capability at a future time. In order to better match generation to load, system dispatchers frequently have to resort to manual rescheduling of units. A dynamic economic dispatch, which determines the economic allocation of generation with knowledge of both the present and future load could lessen these problems. The "look ahead" capability enables a better allocation of regulating margin in the near future. For instance, it can aid in reserving rate-of-response capability so that generation can match rapidly changing load.

- The potential benefits of valve-point loading cannot be obtained without having load prediction capability, and using it to dynamically dispatch generation (some units being dispatched to valve-points). As discussed in [1], one basic requirement for successful implementation of valve-point loading is that the amount of regulating capacity necessary to take up the difference between block-loaded generation and actual load is a function, among other things, of the amount of time required to pick up or drop one or more blocks of generation. Furthermore, some minimum amount of time, say 10 minutes, must be provided during which a unit remains at a given valve position without a reversal of load, otherwise the economic benefit of the valve-point loading will not be achieved. These considerations mean that successful valve point loading requires foreknowledge of the load trend.

In summary, dynamic economic dispatch, operating over a time horizon of up to a few hours, has potential for improving automatic generation control. This paper discusses a new approach taken in developing a dynamic economic dispatch method suitable for use in today's automatic generation control systems. The method is based upon successive approximations dynamic programming [2].

A previous paper [3] discusses the short-term load prediction methodology that provides the basic inputs to the dynamic economic dispatch. The outputs of the dynamic economic dispatch are the economic target trajectories of the generation units' power outputs. These target economic trajectories are then tracked by a load-frequency controller (LFC). A previous paper [4] discusses the LFC logic that has been developed for this tracking function. While the emphasis of this paper is upon dynamic economic dispatch, the work reported here is part of a broader effort to develop an advanced automatic generation control (AGC) software package. This development, a U.S. Department of Energy demonstration project [5], includes the design, implementation and testing of an integrated and coordinated set of AGC algorithms.

PREVIOUS WORK ON DYNAMIC ECONOMIC DISPATCH

Previous work, principally that of [6] - [8], has correctly formulated the AGC problem as a dynamic optimal tracking control problem. In this formulation the economic dispatch function provides target economic trajectories for the generation units. The optimal AGC response tracks these desired unit economic trajectories while simultaneously controlling total area generation to track area load plus schedule [4]. If the dynamic economic dispatch requires changes in units' megawatt output that persist for more than a few seconds, then the rate of change of megawatt output must be limited to a prescribed value for each unit, to satisfy limitations on boiler and combustion equipment response rates.

The importance of such rate limit constraints in determining unit economic trajectories has been previously demonstrated in [6], [7].

The optimal dynamic dispatch of thermal units was originally described in [6], [7]. There economic load allocation and supplementary control action were combined into a single dynamic optimal control problem. An optimal feedback controller was designed using Pontryagin's Maximum Principle. The procedure was limited to a two-generator system due to computational problems in storing complex switching surfaces for more generators.

A multi-pass dynamic programming approach to the dynamic economic dispatch problem was taken in [8]. Optimal trajectories were generated for up to five dispatched units. Valve-point loading was considered. Basically, the approach employed "coarse-grid, fine-grid" methods to reduce the dimensionality problems usually associated with dynamic programming. Ability to handle dynamic valve point loading was an important feature of the method.

Another approach to the dynamic economic dispatch problem was taken in [9]. Optimal generator output trajectories were solved for using quadratic programming. A method was also developed for converting an open-loop control schema, derived from a load forecast, into a feedback control scheme capable of correcting for differences in actual and forecasted load. In addition to the steady-state production cost functions, Ref. [9] considered costs associated with the act of changing the outputs of the generators.

The principal limitations of the past approaches to the dynamic economic dispatch problem have been dimensionality limitations. In the present paper we solve an example dynamic economic dispatch problem involving 15 generating units. In our solution, we require only 360 grid-points (MW discretization levels) per stage. This same problem would require approximately 1.4×10^7 grid-points if the method of [8] were applied. The method of [8], [3] would have been even more burdensome. In short, the successive approximations dynamic programming method developed in the present paper brings large-scale dynamic economic dispatch problems into the realm of feasible solution with modest computer resources.

MATHEMATICAL STATEMENT OF THE PROBLEM

The optimal dynamic dispatch problem is that of allocating generation from n "dispatchable" units so that operating constraints are satisfied and the production costs are minimized. It is assumed that a load prediction is available over the entire dispatch horizon (of two or more hours). Furthermore, it is assumed that the predicted load is specified at uniform discrete time intervals (say, of 5 minutes) indexed as $t = 0,1,2,\ldots,T$. Since (a) not all units will be on AGC and, (b) the area generation requirement must be adjusted for the net scheduled interchange -- it is assumed that the load prediction, the manually-operated generation's output, and planned tie schedules have been combined to obtain the net generation requirements for all units on AGC over the time horizon $t = 0,1,2,\ldots,T$. With these preliminaries, a statement of the optimal dynamic dispatch problem is contained in the discussion below.

The net generation requirement is to be met at each time instant by the sum of the outputs of the generators being scheduled. Formally,

$$\sum_{i=1}^{n} x_i(t) = NETG(t) \qquad (1)$$

$$t = 0,1,\ldots,T$$

where

$x_i(t)$ = output of ith generator at time t

n = number of generating units scheduled

T = number of time intervals in scheduling interval

NETG(t) = net generation requirement for all units on AGC at time t

The output of each generator can be changed directly. Formally,

$$x_i(t+1) = x_i(t) + u_i(t) \qquad (2)$$

where

$u_i(t)$ = change in output of ith generator over time interval t

These changes are bounded through the equations

$$RL_i \le u_i(t) \le RU_i \qquad (3)$$

where

RU_i = maximum increase in output of generator i over one time interval

RL_i = maximum decrease in output of generator i over one time interval

Finally, the cost of operating each generator over the scheduling interval can be expressed as

$$J_i = \sum_{t=1}^{T} f_i(x_i(t)) \qquad (4)$$

where

J_i = total cost of operating generator i over the scheduling interval

$f_i(x_i(t))$ = cost of operating generator i at output $x_i(t)$ over time interval t

The problem can then be written as follows: given a set of generators with initial outputs $x_i(0)$, find a set of changes in output $u_i(t)$, $t = 0,1,2,\ldots,T-1$ such that total cost J, where

$$J = \sum_{i=1}^{n} J_i = \sum_{i=1}^{n} \sum_{t=1}^{T} f_i(x_i(t)) \qquad (5)$$

is minimized, subject to the system dynamic equation

$$x_i(t+1) = x_i(t) + u_i(t),$$

and the constraint on generator outputs (3) and the constraint that the net system load must be met at each time instant (1).

SUCCESSIVE APPROXIMATIONS DYNAMIC PROGRAMMING ALGORITHM

An algorithm for dispatching generation to (predicted) load over a given time-horizon has been developed that uses the dynamic programming successive approximation technique [2]. Normally, this technique involves solving a sequence of dynamic programming problems, each having one state variable. For the reasons given below, the usual approach has been modified to entail solving a sequence of dynamic programming problems, each having two state variables.

If load must be met exactly at each time in the dispatch horizon, then it is not possible to allow independent variation of the output of a single generator. One means of overcoming this difficulty would be to vary one's output while all the remaining units are constrained to move at equal incremental cost within an allowable band constructed about their current trajectories. Yet another, and simpler approach is to allow

one unit's output to be varied while a second unit's output is simultaneously adjusted so that the load constraint is satisfied. In the state space, this constrains the successive approximation searches to lie along the lines depicted in Figure 1.

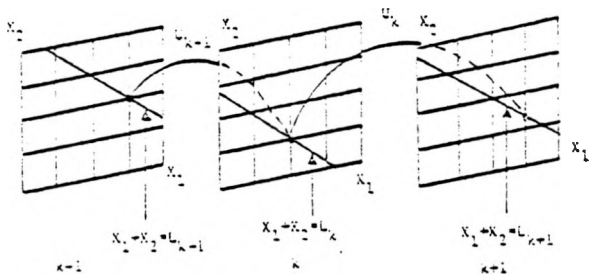

X_1 = output of 1st unit

X_2 = output of 2nd unit

L_k = net generation requirement, k^{th} stage

FIGURE 1 PAIRING OF UNITS IN SUCCESSIVE APPROXIMATIONS DYNAMIC PROGRAMMING

In this pairing approach, various pairing schemes can be applied among the set of dispatchable units. For the example problems given later in this paper, we have experimented with a number of pairing schemes. We have not found any particular scheme to result in the best (with respect to convergence time) overall computational results. One scheme that has been tested we call a "circular" pairing scheme. With this scheme, the units are indexed by $i = 1,2,\ldots,N$ with $i = 1$ corresponding to the "cheapest" unit and $i = N$ corresponding to the "most expensive" unit. The "cheapest" unit is the one whose incremental cost curve lies below all other units' incremental cost curves (within the MW range of this "cheapest" unit). The next cheapest unit is taken to be the one with the next lowest cost curve -- and so on. The circular pairing scheme then considers the units in the pairs: 1 with 2, 2 with 3, 3 with 4,....,(N-1) with N and N with 1.

In the second scheme, which we call a "spiral" pairing scheme, the cheapest unit was first paired with the most expensive unit. On the next successive approximation pass the most expensive unit was paired with the second cheapest unit. On the third pass, the second cheapest unit was paired with the second most expensive unit -- and so forth. A third scheme was tested that was a blend of the first two.

The basic idea of the successive approximations technique is to break the large problem of Equations (1) through (5) containing many control variables (the change in generation variables, $u_i(k)$) into a number of subproblems that each contain only one control variable. By considering the generation units in pairs, each subproblem has only one control variable and only one state variable. Since the computational requirements of dynamic programming increase exponentially with the number of state variables, there is a large reduction in the computational difficulty. Accordingly, although dynamic programming would be infeasible, if applied straightforwardly to the dynamic economic dispatch problem -- it becomes quite feasible if applied iteratively to one pair of units at a time.

The dynamic programming successive approximations (DPSA) algorithm that has been developed for problem (1) - (5) is characterized in three ways: a) the iterations or successive approximations are based upon pairings of units (an "artificial unit" is included among the units, as discussed later), b) each resulting one-dimensional dynamic program is solved by forward dynamic programming, and c) the special structure of the cost function, Equation (4) and the dynamics Equation (2), yield a simple solution procedure for applying Bellman's Principle of Optimality [10,11] at each time-stage of the dynamic program.

Forward Dynamic Programming

As each pair of units is considered for a single successive approximations pass, a single state-variable/single control variable dynamic program is solved to determine the optimum dynamic dispatch for the pair, with the loadings on the other units held fixed. At the time that the dynamic economic dispatch is computed, the outputs of the units at the initial time are known. Accordingly, the dynamic programming proceeds forward in time, starting from the initial unit loadings. Thus the algorithm iterates forward in time-stages, using Bellman's Principle of Optimality:

$$I(x,k) = \min_{u(k-1)} \left\{ \sum_i f_i(x_i(k)) + I(x-u_{k-1}, k-1) \right\} \qquad (6)$$

where $I(x,k)$ is the minimum cost to state x at stage k.

Equation (6) is particularly simple to solve because the unit production costs, $f_i(\cdot)$, are not functions of the control -- but are only functions of the unit outputs.

Special Structure of Cost Function -- and Bellman's Principle of Optimality

At each time-stage, k, of the one state-variable dynamic program, Bellman's Principle of Optimality (6) must be applied to determine the optimum control (generation change) that will bring the unit to an output level, x. Equation (6) is solved for the minimizing control by fixing the output, x, of the unit at time-stage k. Then all controls $u(k)$ that will yield output x at time k, starting from some feasible state x_{k-1} at the previous time-stage are found. The minimizing control is the one that solves Equation (6) for feasible x_{k-1}.

Due to the fact that the production cost functions, $f_i(x_i(k))$, in Equation (6) do not depend explicitly on $u(k-1)$, and also because $x_k = u_{k-1} + x_{k-1}$, Equation (6) reduces to:

$$I(x,k) = \sum_i f_i(x_i(k)) + \min_{\substack{\text{possible} \\ \text{prior} \\ x_{k-1}}} \left\{ I(x_{k-1}, k-1) \right\} \qquad (7)$$

Therefore (6) or (7) is minimized by simply searching among the possible prior state levels for the one that has the minimum cost. This optimum previous state is saved and the new optimum cost through stage k is computed from (7).

Furthermore, the prior stage's feasible states, K_{k-1} that correspond to the given value of K_k are found directly from the unit rate limits, as depicted in Figure 2.

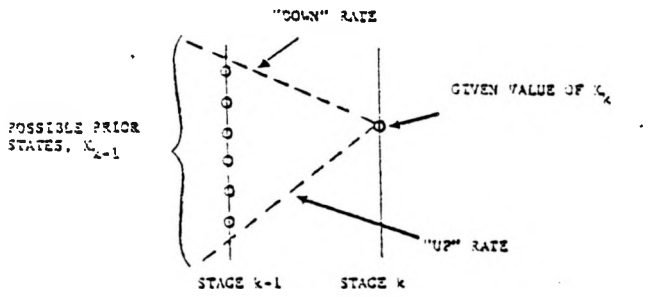

FIGURE 2 PRIOR STAGE FEASIBLE STATES FOUND BY APPLYING KNOWLEDGE OF RATE LIMITS

In summary then, the special structure of the dynamic economic dispatch problem has been used to advantage in simplifying the dynamic program.

Artificial Unit and Initial Feasible Solution

Prior to the application of successive approximations dynamic programming to the problem solution, it is necessary to obtain feasible initial trajectories of unit outputs over the entire dispatch horizon. A static dispatch technique (namely, a minimum marginal cost algorithm which is discussed later) is used to initialize the unit outputs over the dispatch horizon. In order to guarantee that the static dispatch can initialize the units so that their initial trajectories are feasible (meet all constraints), an artifice is used. Namely, an additional fictitious unit, called the "artificial" unit is used in the dispatch. This artificial unit has much higher production costs than the other (actual) units and has very high rate limits. It is loaded by the static dispatch algorithm at time-stages for which the other units cannot satisfy the net generation requirement. The artificial unit therefore expands the total number of units from N to N + 1.

The minimum marginal cost algorithm for initializing unit trajectories considers all units together; that is, there is no need for it to use successive approximations. Once, however, the initial unit trajectories are passed to the DPSA algorithm, the final dynamic dispatch is achieved by the successive approximations method with pairing of two units at each iteration. In effect, DPSA iteratively attempts to both: (a) unload the (expensive) artificial unit — shifting its generation to the (cheaper) actual units while obeying rate limits on the units, and (b) shift generation, for two units at a time, among the actual units to further reduce the total production costs.

The principal steps in the minimum marginal cost algorithm (executed once for each time-stage in the dynamic dispatch horizon) are:

- The rate limits (in both up and down directions) on each unit determine the number of generation increments by which the unit output can be raised/lowered from its last output value. These become the candidate increments available on each unit. The candidate increments for the artificial unit are its entire output range.
- Before determining which of the available generation increments will be used on each unit, the algorithm assumes that each unit starts from the lowest output level within its current range of increments.
- The candidate increments among all units are placed in a list called the "candidate list".
- The increments on the candidate list are ranked by their cost into a ranking array.
- The increments are chosen one-by-one until the total generation requirements for the time-stage is met. Increments are chosen in the order of increasing cost under the further condition that a new increment may not be allocated to a unit unless all other increments between the low and of the available increments and the new increment have already been allocated. As increments are thus chosen from the ranking array, they are placed on a "solution list".
- The solution list gives the new economic dispatch results for the units. The new unit loadings become the last output values considered again at the next time-stage.

A few final comments concerning the use of the artificial unit are:

- It guarantees a feasible solution from DPSA, even when actual load rate exceeds area generation response capability (e.g., during a schedule change). In such cases, the amount of residual generation on the artificial unit corresponds to the drawing of power over the tie lines.
- It admits the possibility of adjusting the production costs on the artificial unit to obtain either rigid matching of generation to load or an approximate matching of generation to load that perhaps takes the rate-of-response limits of the units less.

Valve-Point Loading

The successive approximations dynamic programming algorithm (DPSA) and the minimum marginal cost algorithm (MINMAR) have been adapted to handle valve point loading of units. The algorithms themselves needed no modification for this function; valve-point loading is accomplished via the representation of the valve points in both the unit incremental production cost functions (used by MINMAR) and the unit production cost functions (used by DPSA). The valve-point representation in the cost functions is discussed later.

RESULTS

Descriptions of Units and Load Scenarios

Example dynamic economic dispatch results are presented below for a utility that dispatches 15 generating units. All unit data required for the dynamic economic dispatch are listed in Table 1 except for the artificial unit, which is discussed later. The production cost curve for each actual unit was approximated by a quadratic function of net generation output. That is, the production cost for each unit at a generation output of

x megawatts was approximated by:

$$\text{Production Cost (\$/HR)} = ax^2 + bx + c \qquad (8)$$

Correspondingly, the incremental cost at the generation output was approximated by:

$$\text{Incremental Production Cost (\$/MWH)} = 2ax + b \qquad (9)$$

Both the production cost and the incramental cost of the artificial unit are set to very large values. The rate-of-response of the artificial unit is assumed to be much larger than the 15 dispatched units; a value of 100 MW/MIN was arbitrarily selected for the artificial unit. The artificial unit was assumed to be dispatchable in a -50 MW to +50 MW output range. Finally, the production cost function for this unit was arbitrarily selected to be:

$$\text{Production Cost (\$/HR)} = b|x|, \qquad b = 100 \text{ \$/MWH}$$

Look-Ahead Capability

Figures 4 and 5 show optimal economic dispatching of generating units for Case 1. Since the available aggregate rate of response was never less than the rate of change of the generation requirement in the static dispatch, the results from the static dispatch of MIXMAR and the dynamic dispatch of DPSA should theoretically be identical. However, due to the integer discretization of both MW outputs and cost curves in the program it was found that there were slight differences in unit outputs which are not greater than $\pm$ 1 MW at any time. Figure 4 and 5 show that differences are very minor. These differences do not cause total production cost to differ by more than the cost tolerance (convergency threshold for the successive approximations scheme; a value of $1 was used) which was input to the DPSA program.

TABLE 1

PRODUCTION COST DATA FOR GENERATION UNITS

UNIT NUMBER	RATE LIMIT (MW/MIN)	a*	b*	c*	UPPER ECONOMIC LIMIT (MW)	LOWER ECONOMIC LIMIT (MW)	INITIAL GENERATION (MW)
1	3.000	.005	5.627	261.196	225.000	70.000	130.000
2	3.000	.006	5.506	264.634	240.000	70.000	173.000
3	5.000	.004	6.383	190.502	285.000	110.000	162.000
4	5.000	.005	6.295	230.154	282.000	110.000	140.000
5	1.500	.007	6.654	112.922	114.000	30.000	64.000
6	1.500	.012	6.362	143.092	91.000	30.000	51.000
7	1.500	.012	6.515	135.334	105.000	40.000	45.000
8	1.500	.016	6.268	154.298	104.000	30.000	44.000
9	1.800	.022	7.750	93.100	70.000	35.000	35.000
10	1.800	.024	8.062	80.200	63.000	35.000	35.000
11	1.800	.030	7.667	99.960	77.000	35.000	35.000
12	1.800	.029	7.716	105.840	66.000	35.000	35.000
13	1.800	.030	8.317	91.140	77.000	35.000	35.000
14	3.000	.010	11.752	100.659	118.000	20.000	20.000
15	3.000	.009	11.993	101.790	118.000	20.000	20.000

* Note: a, b, and c are the coefficients appearing in Equations (8) and (9).

Figure 3 shows the two load scenarios of this example. These two scenarios are labeled Case 1 and Case 2. Case 1 is a morning load pickup that occurs over a one hour and twenty minute period for which the aggregate generation requirement increases by approximately 530 MW. Case 2 is constructed from Case 1 by the introduction of a large scheduled power import of 325 MW that is ramped over a 10-minute interval starting 55 minutes into the scenario. The time scale of Figure 3 is labeled in terms of stages; a stage is 5 minutes which is the assumed time between successive economic dispatches. In both cases, aggregate maximum generation of all actual units is greater than the generation requirement and the aggregate rate limit of all actual units is greater than the change in the generation requirement. Therefore, the generation requirement should be able to be met at all times.

These two cases illustrate advantages of the dynamic economic dispatch approach. Two advantages: (1) look-ahead capability, and (2) ability to valve-point load units are discussed below.

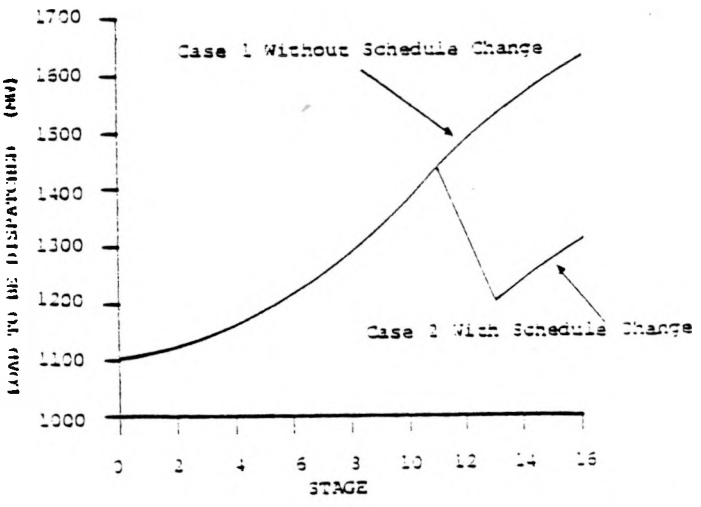

FIGURE 3 TIME PROFILE OF LOAD TO BE DISPATCHED

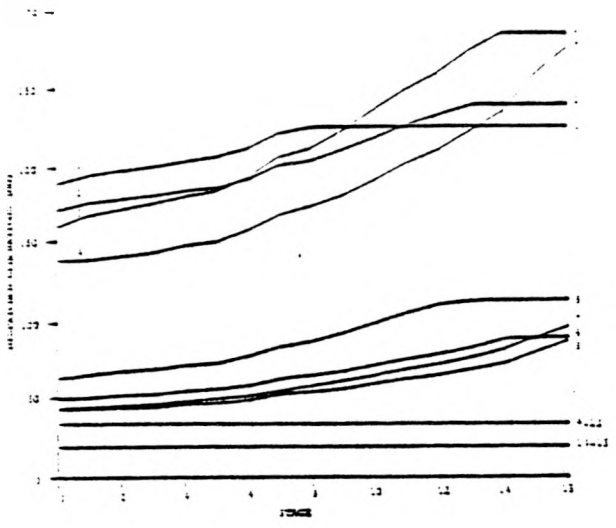

FIGURE 4 MINMAR ECONOMIC DISPATCH OF GENERATING UNITS FOR CASE 1

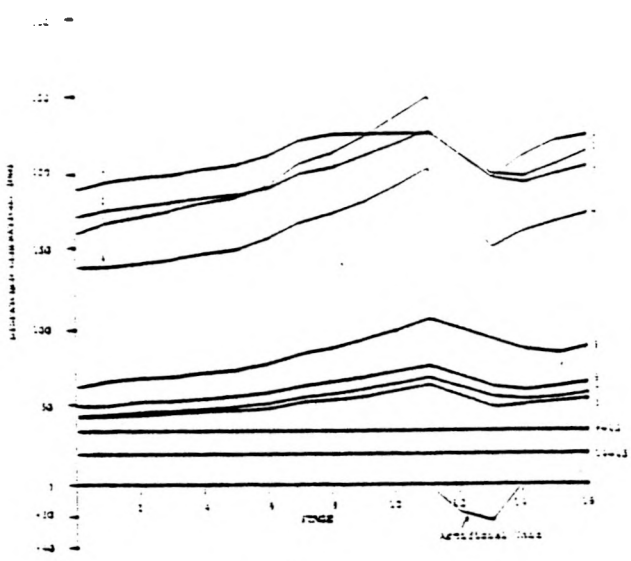

FIGURE 6 MINMAR ECONOMIC DISPATCH OF GENERATING UNITS FOR CASE 2

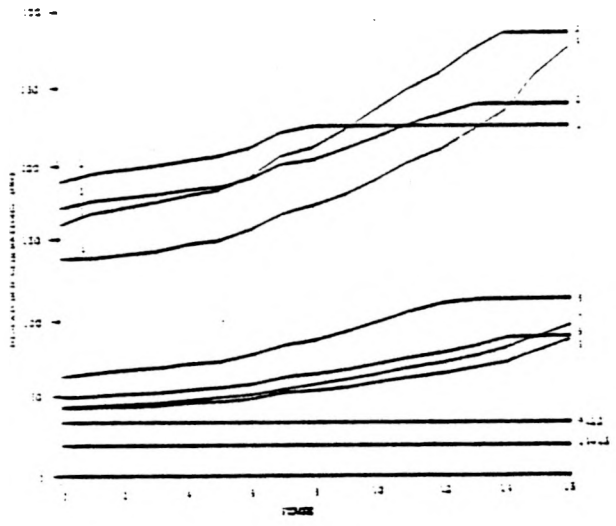

FIGURE 5 DPSA ECONOMIC DISPATCH OF GENERATING UNITS FOR CASE 1

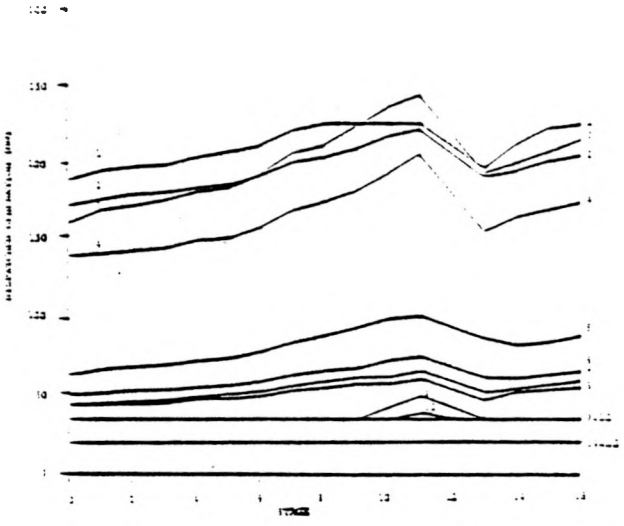

FIGURE 7 DPSA ECONOMIC DISPATCH OF GENERATING UNITS FOR CASE 2

Figure 6 and 7 are optimal economic dispatching of generating units for Case 2 using MINMAR and DPSA respectively. Here, we notice that on Figure 6 the artificial unit is dispatched at 12th and 13th stage. The negative output dispatch of the artificial unit indicates that the generation requirement was decreasing at the higher rate than the static dispatch of MINMAR can handle. Even though the aggregate rate of response of actual units is sufficient to follow the sudden schedule change, the static dispatching approach of MINMAR could not follow it without using the artificial unit. The reason for this is that Units 9 through 15 had been operated at their lower economic limits during the previous stages and therefore could not contribute to meeting the sudden decrease in the generation requirement without the look ahead capability. However, using the trajectories given by MINMAR as the initial trajectories, DPSA is able to remove the output of the artificial unit and reallocate it to the actual units as shown in Figure 7. Also to be noted on DPSA dispatch

is that Units 9 and 10 generate more output at the 10th and 11th stages than in the stage-wise dispatch of MINMAR which is compensated for by slight drops in the outputs of Units 2, 3 and 5 through 8. Even though the total units' output at these stages exactly meets the net generation requirement, the rate of response capability for later time stages has been increased by moving Units 9 and 10 up from their minimum outputs. This extra generation of Units 9 and 10 at stages 10 and 11 is later used as "reserved" rate of response when there is a sudden decrease in the load.

In summary, the Case 1 results demonstrate the equivalence of the MINMAR and DPSA results when collectively the units have an aggregate response rate which is never less than the rate of change of generation requirement. The Case 2 results demonstrate the possible failure of a static dispatch (MINMAR) to satisfy the generation requirement when it is changing rapidly. This failure can occur because the aggregate rate of response is not available due to operating limit constraints. Case 2 also demonstrates how the look-ahead capability of the dynamic economic dispatch of DPSA enables it to succeed where the static dispatch method failed.

Valve Point Loading

The Case 1 and Case 2 scenarios can also be used to illustrate the use of DPSA for valve-point loading of generation units. Consider valve-point loading of generation unit No. 5 from our example. Assume that this unit's valve-points are located at approximately outputs of 30, 60, 90 and 114 MW. Figure 8 depicts two versions of the production cost curve of Unit 5. One version accurately represents the valve point phenomenon, namely that the incremental production cost increases sharply as each valve starts to open. The other version is a smoothed production cost curve (a quadratic function whose parameters were given in Table 1) that ignores the valve point phenomenon.

Figure 9 and 10 show the results for Unit 5 when DPSA is executed for Cases 1 and 2, respectively. Figure 8 shows that when the valve points are represented in the production cost curve that the output of Unit 5 tends to stay at the 90 MW valve-point as long as possible (based on economics), and when the output increases to the 114 MW valve point, it essentially does so at the full rate limit. Figure 10 has Unit 5 staying at its 90 MW valve point for most of the Case 2 scenario. However, for the initial time stages its output is increasing at the rate limit toward the 90 MW valve point. Later the output departs, temporarily, from the valve point for the duration of the abrupt schedule change--eventually returning to the 90 MW valve point once the schedule change is complete.

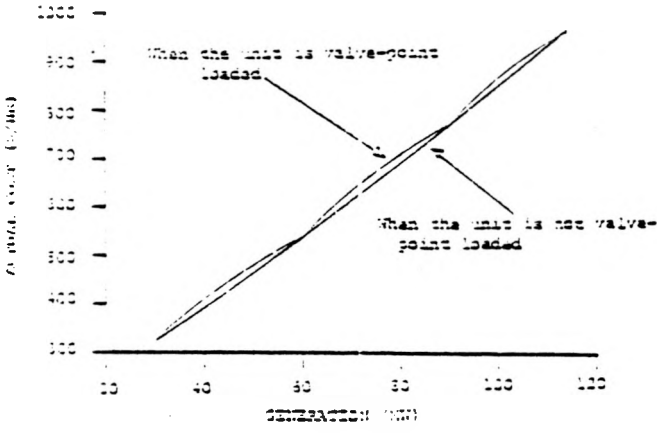

FIGURE 8 COST CURVE FOR UNIT 5

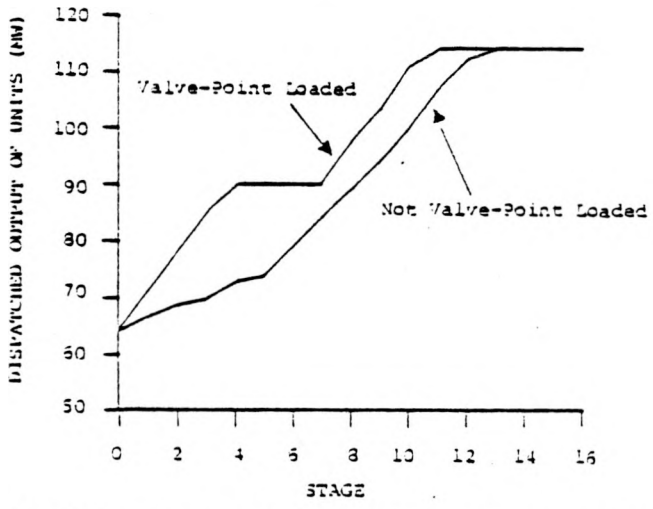

FIGURE 9 COMPARISON OF DISPATCHED OUTPUTS OF UNIT 5 BETWEEN WHEN IT IS VALVE-POINT LOADED AND WHEN IT IS NOT (CASE 1)

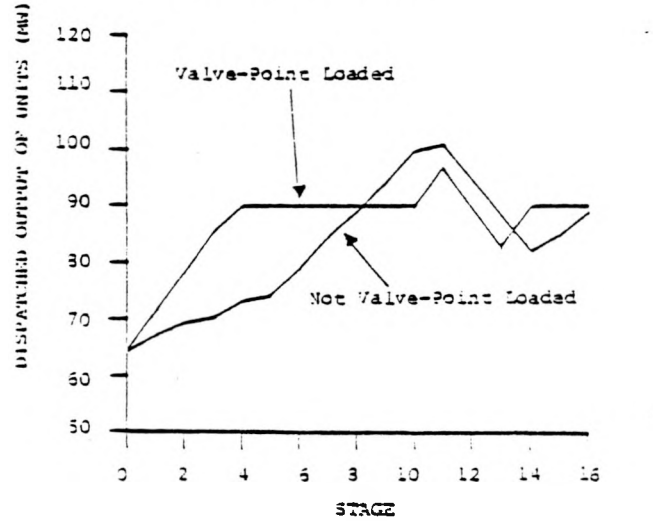

FIGURE 10 COMPARISON OF DISPATCHED OUTPUTS OF UNIT 5 BETWEEN WHEN IT IS VALVE-POINT LOADED AND WHEN IT IS NOT (CASE 2)

Computational Requirements

Computational experience with the dynamic economic dispatch program, DPSA, has been obtained at SCI on a UNIVAC 1108 computer. The computational requirements will vary approximately linearly with the number of units to be dispatched, the time horizon and the dispatch interval, the upper and lower bounds of economic generating limits of all units and the discretization size of the generation. The experience summarized in Table 2 was obtained for the following conditions:

- Number of Units: 16 generating units, including artificial unit
- Number of Stages: 16 5-minute stages

- Number of discretization levels specified: 360 discretization levels*

Factors Determining the Number of Discretization Levels

Upper Bound of Economic Generation among all units	285 MW of Unit 3
Lower Bound of Economic Generation among all units	-50 MW of Artificial Unit
Discretization size	1 MW
Actual number of Discretizations needed	(285-(-50))/1=335*

* Note that the discretization array size is greater than the actual number of discretizations needed.

- Number of pairs 30

TABLE 2
EXPERIENCE WITH COMPUTATIONAL REQUIREMENTS

	MINMAR	DPSA	COMBINED
CORE REQUIREMENT	16.44 K	29.13 K	34.39 K
COMPUTATIONAL TIME REQUIREMENT	5.39 CPU SEC	0.8 CPU SEC PER PAIR PER ITERATION	77.39 CPU SECONDS*

* On average, it took less than three iterations to converge within the cost tolerance of $1. For three iterations, CPU requirement can be estimated as

$$5.39(\text{CPU SEC}) + 0.8\ \frac{\text{CPU SEC}}{\text{PAIR}\cdot\text{ITER}} \times 30(\text{PAIRS}) \times 3(\text{ITER})$$

$$= 77.39(\text{CPU SEC})$$

CONCLUSIONS

A method has been developed that performs an optimal dynamic economic dispatch of a large number of generation units, while using only modest computing resources. The method can also perform dynamic valve-point loading. When used together with a short-term load prediction technique, dynamic economic dispatch can provide benefits of better load tracking and improved generation economics. Use of dynamic economic dispatch is consistent with the formulation of the automatic generation control problem as a dynamic optimal tracking control problem. The dynamic economic dispatch function provides target economic trajectories for the generation units and the optimal AGC response tracks these target trajectories while simultaneously controlling total area generation to track area load plus schedule. The feasibility of the method has been demonstrated on two examples, both of which involve a relatively large number of generation units.

ACKNOWLEDGEMENT

The work reported in this paper is supported by the Systems Management and Structuring Division of Electric Energy Systems, U.S. Department of Energy under Contract No. EC-77-01-2113, includes the design, implementation and testing of an integrated and coordinated set of algorithms for AGC. Systems Control, Inc., Wisconsin Electric Power Company (WEPCO), and Control Data Corporation are jointly conducting the effort. The individual assistance and guidance of Lester H. Fink, U.S. DOE Project Manager, is gratefully acknowledged. Many useful suggestions made by our colleagues at SCI have contributed to this work; in particular, we have benefited from the assistance of Robert E. Larson, Robin Podmore and Sudhir Virmani.

REFERENCES

1. L.H. Fink, H.G. Kwatny, J.P. McDonald, "Economic Dispatch of Generation Via Valve-Point Loading", IEEE Trans. on Power Apparatus and Systems, Vol. PAS-88, No. 6, pp 805-811, June 1969.

2. A.J. Korsak and R.E. Larson, "A Dynamic Programming Successive Approximations Technique with Convergence Proofs - Parts I & II", Automatica, Vol. 6, December 1969.

3. D.W. Ross, et.al., "Short-Term Load Prediction for Economic Dispatch of Generation", accepted for presentation at 1979 Power Industry Computer Application Conference; Cleveland, Ohio, May 15-18, 1979.

4. T.M. Athay, H.G. Kwatny, R.G. Smith, "Area Load-Frequency Control", Proceedings of Sixteenth Annual Allerton Conference, Monticello, Illinois, October 4-6, 1978.

5. "Development and Implementation of Advanced Automatic Generation Control Software Package", U.S. Department of Energy Contract EC-77-01-2113, Systems Control, Inc., Palo Alto, California, (L.H. Fink, U.S. Department of Energy Project Manager).

6. T.E. Bechert, and H.G. Kwatny, "On the Optimal Dynamic Dispatch of Real Power", IEEE Trans. Power App. Syst., Vol. PAS-91, May/June 1972, pp. 889-98.

7. H.G. Kwatny and T.E. Bechert, "On the Structure of Optimal Area Controls in Electric Power Networks", IEEE Trans. Automatic Control, Vol. AC-18 No. 2, April 1973, pp 167-172.

8. T.E. Bechert, N. Chen, "Area Automatic Generation Control by Multi-Pass Dynamic Programming", IEEE Trans. on Power Apparatus and Systems, Vol. PAS-96, No. 5, Sept./Oct., 1977.

9. A.D. Patton, "Dynamic Optimal Dispatch of Real Power for Thermal Generating Units", Proc. 8th Power Industry Computer Application Conference, Minneapolis, Minnesota, June 4-6, 1973; IEEE Publication 73 CHO 740-1 PWR.

10. R.E. Bellman, Dynamic Programming, Princeton University Press, New Jersey, 1957.

11. R.E. Bellman, S.E. Dreyfus, Applied Dynamic Programming, Princeton University Press, New Jersey, 1962.